Assessing Pain and Inflammation in Arthritis Using Novel Imaging Methods

A thesis submitted in candidature for the degree of Doctor of Philosophy

By

Lauren Amy Jordan

July 2016

Infection and Immunity

School of Medicine

Cardiff University

Cardiff

CF14 4XN

TABLE OF CONTENTS

List of Figures

List of Tables

Abbreviations

α	Alpha
β	Beta
µ-CT	Micro- Computed Tomography
2-D	Two Dimensional
3-D	Three Dimensional
A.I.	Arthritic Index
Ab	Antibody
ADAs	Anti-Drug Antibodies
ADAM10	A Disintegrin And Metalloproteinase domain-containing protein-10
ADAM-12	A Disintegrin And Metalloproteinase domain-containing protein-12
ADAM17	A Disintegrin And Metalloproteinase domain-containing protein-17
ADAM-8	A Disintegrin And Metalloproteinase domain-containing protein-8
AIA	Antigen Induced Arthritis
Akt	Protein Kinase B
ANOVA	Analysis of Variance
ASIC	Acid Sensing Ion Channel
BAD	Bcl-2 Associated Death promoter
Bcl-2	B cell lymphoma-2
BMU	Basic Multicellular Unit
BSA	Bovine Serum Albumin
Ca^{2+}	Calcium
CATK	Cathepsin K
CCL2 (MCP-1)	C-C chemokine ligand 2 (monocyte chemotactic protein)
CCL20	C-C chemokine ligand 20
CCL3 (MIP-1α)	C-C chemokine ligand 3 (macrophage inhibitory protein 1 alpha)
CCL5 (RANTES)	C-C chemokine ligand 5 (Regulated on Activation, Normal T Expressed and Secreted ligand)
CCL9	C-C chemokine ligand 9
CCR1	C-C chemokine receptor 1
CCR10	C-C chemokine Receptor 10
CCR2	C-C chemokine receptor 2
CCR4	C-C chemokine receptor 4
CCR5	C-C chemokine receptor 5
CD14	Cluster differentiation 14
CD8	Cluster Differentiation 8
CFA	Complete Freund's Adjuvant

c-fms	Colony stimulating factor 1 receptor
CGRP	Calcitonin Gene Regulated Protein
CIA	Collagen Induced Arthritis
Cl^-	Chloride ion
CLSM	Confocal Laser Scanning Microscopy
COPD	Coronary Obstructive Pulmonary Disease
CRP	C-Reactive Protein
CT	Computed Tomography
CTR	Calcitonin receptor
CTX-1	C-terminal peptide
CV	Cardiovascular disease
CXCL1	C-X-C Chemokine ligand 1
CXCL10	C-X-C Chemokine ligand 10
CXCL12	C-X-C Chemokine ligand 12
CXCL6	C-X-C Chemokine ligand 6
CXCL7	C-X-C Chemokine ligand 7
CXCL8	C-X-C Chemokine ligand 8
CXCL9	C-X-C Chemokine ligand 9
DCs	Dendritic Cells
DC-STAMP	Dendritic Cell – Specific Transmembrane Protein
DCT	Discrete Cosine Transform
DMARDs	Disease Modifying Anti-Rheumatic Drugs
DRG	Dorsal Root Ganglion
EDTA	Ethylenediaminetetraacetic acid
EGCG	Epigallocatechin Gallate
ELISA	Enzyme Linked Immunosorbent Assay
ERK	Extracellular signal Related Kinase
FACS	Fluorescently Activated Cell Sorting
FCS	Foetal Calf Serum
FITC	Fluorescein isothiocyanate
Fra-2	Fos-related anitigen-2
FSC-A	Forward Scatter- Area
FSC-H	Forward Scatter-Height
GM-CSF	Granulocyte macrophage colony stimulating factor
gp130	Glycoprotein 130
GPCR	G Protein Coupled Receptor
GUI	Graphical User Interface
H^+	Hydrogen ion
HBSS	Hanks Buffered Saline Solution
HCl	Hydrochloric acid
HLA/MHC	Human Leukocyte Antigen/ Major Histocompatibility Complex
HRP	Horseradish Peroxidase
ICAM-1	Intracellular Adhesion Molecule-1

IFA	Incomplete Freund's Adjuvant
IFN-γ	Interferon gamma
IgG	Immunoglobulin G
IL-1	Interleukin-1
IL-11	Interleukin-11
IL-12	Interleukin-12
IL-13	Interleukin-13
IL-15	Interleukin-15
IL-17	Interleukin-17
IL-18	Interleukin-18
IL-1R	Interleukin-1 receptor
IL-27	Interleukin-27
IL-4	Interleukin-4
IL-6	Interleukin-6
IL-6R	Interleukin-6 receptor
IL-7	Interleukin-7
IL-8	Interleukin-8
IMS	Industrial Methylated Spirit
JIA	Juvenile Idiopathic Arthritis
JNK	c-Jun N-terminal Kinases
LIF	Leukemia Inhibitory Protein
MACS	Magnetic Activated Cell Sorting
MAPK	Mitogen Activated Protein Kinases
MATLAB	Matrix Laboratory
MCP	Metacarpals
m-CSF	Macrophage colony stimulating factor
MM	Multiple Myeloma
MMP	Matrix Metallloproteinase
MMP-13	Matrix Metalloprotease-13
MMP-2	Matrix Metalloprotease-2
MMP-3	Matrix Metalloprotease-3
MMP-9	Matrix Metalloprotease-9
MRI	Magnetic Resonance Imaging
mRNA	Messenger Ribonucleic acid
MS	Magnetic Separation
MTP	Metatarsals
NFATc1	Nuclear Factor of Activated T cells 1
NF-κβ	Nuclear factor- kappa beta
NGF	Nerve Growth Factor
NTX	N-terminal peptide
OA	Osteoarthritis
OC-STAMP	Osteoclast Stimulatory Transmembrane Protein
OPG	Osteoprotegrin
OVX	Ovariectomized mouse

PBMCs	Peripheral Blood Mononuclear Cells
PBS	Phosphate Buffered Saline
PBS-T	Phosphate Buffered Saline with Tween
PGs	Prostaglandins
PI3K	Phosphoinositide 3-kinase
PMT	Photon Multiplier Tube
PTH	Parathyroid Hormone
qPCR	Quantitative Polymerase Chain Reaction
RA	Rheumatoid arthritis
RANK	Receptor Activator of Nuclear Factor K-B
RANKL	Receptor Activator of Nuclear Factor K-B Ligand
RNA	Ribonucelic Acid
RPMI	Roswell Park Memorial Institute Medium
RT-PCR	Real time PCR
RUNX2	Runt-related transcription factor-2
SASP	Senescence-Associated Secretory Phenotype
SDSPMM	Super Depth Surface Profile Measurement Microscope
SEM	Scanning Electron Microscopy
SEM	Standard Error of the Mean
SF	Synovial Fluid
sgp130-Fc	Soluble Glycoprotein 130-Fc
sIL-6R	Soluble Interleukin-6 receptor
siRNA	Small interfering RNA
SSC-A	Side Scatter -Area
ST	Synovial Tissue
STAT1	Signal Transducer and Activator of Transcription 1
STAT3	Signal Transducer and Activator of Transcription 3
TB	Tuberculosis
TEM	Transmission Electron Microscopy
TGF-β	Transforming Growth Factor beta
TMB	Tetramethylbenzidine
TNFR	Tumour necrosis factor receptor
TNF-α	Tumour necrosis factor- alpha
TRAF6	TNF receptor associated factor-6
TRAP	Tartrate resistant acid phosphatase
TrkA	Tropomyosin receptor kinase A
TRPV1	Transient Receptor Potential Vanilloid 1
US	Ultrasonography
VCAM-1	Vascular Cell Adhesion Protein-1
VIP	Vasoactive Intestinal Peptide
WT	Wild-Type

Acknowledgements

Over the past 4 years I have received a considerable amount of help and support from many of my friends and family. I would like to thank my supervisors Anwen and Ann for their continued support, advice, and above all patience throughout the last 4 years. I know times were trying at times but your input has always been greatly appreciated. At Cardiff University I would like to thank the Rheumatology Department and all those who have listened to presentations and given constructive feedback, and of course my review panel for their guidance at the end of each year and building up my confidence as a researcher. I would also like to thank the William Morgan Thomas fund and the BSI travel award which enabled my travel to two international conferences to present my research.

Following this, my time at Cardiff University would not have been the same without my girls; Rav, Jess, Ruth, Katie, Charlie and Kate. I cannot express in words the gratitude I have for you girls. Rav and Jess, you have simply been amazing. You've kept me sane, healthy, fit and topped up with kebabs! Thank you also to Anne and Saydul, your constant support, love, shoulder to cry/moan/nag on, has helped me so much through the last 4 years. You have all been my rock in one way or another, both in my professional and my personal life, and I hope the new distance between us all won't change that. Thank you to Mr Alastair Robertson, through tough times you supported and encouraged me to keep going, and I will always remember the good memories. Special thanks also go to Mr Mitchell. You have brightened up the last couple of months and been evidence of the light at the end of the tunnel in more ways than one, thank you.

Finally to my family; Mum, Dad, Ka Ha, Grandma and Granddad, thank you for supporting me and my decisions in life. The last 4 years have definitely been trying but I could not have made it without your constant love, support and optimism. A special thank you goes to Uncle David for his ability to move my life and its belongings around the entire country! Thank you all for putting up with me and providing constant encouragement and cake!

Declaration

This work has not previously been accepted in substance for any degree and is not currently submitted in candidature for any degree.

Signed.....(Lauren Amy Jordan)

Date.....30 March 2017.....

Statement 1

This thesis is being submitted in partial fulfilment of the requirements for the degree of PhD.

Signed.....(Lauren Amy Jordan)

Date.....30 March 2017.....

Statement 2

This thesis is the result of my own independent work/investigation, except where otherwise stated. Other sources are acknowledged by explicit references.

Signed.....(Lauren Amy Jordan)

Date.....30 March 2017.....

Statement 3

I hereby give consent for my thesis, if accepted, to be available for photocopying and for inter-library loan, and for the title and summary to be made available to outside organisations.

Signed.....(Lauren Amy Jordan)

Date.....30 March 2017.....

Statement 4

I hereby give consent for my thesis, if accepted, to be available for photocopying and for inter-library loans **after expiry of a bar on access previously approved by the Graduate Development Committee.**

Signed.....(Lauren Amy Jordan)

Date.....30 March 2017.....

ABSTRACT

Enhanced bone resorption is a common pathology in destructive bone diseases. Many cytokines (*e.g.* IL-6 and TNF-α) and chemokines (*e.g.* CCL2, CCL3 and CCL5) elevated in patients exert pathological roles in leukocyte migration and inflammation, but their effect on direct bone destruction remained elusive. Published research into osteoclastogenesis was carried out in co-cultures, from which osteoclast differentiation, resorption and mediator secretion data was obtained. The main objective of this thesis was to establish a working methodology for the *in vitro* differentiation of $CD14^{+ve}$ mononuclear cells into osteoclasts and to decipher the direct effects of IL-6 and CCL3 on osteoclastogenesis and bone resorption.

IL-6 trans-signalling exerted an effect in both basal and pathological osteoclastogenesis, whereas its inhibition *via* sgp130-Fc significantly reduced osteoclast formation and bone resorption *in vitro*. Although not examined *in vivo*, the translational use of sgp130-Fc as a therapeutic for destructive bone pathology was postulated from data showing a reduction in osteoclast differentiation and resorption after stimulation with HYPER-IL-6.

Secondary to IL-6 trans-signalling, it was hypothesised that the neutralisation of CCL3 *in vitro* and *in vivo* would significantly reduce osteoclast differentiation and resorption. Osteoclast number significantly reduced in the presence of anti-CCL3, but $TRAP^{+ve}$ cell count was unaltered, suggesting an early role of CCL3 in osteoclast multi-nucleation/fusion. Additionally, *in vivo* data showed a protective effect of anti-CCL3 with significantly reduced bone erosive scores and osteoclast counts thereby presenting CCL3 as a novel biomarker of disease activity in destructive bone disease. In contrast, TNF-α, CCL2, and CCL5 were shown to have no role in direct osteoclast differentiation in our monocultures.

In conclusion, for the first time this work documents novel and important roles of IL-6 trans-signalling and CCL3 in increased osteoclast differentiation and bone resorption. Our data highlights the importance of IL-6 trans-signalling and provides evidence for the use of CCL3 as a predictive biomarker in destructive bone diseases.

Chapter 1:General Introduction

1.1 Bone Homeostasis

The human skeleton consists of an average of 206 bones and has many important functions; supporting body structure, mechanical levers for movement, protecting internal organs (including the central nervous system), maintaining an ionic environment (Ca^{2+}), and in the generation and replenishment of haematopoietic cells. Bone homeostasis and remodelling is therefore essential to many biological functions. Bone remodelling is a tightly coupled and regulated process in which the rapid destruction of bone by osteoclasts occurs (taking 14-21 days), followed by the formation of osteoid and new bone matrix by osteoblasts (taking ≥3 months; Figure 1.1); referred to as the basic multicellular unit (BMU; *Raisz 1999, Jilka 2003*).Multiple factors play a role in the regulation of bone homeostasis, where the release of humoral factors including calcium, growth factors and degradation products induce osteoblastogenesis and bone formation (*i.e.* parathyroid hormone (PTH), vitamin D, TGF-β, prostaglandin E, osteocalcin and several pro-inflammatory cytokines; *Chenu et al. 1988, Rodan et al. 1998,Neer et al. 2001, Kanazawa et al. 2015*).

Differences in bone turnover kinetics can lead to several pathological outcomes related to enhanced osteoblast or osteoclast activity, where diseases such as osteopetrosis, rickets, osteomalacia, and osteophyte formation result due to increased osteoblastogenesis (*Rogers et al. 1997, Stark & Savarirayan 2009, Elder & Bishop 2014*) or alternatively diseases including osteitis fibrosa cystica, Paget's disease and osteoporosis result due to elevated osteoclastogenesis (*Sleiman et al. 2004*, *Ralston et al. 2008, Jobke et al. 2014*). Under both pathological circumstance, changes in joint structure results. Extensive research relating to synovial components in bone diseases was reported, but limited research of how arthritic diseases directly affect the homeostasis of osteoblasts and osteoclasts (*i.e.* the BMU) is currently available. Due to the major implications of bone destruction in joint structure and overall patient health and well being, this thesis will focus upon the only cell capable of resorbing bone; the osteoclast. A relationship between the osteoclast, synovial infiltrate and the cartilage in arthritic diseases must however be

kept in mind (*Danks et al. 2002, Kinne & Burmester 2007, Schett 2007, Schett 2007,Schett & Teitelbaum 2009, Hitchon & El-Gabalawy 2011, Knowles et al. 2012*).

1.1.1 An overview of osteoblasts and osteocytes

Osteoblasts are mononuclear cells differentiated from mesenchymal stem cells in the presence of RUNX2 and its downstream signalling protein Osterix (*Ducy et al. 1997, Nakashima et al. 2002*). The association of osteoblasts via tight junctions at bone-forming sites facilitates the secretion of bone matrix, which after ~10 days becomes calcified (*Nijweide et al. 1982*). In addition to bone matrix, osteoblasts secrete the major osteoclast-stimulating mediator RANKL (receptor activator nuclear factor κβ (RANK) ligand) which is essential for osteoclast differentiation, along with the main natural osteoclast inhibitor; Osteoprotegrin (OPG), RANKL decoy receptor.

When an osteoblast becomes ensnared in bone lacunae, the secretion of bone matrix stops and terminal differentiation into osteocytes ensues. Osteocytes are found in plentiful numbers and act as modulators in osteoblast and osteoclast stimulation due to their mechanosensory phenotypes (*Caetano-Lopes et al. 2007*).

1.1.2 An overview of osteoclasts

Osteoclasts are differentiated from a haematopoietic origin as originally performed and reported by *Donald Walker* in the 1970s, where osteopetrotic mice were cured through treatment with wild-type spleen cells (*Walker 1975*). This finding was later translated into humans by *Coccia et al. (1980)* who treated an osteopetrotic 5 month old girl with bone-marrow from her brother (HLA-MLC identical) resulting in active osteoclasts (containing Y chromosome) alongside her own osteoblasts, which in tandem reduced disease pathogenesis. Osteoclast differentiation was subsequently well studied through the use of gene knock-out models in osteopetrosis which highlighted essential genes in osteoclastogenesis, and in 2006 $CD14^{+ve}$ cells were identified as osteoclast precursor cells (*Komano et al. 2006*). Osteoclast differentiation relies on the essential presence of macrophage colony stimulating factor (m-CSF) and RANKL. Terminally differentiated osteoclasts are

giant multinucleated, tartrate resistant acid-phosphatase^{+ve} (TRAP^{+ve}), cathepsin K^{+ve} (CATK^{+ve}), vitronectin receptor^{+ve} cells (*Davies et al. 1989, Simpson & Horton 1989 Motyckova et al. 2001, Takayanagi et al. 2002*). Osteoclast polarisation facilitates adhesion to bone matrix and results in a ruffled membrane at the resorptive edge. The secretion of acid, TRAP and enzymes (CATK and matrix metalloproteases; MMPs) at the ruffled membrane leads to bone resorption and cartilage destruction. Bone degradation products (*e.g.* collagen fragments C-terminal telopeptide of type-I collagen, CTX-1, or N-terminal telopeptide of type I collagen, NTX-1) and growth factors (e.g., TGF-β) are released from the matrix and thought to contribute in the stimulation of osteoblastogenesis; thus, a self-regulatory loop for bone homeostasis is maintained (*Boyle, Simonet & Lacey 2003*). The process of osteoclastogenesis will be further introduced in Section 1.2.

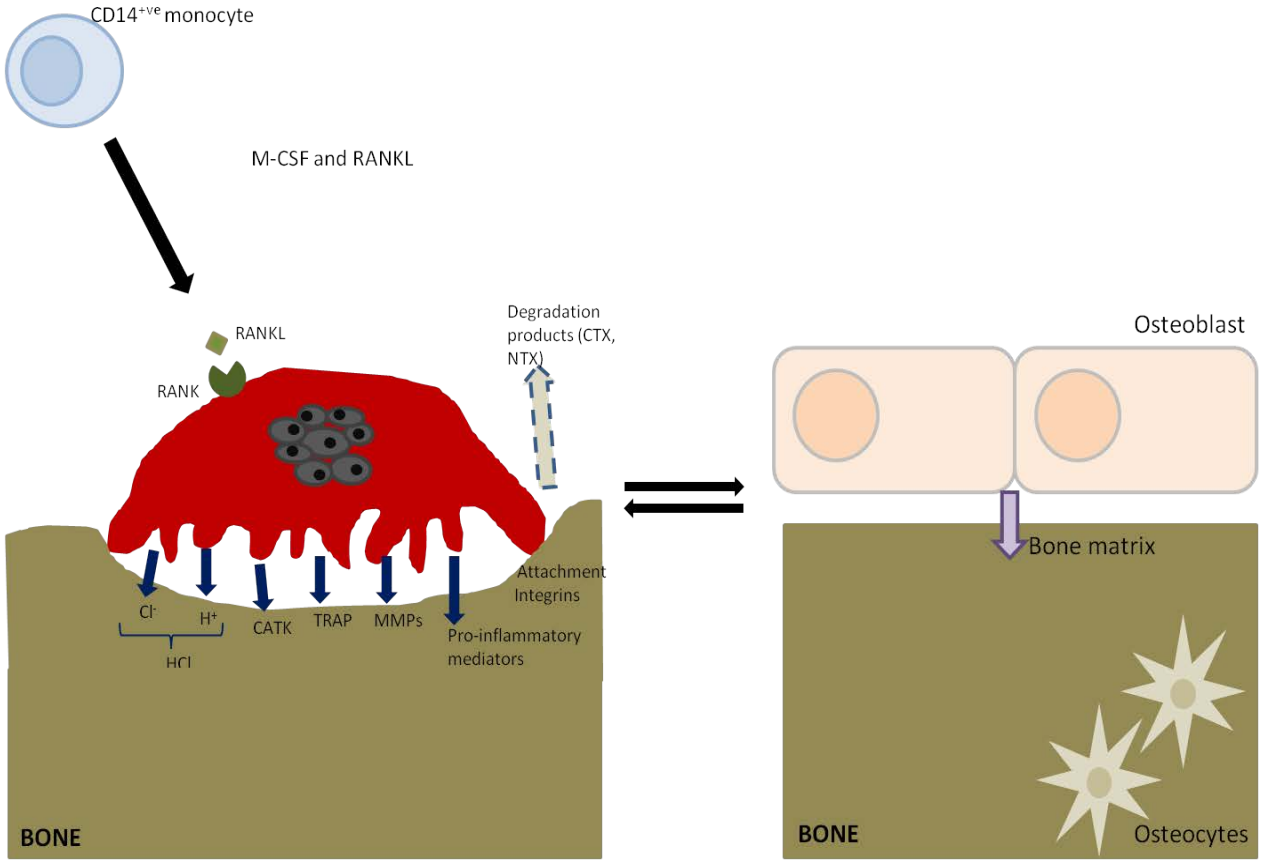

Figure 1. 1 - An illustration of cellular involvement in bone homeostasis.In the presence of osteoclast stimulating factors (m-CSF and RANKL) $CD14^{+ve}$ mononuclear cells differentiate into osteoclasts, classified by their giant multinuclear phenotype and expression of vitronectin, TRAP and CATK. The expression and secretion of TRAP and degradative enzymes (CATK and MMPs) from the osteoclast results in bone resorption, leading to the dissolution of bone matrix (*e.g.* collagen fragments) and the secretion of growth factors (*e.g.* TGF-β). Following bone resorption, bone formation is stimulated via the osteoblast where new osteoid is laid down and calcified.

1.2 Osteoclastogenesis

Osteoclast precursors undergo six main steps in becoming mature osteoclasts. Firstly, $CD14^{+ve}$monocytes migrate into local areas due to a concentration gradient of pro-inflammatory cytokines and chemokines; *i.e.* TNF-α, IL-1 and IL-6 (*McInnes and Schett, 2007*).The retention of these precursors in the joint occurs until a high cell density is obtained, priming the cells for fusion and differentiation. In tandem to the secretion of pro-inflammatory cytokines and chemokines, m-CSF and RANKL are secreted from co-localised cells (stromal cells, osteoblasts, T cells) and are the main instigators of monocyte fusion and differentiation (*Susa et al. 2004*). M-CSF stimulates cell proliferation through its receptor (c-fms) expression on precursor cells. Ligand binding also enhances further secretion of chemotactic mediators which facilitate the initial migration of cells and increasing cell survival (*Nemunaitis 1993, Yang et al. 1996 ,Ross et al. 2006*).The importance of m-CSF was shown in osteoclast differentiation where $c\text{-}fms^{-/-}$ mice lack terminally differentiated osteoclasts (*Kikuta & Ishii 2013)*.

RANKL originates either from proteolytic cleavage by matrix-metalloprotease-3 and -7 secreted from the osteoblast/osteoclast respectively, or is secreted directly from mesenchymal cells, osteoblasts and T cells (*Jimi et al. 1999, Yu et al. 2004, Blair et al. 2005, Wada et al. 2006*).RANKL binds to RANK on pre-osteoclasts and initiates its signalling pathway (Figure 1.2). In brief, there-localisation of TNFR-associated cytoplasmic factor 6 (TRAF6) results from RANKL-RANK binding stimulating downstream signalling and leading to cell fusion. Primarily this occurs through dendritic cell-specific trans-membrane protein (DC-STAMP), a protein found at significantly increased levels in arthritic joints (*Han et al. 2001, Yagi et al. 2005, McInnes & Schett* 2007*, Mizutani et al. 2009, Kikuta & Ishii, 2013*). In addition to DC-STAMP, TRAF6 also stimulates the activation of NF-κβ and ERK signalling in addition to osteoclast-specific target genes; NFATc1, c-fos, CATK, TRAP, adhesion integrins, chemokine/cytokine secretions and calcitonin (CTR) receptor (*Jimi et al. 1999, Yu et al. 2004, Blair et al. 2005, Wada et al. 2006, McInnes and Schett, 2007*). The importance of c-fos in osteoclast-macrophage lineage determination has been reported both *in vitro* and *in vivo*. *In vivo* c-fos deficient mice develop osteopetrosis

which can be rescued through bone marrow transplantation, and in bone marrow macrophage cultures p38 inhibition resulted in attenuated c-fos and decreased osteoclast differentiation (*Grigoriadis et al. 1994, Huang et al. 2006*).

The multinucleation of precursor cells is paramount to the transcription and expression of osteoclast-specific genes, and their subsequent resorptive capabilities. A correlation between nuclei number and the resorptive potential of the osteoclast has previously been shown by *Piper, Boyde & Jones (1992),* highlighting the importance of multinucleation. An association between osteoclast size due to Fra-2 (Fos associated protein) and bone destruction has also been made by *Bozec et al. (2008)* who reported increased size to link to destructive bone diseases. Additional to multinucleated cells, the adhesion integrin αvβ3 is also paramount for attachment of differentiating osteoclasts to bone, whilst also playing a role in cytoskeletal reorganisation (*Kikuta & Ishii 2013)*. Of importance is the transition of αvβ5 integrin, which is present prior to multi-nucleation but reduced after differentiation, to αvβ3 integrin which presents with opposite expression patterns (*Sago et al. 1999*).

Finally, a vital step for osteoclast adhesion to bone matrix is the polarisation of the cell body resulting in the formation of a ruffled membrane at the resorptive edge due to actin cytoskeleton rearranging. This ruffled membrane facilitates the transportation of acidifying vesicles along microtubules to the plasma membrane where a tight junction has formed between bone and osteoclast. A proton pump is relocated to the osteoclast-bone interface, and H^+ are secreted which associate with Cl^- (pumped out of the cell) forming HCl, leading to the acidification of bone mineral (pH4.5). The secretion of MMPs and enzymes (CATK and TRAP which function at low pH) leads to the further destruction of bone and mineralised cartilage, leading to the formation of resorption pits/lacunae(*Boyle, Simonet& Lacey 2003*). The degradation products (*e.g.* C-terminal telopeptide of type-I collagen, CTX-1, or N-terminal telopeptide of type I collagen, NTX-1) can be quantified *in vitro* to determine osteoclast resorptive activity.

Within bone homeostasis, a regulatory mediator of osteoclast differentiation and resorption is secreted from co-localised cells (osteoblasts and bone marrow stromal cells) in response to osteoclast-stimulating mediators. This decoy receptor of RANKL is termed osteoprotegerin (OPG), and a close regulatory role between OPG and RANKL exists. In destructive bone diseases, an unbalance between osteoclast inhibitory and stimulatory signals occurs often resulting in enhanced osteoclast formation and/or activity. As a consequence substantial bone erosions develop and progressively get extenuated over time. Although there are many pathogenic instigators leading to the uncoupling of bone homeostasis, many of these are hormones and inflammatory mediators. Within this thesis the term destructive bone disease will be used to describe diseases of the joint or alveolar bone where substantial bone resorption has occurred; *i.e.* osteoporosis, periodontitis, rheumatoid arthritis.

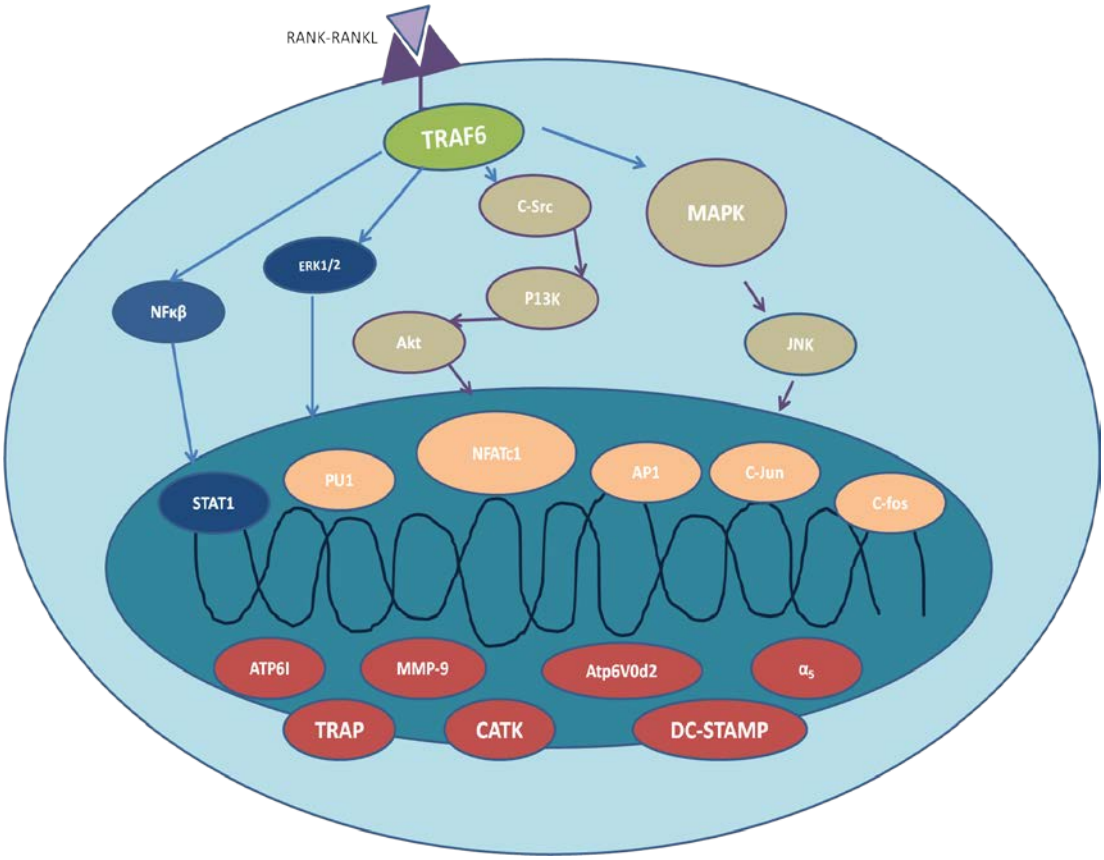

Figure 1. 2 - Signalling pathways activated by RANKL-RANK.The binding of RANKL to its receptor RANK activates TRAF6 stimulating downstream signalling pathways leading to the transcription and expression of osteoclast-specific genes (*e.g.* ATP, TRAP, CATK, DC-STAMP, Atp6V0d2 and integrins).

1.3 Stimulators of osteoclastogenesis

Hormones, cytokines and chemokines are thought to play a major role in the destructive phenotype identified in many forms of inflammatory arthritis. An overview of the main instigators of osteoclastogenesis follow, specifically those with direct links.

1.3.1 Hormonal impact on osteoclastogenesis

Many hormones are known to exert a role in osteoclastogenesis and are pivotal to pathological bone destruction.

1.3.1.1 Oestrogen

Oestrogen inhibits osteoclastogenesis and associated bone resorption in mammals, and is essential in bone development due to its role in epiphyses closing. The precise means of how this occurs is still unclear, but it is likely to be associated with precursor cell differentiation, and pro-inflammatory cytokine secretions (*i.e.* IL-6).The expression of oestrogen receptor (ERα) has been confirmed on osteoblasts, pre-osteoclasts and osteoclast; exerting a dual mechanism on osteoclast activity (*Oreffo et al. 1999*). Firstly, direct binding of oestrogen to its receptor on the osteoclast induces the osteoclast to lose attachment to bone surfaces, and increases osteoclast apoptosis (*Liu & Howard 1991, Kameda et al. 1997*). However, oestrogens effects on osteoclastogenesis are primarily induced by its impact on osteoblast activity. After activation by oestrogen the osteoblast secretes OPG which acts as a decoy receptor to RANKL and thus prevents osteoclastogenesis(*Bord et al. 2003*).Oestrogen therefore exerts an effect on both mature (directly through receptors on the osteoclast) and differentiating (indirectly through the osteoblast) osteoclasts. In females oestrogen is defined as an evolutionary advantage which allows the retention of calcium in the body for embryo development (*Riggs, Khosla & Melton 2002*).

1.3.1.2 Testosterone

Similar inhibiting effects of testosterone on osteoclastogenesis have been reported to oestrogen, but these may occur via two mechanisms; conversion of testosterone into oestrogen via aromatase, and direct effects mediated through androgen receptors (*Chen et al. 2001, Michael et al. 2005*). These two mechanisms are

known to be independent of each other where inhibiting the ER or aromatase has no effect on the reduction of osteoclastogenesis as a result of testosterone/androgen receptors, and vice versa (*Chen et al. 2001*). Testosterone also exerts an inhibiting effect on osteoclastogenesis in the presence of its stimulator PTH (see Section 1.3.1.5) in a concentration dependent manner, due to the expression of androgen receptors (*Chen et al. 2001*). In cultures containing $CD14^{+ve}$ cells only, and in co-cultures of mononuclear cells and osteoblasts, testosterone at physiological concentrations, and also over a dose-range, reduces osteoclast differentiation and resorptive activity, and in co-cultures leads to increased OPG secretions from osteoblasts (*Michael et al. 2005*).

1.3.1.3 Calcitonin

Calcitonin also plays an essential role in the regulation of osteoclast activity. Calcitonin hormone controls serum levels of calcium, firstly by enhancing calcium excretion from the kidneys, and secondly by directly inhibiting bone resorption through activating the calcitonin receptor on the osteoclast, leading to a reduction in cellular movement and secretion of resorptive enzymes (*Copp et al. 1962, Warshawsky et al. 1980, Takahashi et al. 1988, Zheng et al. 1994*).

1.3.1.4 Prostaglandin

Prostaglandin, specifically E_2, is a pivotal mediator in bone homeostasis. PGE_2exerts a dose-dependent stimulatory effect on osteoclastogenesis and bone resorption, and this is mediated through its receptors EP2 and EP4 (*Lader & Flanagan 1998*). PGE_2 exerts this effect through increasing RANKL signalling and facilitating cross-signalling between downstream RANKL and EP2 and EP4 signalling pathways; an indirect effect mediated by the osteoblast (*Kobayashi et al. 2006*). Through the inhibition of prostaglandin synthesis by addition of indomethacin, a significant decrease in osteoclast number and bone resorption results, identifying its importance (*Kaji et al. 1996, Lader & Flanagan 1998*).

However, contradictory results are published for the direct effects of PGE_2 on osteoclastogenesis, where PGE_2 has been reported to reduce osteoclast number and resorption. *Kobayashi et al. (2005)* concluded that this effect was due to a

changing expression of EP receptors, where mononuclear cells could auto-reduce their surface expression of EP2 and EP4 to evade the direct inhibiting action of PGE_2 in cultures.

1.3.1.5 Parathyroid hormone (PTH)

Parathyroid hormone regulates calcium by leading to its release or resorption in bone, the kidney and/or the intestine. PTH release is increased due to low calcium or due to elevated levels of serum phosphate. PTH then activates the osteoblast and causes an increase in RANKL and an attenuation in OPG secretion, leading to an indirect stimulation of osteoclast differentiation and subsequent resorptive activity. PTH is often increased in destructive diseases and causes an increased release of calcium from the bone due to enhanced osteoclast formation and resorption (*Poole &Reeve 2005*).

Additional to PTH, growth hormone, thyroid hormone vitamin D and glucocorticoids are all also associated with increased bone resorption.

1.3.2 Pro-inflammatory cytokines in destructive bone diseases

In addition to the above hormones many cytokines are found elevated in inflammatory destructive bone diseases (*i.e.* RA), including IL-1, TNF-α and IL-6 (*Hopkins et al. 1988, Issekutz et al. 1994*). The secretion of these pro-inflammatory cytokines is likely to occur from infiltrating leukocytes (*e.g.* T cells, neutrophils), chondrocytes, stromal cells, osteoblasts or osteoclasts (*Firestein et al. 1994, Braun et al. 1999, Raza et al. 2005, Joosten et al. 2009*). Although the direct mechanism of action of cytokines on osteoclast differentiation is still under investigation, these cytokines are involved in the migration of precursor cells and the secretion of RANKL which in tandem increases osteoclastogenesis.

1.3.2.1 IL-1 and TNF-α

Interleukin-1 (IL-1) is a stimulator of osteoclast differentiation and functional resorption *in vitro* and *in vivo* via three main ways; osteoclast stimulation, indirectly enhancing RANKL secretion from neighbouring cells (T cells), and increasing co-

stimulating mediators *i.e.* prostaglandins (PGs; *Klein& Raisz1970*, *Jimi et al. 1999*). IL-1 has two main receptors (IL-1R type I and II) to which it binds, each of which has differing downstream signalling pathways with divergent effects. IL-1R type I is the receptor of main interest in inflammatory arthritis due to its role in inflammation. Type II however, acts as an endogenous suppressor of IL-1 activity by competitive binding (*Kuno & Matsushima 1994*).Following IL-1 binding to IL-1R type I, TRAFs and NF-κβ signalling pathways (identical to RANKL signalling) are activated, amplifying both IL-1 and RANKL signals (*Eder 1997*). Similarly to IL-1, tumour necrosis factor-alpha (TNF-α) stimulates the recruitment and differentiation of osteoclast precursors from bone marrow (*Bertolini et al. 1986*).TNF-α binds to TNF receptors (TNFR) found on cell membranes or as soluble forms (*i.e.* TNFR1). An adaptor protein such as TRAF is again utilised and effects on inflammation, proliferation or cell survival are exerted (*Gravestein & Borst 1998*).Direct mechanisms of TNF-α on osteoclastogenesis are controversial, where the majority suggest a RANKL-dependent mechanism of action due to co-localised cells increasing RANKL secretion in response to TNF-α. However, a RANKL-independent mechanism was suggested by *Kobayashi et al.*(*2000*)but data was not reproducible questioning its validity.

1.3.2.2 IL-6

IL-6 is also significantly enhanced in destructive bone diseases and is secreted from stromal cells and osteoblasts in the joint (*Ishimi et al. 1990, Srirangan & Choy 2010*). Specifically, this cytokine enhances monocyte migration in the presence of its receptor IL-6R, and was linked to enhanced osteoclastogenesis due to increasing RANKL secretion (*Hashizume et al. 2008*). IL-6R can be found in both membrane bound and soluble forms, facilitating two independent signalling pathways; classical and trans-signalling. IL-6 classical signalling is known as the pathway resultant of IL-6 binding to membrane bound IL-6R, which then associates and dimerizes with gp130. Membrane bound IL-6R expression was reported on monocytes and macrophages and it is these cells which can respond to IL-6 classical signalling. This classical pathway is thought of as the regulatory pathway for resolution of an immune response and cellular regeneration. However, cells which do not express

membrane bound IL-6R or are not currently known to express it (*i.e.* the osteoclast), can still respond to IL-6 through their ubiquitous expression of gp130 (*Kishimoto et al. 1995, Kotake et al. 1996, Grivennikov et al. 2009, Miyamoto et al. 2009*, *Jones, Scheller& Rose-John 2011*).

IL-6 trans-signalling occurs through the binding of IL-6 to a soluble form of its receptor (sIL-6R), which dimerizes with gp130 on the cell membrane, and activates JAK/STAT pathways. The secretion of sIL-6R was reported from cells of the joint (*i.e.* osteoblasts, stromal cells *etc.*) and occurs due to two mechanisms; proteolytic cleavage and alternative splicing (*Ishimi et al. 1990, Tamura et al. 1993* and *Srirangan and Choy 2010*). Proteolytic cleavage occurs through a disintegrin and metalloproteases domain-containing protein-10 and -17 (ADAM10 and ADAM17respectively), where IL-1 and TNF-α induced neutrophil apoptosis release sIL-6R (*Schumacher et al. 2015*). Alternative splicing of mRNA coding for IL-6R also leads to loss of specific membrane domains, resulting in its soluble form (*Galicia et al. 2004*). Evidence of IL-6 trans-signalling in osteoclast formation was first reported in 1993 by *Tamura et al.* where osteoclast number significantly increased after treatment of murine co-cultures (bone marrow and osteoblasts) with IL-6 (200ng/mL) and sIL-6R (500ng/mL), and not in the presence of these mediators alone. However, the direct effects of IL-6 trans-signalling on pure monocultures of osteoclastogenesis are still unknown. However, it was postulated that any affect IL-6 had on osteoclastogenesis was through sIL-6R and trans-signalling; it's thus believed to be the pathogenic signalling pathway involved in inflammation associated with disease.

In addition, the increased presence of IL-1, TNF-α and IL-8 in destructive bone disease synergistically increases IL-6 secretion (*Pathak et al. 2015*).Other mediators sharing gp130 are also postulated in osteoclastogenesis. Interleukin-11 (IL-11) and leukaemia inhibitory factor (LIF) are both secreted by bone cells and reported to 'stimulate' osteoclast differentiation, but reported data since has not been reproducible and remains controversial (*Lorenzo et al. 1990, Reid et al. 1990,Hill et al. 1998, Lee & Lorenzo 2006*). Alternatively, the opposite effect was reported for

oncostatin M which inhibited osteoclast differentiation and resorption, and pushed cells down a macrophage lineage (*Heymann et al. 1998*).

1.3.2.3 IL-7

Controversial findings are presented for the role of interleukin-7 (IL-7) in bone homeostasis where both stimulatory and inhibitory roles were suggested. *In vitro* supplementation of IL-7 into human osteoclast differentiation cultures increased T cell secretion of RANKL, indirectly increasing osteoclastogenesis but not directly (*Weitzmann et al. 2000*). Supporting this, T cell$^{-/-}$ mice treated with IL-7 showed no change in osteoclastogenesis or bone destruction (*Toraldo et al. 2003*). Opposing this, IL-7 supplemented *in vitro* was reported to decrease osteoclast numbers by *Lee et al. (2003)*, and *in vivo* IL-7$^{-/-}$ mice were shown to have increased osteoclastogenesis (*Lee et al. 2003*). Further work establishing the role of IL-7 in osteoclastogenesis is however needed.

1.3.2.4 IFN-γ, IL-4, IL-13, IL-12 andIL-18

Additional to the main osteoclast-stimulating mediators, inhibitors of osteoclastogenesis also exist; interferon-γ (IFN-γ), interleukin-4 (IL-4), interleukin-13 (IL-13), interleukin-12 (IL-12) and interleukin-18 (IL-18) (*Lee & Lorenzo 2006*). IFN-γ inhibits bone resorption through interfering with the RANK signalling pathway and degrading TRAF6, thus preventing pre-osteoclast differentiation (*Takayanagi et al. 2000*). IL-4 similarly affects RANKL signalling, but this time at the level of NFATc1, therefore disrupting differentiation (*Cheng et al. 2011*). Alternatively, IL-13 inhibits osteoclastogenesis indirectly through reducing PGs, simultaneously increasing OPG and osteoblast migration (*Lind et al. 1995,Palmqvist et al. 2006*). Similar indirect mechanisms are exerted by IL-12 and IL-18, which inhibit osteoclastogenesis through altering T cell behaviour and increasing the secretion of granulocyte macrophage colony-stimulating factor (GM-CSF; directs differentiation of precursors away from the osteoclast) respectively (*Horwood et al. 2001*). In addition, IL-12 has also been linked to the enhanced apoptosis of pre-osteoclasts thus inhibiting osteoclast maturation and subsequent resorption (*Kitaura et al. 2002*).

1.3.3 Pro-inflammatory Chemokines

The reported activity of several inflammatory CXC- and CC-chemokines in inflammatory arthritis was documented over the past 15 years. The main role of these chemokines is in the chemotaxis of neutrophils (CXC- chemokines primarily), monocytes and macrophages (CC-chemokines primarily) via concentration gradients, in addition to a role in angiogenesis. Chemokines thus exert a dual effect in maintaining the diseased joint with nutrients and leukocytes via the new vasculature.CXCL1, CXCL6, CXCL7, CXCL8 (IL-8), CXCL9, CXCL10, CXCL12, CCL2 (monocyte chemotactic protein-1), CCL3 (macrophage inflammatory protein 1-α), CCL5 (regulated upon activation of normal T-cell expressed and secreted) and CCL20 are all elevated in the synovial joint of RA patients due to their enhanced secretion from synovial macrophages and fibroblasts (*Koch 2005, Boyce et al. 2006*). However, only a few of these chemokines were linked to osteoclastogenesis or functional resorptive activity in inflammatory arthritis, where most were identified from co-culture methodologies, making the direct role of these chemokines on osteoclast differentiation elusive.

1.3.3.1 CCL2

CCL2 is elevated in inflammatory arthritis patients and is secreted from fibroblasts, synovial cells and infiltrating leukocytes causing monocyte migration (*Kim et al. 2005, Koch 2005*, *Vangsness et al*. *2011*).CCL2 signals through its membrane-bound receptors CCR2 and CCR4, found on monocytes, macrophages and some T cells (*Vergunst et al. 2008*).In addition, osteoclast and osteoblast secretion of CCL2 can occurs, but only in the presence of RANKL are functional osteoclasts produced (*Kim et al. 2005*).

Direct effects of CCL2 on osteoclastogenesis are currently unknown, although previous studies suggest CCL2 is not pivotal to inflammatory pathogenesis presented in the arthritides; its neutralisation (anti-CCR2) had no effect on reducing inflammation in RA patients (*Vergunst et al. 2008*).However,CCL2 was shown to increase RANKL secretion and DC-STAMP expression, subsequently exerting an indirect role of CCL2 on destructive pathology associated with arthritis (*Kim et al. 2005*). Differential effects ofCCL2 in mouse and human disease were reported,

where CCL2 leads to increased mononuclear fusion in humans and therefore osteoclastogenesis (likely due to increased RANKL; *Kim et al. 2005*), but in mice both stimulatory and inhibitory effects are known (*Quinones et al. 2006*).

1.3.3.2 CCL3

CCL3 is secreted from T cells, fibroblasts, B cells and macrophages and is known to induce the migration of osteoclast precursors (monocytes), neutrophils, T cells and macrophages to high density areas (*Wolpe et al. 1988, Trifilo et al. 2003, Narni-Mancinelli et al. 2007, Enzerink et al. 2009,Zucchetto et al. 2009, Takahashi et al. 2015*). CCL3 exerts its migratory effect after binding to its receptors CCR1 and CCR5. CCR1 is found on leukocytes (including monocytes) and is expressed on osteoclasts (*Yu et al. 2004*). In the process of osteoclastogenesis, CCR1 is thought to be the main receptor for CCL3 due to its elevated presence in destructive bone diseases. A lack of signalling through CCR5 has suggested this receptor as inconsequential in osteoclast formation (*Doodes et al. 2009, Lebre et al. 2011*). CCR5 is therefore suggested as being important to cell migration into arthritic joints, but then CCR1 becomes the dominant receptor for mononuclear cell retention and osteoclastic differentiation.

CCL3 is significantly increased in many destructive bone diseases including RA, OA, JIA and MM, where its concentration was significantly correlated to osteoclastogenesis (*Koch et al. 1994, Choi et al. 2001, Oba et al. 2005, Pharoah et al. 2006, Szekanecz et al. 2010, Vallet et al. 2011, Vangsness et al. 2011*). Although co-cultures have mainly been used, CCL3 was shown as pivotal to the process of osteoclastogenesis, where its inhibition has resulted in decreased osteoclast number. A clear role of this chemokine in osteoclast differentiation is therefore evident, but its mechanism is still elusive. Supporting a role of CCL3 in osteoclastogenesis is its stability at low pH (*Ren et al. 2010*), giving it a major advantage over other chemokines that get denatured in acidic environments; H^+ ions secreted from actively resorbing osteoclasts.

In addition, indirect effects of this chemokine are reported due to its ability of increasing the co-secretion of cytokines and chemokines into the inflammatory

milieu of the joint;IL-6, sIL-6R, CCL2 and CCL5 (*Chintalacharuvu et al. 2005, Koch 2005, Pharoah et al. 2006*).

1.3.3.3 CCL5

Sharing the same receptors as CCL3, CCL5isalso significantly elevated in destructive bone diseases (*Yano et al. 2005, Pharoah et al. 2006*).CCL5 induces monocyte motility in the presence of RANKL in addition to stimulating osteoclast migration across growth substrates (*Yu et al. 2004*). Although very few studies have investigated the effects of CCL5 on direct osteoclastogenesis, CCL5 has been found to enhance monocyte/macrophage migration (*Keophiphath et al. 2010*).The presence of lymphotoxin can lead to augmented CCL5 secretion, as can elevated Ca^{2+} (*Yano et al. 2005, McInnes and Schett. 2007* and *Calmon-Hamaty et al. 2011*). However, such increases in CCL5 could be due to an autocrine regulation loop, where CCL5 in turn prevents further osteoclastogenesis due to the blockade of CCR1 and CCR5 thus preventing CCL3 signalling. Further experiments in monocultures of osteoclast precursors are however needed to determine the role of this chemokine in osteoclastogenesis.

1.3.4 Conclusion on the effects of inflammatory mediators on osteoclastogenesis

The role of inflammatory mediators in osteoclastogenesis is vast, where many complex effects are exerted with causative links to the prevalence of destructive diseases (*Yu et al. 2004, Kokkonen et al. 2010*). Substantial gaps in our knowledge of the direct effects of these hormones, cytokines and mediators in direct osteoclast differentiation are however apparent due to the substantial use of co-culture methodologies.

1.4 The hypothesised role of the osteoclast in pain

A significant impact of the presence of pro-inflammatory mediators on osteoclastogenesis and the resultant pathology was introduced, but additionally a

modulatory role in hyperalgesia and nociception has been postulated. The evidence for this notion is derived from published literature which is summarised in the sections that follow.

1.4.1 Acid-Induced bone pain

Pain is a common symptom associated with destructive bone diseases and in the last 20 years has been linked to the osteoclast. In 2006 *Nagae et al.* published data stating that the inhibition of osteoclastogenesis (bisphosphonates, OPG, alendronate and zoledronic acid) led to a significant reduction in bone resorption and hyperalgesia, compared to controls; a link between the osteoclast and pain perception. Supporting their theory, an increase in mRNA for the acid-sensing ion channel (ASIC) in dorsal root ganglions provided a mechanism behind increased sensitivity under the acidic environment created by the actively resorbing osteoclast. The protection of joint architecture and decreased hyperalgesia was later reported by *Strassle et al. (2010)*. Further evidence was reported by *Abe et al. (2015)*through the analysis of c-fos and transient receptor potential channel vanilloid subfamily member 1 (TRPV1) expression in the dorsal horn of spinal cord ovariectomized (OVX) mice. Both c-fos and TRPV1 were significantly increased in OVX mice compared to matched controls, and this increase was susceptible to inhibition through alendronate treatment; thus linking hormones to pain.

1.4.2 Pro-inflammatory mediator induced pain

In addition, pro-inflammatory cytokines stimulating osteoclastogenesis are also hypothesised as having a role in pain. The secretion of pro-inflammatory cytokines leads to altered nociceptor function effecting pain perception (*Loeser and Melzack, 1999)*. One theory could be that the secretion of cytokines/pain mediators (IL-6, bradykinin, endothelin-1 and nerve growth factor; NGF, *Besson 1999*)could have come directly from the osteoclast simultaneously enhanced pain perception and osteoclastogenesis. However, the direct secretion of these mediators from the osteoclast has not yet been proven, but their nociceptive role is known (*Ren and Dubner 2010).*

1.4.2.1 TNF-α

The direct role of TNF-α in pain is still debated, but increased secretion from receptive cells is known to occur, which sequentially activates and prolongs hyperalgesia (*Richter et al. 2010*).

1.4.2.2 IL-6

IL-6 increases heat-induced and mechanical pain, which through its inhibition (IL-6 neutralising antibody) can be attenuated (*De Jongh et al. 2003)*. Although the mechanism behind this increase is currently unclear, it is thought that the increased expression of gp130 on peripheral nerves in the presence of IL-6 encourages neurite growth and survival (*De Jongh et al. 2002)*. In addition, IL-6 is also linked to the secretion of nerve growth factor (NGF) which is commonly released from injured tissues, thus increasing nociceptor sensitivity whilst preparing the body for injury response (*Anderson & Rao 2001*).

1.4.2.3 NGF

NGF is associated with neurite growth and survival. Previous publication has reported the enhanced secretion of NGF from T cells and mast cells in models of bone destruction, where enhanced pain perception was reported (*Lambiase et al. 1997*). The addition of NGF in animal models leads to heightened heat and mechanical sensitivity through increasing TRPV1 expression and bradykinin receptor binding. Although research into NGF and arthritis is limited, the peptide bradykinin is elevated in rheumatoid arthritis (RA) patients (*Hargreaves et al. 1988, Xie et al. 2014*). Additionally, in murine models a decrease in bradykinin receptor results in decreased arthritis severity. Thus a tentative link between NGF and bradykinin increases in arthritic patients could be postulated.

Our knowledge of the osteoclasts role in different types of pain linked to destructive bone diseases is therefore limited, where extensive further research is needed. However data combined from these studies could be collated with those investigating the destructive pathology caused by the osteoclast (both *in vitro* and *in vivo*; using imaging methodology discussed in the next section), to create an in-depth profile of pathogenicity associated with osteoclastogenesis.

1.5 Imaging destructive bone diseases

To establish the impact of the osteoclast on bone pathology, traditional *in vivo* techniques include ultrasound (US), radiography, computed tomography (CT) and magnetic resonance imaging (MRI), all of which provide an image of joint structure. US is based upon sound waves travelling through the body and being deflected back to the originating probe for detection once a tissue is reached that they cannot travel through. The length of time it takes for the signal to be received depends upon the tissue they reached *(Døhn et al. 2006)*. The advantages of US are that it has a good sensitivity for bone erosions and is relatively cheap; however, the joint imaged has to be easily accessible and this is sometimes problematic.

X-rays (traditional radiography composed of one ray, and CT scans composed of multiple rays), travel in one dimension and are passed through the area of interest before being detecting on the other side. Highly calcified bone absorbs the energy and soft tissue does not (although still visible but hard to distinguish; *Taouli et al. 2004*). In CT scans a computerised 3-D image is composed following cross-sectional analysis *(Dawson et al. 2001)*. This technique offers an advantage over US and x-ray as it reconstructs a 3D image where cross-sectional erosions can be viewed; however, soft tissue is again difficult to distinguish.

Thirdly, MRI utilises radio-waves of low-frequency to penetrate areas of interest and images are acquired from the time it takes for the reflected signal of magnetized spins from H^+ in the object to be detected, defining tissue location, structure and composition *(McQueen 2000).* Although this method yields the most integrated image of bone and soft tissue, it is not as sensitive as CT for calcified tissues, is prone to artefacts and is the most expensive imaging modality.

1.5.1 Imaging methods for the diagnosis of destructive bone diseases

The use of these above *in vivo* methods is highly important in diagnosing and monitoring physiological disease progression, in addition to furthering our knowledge of how these diseases affect the body. In RA patients, during the first two years of disease duration substantial erosions and joint space narrowing are

common pathologies seen (*Ved et al. 2002,Nogueira-Barbosa et al. 2010, Døhn et al. 2012)*. However, by the time these imaging methods highlight such erosions, they are well-established and substantial bone destruction has normally occurred. The need for an early imaging system of disease progression is pivotal to diagnose and hinder osteoclast-associated disease progression.

1.5.2 Possible imaging methods for the early identification of destructive bone disease

For many years osteoclastogenesis and resorption research was carried out utilising many two dimensional (2D) *in vitro* methodologies; *e.g.* counting osteoclast numbers or area of resorption. Imaging methods used for histological quantification of area resorbed commonly include light microscopy, scanning electron microscopy (SEM) and transmission electron microscopy (TEM). Light microscopy is the most common, in which visible light is reflected of the surface of the substrate and magnification lenses facilitate its visualisation. SEM directs a focussed beam of electrons onto the sample which interact and release signals back to the detector regarding surface topography (*Sreeja et al. 2009)*. Methods similar to SEM have also been used by *Sasaki, Debari and Hasemi (1993)* who studied Howship's resorption lacunae through back-scattered electron microscopy (signals reflect off samples and travel back to detector at their source) and scanning probe microscopy (probes scan the surface of a sample and relay information back to a computer). Thirdly, TEM uses electrons which travel through the sample and are detected on the opposite side, thus yielding data regarding internal structures.

Although 2D imaging methods described previously were essential in assessing cell counts and resorption areas, their significant disadvantage is that they cannot quantify 3D processes; *i.e.* two resorption pits may have identical surface areas but their depths and volumes may be significantly different. *In vivo* imaging methods including CT and MRI would therefore be preferable as they facilitate 3D visualisation and subsequent quantification. 3D imaging methods are generally of higher resolution with increased sensitivity, but also have their disadvantages: they're costly, need trained personnel and are challenging in method set up. The benefits of using 3D imaging methods over 2D do outweigh these however, and are

essential when planning experiments to further our knowledge in both osteoclastogenesis and bone resorption; sequentially relating this back to destructive bone diseases.

The use of 3D imaging to quantify osteoclast phenotype has in the last 5 years been reported, although many improvements are still needed. Confocal laser scanning microscopy (CLSM/confocal microscopy) was utilised within *in vitro* studies where it utilises point illumination with a pin-hole to eliminate out-of-focus light, resulting in a high-resolution image with x, y and z dimensions. Using this technique, living or fixed cells can be imaged and identified based on their subcellular structure and 3D parameters can be quantified *i.e.* resorption pits (*Coxon 2012, Goldberg et al. 2012, Mediero et al. 2014*). *Grevers et al. (2011)* used confocal microscopy to highlight the F-actin structural rings in osteoclasts stimulated with S100A8 (RA alarmin responsible for enhanced inflammatory response) which were significantly elevated to those from control cultures. Three years later, *Mediero et al. (2014)* showed intrinsic differences between pre-osteoclasts, differentiating osteoclasts, and mature osteoclasts by nuclei number and F-actin conformation. Furthermore, *Nevius et al. (2015)*used two-photon microscopy to show the effects of EBI2 (a G protein coupled receptor involved in monocyte migration) on osteoclastic movement and giant nucleated cell differentiation. From all of these studies the use of 3D imaging has therefore been proven effective and a useful tool for cell identification and furthering osteoclast knowledge.

In tandem, several researchers investigated the use of CSLM for the quantification of resorption. The first studies investigating the 3D characteristics of resorption pits were reported in the 1990s, where *Jones, Arora & Boyde (1995)* used a 'video-rate, line confocal reflection light microscope' to identify bone mineral density as the rate-determining step in osteoclast resorption and pit volume. In 1999 *James et al* commented on the advantages of using confocal microscopy for data relating to resorption pit number, area and volume. It was concluded that all three parameters are necessary to fully understand the resorptive behaviour of the osteoclast as pit area may be comparable between two pits but their volume may alter significantly (*James et al. 1999)*.

This variation in pit volume was later found to correlate with soluble markers of bone resorption (CTX and NTX). Following this, 13 years passed before a second study investigating pit depth was published. In 2012 *Goldberg et al.* used confocal microscopy paired with Sirius red staining (identifying resorptive edge) to show the role of Rac1 and Rac2 in osteoclast-mediated bone resorption. In $Rac1^{-/-}$cultures resorption pits had a reduced volume and area compared to wild-type cultures, but in $Rac2^{-/-}$ cultures although a reduction in resorption volume was found, pit area was unchanged. However, *Goldberg et al. (2012)* did not further define why this change occurred (*i.e.* probable change in pit depth or anomaly) and therefore the osteoclasts true resorptive capability remained unanswered.

Simultaneously, *Jeon et al. (2012)* also published a confocal microscopy methodology with the aim of producing 3D representations of resorption pits. *Jeon et al. (2012)*reported that multiple pits of relatively small surface area and depth were present at the start of osteoclast differentiation, but that after 14 days of culture pit area increased, and by day 21 pit depth also increased. Therefore pit area was apparently linked to osteoclast size, and pit depth to osteoclast resorptive potential (z dimension).

An alternative method for determining pit characteristics, Super Depth Surface Profile Measurement Microscope (SDSPMM), was also reported by *Soysa et al. (2009)* after the limitations of 2D imaging where reported. In SDSPMM a 3D image was obtained from which pit depth and volume could be calculated, from using data obtained from the z-dimension. *Soysa et al. (2009)* concluded that osteoclasts cultured under stimulatory cytokine conditions yielded enhanced volumes and depths of resorption pits compared to un-stimulated cultures; supporting confocal data obtained by *James et al. 1999* and *Goldberg et al. 2012*. Taken together, all of these studies provide substantial support for the use of 3D imaging techniques in clarifying the role of the osteoclast *in vitro*. Such methodologies are therefore imperative to further our knowledge of the differentiating osteoclast and its resorptive capabilities in both health and disease.

1.6 Destructive Bone Diseases

Through the utilisation of imaging methods described previously, and the combination of biological tests, many destructive bone diseases of the joint can now be identified in clinic. These diseases result due to an unbalanced increase in bone resorption versus osteoid formation, which leads to a multitude of pathological events associated with the bone and overall joint health. The identification, classification and diagnosis of destructive bone diseases was well documented over the past decades (Table 1.1) and the pathological presentation commonly includes inflammation of soft tissues lining the joint, cartilage destruction, osteopenia and periosteal reaction, narrowing of joint spaces, fusion of joints and bone erosions (as shown in Figure 1.3).

Table 1. 1 - A descriptive table of destructive bone diseases in order of UK prevalence.

Destructive Bone Disease	Description
Periodontal disease	A disease caused by excessive and highly pressurised oral activity which enhances osteoclastic resorption of alveolar bone. Resulting inflammation may ensue with further trauma and possible infection (*Repeke et al. 2010*).
Osteoarthritis (OA)	A degenerative disease of joints with gradual destruction of cartilage exposing underlying bone surfaces heightening bone resorption leading to pain on movement. (*Hayami et al. 2004)*.
Osteoporosis	A disease of low bone mass (often diagnosed after a fracture) thought to occur due to uncontrolled resorption and insufficient new bone formation. Common in post-menopausal women due to the link between oestrogen and osteoclast differentiation and resorption (*Raisz 2005*).
Rheumatoid arthritis (RA)	A chronic systemic inflammatory disease primarily of the extremities presenting with inflamed & tender joints and bone destruction visible from radiological assessment. Affects 1% of the male population and 3% of the female population. Prevalence >55 years old. Autoimmunity is thought to play a major role (*Ichikawa et al. 2016*, *Toma et al. 2007*).
Osteitis fibrosa cystica	Destruction of the skeleton due to enhanced osteoclastogenesis results from hyperparathyroidism thus predisposing the patient to fractures. Brown tumours are commonly found on bone structures as they are resorbed (*Maina & Kraus 2012*).
Paget's disease	A disease associated with pathological osteoclast and osteoblast activity. Enhanced osteoclast differentiation leads to substantially increased osteoclast size and resorption. To compensate, osteoblasts rapidly lay down new bone matrix which is inadequately organized with poor structure, leading to enlarged and misshapen bones (*Doyle, Banks& Pennock1980)*.
Multiple myeloma	Multiple myeloma is a hematologic malignancy coupled to significantly enhanced osteoclast resorption and bone destruction. Pathogenic mechanisms behind enhanced destruction are currently thought to be due to excessive secretion of osteoclast stimulating and osteoblast inhibiting factors from tumours (*Pearse et al. 2001*).

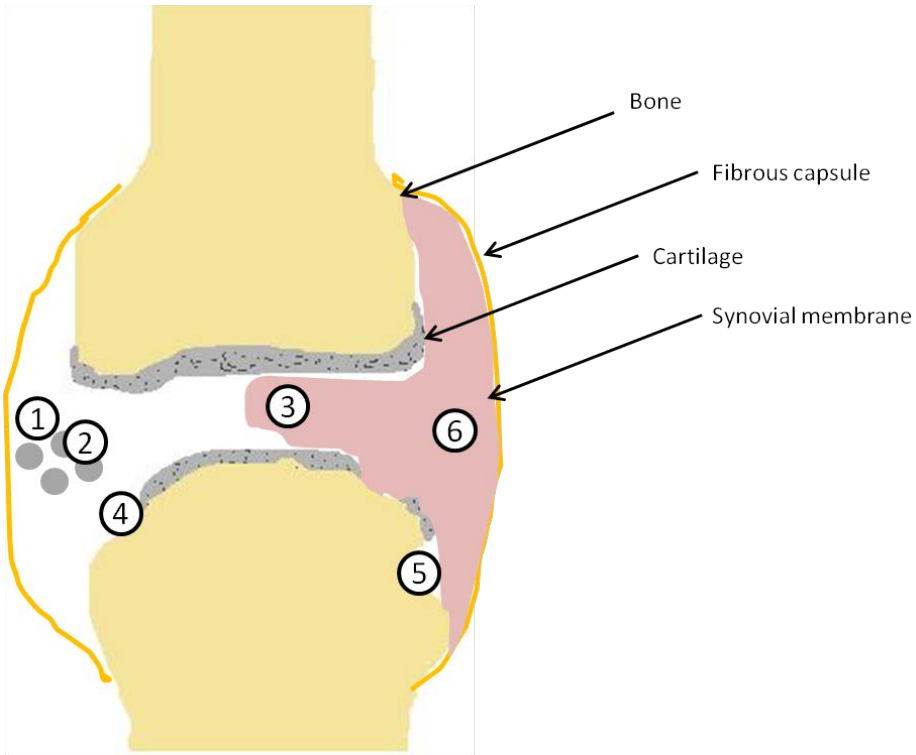

1 **Inflammatory cell infiltrate (monocytes/macrophages/T cells/B cells)**
2 **Increased pro-inflammatory cytokines**
3 **Hyperplasia**
4 **Cartilage destruction**
5 **Bone destruction**
6 **Pannus formation**

Figure 1. 3 - An illustration of the joint pathology associated with the arthritides.In arthritic joints 6 aspects of pathology are commonly seen. Inflammatory cells (monocytes/macrophages/T cells/B cells) infiltrate into the joint due to elevated pro-inflammatory cytokines and chemokines (IL-6 and CCL3). Such elevated levels of inflammatory mediators results in both hyperplasia and pannus formation in the joint. Additionally, cartilage is slowly degraded by enzymes, revealing unprotected bone underneath which is subject to destruction.

The inflammatory phenotype of a joint is common between destructive bone diseases. The influx of inflammatory cells (monocytes/macrophages/B cells/T cells) into the synovial capsule precedes the localised secretion of several pro-inflammatory cytokines (TNF-α, IL-6, IL-1 and IL-8; *Schett 2007*). These pro-inflammatory cytokines lead to several effects; enhanced fibroblastic proliferation, concurrent hyperplasia, co-secretion of inflammatory cytokines, enhanced cartilage damage and bone destruction. In tandem, infiltrating inflammatory cells secrete

matrix metalloproteases (MMPs) which degrade cartilage and reveals underlying bone, enabling further bone resorption (*Danks et al. 2002, Hirayama et al. 2002, Schett, 2007*). The invasion of the whole joint thus progresses, often resulting in pannus formation (Figure 1.3), and periosteal reaction (uncontrolled bone proliferation in psoriatic and reactive arthritis), further enhancing the pathogenesis of the disease (*Schett 2007*, *Rana et al. 2009*).

Additional to the inflammatory changes, four common structural joint changes also occur. Joint space narrowing, joint fusion (especially in spondyloarthritides patients where sacroiliac joints are remodelled), excessive bone formation resulting in osteophytes (thought to result from a lack of Dickkopf-1; Wnt inhibitor), and joint destruction (*Uderhardt et al. 2010, Ichikawa et al. 2016*). Although several reasons exists for increased bone resorption (*i.e.* decreased osteoblast activity), in this thesis the main focus is upon the uncoupling due to inflammatory cytokines and chemokines which facilitate bone destruction as already discussed (*Heymann et al. 1998, Uderhardt et al. 2009, Kitaura et al. 2014*). As the osteoclast is the only cell capable of bone destruction, it is of paramount importance. Understanding the role of the osteoclast in destructive bone diseases is therefore essential to fully explore the complex relationship between pain, inflammation and pathology in arthritis.

1.7 *In vivo* models of arthritis

To further our understanding as to how osteoclasts mediate a role in the inflammation, pathology and pain associated with destructive bone diseases, *in vivo* models of arthritis are needed. The use of these models is pivotal in providing the most up-to-date translational research for both disease pathogenesis and novel treatment strategies (*Bendele 2001*).Many murine models for the arthritides are available and include the following; adjuvant induced arthritis, antigen induced arthritis, streptococcal cell wall arthritis, immune complex induced arthritis, surgically induced osteoarthritis and collagen induced arthritis(*Brackertz, Mitchell& Mackay1977, Cromartie et al. 1977, Trentham et al. 1978, Holmdahl et al. 1992,*

Van Lent et al. 1995, Bendele et al. 1999, Finnegan et al. 1999, Nandakumar et al. 2003, Dinser 2008, van der Berg 2009).

Adjuvant arthritis is the original model of arthritis commonly used to establish the effects of novel drugs. This model is induced by injection of complete Freund's adjuvant into the joint resulting in the presentation of a polyarticular disease after 1-2 weeks, where inflammation and bone destruction present (*Bendele et al. 1999*).Acute arthritis results when using this model as clinical symptoms last less than a month, presenting a major disadvantage for the relevance to human disease. A second model, antigen-induced arthritis, was developed over 40 years ago by *Dumonde & Glynn*(*1961)* and differs from adjuvant arthritis by the injection of a known antigen (fibrin or methylated bovine serum albumin) into the joint, which contains the arthritis to the injected joint (*van den Berg et al. 2007*). Histological, inflammation, bone and cartilage destruction are presented, likening it human RA (*van den Berg et al. 2007*). However due to the lack of penetrance its use to study human RA is questionable.

A third model known as streptococcal cell wall induced arthritis can be induced through the injection of cell wall components from streptococcal cultures into the joint space. The resulting disease presents as a chronic polyarthritis with erosive phenotype, although a secondary 'reactivation' phase may be necessary; limiting its translation to human disease (*Schimmer et al. 1998*). Alternatively, inflammatory arthritis could be induced through injection of anti-bovine serum albumin IgG antibodies followed by BSA, thus evoking an immune-complex. This type of inflammatory arthritis results in enhanced infiltration of polymorphonuclear cells and joint pathology (*Rocha, Andrade & Jancar 1996*).

Alternatively, a model of non-inflammatory arthritis could be used, known as surgically induced arthritis. This model is commonly used to study human arthritides such as OA. The model is induced through surgical trauma to the joint, mimicking that which would occur in the human disease. In contrast to the human disease however, arthritis develops quickly, but this is advantageous for therapy testing (*Bendele et al. 1999*).

Lastly, the most utilised animal model for arthritis is collagen-induced arthritis (CIA) which was first reported by *Trentham et al.* (*1978*). CIA presents with systemic immune system involvement and is a poly-articular erosive disease like human RA. Characteristic histology findings of synovial joints include; enhanced leukocyte infiltration, synovial hyperplasia, inflammatory pannus formation, cartilage destruction and bone erosions (*Song et al. 2015*). Commonly, male DBA/1 mice are used to study CIA due to an average of 90% showing full disease penetrance, and successful presentation (*Dinser 2008*). The high penetrance of this disease is a major advantage making this an ideal model for RA and potential therapeutics; increases reportable data, and decreases the need for high sample numbers and cost (*Kannan et al. 2005*). In addition, it was reported that the same pro-inflammatory cytokines are involved in both the pathogenesis of CIA and RA, including IL-1, IL-6, and TNF-α, where the development of pharmacological RA treatments have arisen from CIA animal studies (*Goldring et al. 2000* &*Kannan et al. 2005*). Furthermore, auto-antibodies to type II collagen are also found in murine samples, presenting with similar immune involvement as human RA.

Although the above models have all been used with varying degrees of success for the presentation, evaluation and treatment of human arthritis, the CIA model is the most commonly used due to its similarity in disease presentation to human RA. However, CIA only ensues after induction and therefore is not a natural progression as RA is. Additionally, CIA shows greater penetrance in male mice, compared to RA showing increased penetrance in females. Although the reason behind this is still unknown, the difference is thought to be due to the involvement of the sex hormone testosterone, but this does raise an interesting question of sex bias. Despite this, procedural induction is relatively easy, produces high incidence and penetrance, and can be used to develop pharmacological target therapies (*Bendele 2001*). Reproducible results are generally collated through this model, although intra-experiment differences do arise. However, in human RA no two patient cases are the same, thus this model also provides insight into patient individuality (*Kannan et al. 2005*).

1.7.1 Collagen-induced arthritis (CIA)

The basis for CIA use was first proposed in 1978 by *Trentham et al.* where the self-recognition of type II collagen by auto-antibodies was described in joints after the induction of CIA (emulsion of complete Freund's adjuvant (CFA) and type II collagen). The importance of many cytokines, chemokines and growth factors in the arthritides and their therapeutic potential was illustrated and reported through the use of CIA over the past 40 years. For example, *Lubberts et al. (2004)* defined the role of the novel cytokine IL-17 in osteoclast-mediated pathology. In their study, the treatment of mice at first presentation of CIA with anti-IL-17 significantly decreased bone and cartilage degradation in hind limbs, coinciding with reduced inflammation; later reported to be due to significantly decreased systemic IL-6. Additionally, treating well-established CIA mice with anti-IL-17 (a later time-point) also yielded promising results in deliberating the progression of joint pathology (*Lubberts et al. 2004*). The above reported use of CIA therefore highlights the utility of such an *in vivo* model in distinguishing the role of inflammatory mediators previously shown to exert a significant role on osteoclastogenesis *in vitro,* and to then postulate potential novel pharmacological targets in destructive bone diseases.

1.7.2 Therapeutic drug development

The importance of the above models was pivotal in the development of novel therapeutics targeting inflammatory arthritis and destructive bone diseases. Although past the scope of this project, it is important to appreciate the translational impact of potential therapies from *in vitro* to *in vivo*. Several therapeutic drugs (biologic DMARDs) are currently available and used in the treatment of inflammatory arthritis and some of these are highlighted in Table 1.2. From the collated data it is evident that further research into pharmaceutical agents which will inhibit, block or reduce the formation or resorptive activity of the osteoclast is going to be crucial for developing treatments against destructive bone diseases, where pathogenic inflammatory components are already reduced.

Table 1. 2 - An overview of currently available biologics.

Drug	Mechanism of action	Tested in
Etanercept	A TNFR fusion protein that binds to TNF-α and blocks its binding to membrane bound TNFR, thus inhibiting TNF activity (*Anandarajah et al. 2008*)	RA, JIA, psoriatic arthritis and ankylosing spondylitis
Adalimumab	A monoclonal antibody that binds to TNF-α and prevents its signalling through membrane bound TNFR (*Kempeni 1999*)	RA, psoriatic arthritis, ankylosing spondylitis and Crohn's disease
Infliximab	A monoclonal antibody which binds to TNF-α and again prevents its binding to membrane TNFR (*Gengenbacher et al. 2007*)	RA, psoriatic arthritis, ulcerative colitis Behçet's disease and Crohn's disease
Anakinra	This receptor antagonist competitively inhibits IL-1R preventing IL-1 from binding to its receptor (*Fleischmann et al. 2006*)	RA and some inflammatory skin diseases
Tocilizumab	A monoclonal antibody which binds membrane bound and soluble forms of IL-6R, thus blocking IL-6 binding and cell signalling (*Genovese et al. 2008*)	RA, JIA, MM, Castleman's disease
Denosumab	Inhibits RANKL by acting as its decoy receptor (modelled on OPG), thus reduces osteoclast formation and bone resorption, leading to increase bone mineral density (*Andrews 2008 , Baron et al. 2011, Sims and Romas 2015*)	Osteoporosis, bone metastases, post-menopausal women

1.8 Project Summary

In destructive bone diseases many pro-inflammatory cytokines and chemokines are known to be involved in the enhanced erosive phenotype presented. However, the direct role of these mediators on the differentiation of $CD14^{+ve}$ mononuclear cells into osteoclasts and their corresponding resorptive activity was still unknown. Monocultures were therefore preferred over co-culture methodologies to gain a greater understanding. No current methodology existed for the automated counting of adhered cells, which presented itself as an issue when previously trying to count extensive numbers of osteoclasts due to their highly adherent phenotype. In addition to this, the quantification of resorptive activity is traditionally performed using 2D imaging modalities, but research publications have described the limitations and short-falls of these methods in masking the complete resorptive phenotype of the osteoclast. For this reason, novel methodologies for both counting adherent cells (osteoclasts) and for the quantification of resorptive activity through 3D imaging will both be reported in this thesis. Following this, an assessment of specific pro-inflammatory mediators highlighted from Chapter 3 was completed to determine their role on direct osteoclastogenesis and bone destruction using these novel methodologies, and the targeting of each as a therapeutic will be assessed.

1.8.1 Project Aim and Hypothesis

The overall aim of this thesis was to establish the role of pro-inflammatory mediators in the direct differentiation of human osteoclasts and their resorptive activity using novel imaging methodologies which will determine their impact on associated pain and pathology related to arthritis. Data reported from this thesis would subsequently lead us to accept or reject our hypothesis that IL-6, TNF-α, CCL2, CCL3 and CCL5 significantly increase the differentiation of the osteoclast and its resorptive potential heightening bone destruction. This hypothesis was addressed in the proceeding chapters through the following aims;

- Aim 1- to establish a reproducible monoculture method for human osteoclasts *in vitro* and to create a novel, high-throughput, automated computer algorithm for adherent total cell counts.
- Aim 2- to define the direct role of IL-6 trans-signalling in osteoclast differentiation stimulated by m-CSF and RANKL through the use of sgp130-Fc.
- Aim 3- to decipher the role CCL3 plays in the differentiation and functional resorptive activity of the osteoclast *in vitro*.

Chapter 2:Materials and Methods

2.1 Materials

All chemicals were purchased from Sigma-Aldrich (unless stated otherwise). Solvents were supplied by Fisher Scientific (unless stated otherwise). A Millipore Milli-Q system produced dH_2O that was used to prepare buffers, reagents and stains. Phosphate Buffered Saline (PBS) pH7.2 was supplied by Life Technologies Ltd. All plastic-ware, sterile tissue culture plates and ELISA plates were obtained from Greiner Bio-One Ltd. Antibodies (Anti-human CD14-FITC and Isotype Control FITC) used for flow cytometry were purchased from eBiosciences.

2.1.1 Human osteoclast assay culture media

Reagent were supplied by Life Technologies unless specified otherwise.

A *basic medium* containing Roswell Park Memorial Institute medium 1640 (RPMI-1640) was supplemented with 10% heat-inactivated foetal calf serum (FCS, Biosera), 20mM L-glutamine, and penicillin (50 units/mL)/Streptomycin (50µg/mL).

Human proliferation medium was prepared by adding 5ng/mL or 10ng/ml m-CSF (R&D systems) into basic medium.

Human osteoclast differentiation medium was prepared from *basic medium* supplemented with 5ng/mL m-CSF, 5ng/mL RANKL and 2.5µg/mL polyHistidine (all from R&D systems).

2.1.2 Treatment of *in vitro* human osteoclast differentiation cultures with either sgp130-Fc, HYPER-IL-6 or sgp130-Fc and HYPER-IL-6

Human osteoclast differentiation medium from Section 2.1.1 was supplemented with soluble gp130-Fc (sgp130-Fc) at 500ng/mL and/or a fusion protein of IL-6 linked to sIL-6R (HYPER-IL-6), both generous donations from Professor Rose-John, University of Kiel) over a concentration range of 0.5-10ng/mL.

2.1.3 Treatment of *in vitro* human osteoclast differentiation cultures with anti-CCL3

Human osteoclast differentiation medium from Section 2.1.1 was supplemented with human anti-CCL3 antibody reconstituted with sterile PBS over a range of 0-8ng/mL (MAB270; mouse IgG1 source, R&D systems). As a control, *human osteoclast differentiation medium* was supplemented with mouse IgG1 isotype at the same concentrations as anti-CCL3 in assays (MAB002, R&D systems). *Human osteoclast differentiation medium* was also supplemented with recombinant human OPG reconstituted with sterile PBS containing 0.1% BSA at 8ng/mL and 100ng/mL (185-OS, R&D systems).

2.1.4 Buffers, staining solutions and mountants

The solutions used for this project are listed Table 2.1.

Table 2. 1 - Buffers, staining solutions and mountants.

• **Tissue culture 70% alcohol spray**
350mL methanol was diluted with 150mL dH_2O.
• **MACS CD14^{+ve}cell fraction isolation**
MACS buffer – 58mg EDTA and 500mg bovine serum albumin (BSA) were dissolved in 100mL PBS prior to sterile filtration.
• **Flow Cytometry Reagents**
Flow cytometry buffer – 150µL FCS was diluted in 15mL PBS. *4% Formaldehyde* – 10.8mL formaldehyde (37%) in 89.2mL PBS.
• **Cellular fixation**
Glutaraldehyde solution (10%) – 400µL glutaraldehyde stock diluted with 600µL dH_2O.
• **TRAP staining of ivory disks**
Sodium acetate solution 0.2M – 0.164g sodium acetate dissolved in 10mL dH_2O. *Acetic acid solution 0.2M* – 115µL acetic acid diluted in 10mL dH_2O. *Sodium tartrate solution 0.35M* – 0.69g sodium tartrate was dissolved in 10mL dH_2O. *Naphthol AS-MX phosphate disodium salt solution* – 3mg naphthol AS-MX phosphate disodium salt was dissolved in 300µL dH_2O. *Acetate buffer 0.1M* – 3.52mL sodium acetate solution (0.2M) and 1.48mL acetic acid solution (0.2M) were added into 5mL dH_2O. *TRAP buffer* – 1mL sodium tartrate solution* (0.3M), 100µL naphthol AS-MX phosphate disodium salt solution and 10µL Triton X-100 were added to 5mL acetate buffer (0.1M). 3.89mL dH_2O was then added into the solution. *TRAP staining solution* – 3mg Fast red violet LB salt was dissolved in the TRAP buffer. *resulting in a final 30mM tartrate solution eliminating phosphatase sensitive to tartrate (*Li et al. 1970*).
• **Haematoxylin Stain**
Equal quantities of Harris' Haematoxylin Stain and dH_2O were mixed together.

• **Resorption Pit Staining**
Bleaching solution (1%) – 333µL hydrogen peroxide (30%) was diluted in 10mL dH_2O. *Toluidine blue stain (0.5%)* – 0.25g toluidine blue stain was dissolved in 50mL dH_2O. *Calcein staining solution* – 5mg calcein was dissolved in 10mL dH_2O.
• **Confocal microscopy disk mountant**
Harvested disks were mounted using CyGEL (a liquid between 2-6^oC, a solid at ≥6^oC).
• **ELISA Reagents**
Wash buffer (0.05% PBS-T) – 10 PBS tablets dissolved in 2L of dH_2O, containing 1mL of Tween-20. *Blocking buffer* – 1g BSA dissolved in 100mL PBS. *Citrate buffer pH 3.95* – 4.2g citric acid (0.2M) dissolved in 100mL dH_2O (pH adjusted using sodium hydroxide solution). *Sodium hydroxide solution* – 2mg NaOH in 50mL dH_2O. *Tetramethylbenzidine (TMB)* – 240mg (TMB) was dissolved in a solution containing 5mL dimethyl sulphoxide (DMSO) and 5mL of absolute ethanol. *Development buffer* – 10µL hydrogen peroxide (30%) and 100µL TMB were dispersed in 10.5mL citrate buffer. *Stop solution (12% sulphuric acid)* – 60mL of 99.99% sulphuric acid in 440mL of dH_2O.
• **Preparation of Complete Freund's Adjuvant (CFA; an immuostimulator**)
100mg Tuberculosis (TB) was ground up into a fine powder. Small amounts of incomplete Freund's adjuvant (IFA) were added to create a suspension of TB, 20mL of IFA in total. Once at 5mg/mL the solution was aliquoted into 2.5mL vials and frozen (-80^oC)
• **Preparation of collagen solution**
5mg of collagen from chicken sternal cartilage (C9301) was dissolved in 2.5mL 10mM acetic acid and placed at 4^oC mixing overnight
• **Preparation of CFA + collagen (stimulates immune response to collagen)**
2.5mL CFA and 2.5mL collagen solution was mixed for 5 minutes until a thick emulsion which floated on water formed
• **Fixation of joints using 10% neutral buffered formalin solution**
10% neutral buffered formalin solution (200mL) was used to submerge joints
• **Storage buffer for murine joints – 70% alcohol**
700mL methanol was diluted with 300mL dH_2O
• **EDTA decalcification solution (demineralisation of bone to allow for wax histology)**
5 PBS tablets were dissolved in 1L of dH_2O 70g EDTA was then added and the pH was adjusted to 7.1 using sodium hydroxide
• **Rehydration solutions (essential for staining as hydrophobic after embedding)**
Xylene (100%) – 500mL 90% alcohol – 450mL industrial methylated spirit (IMS) diluted with 50mL dH_2O 100% alcohol – 500mL IMS
• **Dehydration solutions (minimizes cell damage and maintains sample integrity)**
100% alcohol – 500mL IMS 90% alcohol – 450mL IMS diluted with 50mL dH_2O Xylene (100%) – 500mL
• **TRAP preparation buffer for histological sections (shoulders/knees/ankles**)
0.82g of sodium acetate and 0.58g of tartaric acid dissolved in 50mL dH_2O
• **TRAP stain for histological sections (shoulders/knees/ankles)**
0.5mg/mL naphtol AS-MX phosphate and 1.1mg/mL fast red TR salt dissolved in 50mL preparation buffer
• **Haematoxylin stain**

Undiluted Harris' Haematoxylin (50mL)
• **Scott's tap water (blueing reagent for staining)**
1 part Scott's tap water concentrate was dissolved in 9 parts of dH_2O and stored for a month or until discolouration

2.1.5 Murine CIA model

Male DBA/1 mice (n=12) were obtained from Charles River and divided into two treatment groups. 6 mice received an antibody against mouse CCL3 which was reconstituted in sterile PBS (MAB450; monoclonal rat IgG source, R&D systems), and the remaining 6 received a monoclonal rat IgG isotype antibody reconstituted in sterile PBS (MAB006, R&D systems). Delivery of both was by 100µL intraperitoneal injection (i.p.) at 5mg/kg.

2.1.6 Hardware and Software

Hardware and software used in this thesis are listed in Table 2.2.

Table 2. 2 - Hardware and software used to observe, measure and quantify cells and or cell activity.

Equipment/Software	Supplier	Purpose
BD Accuri C6 flow cytometer	BD Biosciences	Flow cytometry
BD CFlow Plus software	BD Biosciences	Flow cytometry analysis
Olympus BX41 Microscope	Olympus	Visualisation of cells
Olympus Camedia C-3030 Digital Camera	Olympus	Image acquisition
Canon EOS 100D Digital Camera	Canon	Image acquisition
Matrix Laboratory (MATLAB)	Mathworks	Image analysis for cell number and characteristics
Corel Paint Shop Pro X5	Corel UK Ltd.	Image analysis for cell number and characteristics
Image J. Ink	National Institute of Health (NIH)	Resorption pit analysis for cell activity
LaserSharp	Bio-Rad	Confocal image acquisition
MetaMorph	BioImaging Solutions Inc.	Confocal image analysis for 2D and 3D characterisation of resorption pits
Omega Control/ Omega Data Analysis	BMG LabTech	ELISA plate reader to measure presence of soluble mediators for pain, inflammation and pathology
GraphPad Prism 4	GraphPad Software Inc.	Data analysis and presentation
Microsoft Office 2013	Microsoft	Data analysis and presentation

2.2 Methods

A comprehensive account of the methods used to culture, count and characterise human osteoclast differentiation assays are detailed in this section. For a more comprehensive list of methods used for osteoclast culture, resorption pit quantification, erosive pathology imaging, and *in vivo* techniques, the following reference can be used; *Bone Research Protocols* (specifically Chapters 11, 24, 25, 26, 27, 29, 33 and 38).

2.2.1 The acquisition and isolation of $CD14^{+ve}$ cells from peripheral blood of healthy human volunteers

Consent from healthy human volunteers was taken under a project reviewed by the Research Ethics Committee for Wales (Reference No 12/WA/0045), for the acquisition of venous peripheral blood. From each donor enrolled into the study, 40mL whole blood was collected and immediately placed into a falcon tube containing heparin, preventing coagulation. Blood (10mL) was then layered onto 5mL histopaque-1077 (Sigma-Aldrich) and centrifuged at 400g for 30 minutes leading to the separation of blood components due to differing cell densities. Plasma was removed from all tubes allowing the interface layer of peripheral blood mononuclear cells (PBMCs) to be collected and transferred into separate sterile falcon tubes containing 10mL Hanks Buffered Saline Solution (HBSS) (Life Technologies), and were then centrifuged for 10 minutes at 300g. Post-centrifugation, the HBSS was removed from all tubes and 10mL of fresh HBSS was added to each tube and the pellet of PBMCs was re-suspended. The cells were washed three times in HBSS before being re-suspended in 5mL human basic medium and placed on ice. A sample of the PBMC population was diluted 1:10 with human basic medium and a cell count was performed using a haemocytometer (Section 2.2.2). After this initial cell count 2 x 10^5 cells were removed and placed on ice ready for further preparation and analysis using flow cytometry (Section 2.2.3).

The PBMC suspension was centrifuged for a further 10 minutes at 300g and all medium was carefully removed from the tube. The pellet was then re-suspended in a solution of anti-human CD14 MACS microbeads (20µL per 10^7 cells) and MACS

buffer (80µL per 10^7 cells), which was then incubated on ice for 15 minutes. Following this the cell suspension was put through a pre-separation filter (pre-rinsed with 500µL MACS buffer) over the MS column. $CD14^{-ve}$ cells were collected in a waste falcon tube and disposed of, and $CD14^{+ve}$ cells were maintained within the magnetic column. The column was washed through three times using 500µL MACS buffer prior to the removal of the column from its magnet to a new, sterile falcon tube. The $CD14^{+ve}$ cells were flushed out of the column into the sterile tube using 1mL MACS buffer and 1mL human basic medium. A second cell count with a 1 in 5 dilution was performed on the $CD14^{+ve}$ cell population (Section 2.2.2). After this second cell count, 2 x 10^5 cells were removed and placed on ice ready for further preparation and analysis using flow cytometry (Section 2.2.3). Finally, cells were spun at 300g for 10 minutes prior to be re-suspended in human basic medium to a concentration of 3.2 x 10^6 cells/mL. This cell suspension was then used to seed the ivory disks used in the human osteoclast assay (Figure 2.1, Section 2.2.4).

2.2.2 Manual cell counting using a haemocytometer

Cell counts during the human $CD14^{+ve}$ cell isolation stages were performed using a haemocytometer. The cell suspension was diluted either 1 in 5, or 1 in 10 using human basic medium and then applied to a haemocytometer. Cells within the four corner sections of the haemocytometer were counted and total number of cells/mL were calculated using the formula in Figure 2.2.

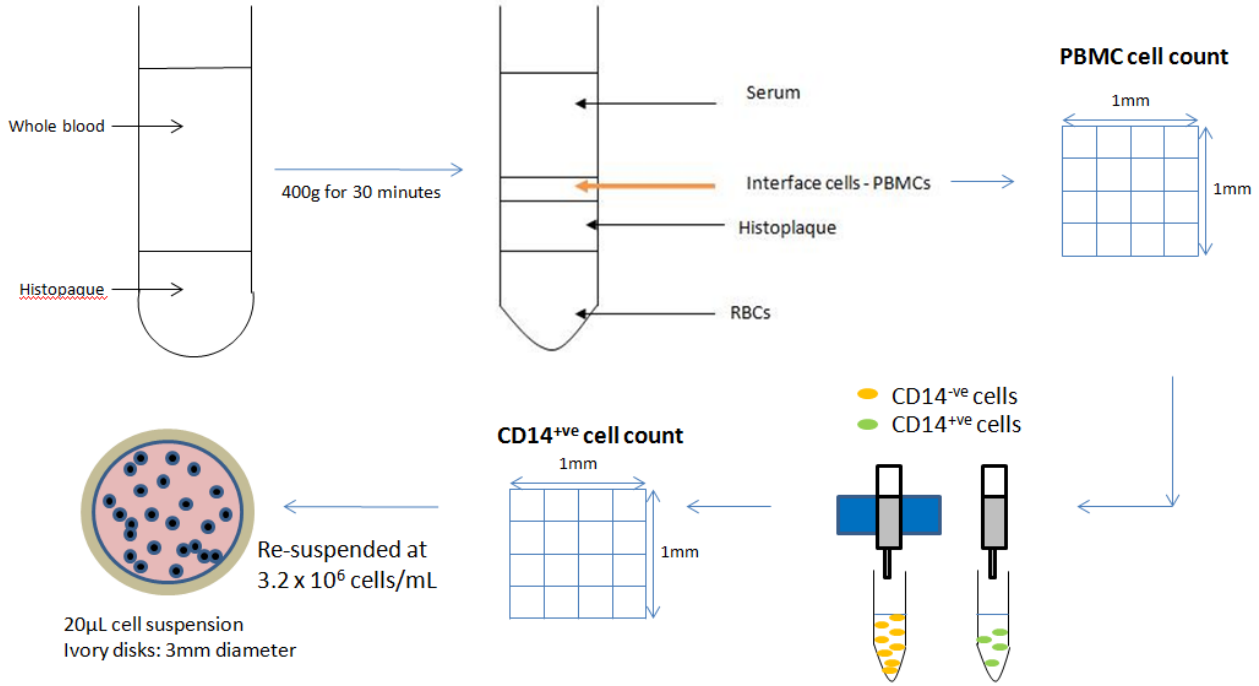

Figure 2. 1 - The acquisition and isolation of CD14^{+ve} mononuclear cells from human whole blood. Whole blood (10mL) was layered on top of histopaque (5mL) and spun at 400g for 30 minutes. PBMCs were isolated and transferred into a sterile tube prior to washing 3x in HBSS (10mL). Cell counts were carried out to calculate MACS buffer and bead volumes for CD14^{+ve} mononuclear cell isolation. After magnetic separation, these cells were counted, and seeded on ivory disks at 3.2 x 10^6 cells/mL.

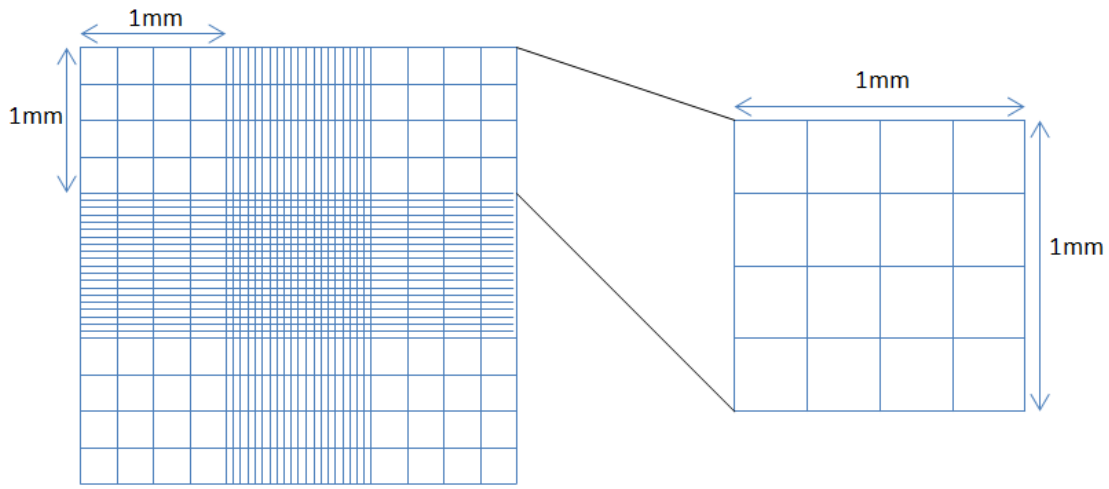

$$Total\ number\ of\ cells\ per\ mL = \ average\ of\ the\ 4\ quadrants\ x\ dilution\ factor\ x\ 10^4$$

Figure 2. 2 - Example view of a haemocytometer.Cell counts were obtained from the top left, top right, bottom left and bottom right quadrants (1mm^2 in total). An average from these four quadrants was taken, multiplied by the dilution factor, and then multiplied by 10^4 to yield a cell count/mL.

2.2.3 Analysis of human CD14^{+ve} mononuclear cell purity using flow cytometry

Flow cytometry was used to determine the percentage of CD14^{+ve} cells within the PBMC population initially isolated using histopaque, and within the final mononuclear cell population used to seed the ivory disks. Samples containing 2 x10^5 cells from each of these populations were taken and spun at 800g for 2 minutes. The pellet was then re-suspended in FACS buffer (400µL), and each suspension was divided into two tubes. A monoclonal anti-CD14 FITC antibody or its corresponding isotype (both eBiosciences, San Diego, CA) was then supplemented into the sample vials and placed on ice for 30 minutes. After this incubation cells were again spun at 800g for 2 minutes prior to being washed in FACS buffer. This was repeated 3 times. Following the final removal of the supernatant, cells were re-suspended in 200µL FACS buffer and 200µL 4% formaldehyde, fixing the cells. Once fixed, cells were then run through a flow cytometer (Accuri C6, BD) at 40,000 events, and the data collected was analysed using the partner software CFlow Plus (BD). To remove cell debris and doublets forward scatter area (FSC-A) against height (FSC-H) plots and side-scatter area (SSC-A) against FSC-A plots were drawn. CD14^{+ve} cells were then gated from scatter plots, and samples were compared against those labelled with the isotype. A percentage purity of CD14^{+ve} cells was then acquired.

2.2.4 The *in vitro* monoculture of human osteoclasts

Ivory disks, which mimicked the physiological matrix of bone, were seeded with 3.2 x 10^6 CD14^{+ve} mononuclear cells of ≥90% purity. These disks were initially incubated at 37^{o}C for 2 hours to allow cellular adhesion to the ivory disks. After two hours the disks were placed within a 48 well culture plate containing 500µL of proliferation medium for 7 days. Culture supernatants were collected and stored at -80^{o}C and wells were replenished with fresh medium every 3-4 days. To ensure cell density was of a high enough value to facilitate osteoclast differentiation, two disks from each experiment were harvested at day 0. These disks were fixed and stained using glutaraldehyde, haematoxylin and TRAP stains. Assays containing disks with adequate cell density (>500 cells/mm^2) were further cultured in differentiation medium containing 5ng/mL m-CSF and 5ng/mL RANKL (Figure 2.3).

After initial analysis of total cell counts obtained from a previously established method (Dr F. L. Collins) using 5ng/mL m-CSF, a reduction in total count was noted (counts were quantified by two individual analysts and results reported in Chapter 3). The concentration of m-CSF in proliferation medium was therefore increased to 10ng/mL. All subsequent assays and the validation of the automated counting algorithm were cultured in 10ng/mL m-CSF proliferation medium prior to culture in differentiation medium for 14 days which contained 5ng/mL. Control culture conditions containing only proliferation medium were run alongside disks cultured in differentiation medium to establish the effects of RANKL addition (Figure 2.4). From initial results a power calculation was carried out to reveal a total of 8 individuals were needed to determine whether a significant effect could be seen in the osteoclast differentiation assay.

2.2.5 The addition of sgp130-Fc and HYPER-IL-6 into osteoclast cultures

Sgp130-Fc was supplemented into differentiation cultures at 500ng/mL across the 14 day time-course, alongside its addition into m-CSF control cultures (n = 8). HYPER-IL-6 was initially supplemented into cultures at 10ng/mL (n=7) but after low cell counts a dose range of 0.5ng/mL to 5ng/mL was tested in differentiation medium (n=1). Following this the optimal dose of 0.5ng/mL HYPER-IL-6 was added into differentiation medium (n=8) across the 14 day culture period. Finally, the combination of sgp130-Fc (500ng/mL) and HYPER-IL-6 (0.5ng/mL) was supplemented into differentiation cultures across the time-point (n=6). Medium was collected, refreshed and treated every 3-4 days, and at day 14 disks were harvested and stained with haematoxylin and TRAP.

2.2.6 Treatment of *in vitro* human osteoclast differentiation cultures with anti-CCL3

Ivory disks were seeded and cultured as previously stated in Section 2.2.4. At day 0 anti-CCL3 was supplemented into differentiation cultures at 0, 2, 4 and 8ng/mL, alongside their addition into m-CSF control cultures (n=8). Medium was collected, refreshed and treated every 3-4 days, and at day 14 disks were harvested and stained with haematoxylin and TRAP.

2.2.7 Treatment of *in vitro* human differentiation assays with recombinant human IgG1

Seeded disks from Section 2.2.4 were cultured for seven days in proliferation medium prior to being treated with differentiation medium containing 8ng/mL recombinant human IgG1 antibody for 14 days (n=8). Control cultures containing m-CSF (5ng/mL) and IgG1 isotype (8ng/mL) were run in parallel (n=4). Medium was harvested and replenished every 3-4 days and assays were terminated on day 14, where disks were fixed and stained with haematoxylin and TRAP.

2.2.8 Treatment of *in vitro* human osteoclast differentiation cultures with OPG

Methodologies outlined in Section 2.2.4 were used to seed disks and culture them in proliferation medium for seven days. At day 0 either 8ng/mL OPG or 100ng/mL OPG were supplemented into differentiation cultures. Medium was harvested and replenished every 3-4 days. At day 14 disks were harvested, fixed and stained for total, TRAP, osteoclast cell number and functional activity.

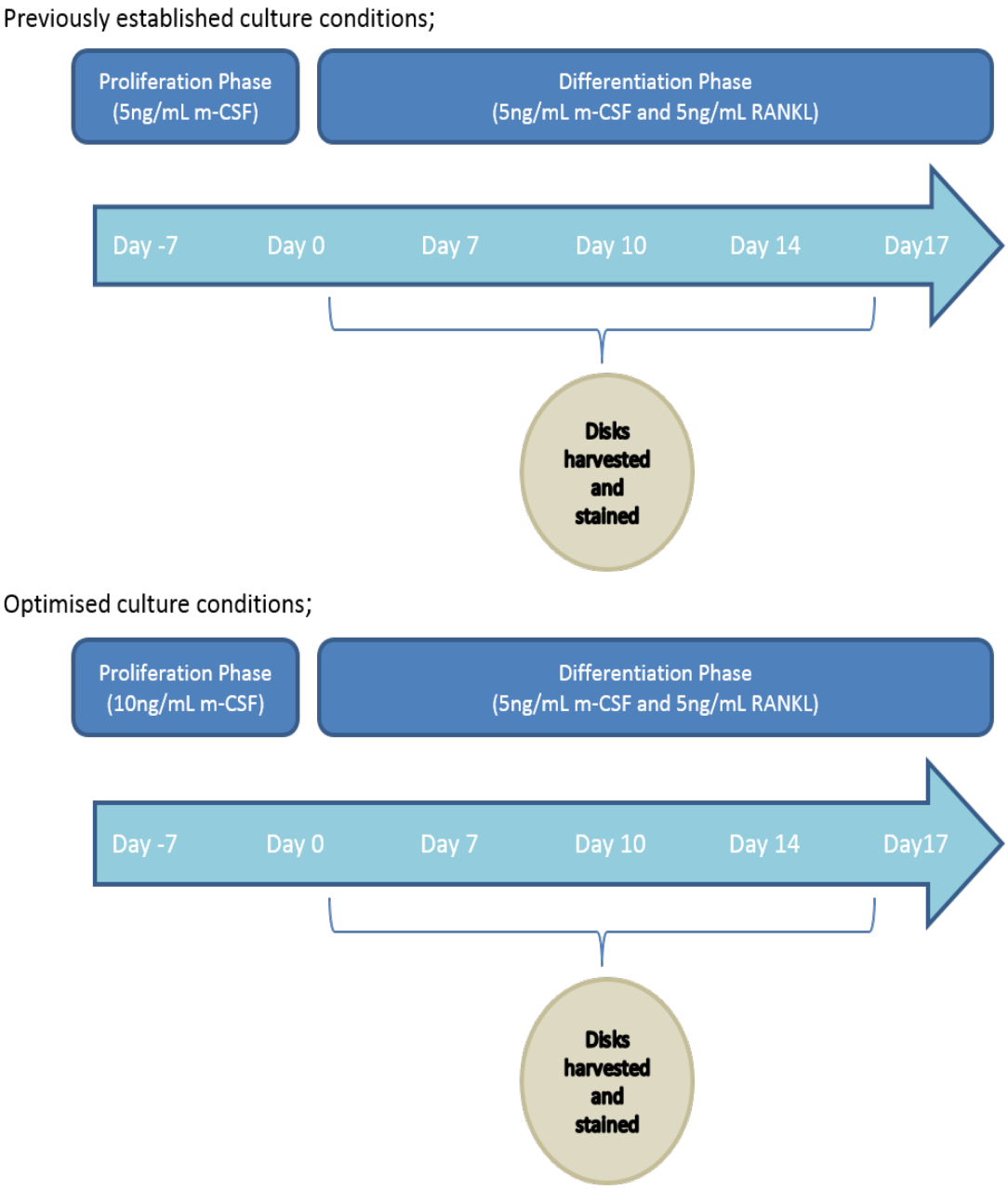

Figure 2. 3 - The time-course for the culture of human CD14^{+ve} mononuclear cells in the proliferation and differentiation phase of the osteoclast assay. Previously established proliferation medium containing 5ng/mL was used to culture CD14^{+ve} cells for seven days prior to addition of differentiation medium (5ng/mL m-CSF and 5ng/mL RANKL).The optimisation of these conditions led to an increase to 10ng/mL m-CSF in proliferation medium for seven days prior to addition of differentiation medium at the same concentrations as used previously used. Every 3-4 days medium was harvested, replenished, and sample disks were fixed and stained. In later experiments supernatant was harvested and replenished on days 1 and 3 to assess the early secretion of mediators.

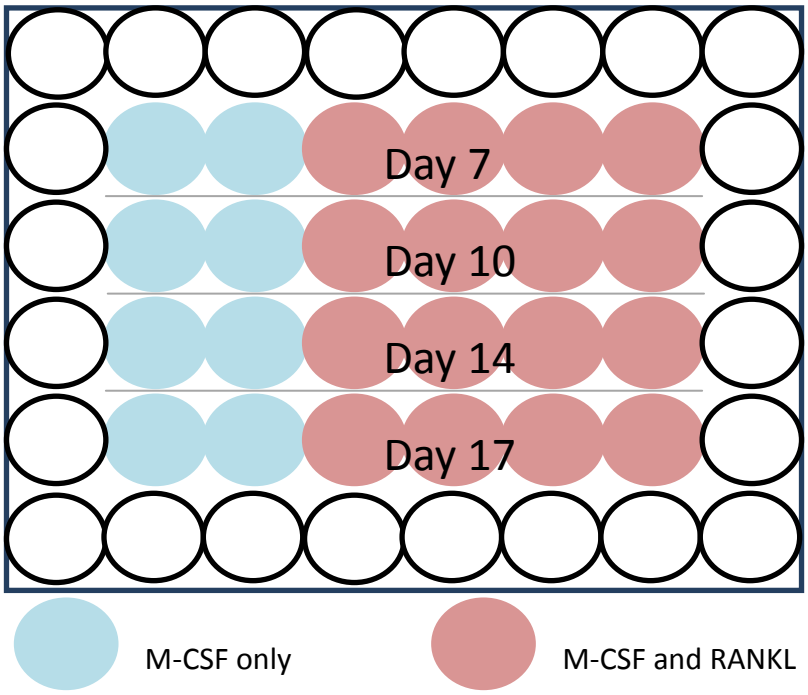

Figure 2. 4 - Example plate map from a human differentiation assay.A representative plate map from an osteoclast differentiation assay illustrates multiple disks per time-point were run under each condition, accounting for inter- and intra-donor variability; two control disks from m-CSF only cultures were run alongside four discs cultured in differentiation medium. Time-points within assays varied and including the following days; 0, 1, 3, 7, 10, 14 and 17.

2.2.9 Histological staining for the identification of nucleated and TRAP+ve cells

Disks were harvested at days 0, day 1, day 3, day 7, day 10, day 14 and day 17 of the human osteoclast differentiation assay (Figure 2.3 and 2.4). At these time-points disks were removed from culture and washed twice with PBS. Cells adhered to the ivory disks were fixed with glutaraldehyde solution for 15 minutes at 37^{o}C, prior to being washed twice in PBS and left to dry for 5 minutes. To identify the presence of pre- and mature osteoclasts, disks were incubated with 300µL TRAP staining solution for 6 minutes at 37^{o}C, prior to being washed twice in PBS to remove the stain. Haematoxylin (300µL) was then used as a counter-stain for nuclear material within the cells and was applied to each disk for 10 seconds at room temperature, prior to its removal by two washes with dH_2O.

2.2.10 Image acquisition across the x and y dimension of the disks

Every disk was visualised and imaged using either a 4x magnification taking 4 areas of interest (4.375mm^2 each using a Canon EOS 100D camera) or a 10x magnification capturing 13 areas of interest/ROIs (1.375mm^2 each using the Olympus Camedia C-3030 Digital Camera), Figure 2.5. Following this the image was then processed for either cell counts or area resorbed.

2.2.11 Manual total cell counting of human osteoclast assays

Preliminary total cell counts were obtained manually through counting and electronically marking every cell adhered to each disk (Figure 2.6). This method was carried out for all sections of the disk, equating to a total cell count for 17.5mm^2. Within each culture condition, a minimum of 3 replicate disks were used to reduce to intra-assay variability. As a result, the time for total cell counts using a manual method was >130 hours. A novel, high-throughput and automated method for cell counting was then developed and validated.

i.) x4

ii.) x10

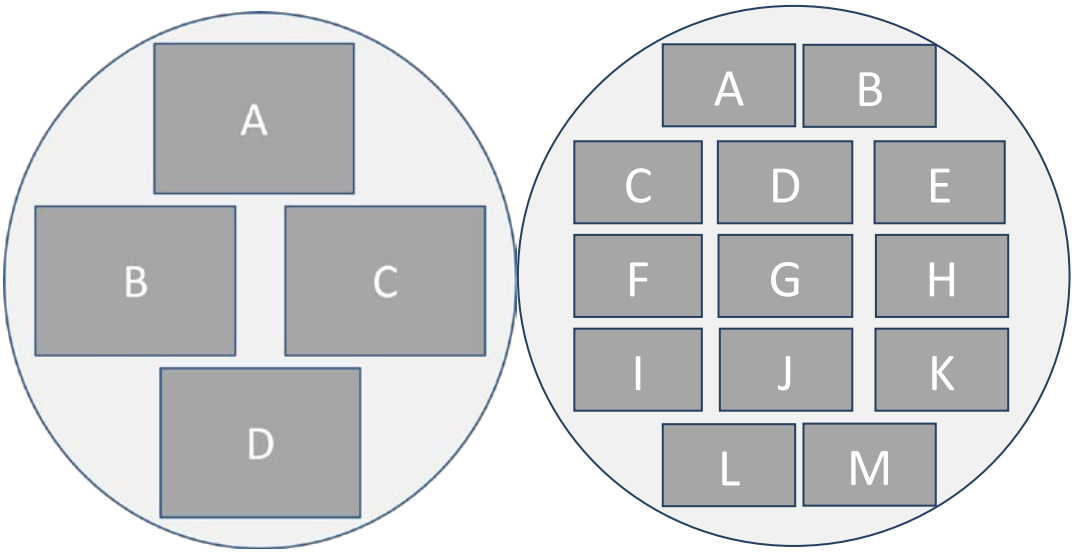

Figure 2. 5 - Schematic diagram of disk area imaged.Two methods were used for the collection of images across the x and y dimensions of the disks, which resulted to a total of 17.5mm^2. i.) 4 images at x4 magnification were acquired using the Canon EOS 100D camera. ii.) 13 images at x10 magnification were acquired using the Olympus Camedia C-3030 Digital Camera.

i.)

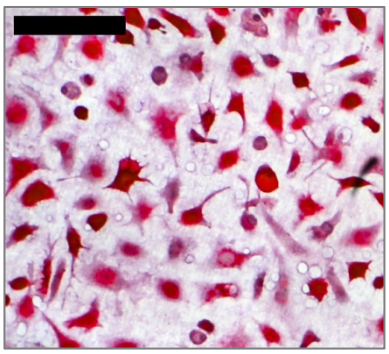

ii.)

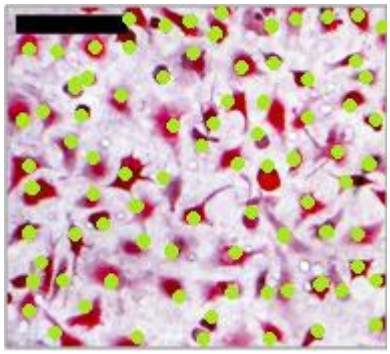

Figure 2. 6 - Manual total cell counting method.**i**.) The original image. ii.) An image which was manually counted; each cell was marked with green documenting its inclusion and then the image was saved. Scale bar = 100µm.

2.2.12 Development of a novel, high-throughput, automated cell counting algorithm

A computational algorithm which facilitated high-throughput, reproducible and accurate total cell counts was necessary due to the large number of cells seeded on each ivory disk. MATLAB was used to develop this algorithm due to its functionality for manipulating images in the raw data format. The process used within every step of this algorithm is described below where example pseudocode can be found along with illustrative figures of the commands. At each step of the algorithm figures could be produced and saved for comparison with the manual counting method. The full code for the final development of this algorithm can be found in Appendix 1.

2.2.12.1 The selected image was loaded into the workspace

All axes were cleared and the sample image loaded into the workspace; known as (I). (I) was then presented in an axis as shown in Figure 2.7, using the command *imagesc(I)*.

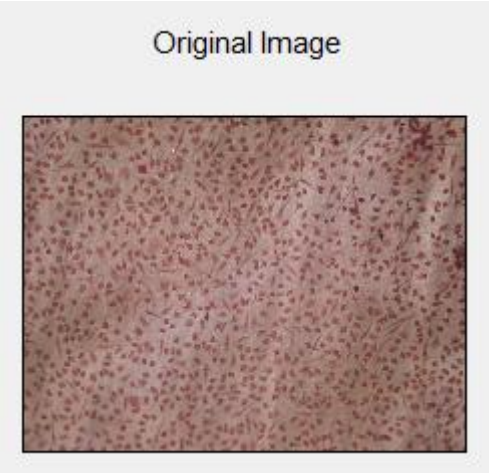

Figure 2. 7 - Loading an image into the workspace.An example image from day 0 of the differentiation assay was loaded into the workspace and displayed within a new figure.

2.2.12.2 Conversion into a binary image and application of a threshold

The selected image was converted into a binary image through the command '*im2bw*' which utilised a default threshold determined using the command '*graythresh(I)*'. This binary image consisted of '0' or '1' only, indicating either the presence or absence of a signal; i.e. the binary number system (*Kerman, 2002*). A second binary image was then produced which utilised a threshold manually set at 50 and defined by the function '*P.noise_thresh',* to remove all objects below this threshold (considered noise due to their small size). A second parameter of pixel connectedness was also set, '*P.conn=4*' which allowed only '0' pixels with 4 other '0' pixels located directly next to them to be defined as an object. Total number of objects within the binary and denoised binary images was then expressed underneath each image when shown as a figure using the '*imagesc*' command (Figure 2.8).

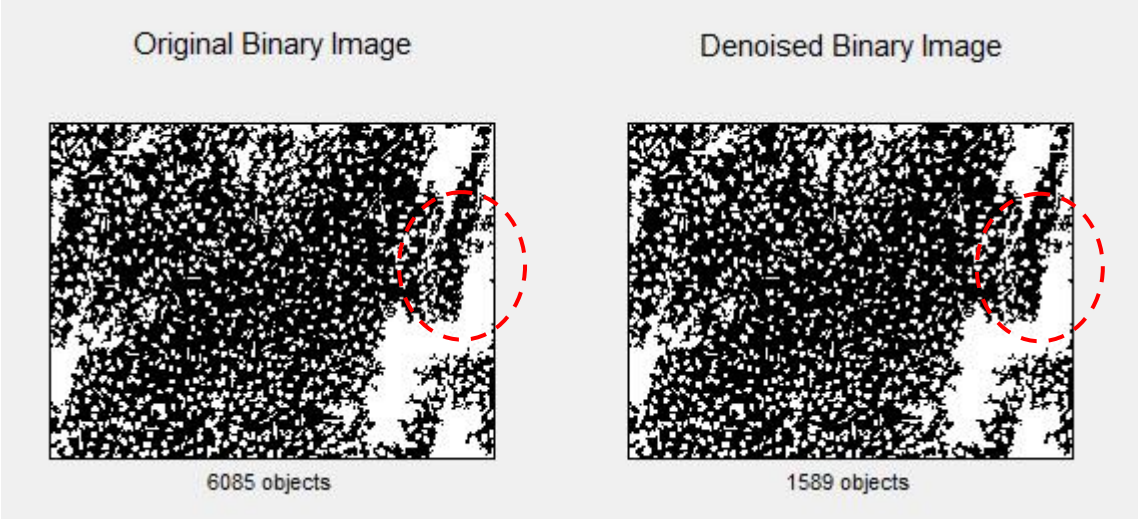

Figure 2. 8 - Conversion into a binary image and background noise reduction.A default threshold was set from the original binary image, where any objects falling below this threshold were removed (see dotted red circles), resulting in the reduction of total object count (stated under the image).

2.2.12.3 The selected image was normalised to ensure a constant background illumination across the disks

The conversion of the image into a de-noised binary image led to clear areas of the original image being extensively covered with '0' signal due to an uneven background illumination. Initially it was thought that these disks could have undulations on their surface from disk preparation procedures. However, after maximising the effectiveness of the high-speed saw, no differences in the uneven background illuminations were seen, and areas of '0' signal still remained (Figure 2.9). It was concluded that the areas of uneven background were inherent and natural within the disks, and would therefore be unavoidable.

To overcome the inconsistent background illumination, a piece of code used within facial recognition software was used. In theory this code was able to reduce alterations in facial illumination; i.e. 'shadowing'(*Haritha et al., 2012*and*Struc, 2009*). It was this principle that was used to remove the uneven illumination from the images of the disks and facilitate the accurate visualisation of the objects 'hidden' under the large areas of '0' signal. First, the original image was converted from the red-green-blue colour model (RGB model) into greyscale using the '*rgb2gray*' command, and then the '*DCT_normalisation'* function was applied which led to the normalisation of the image; (*Struc, 2009* and*Haritha et al., 2012*). The normalised image was then denoised, presented in the figure, and the number of objects within the image were shown beneath (Figure 2.9).

i.)

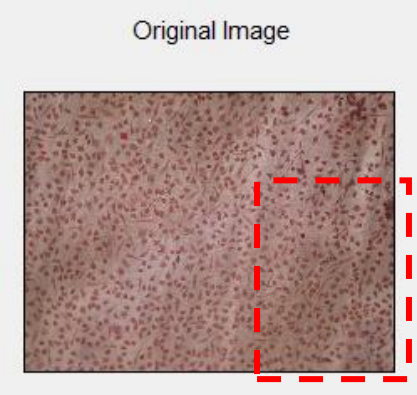

ii.)

iii.)

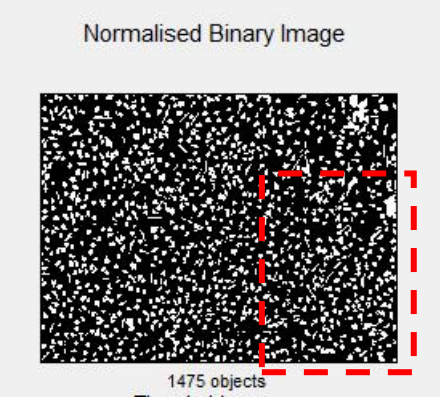

Figure 2. 9 - Accurate visualisation of total cells was achieved through image normalisation.When compared back to the original image (i), the denoised image (ii) showed several areas of high '0' values in the image, which were known as areas of inconsistent background illumination(red boxes). Through utilising the 'DCT_normalisation' code, a constant background illumination was maintained (iii) and total cell number obtained.

2.2.12.4 *Objects counted within the image were segmented for clarification*

In order to confirm the algorithm's definition of an object, all objects within the image were 'segmented' using the MATLAB command '*bwperim*', resulting in an aqua-coloured perimeter appeared around each counted object. Using '*imagesc*' a subsequent figure demonstrated those counted, Figure 2.10.

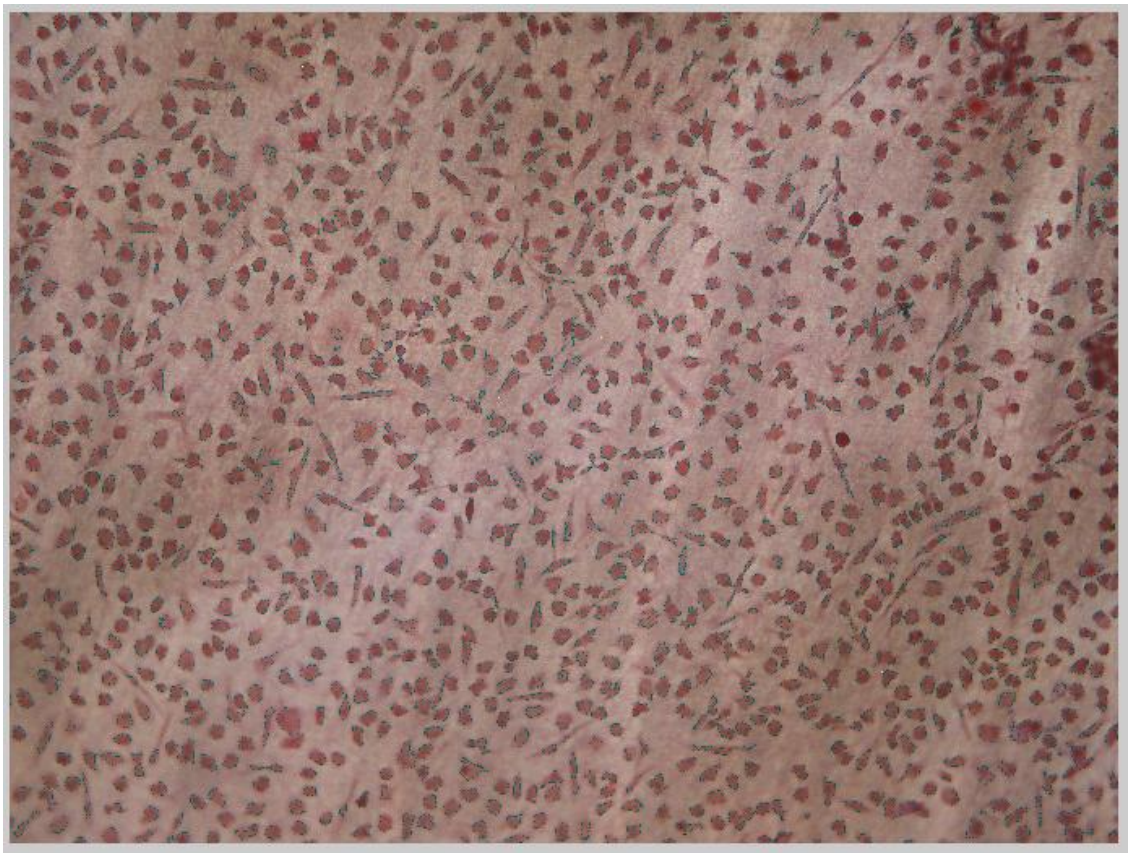

Figure 2. 10 - Segmentation of objects included in automated counts.The counted objects within the image were marked with an aqua perimeter allowing the comparison between the previous manual cell counts and the automated object counts.

2.2.12.5 Histogram of total object count

After visualisation each counted object was placed into a histogram bar depending upon its size in pixels. A histogram was coded for through defining the x and y dimensions, along with setting up the histogram bin sizes. There were 21 histogram bins which were defined as follows; bin 1- objects of size 0-100 pixels, bin 2- objects of size 101-200 pixels, and so forth up to bin 20 which contained objects of 1,901- 2,000 pixels, and bin 21 with objects >2,000 pixels, ensuring all larger objects were accounted for. A loop was then set up to ensure that all objects within the denoised normalised image would be 'selected' and 'placed' into one of the bins defined. Objects in the top left of the image were 'selected' first, and objects in the bottom right of the image were of the last to be 'selected'.

This histogram was then shown within a new figure using the command '*bar*' and the number of objects within each bin were displayed on top of the histogram bars (Figure 2.11). Along with the visual representation of the histogram, a separate figure containing a subplot, '*subplot*', was used to show the individual histogram bins as separate axes, and reveal which, and how many objects were in each bin, along with their physical distribution within the denoised, normalised image. The total object counts from within each histogram bar was then exported out of MATLAB and into an excel spreadsheet using the command '*xlswrite*', which was then saved and analysed further (Figure 2.11).

i.)

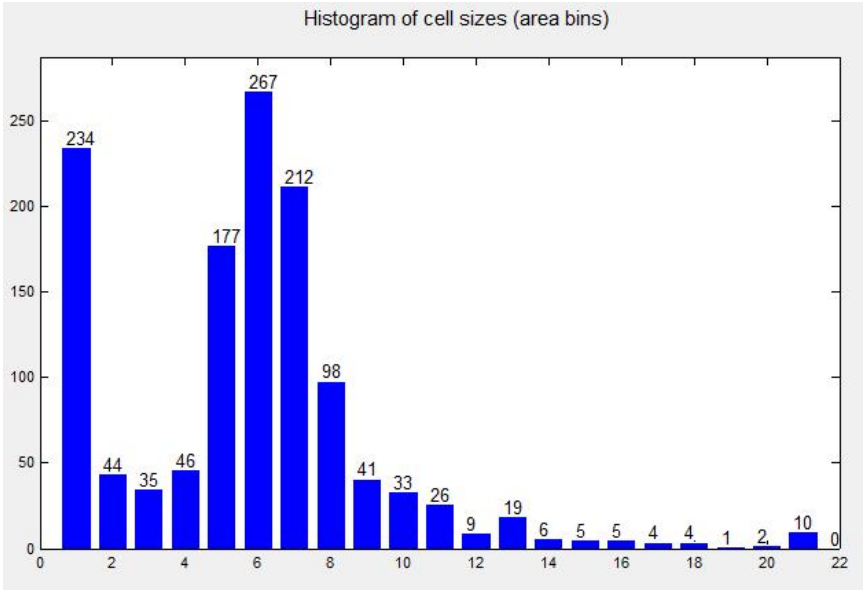

ii.)

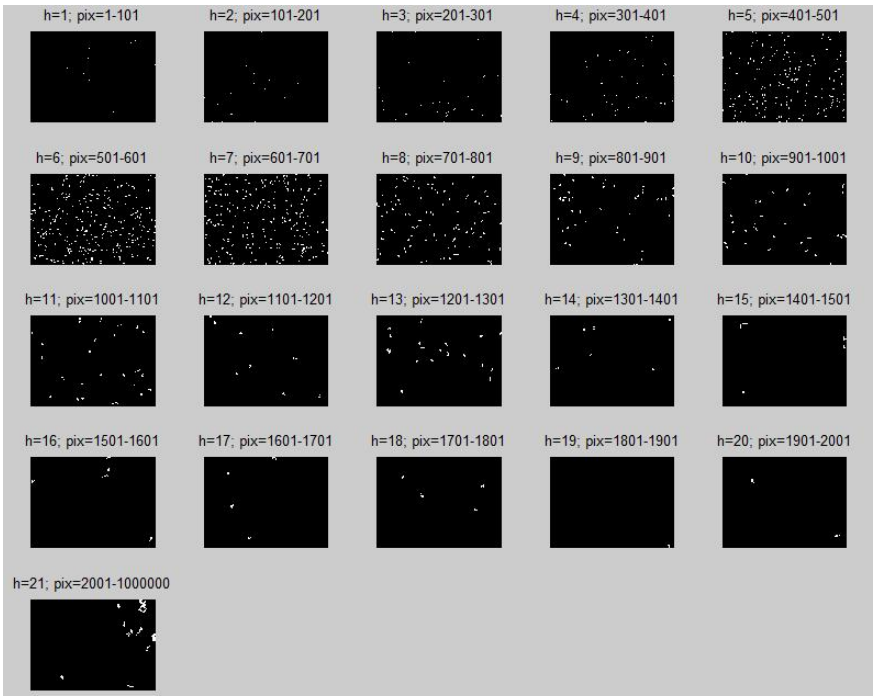

Figure 2. 11 - A histogram illustrating cell size distribution and frequency.(i) A histogram illustrating cell size and distribution from automated cell counts shows the highest cell frequencies at the lower cell sizes (day 0 image). (ii) Through further analysis a subplot of the histogram highlights that the majority of cells were present within the first 7 histogram bins, after which the number of objects decreases in subsequent bins.

2.2.13 Development of a semi-automated method for total object count using a graphical user interface (GUI)

In order to reduce the user input needed to carry out the above algorithm, a graphical user interface (GUI) was designed, with the basic principle of 'one click, one figure'; *i.e.* the automatically runs. The GUI for total object counts, shown in Figure 2.12, was initiated through selecting 'Load Image', which would run the code described in Section 2.2.12.1 and result in the original image being uploaded into the GUI. The second button 'Threshold Image' (section 2.2.12.2 code) would result in the images being displayed within the 'Original Binary Image' and 'Denoised Binary Image' axes. The 'Normalise Image' button (section 2.2.12.3 code), shows the normalised image within the Normalised Binary Image axes. The 'Segment Cells' button (section 2.2.12.4 code) shows all objects within the image highlighted through an aqua-coloured perimeter. The final two steps 'Make Histogram' and 'Save Results' (section 2.2.12.5 code) together resulted in a histogram plot of object count, size and distribution, and also allowed the total object count data to be exported out of MATLAB and saved as an excel spreadsheet. Two examples are shown in Figure 2.13; one illustrating smaller mononuclear cells, and the other showing a more diverse range of adhered cells.

i.)

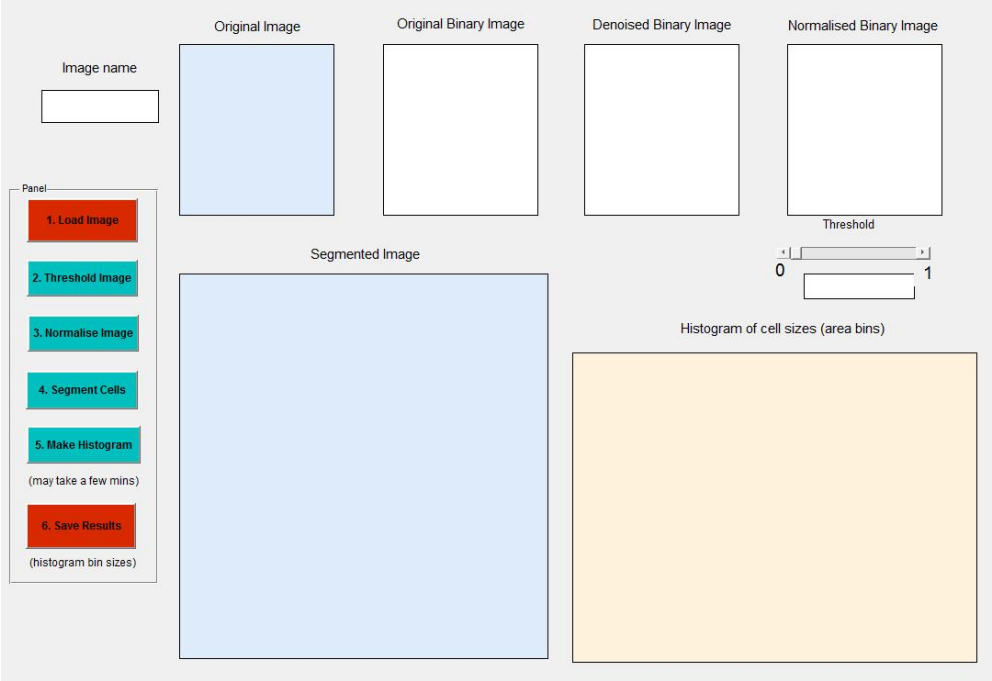

Figure 2. 12 - GUI example for automated cell counts.i.) The user inputs the image through the command buttons found within the 'Panel' which then facilitates the following; image thresholding, normalisation, segmentation, and the formation of a histogram of cell size, frequency and distribution to be created.

i.)

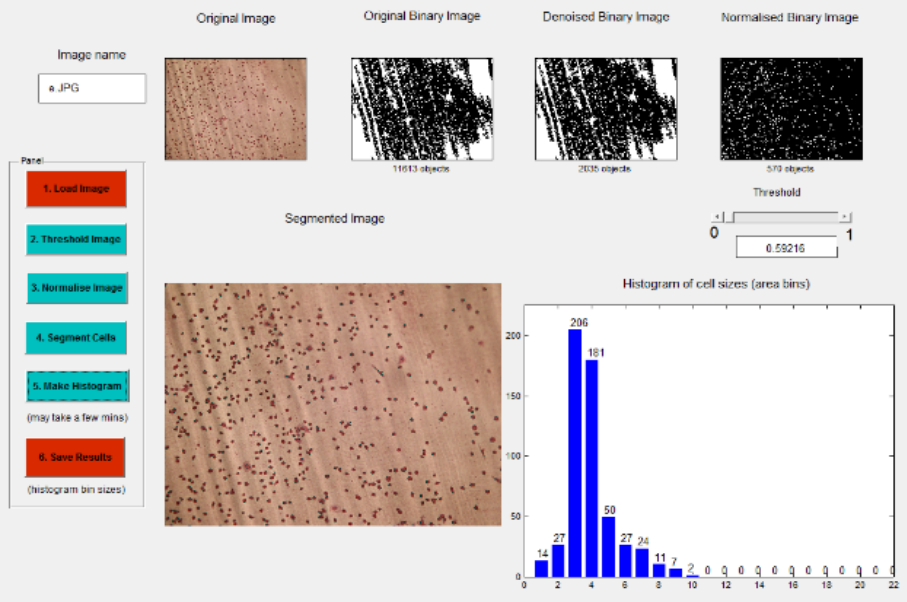

ii.)

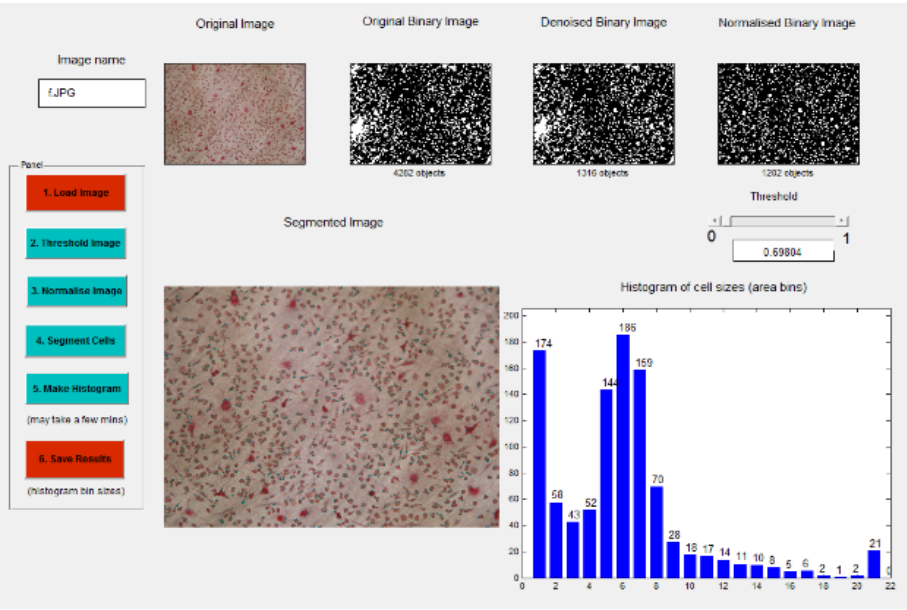

Figure 2. 13 - Two examples from the GUI illustrating the diverse cell populations adhered to the ivory disks. (i) Image from an m-CSF only culture showing peak cell distribution on the left hand side of the histogram, being indicative of small objects. (ii) Image acquired after 10 days of culture in m-CSF and RANKL. The main distribution of cells has shifted to the right, and a peak in histogram bar 21 can be seen, indicative of larger objects, most likely to be osteoclasts.

2.2.14 A fully automated, high-throughput algorithm for total object count was coded

The pre-described GUI for total object counts provided a semi-automated method for cellular counting which was found to be 7.5-fold faster than the manual counting methods previously used. However, user-input was still needed which slowed the process down and still took the analyst 13.5 hours of user input to analyse one experiment. To fully automate the algorithm, the previously described code was modified which allowed it to loop through all images in a folder, processing and saving the results with just one click, thereby enabling it to be run overnight. The computational code previously described was transformed into a *function* named '*Count_Cells_fxn*', which when then used in a new script.

2.2.15 Analysis of TRAP^{+ve} and osteoclast counts in human osteoclast assays

The automated algorithm provides a count for total cells but could not provide an accurate count for TRAP^{+ve} and osteoclast number. For this reason, TRAP^{+ve} and osteoclast count from disks harvested were obtained manually. The TRAP stain allows cells expressing TRAP to be distinguished from TRAP^{-ve} cells, which were stained with haematoxylin only. Within this thesis, TRAP^{+ve} cell count corresponds to the total number of cells stained with TRAP. The presence of osteoclasts was assessed through TRAP and haematoxylin staining by the following definition; an osteoclast was a multinucleated (≥3 nuclei) TRAP^{+ve} cell of ≥30µm diameter in the smallest dimension of the cell. TRAP^{+ve} cells (green circles)and osteoclasts (blue circles)were counted manually and marked within each image using PaintShop Pro, thus allowing an electronic copy of each count to be maintained (Figure 2.14). These parameters were then exported into excel and saved alongside the automated total cell count data. The percentage of osteoclastogenesis was then calculated using the automated total cell count and manual osteoclast count (both at day 14), facilitating comparisons between donors.

i.) ii.)

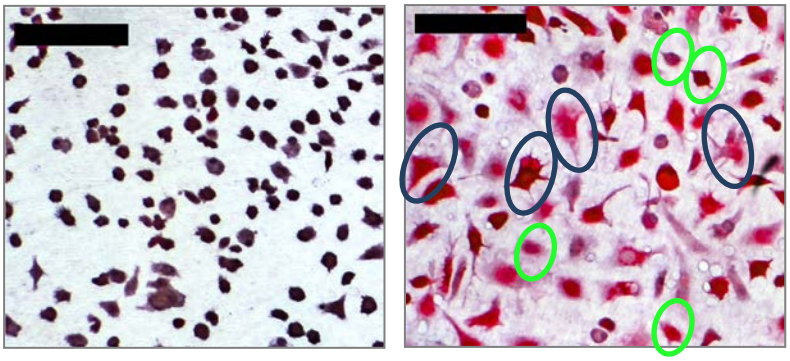

Figure 2. 14 - The identification of TRAP^{+ve} mononuclear and TRAP^{+ve} multinucleated cells within osteoclast differentiation cultures.The presence of only TRAP^{-ve} cells can be seen within (i) where cultures have only been supplemented with m-CSF. TRAP^{+ve} mononuclear cells were evident within (ii) and are circled in green, whereas TRAP^{+ve} multinucleated cells are circled in blue. Both images are stained with TRAP and haematoxylin; scale bar = 100µm.

2.2.16 Assessment of osteoclast functional activity through resorption pit analysis

A traditional method for the calculation of area resorbed through osteoclast activity was utilised and compared to a novel method of analysis for images acquired through confocal microscopy.

2.2.16.1 *Identification of resorption pits using toluidine blue staining and light microscopy*

Once cells adhered to ivory disks were imaged, disks were scraped with 70% alcohol and incubated overnight in 300µL 1% H_2O_2 with mechanical shaking. This method removed attached cells and bleached the disks of TRAP and haematoxylin stain prior to further staining. The H_2O_2 was removed and disks were washed twice with dH_2O. 300µL of toluidine blue stain (0.5%) was applied to the disks and incubated for 1 minute at room temperature. The stain was removed and disks were washed twice with dH_2O prior to imaging and analysis (Figure 2.15). Mimicking the images obtained for cell counts, sections of each disk were obtained, resulting in a total area of 17.5mm^2 imaged. Analysis of area resorbed was carried out within ImageJ, where pits outlined by the toluidine blue stain were circled and the area within them calculated based upon the known parameters of the image; 2064 pixels = 1 mm. Where tracks of resorption or conjoining pits were visible, one continuous area was analysed. All areas of resorbed bone within each image were analysed creating a total area of resorption per 17.5mm^2, along with data yielded regarding the number of resorption events and the range of resorption pit size.

2.2.16.2 Identification of resorption pits using calcein staining and confocal microscopy

To decipher whether confocal microscopy produced a more detailed and sensitive method of calculating total area resorbed per 17.5mm^2, results were compared back to toluidine blue staining. Disks for confocal microscopy were scraped within 70% alcohol and left overnight in H_2O_2 prior to being washed twice in dH_2O. Disks were incubated in calcein stain (300µL) overnight on a mechanical shaker at room temperature. Following this, the calcein was removed and disks washed twice in dH_2O. Disks were then mounted in 24 well glass-bottomed plates at <4^{o}C using

CyGEL. Once the disks were in place, the plate was removed and placed at room temperature enabling the solidification of CyGEL ensuring a firm mount reducing sample movement when imaging. This thermoreversible property allowed the disks to be retained after imaging. Once disks were mounted, laser scanning confocal images were acquired using a x20 objective lens and Nikon Eclipse TE300 linked to the LaserSharp 2000 software. Through this software the orientation and location of the field of view could be controlled, along with the precise parameters of the confocal set-up. Along with an Argon laser, two photon multiplier tubes (PMT) were active to detect signals at 480-490nm (PMT1 = scattered light) and >520nm (PMT2 = calcein signal output), and a transmission detector was active in collecting transmitted signals through the sample. Specific data collection parameters were recorded for each disk and kept constant to ensure continuity across the data collection process. For each data collection the following parameters were never changed; zoom: 1.5, pixels-by-lines: 512 x 512, step: 0.2µm, xy pixel: 0.8µm, objective: 20X. Using the x20 objective lens, images were acquired and then saved, exported and analysed using ImageJ as before in Section 2.2.16.1 for total area resorbed (Figure 2.16). The results from these two methods for calculating total area resorbed were then compared (Chapter 3).

To determine pit depth, laser scanning confocal images were also acquired at x60, using PMT set to detect signals at 480-490nm (PMT1 = scattered light) and >520nm (PMT2 = calcein signal output). Transmitted light was also detected. Set parameters remained constant in data collection to ensure reproducibility and accuracy in sample analysis; zoom: 1.5, pixels-by-lines: 512 x 512, step: 0.2µm, xy pixel: 0.27µm, objective: 60X. Data sets could then be saved and exported ready for analysis in MetaMorph.

i.) ii.) iii.)

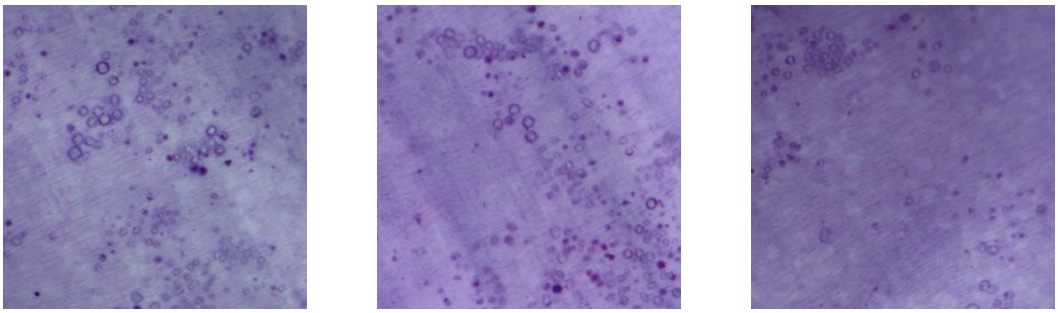

Figure 2. 15 - Representative images of toluidine blue staining acquired via light microscopy. To assess area resorbed in human osteoclast differentiation assays toluidine blue staining was utilised. Representative images (i, ii and iii) above illustrate areas of resorption through concentrated areas of toluidine blue stain. Images were taken at x4 magnification and are from 3 individual donors.

i) ii.) iii.)

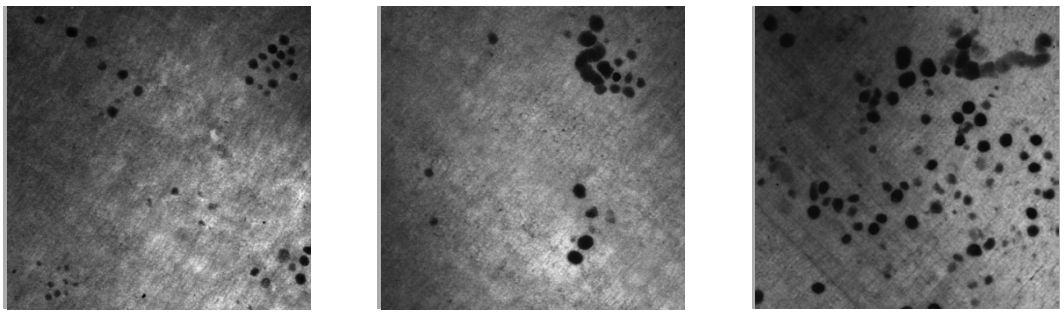

Figure 2. 16 - Representative images of calcein stained disks acquired via confocal microscopy. Areas of resorption can be identified through distinct regions of no signal (black pits) from confocal images obtained after calcein staining. Individual pits were seen along with 'tracking' and areas of slight erosion (i, ii and iii). Calcein stained disks were compared to previously acquired toluidine blue stained disks to assess the benefit of using novel imaging methods for calculating area resorbed. Images were acquired using x20 Oil lens, with the following parameters; zoom: 1.5, xy pixel: 0.8µm, pixels x lines: 512 x 512.

2.2.17 The three dimensional characterisation of resorptive pits

Data sets known as stacks were loaded into Metamorph (Molecular Devices Corp., CA). Region measurements were used to calculate the average intensity of pits in each image, thereby defining the presence of a pit. An inclusive threshold equivalent to this average intensity was applied to the stack thus identifying pits, and through the application of a median filter (3-by-3 pixels) a reduction of noise ensued. This median filtered stack was then transformed into a binary image, allowing the creation of a single intensity image from the summation of all the data sets. The background signal in this image was then equalised and subtracted from the original, leaving only intensity signals from the eroded pits. Each pit was then analysed as a collective, and data regarding the following were documented; total area, total intensity, maximum intensity, perimeter, centroid X and centroid Y. Appendix 1 demonstrates this process using visual guides as does Figure 2.17. Additional to these, from total intensity the volume of a pit could be calculated using a correction factor (necessary due to differences in refractive index of the lens and mountant) and by determining the size of a 1-by-1 pixel;

$$1\ pixel\ by\ 1\ pixel = \ 0.27\ x\ 0.27\ x\ (0.2\ x\ 0.8) = \ 0.011664\mu m^3$$

$xy\ pixel = 0.27$

$Step\ in\ z\ dimension = 0.2$

$Correction\ factor = 0.8$

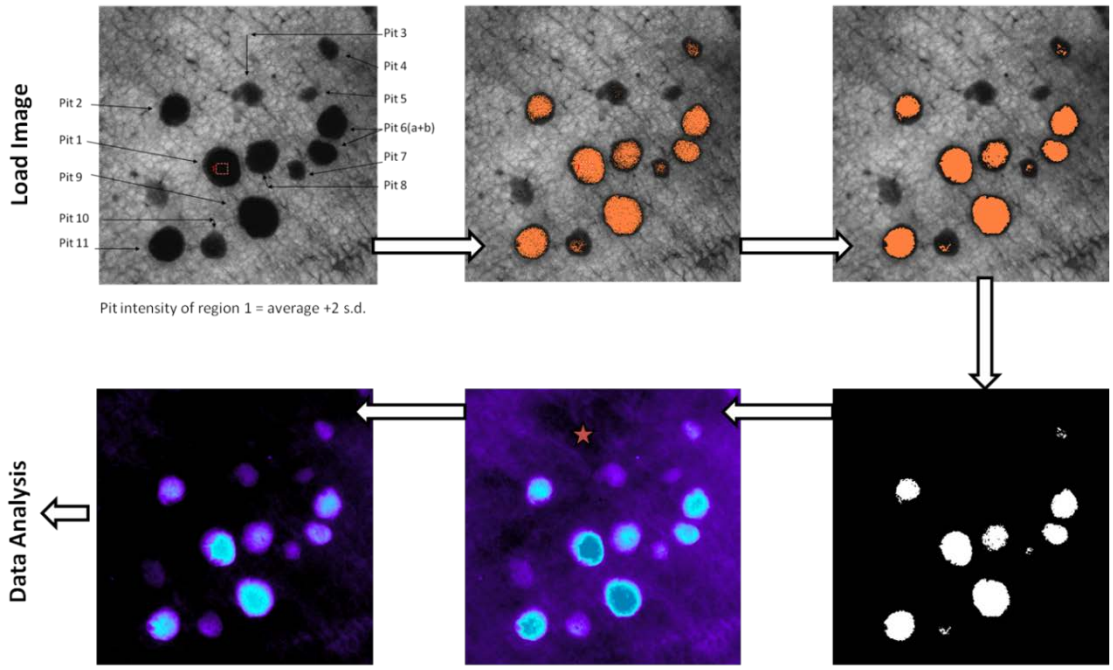

Figure 2. 17 - Flow diagram for the calculation of depth and volume of pits from 3D confocal stacks.Data collected at x60 was loaded into metamorph and the average intensity of a pit was defined. Through the application of an inclusive threshold and a median filter, both background noise and data slices below the base of the pit were removed. A binary image was then produced which could be summed to allow the removal of background signal and facilitate the creation of an intensity profile for each pit.0.27µm = pixel.

2.2.18 Analysis of soluble mediators linked to osteoclast differentiation and function by ELISA

Supernatants collected from osteoclast assays were analysed within ELISAs (R&D Systems) for chemokines and cytokines implicated in destructive bone diseases; CCL2, CCL3, CCL5, IL-6, and TNF-α. The specific dilutions and concentrations of the ELISAs used are contained within Table 2.3. Additional ELISAs were run assessing the presence of soluble NGF (R&D systems), CTX-1 and TRAP5b (Immunodiagnostic Systems).

The following standard protocol was used for the ELISAs; 100µL of capture antibody diluted in PBS was coated onto 96 well plates and incubated overnight at room temperature. The next day each plate was washed 3 times using wash buffer (0.05% PBS-T) and dried prior to the addition of 300µL of blocking buffer (1% BSA in PBS) for 2 hours at room temperature with mechanical shaking. During this incubation step samples were diluted if needed and standards were prepared in reagent diluent (1% BSA in PBS). After blocking, plates were washed 3 times in wash buffer, and 100µL of samples and standards were applied to representative wells, where standards were run in duplicate. The samples were incubated on the plates for 2 hours with shaking, prior to being washed 3 times with wash buffer. Following this, 100µL of detection antibody (specific for each ELISA) was added to each well and incubated on the plate shaker for 2 hours again. Plates were washed 3 times in wash buffer, dried, and streptavidin-HRP was added to each well (100µL). Plates were incubated for 20 minutes at room temperature away from direct sunlight, prior to being washed 3 times with wash buffer. Finally, the addition of the substrate reagent which facilitated a colour change (100µL), and once developed the reaction was stopped through the addition of 50µL sulphuric acid (12%). Plates were then read at 450nm using a plate reader.

Table 2. 3 - ELISAs utilised throughout the project..

ELISA	Capture Ab	Detection Ab	Standard
Human CCL2	1.0µg/mL	50ng/mL	1000pg/mL – 15.6pg/mL
Human CCL3	0.4µg/mL	200ng/mL	500pg/mL – 7.8pg/mL
Human CCL5	1.0µg/mL	20ng/mL	1000pg/mL – 15.6pg/mL
Human IL-6	2.0µg/mL	50ng/mL	600pg/mL – 9.375pg/mL
Human TNF-α	4.0µg/mL	350ng/mL	1000pg/mL – 15.6pg/mL
NGF	2.0µg/mL	50ng/mL	31.20 – 2,000pg/mL
CTX-1	Kit specific		0 – 3.38ng/mL
TRAP5b	Kit specific		0.5 – 10U/L

2.2.19 Collagen-Induced Arthritis (CIA)

All animal experiments were conducted in line with ARRIVE guidelines and ethical permissions were granted under Home Office project licence 30/2928. DBA-1 male mice aged 8 weeks (12 in total) were ear tagged and divided into two groups (control group and an experimental group; 6 in each) with equal weight distributions prior to being immunized at day 0 with 2 x 50µL of CFA containing 2mg/mL collagen by intradermal (i.d.) injection. Animals were observed every other day for sores and scabs located on their hind-quarters and were treated with iodinated povidone when necessary. At day 21, each animal received 2 x 50µL i.d. of CFA and collagen, injected on the opposite side to previous injections, and were divided into two equal groups (n=6 in each). One group were given 100µL intraperitoneal injection of isotype control IgG antibody (5mg/kg), and the other anti-CCL3 antibody (5mg/kg). Animals received an additional 5 doses every other day prior to being culled by schedule 1 procedures.

Callipers were used to measure paw diameter. Arthritis severity (by clinical score) was assessed in each mouse by scoring each paw on a scale from 1 to 4; 0= no evidence of swelling or erythema, 1= swelling of the tarsals or ankle joint along with erythema, 2= swelling of the tarsals and ankle joint along with erythema, 3= reasonable swelling of the tarsals and ankle joint along with erythema, 4 = substantial swelling of the entire foot and the presence of erythema. An observed maximum clinical score 14 or loss of 20% of body weight (from baseline on Day 21)

necessitated humane killing of the animal in accordance with the severity limits of our Project Licence issued under Home Office regulations. The physical appearance, clinical signs, and the natural behaviour of the mouse were also monitored daily and any changes noted. A schematic of CIA induction in mouse is presented in Figure 2.18.

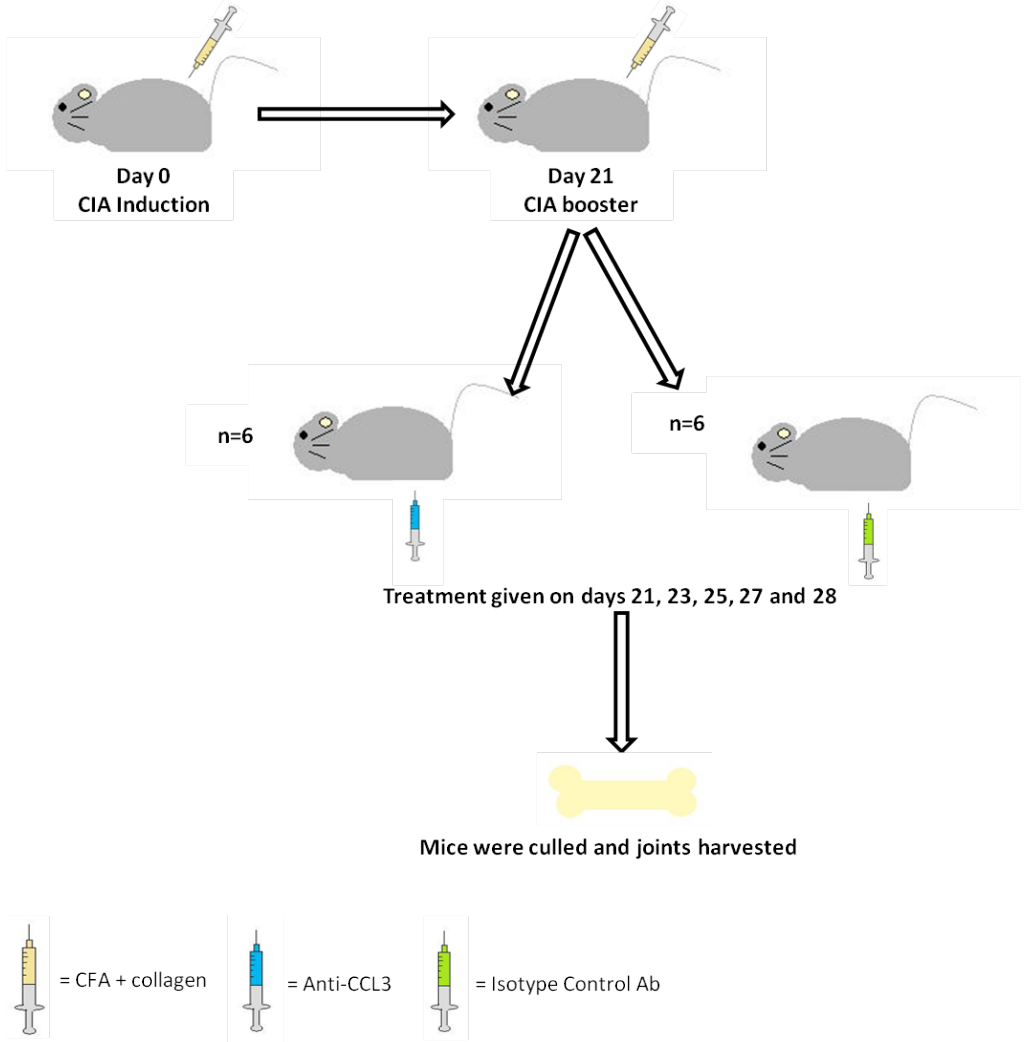

Figure 2. 18 - The induction of CIA.Mice aged 8 weeks were weighed and injected at day 0 with 2 x 50µL CFA containing 2mg/mL collagen by i.d. on the right hand side of their lower hindquarter. Every other day mice were checked for clinical and physical signs of arthritis. If scabs formed they were treated with iodinate povidone. At day 21, mice were again weighed and divided equally into two groups of n=6. All mice received a booster of 2 x 50µL again by i.d. on the left hand side of their lower hindquarter. One group received an i.p. injection of 100µL anti-CCL3 (5mg/kg), and the other an i.p. of 100µL isotype control antibody (5mg/kg) every other day. Every day mice were weighed, assessed for clinical signs of arthritis (scored from 0-4) and the diameters of their paws measured using callipers. Mice were culled and joints harvested on day 29.

2.2.20 Fixation of murine CIA joints

Mice were culled on day 29 and joint tissues from both fore- and hind-limbs were harvested. All fur/skin was removed from the joints ahead of fixation. Shoulder joints obtained were fixed in 10% neutral buffered formalin solution for 24 hours at room temperature and then placed into 70% alcohol for 2 weeks. Knee and ankle joints were fixed and stored in 70% alcohol immediately after the animal was culled until they were decalcified (section 2.2.23). Radiological images of hind- and forepaws were acquired prior to processing through to paraffin wax blocks for histological evaluation.

2.2.21 Radiological imaging and analysis of erosions in murine paw joints

Hind- and forepaws were imaged using a KODAK-pro and were assessed for erosions by a rheumatology clinical research fellow and an orthopaedic surgeon. In total 12 joints of the forepaw were assessed for erosions including; 2nd Distal Carpal - Radiale and Intermedium, Fused 4th-5th Distal Carpals – Ulnare, 1^{st} to 5^{th} MCP – Carpal and the 1^{st} to 5^{th} PIP – MCP (Figure 2.19). Hind paw assessment criteria consisted of the following; Centrale – Intermedium, 4th-5th Distal Tarpals – Fibulare, 1^{st} to 5^{th} MTP – Tarsal and the 1^{st} to 5^{th} PIP to MTP (Figure 2.19).

2.2.22 3D reconstructions of murine joints using micro-computed tomography (µ-CT)

Murine hind paws were sent to a collaborator at Gothenburg University (Professor Maria Bokarewa) where they were imaged using the µCT Skyscan1176 and reconstructed using the partner Bruker software. Once the data was collected, reconstructed images of the hind paw, MTPs, talus and calcaneus were created.

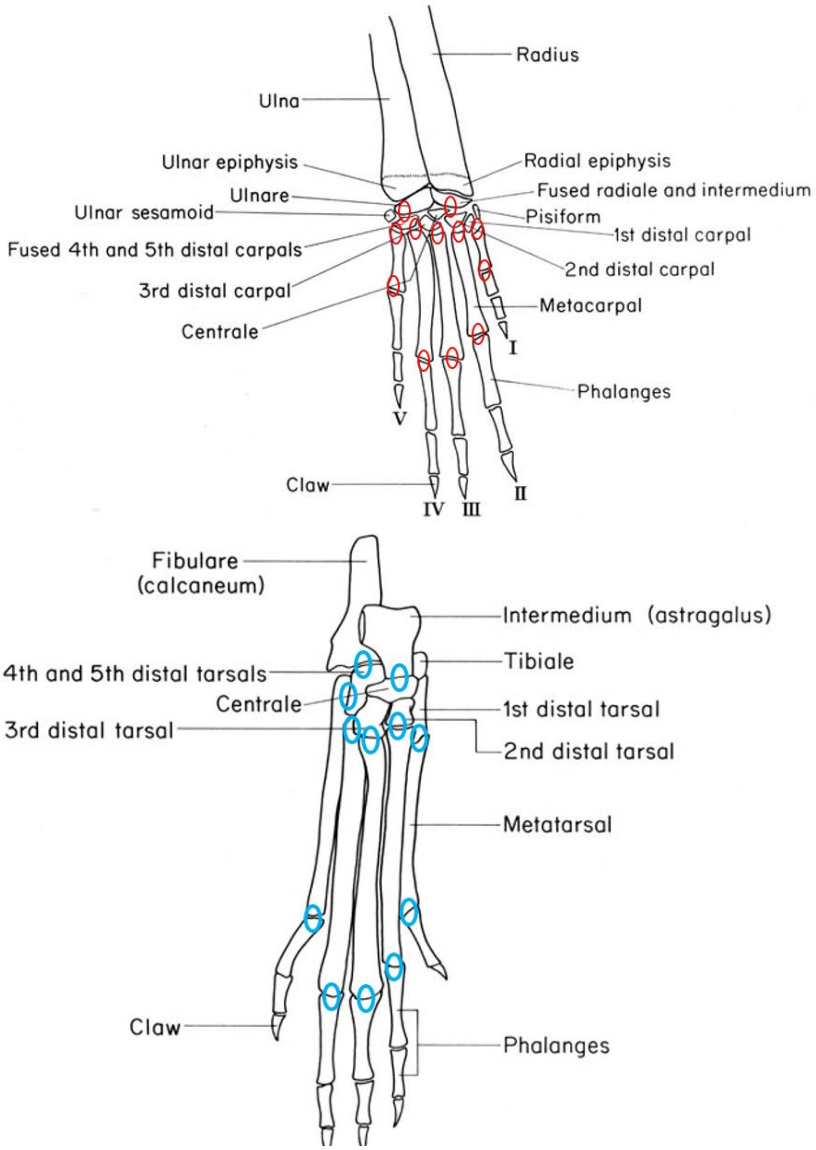

Figure 2. 19 - Radiological assessment of erosions present within the fore- and hind paws.After joints were harvested from CIA mice, fore- and hind- paws were fixed prior to acquiring x-rays. 12 areas of interest were assessed within x-rays. Forepaw joint of interest are circled in red; 2nd Distal Carpal - Radiale and Intermedium, Fused 4th-5th Distal Carpals – Ulnare, 1st to 5th MCP – Carpal and the 1st to 5th PIP – MCP. Hind paw joints of interest are circled in blue; Centrale – Intermedium, 4th-5th Distal Tarpals – Fibulare, 1st to 5th MTP – Tarsal and the 1st to 5th PIP to MTP. Images taken from *Cook 1965*.

2.2.23 Decalcification and processing of murine joints

After fixation and imaging, shoulder, knee and ankle joints were decalcified in EDTA solution for a total of 3 weeks at room temperature. Every 3 days the EDTA solution was replenished. Joints were then x-rayed to confirm successful decalcification, and left in dH_2O for 48 hours (refreshing after 24 hours) at room temperature. Joints were then processed and embedded in paraffin prior to sectioning.

2.2.24 Histochemical staining

Sections of 7µm thickness were cut from paraffin-embedded knee and ankle joints. All sections were taken through the same rehydration and dehydration processes irrespective of the staining process they were subjected to. Rehydration was achieved through samples going a set of incubation periods in varying percentages of xylene and alcohol to gradually increase their solubility (described in Table 2.4). Following this rehydration, the stain was applied to the section and incubated for the specified amount of time. After this, the section was rinsed in running water then distilled water or Scott's tap water, prior to completion of the dehydration steps; a series of varying percentage alcohols followed by immersion in xylene for set incubation times. Sections were then mounted using DPX (Sigma) and left to dry overnight prior to analysis and enabling long-term storage.

Table 2. 4 - Rehydration and dehydration procedures used throughout the immunohistochemical staining of murine sections.

Process	Incubation	Purpose
Xylene 1 (100%)	5 minutes	Rehydration allowing water soluble stains to penetrate sample
Xylene 2 (100%)	5 minutes	
Xylene 3 (100%)	5 minutes	
100% IMS 1	3 minutes	
100% IMS 2	3 minutes	
90% IMS 1	3 minutes	
dH_2O	2 minutes	
dH_2O	5 minutes	Dehydration of specimens allowing long-term storage of samples mounted in xylene based DPX
90% IMS 2	3 minutes	
100% IMS 3	3 minutes	
100% IMS 4	3 minutes	
Xylene 4 (100%)	5 minutes	
Xylene 5 (100%)	5 minutes	
Xylene 6 (100%)	5 minutes	
DPX mountant	-	Mounts slides enabling long-term storage

2.2.25 Haematoxylin staining

Following rehydration, slides were immersed in Harris' haematoxylin stain for 3 minutes prior to being rinsed in running tap water. Once the tap water ran clear, slides were placed in Scott's tap water for 1 minute to develop and fix the 'blue' stain. Slides were then dehydrated (Table 2.4) prior to imaging (Canon EOS 100D) and analysis.

2.2.26 TRAP staining in tissue sections

Osteoclasts were observed in murine joints using TRAP stain. The TRAP solution and TRAP preparation buffer were prepared as described in Table 2.2. After rehydration, slides were placed in TRAP preparation buffer overnight at room temperature. pH5 for the preparation buffer was maintained, and the next morning slides were placed in a moist incubation chamber where specimens were immersed in TRAP stain for 6 hours at 37^{o}C. After 6 hours, slides were washed for 5 minutes in dH_2O and ready for haematoxylin staining as in Section 2.2.25. If no

haematoxylin staining was carried out, slides were then taken through the dehydration procedure as described in Section 2.2.24. Once mounted, sections were visualised and imaged (Canon EOS 100D) prior to analysis.

2.2.27 Histological analysis: calculating the arthritis index, inflammatory index score, erosive score and osteoclast count

All stained sections were analysed using an established method (arthritis index; *Coppieters et al. 2006, Seeuws et al. 2010* and *Yang et al. 2013*). Scoring inflammatory infiltration of synovial tissue, joint exudate, synovial hyperplasia and bone erosion. The assessment of the arthritis index was carried out as described in Table 2.5 and Figure 2.20. Osteoclast-associated TRAP staining was counted manually and analysed using image analysis software (PhotoShop). An area of interest was created and the total number of pixels per area reported. A pre-set colour identifier (red) was then placed on top of the selected area where all pixels relating to that colour were identified and counted automatically, yielding the total TRAP pixels per unit area. This number was then converted into a percentage for comparison between joints. Finally, a manual count was completed identifying the number of $TRAP^{+ve}$ osteoclasts located in every joint.

T**able 2. 5 - Arthritis Index Scoring**.

Arthritis Index	Inflammatory Score	Synovial inflammation	0-Normal 1-Some inflammatory infiltrate but adiposity hardly affected (10% inflammatory, 90% adipose) 2-Similar amounts of inflammatory infiltrate to adipose tissue (50% inflammatory, 50% adipose) 3-Inflammatory cells dominate tissue with small amount of adipose tissue (70% inflammatory, 30% adipose) 4-Majority inflammatory cells with minimal adipose tissue (90% inflammatory, 10% adipose) 5-No adipose tissue, all inflammatory infiltrate (100% inflammatory, 0% adipose)
		Exudate	0-Normal 1-Inflammatory cells in exudate 2-High proportion of inflammatory cells in exudate with some fibrin deposits 3-High proportion of inflammatory cells in exudate with substantial fibrin deposits
		Hyperplasia and pannus formation	0-Normal 1-Synovial layer showing signs of thickening 2- Synovial layer creeping over the bone surface and invading the joint space 3- Synovial layer creeping over the bone surface and invading the joint space with visible signs of cartilage loss
	Degenerative Score	Bone erosions	0-Normal 1-Early stages of bone erosion including bone thinning 2-Detectable erosion of bone by pannus formation 3-Large area of bone eroded due to pannus

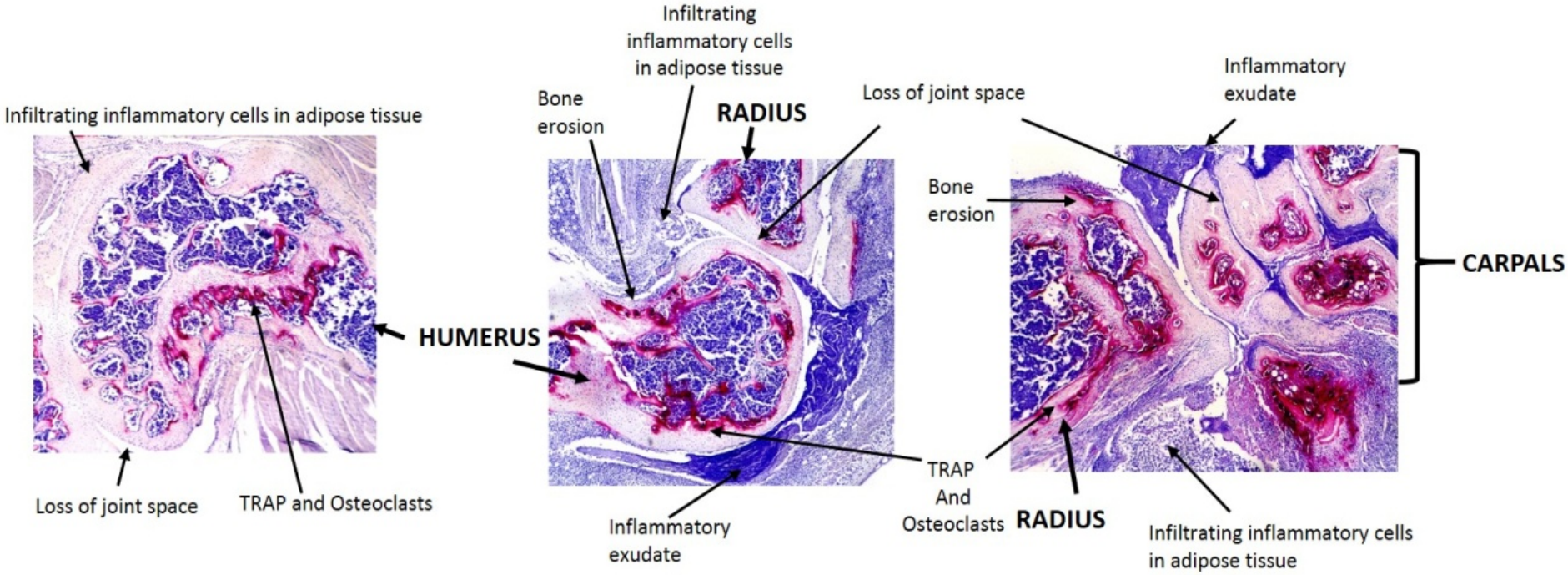

Figure 2. 20 - Arthritic Index Scoring. Each joint was assessed for visible signs of the four following categories; synovial inflammation, exudate, hyperplasia with pannus formation and bone erosions. In the shoulder joint only the head of the humerus was assessed, in the elbow joint the base of the humerus and radius were both assessed, and in the wrist joint the radius and carpals were assessed. The above example shows defined areas where these four parameters are met as indicated by the arrows.

2.2.28 Statistical Analysis

Data obtained in this thesis was processed using Microsoft Excel and GraphPad Prism, facilitating the graphical representation of the data. All results were reported as the mean ± standard error of the mean (SEM) unless otherwise stated. Prior to statistical analysis, significant outliers ($p \leq 0.05$) were identified through the Grubb's outlier test (GraphPad Quick Calcs) and removed from data sets. Multiple statistical tests were carried out in this thesis including a two-tailed Student's t-test (used for a comparison of two normally distributed individual data sets), one-way and two-way analysis of variance (ANOVA; for comparing time-courses or dose responses of multiple data sets) which utilised a Bonferroni post-test to highlight groups with significant differences, and finally Spearman's rank coefficient tests (to show correlational relationships between data sets) were reported. Where statistical significance was reported, a minimum p value of ≤ 0.05 was considered significant.

Chapter 3:Creating an automated computational algorithm for counting cells in human osteoclast differentiation assays

3.1 Introduction

Over the past 20 years, the study of *in vitro* human osteoclast differentiation has become common practice. In the 1980's the differentiation of the osteoclast from monocytes was discovered, where their distinct haematopoietic lineage from $CD14^{+ve}$ mononuclear cells was demonstrated providing definitive evidence (*Massey & Flanagan. 1999*). Several research groups supported the haematopoietic origin of the osteoclast and identified macrophage colony stimulating factor (m-CSF) and receptor activator of nuclear factor κβ ligand (RANKL) as critical soluble factors necessary for the differentiation and maturation of osteoclasts (*Nicholson et al. 2000)*.

The culture of osteoclasts was reported via two main techniques; monocultures and co-cultures. In monocultures m-CSF and RANKL are exogenously supplemented into the medium, whereas in co-cultures these soluble factors are endogenously secreted from bone marrow cells, osteoblasts or T cells (*Lacey et al. 1998, Takahashi et al. 1988, Nicholson et al. 2000, Boyle, Simonet & Lacey 2003, Lutter et al. 2010*). m-CSF is used across a broad concentration range (5-25ng/mL) in the literature to facilitate the proliferation and survival of $CD14^{+ve}$ mononuclear cells in culture (*Massey & Flanagan, 1999, Nicholson et al. 2000, Kim et al. 2005, Hodge et al. 2011)*. RANKL, at concentrations from 3 to 100ng/mL, is reported to induce mononuclear cell differentiation into osteoclasts (*Quinn et al. 1998, Udagawa et al. 2000, Nicholson et al. 2000, Han et al. 2001)*. The range of RANKL concentration can be applied to cultures due to differences in precursor cell purity, number, source, cell subset, culture medium and substrate/adherent surface supporting cell culture. m-CSF and RANKL concentrations are generally lower in co-culture methods using $CD14^{+ve}$ cells cultured with T cells due to their ability to secrete RANKL. Furthermore, concentration may alter depending on the length of the assay and pre-defined primary outcomes; RANKL concentrations are generally lower for extended time-courses measuring osteoclast function versus shorter experiments studying osteoclast differentiation (*Nicholson et al. 2000, Lutter et al. 2010)*.

The interpretation of osteoclast differentiation assays is usually a result of several assessment criteria including; total cell count, osteoclast count, osteoclastogenesis

(as a percentage of total cells) and area of bone substrate resorbed. Substantial variability in the published literature with regard to each parameter due to their dependence on culture methodologies does exist; [m-CSF and RANKL], length of culture, seeding density, total area seeded, intra-assay reproducibility and inter-donor variability. To acquire such data, the methodologies used required consideration. Counting methods generally apply to cells in suspension (haemocytometer, fluorescent activated cell sorting, a spectrophotometer, electrical gating, medical imaging and manual counts) and cannot be utilised during the course of the osteoclastogenesis assays which rely upon cells adhering to matrix (*Tzur et al. 2011, Bonetta et al. 2005)*. Adherent cells would therefore need to be counted manually using a slow, laborious, time consuming microscopic method. The first aim of the project, was therefore to create a novel, automated computer algorithm to count adhered cells that was accurate, reduced analysis time and minimised inter-analyst errors in counting. It was considered an essential first step for delivery of data from the multiple osteoclast assays planned for this thesis.

Additional to total cells, $TRAP^{+ve}$ cell data is also important when interpreting osteoclast assay data (*Nicholson et al. 2000, Boyle, Simonet& Lacey 2003)*. In addition to this cell specific marker for osteoclasts, secondary soluble factors (e.g. TRAP5b and CTX-1) are frequently measured (sample/tissue culture supernatants, blood and synovial fluid) as surrogate markers of osteoclast activation and bone resorption (*Halleen et al. 2000*, *Chailurkit et al. 2001, Shidara et al. 2008, Chubb et al. 2012)*. Resorption of bone matrix/bone substrate is identified *in vitro* with toluidine blue staining of areas resulting in a blue perimeter around the resorbed area (*Keller et al. 2012*). Osteoclastogenesis cultures are also suggested to secrete several pro-inflammatory cytokines (IL-6, IL-1, TNF-α) and chemokines (CXCL8, CCL3, CCL2 and CCL5), which have all been implicated in the indirect differentiation and function of the osteoclast (*Scheven et al. 1999, Kobayashi et al. 2000, Wintges et al. 2003, Kim et al. 2005, Yoshitake et al. 2008, Dapunt et al. 2014)*. The direct link between these cytokines/chemokines, the differentiation of $CD14^{+ve}$ mononuclear cells into osteoclasts and their subsequent resorption has not yet been fully determined in a monoculture system.

The aim of this chapter was to establish a reproducible monoculture method for human osteoclasts *in vitro* to assist in the creation and validation of a novel, high-throughput, automated computer algorithm for acquiring total cell counts in adherent cell cultures. Characterisation of adhered cells, resorption pit analysis and the quantification of cytokines and chemokines in culture supernatants were also performed. Osteoclast-associated soluble factors with potential importance for modulating pain, inflammation and bone pathology during inflammatory arthritis could therefore be postulated. This chapter details methodology, results and discussion points under the following objectives:

- To validate a reproducible and reliable method of osteoclast differentiation from $CD14^{+ve}$ monocultures over a 17-day time course in differentiation medium.
- To create and validate a novel, automated, high-throughput and sensitive method for counting total number of cells on a plate.
- To identify and measure potential early surrogate soluble markers of osteoclast differentiation from $CD14^{+ve}$ monocultures exposed to m-CSF and RANKL.

3.2 Essential Methodology

The below diagrams highlight the essential methods used throughout this chapter. Full detail of all these methods can be found in their respective sections in Chapter 2 as stated.

- ***Osteoclast assay set up (Chapter 2 Sections 2.2.1 - 2.2.4)***

Condition	Number of Donors	Number of Replicate Disks per donor	Comments
m-CSF only	8	3	Used within Sections 3.3.2 to 3.3.5. Mean of replicates plotted for each time-point
m-CSF and RANKL	8	3	
m-CSF only	8	3	Used within Sections 3.3.7 to 3.3.9 and Section 3.2.11. Mean of replicates plotted for each time-point.
m-CSF and RANKL	8	3	

-PBMCs isolated from healthy human whole blood via density centrifugation went through magnetic activated cell sorting to yield a pure suspension of $CD14^{+ve}$ monocytes (as illustrated below).

- Disks were seeded with 3.2 x 10^6 cells and cultured with m-CSF alone (5ng/mL) or in combination with RANKL (5ng/mL). Culture supernatants collected and replenished every 3-4 days. Disks harvested at each time-point.

Caption 1 - Isolation of human $CD14^{+ve}$ monocytes from peripheral blood. Human blood layered onto hisotpaque is centrifuged yielding peripheral blood mononuclear cells. $CD14^{+ve}$ monocytes isolated by magnetic activated cell sorting and 3.2 x 10^6 cells/mL are seeded onto ivory disks prior to culture in osteoclast proliferation/differentiation medium.

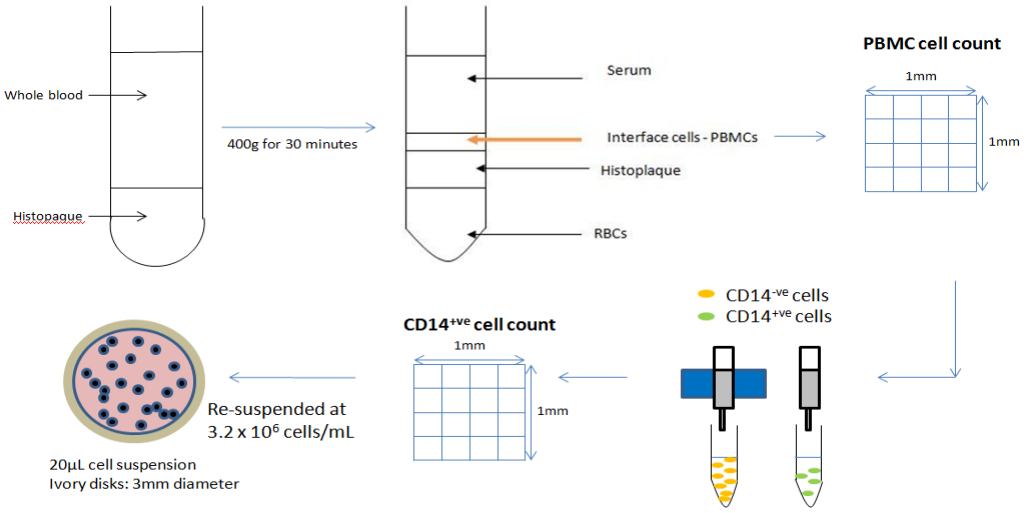

- ***Quantitative parameter assessment of the osteoclast assay***

-Disks harvested at days 0, 7, 10, 14 and 17 were fixed with glutaraldehyde prior to staining with TRAP and haematoxylin to identify total cells and osteoclasts; quantified through MATLAB and manual counts. Following cell counts adhered cells were removed and disks stained with toluidine blue or calcein to facilitate quantification of resorbed area. Harvested supernatants were analysed by ELISA.

Caption 2 - The osteoclast assay and functional analyses. Disks seeded with $CD14^{+ve}$ monocytes are cultured up to day 17 in the presence of M-CSF and RANKL. Every 3-4 days disks and their supernatants were harvested and used for one of the following analyses; cell staining (TRAP and haematoxylin), area of resorption quantification (toluidine blue or calcein) and ELISA.

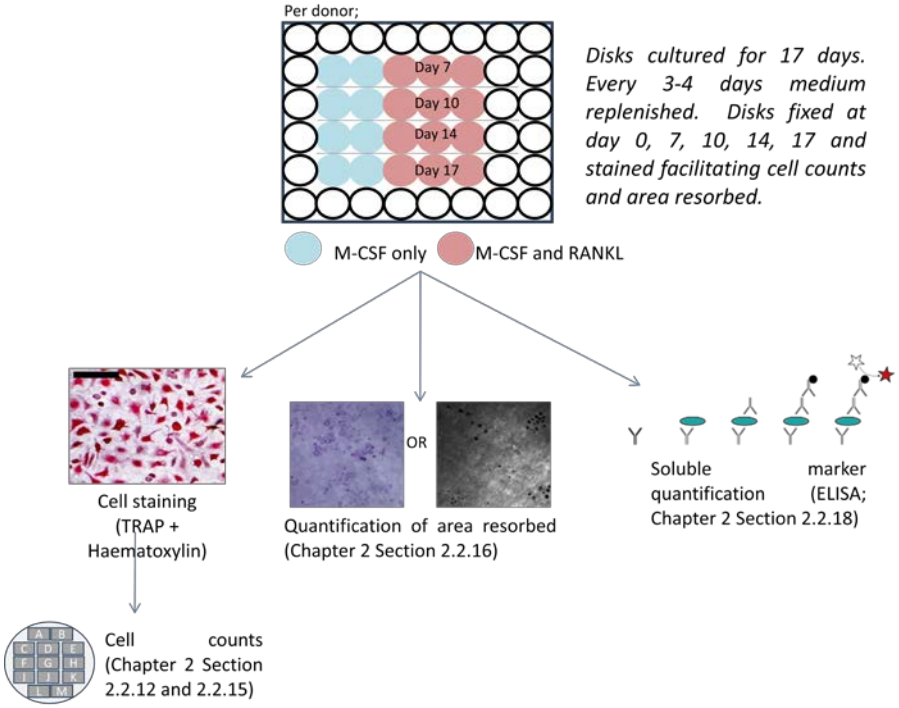

3.3 Results

3.3.1 Proliferation medium supplemented with 10ng/mL m-CSF resulted in increased mononuclear cell number

Human osteoclast assays established by a previous PhD student utilized m-CSF concentrations of 5ng/mL which yielded approximately 518 ± 56 cells/mm^{2}at day 0. In the initial assays conducted for this thesis, at day 0 cell numbers were substantially lower at 311 ± 15 cells/mm^2, when using the same reagents and culture conditions. These low cell numbers were found to be insufficient for the completion of osteoclast differentiation assays.

Altering the concentration of m-CSF to 10ng/mL increased the total cell count to 565 ± 31cells/mm^2 at day 0 (Figure 3.1), and restored the cell density to a level that was comparable to previously established assays. All subsequent assays used m-CSF at 10ng/mL for the proliferation phase. Assays where <500 cells/mm^2 were recorded at day 0 were terminated due to insufficient cell number. Assays with >500 cells/mm^2 were then supplemented with differentiation medium (5ng/mL m-CSF and 5ng/mL RANKL) inducing osteoclast differentiation.

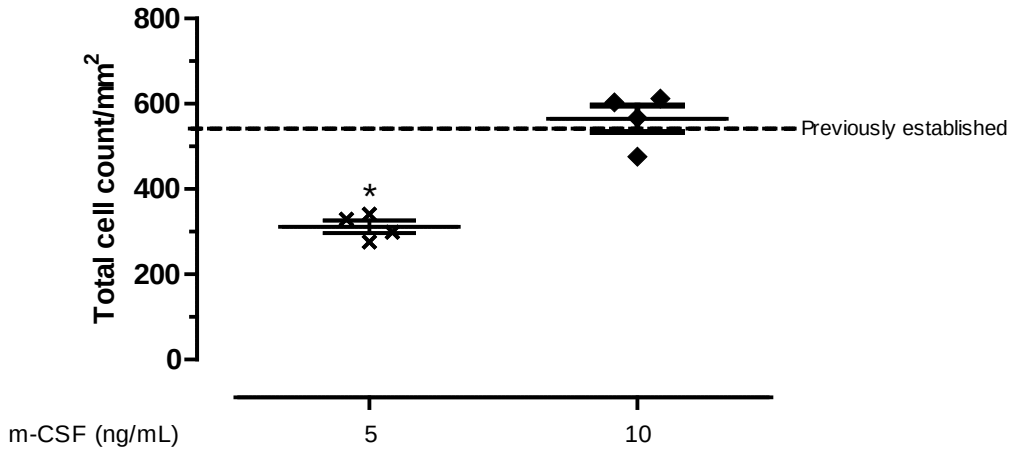

Figure 3. 1 - Supplementation of proliferation medium with 10ng/mL m-CSF led to an increase in total cell count at day 0. Previously established assays using 5ng/mL m-CSF (completed by previous PhD student) yielded a significantly higher number of total cells (dashed line) when compared to those initially ran in this project (presented as crosses). Optimisation to 10ng/mL m-CSF in proliferation medium led to comparable total cell counts to previously reported, and showed a concentration dependent effect of m-CSF (presented as filled diamonds). Statistical analysis using a Student's t-test was performed between values obtained at both 5ng/mL and 10ng/mL m-CSF compared to previously established values, and mean ± SEM data values are shown; Significance * refers to $p \leq 0.05$. (Data plotted refers to 4 disks from 1 donor).

3.3.2 Visualising the differentiation of human osteoclasts across a 17 day time-course

Human $CD14^{+ve}$ mononuclear cells were cultured in differentiation medium for a total of 17 days resulting in the formation of osteoclasts. Throughout the time-course of the assay disks were harvested, fixed and stained with haematoxylin and TRAP. Representative images across the time-course illustrate cell phenotypes adhered to disks; mononuclear cells, $TRAP^{+ve}$ nucleated cells (up to, and including, 2 nuclei) and $TRAP^{+ve}$ multinucleated osteoclasts (Figure3.2). At day 0, cells present were small (32µm in diameter), mononucleated cells stained only with haematoxylin and were found within close vicinity to each other. Seven days later, the presence of larger $TRAP^{+ve}$ multinucleated cells were evident, reaching around 37µm in diameter, where a reduction in total cell coverage of the disk was noted. Along with these larger cells, a small number of $TRAP^{+ve}$ mononuclear cells were also present. After a further 3 days (day 10), the presence of $TRAP^{+ve}$ multinucleated osteoclasts was seen, along with a further reduction in cell density. The diameter of these large $TRAP^{+ve}$ osteoclasts ranged from 61µm to >100µmwith no pattern in shape or surface area occupied. At day 14, $TRAP^{+ve}$ osteoclasts and $TRAP^{+ve}$ multinucleated cells were still present, although fewer total cells were visualised adhered to the disks, possibly due to multinucleation. At the final time-point of day 17, $TRAP^{+ve}$ multinucleated cells were present but cells expressed unusual phenotypes, possibly characteristic of cell death.

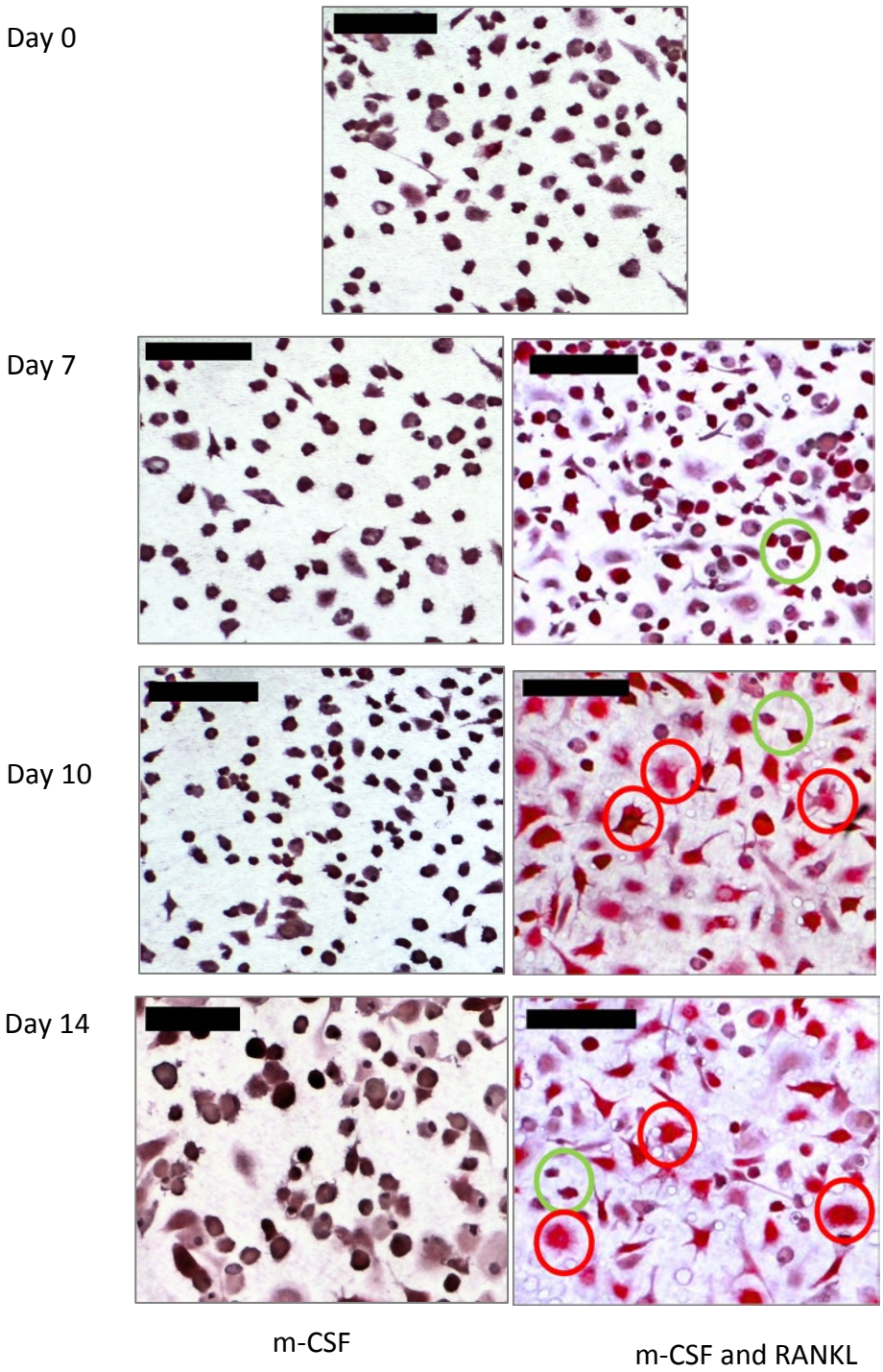

Figure 3. 2 - Representative images across the time-course of the osteoclast differentiation assay. At day 0, 7, 10, and 14 of the osteoclast assay, disks were harvested, fixed and stained using haematoxylin and TRAP. Multiple TRAP^{+ve} mononuclear cells (green circles)and multinucleated osteoclasts (red circles)were visualised in cultures supplemented with RANKL across the time-course. In m-CSF only cultures only haematoxylin stained cells were visible. Scale bar = 100µm.

3.3.3. Total cell counts were highly labour intensive but did show a decrease across a 17-day time-course

The number of total cells adhered to the ivory disks was counted manually. At day 0, 15,288 ± 2,296 cells/disk were reported which substantially reduced to 4,713 ± 1,494 cells/disk at day 17 (no statistics carried out as disks arose from n=1 donor, 3 disks per time-point; Figure 3.3). The manual counting process used took >100 hours to complete due to the necessity of replicates from just one donor. This manual cell counting was also prone to analyst variability (two analysts) due to the high number of cells to be counted.

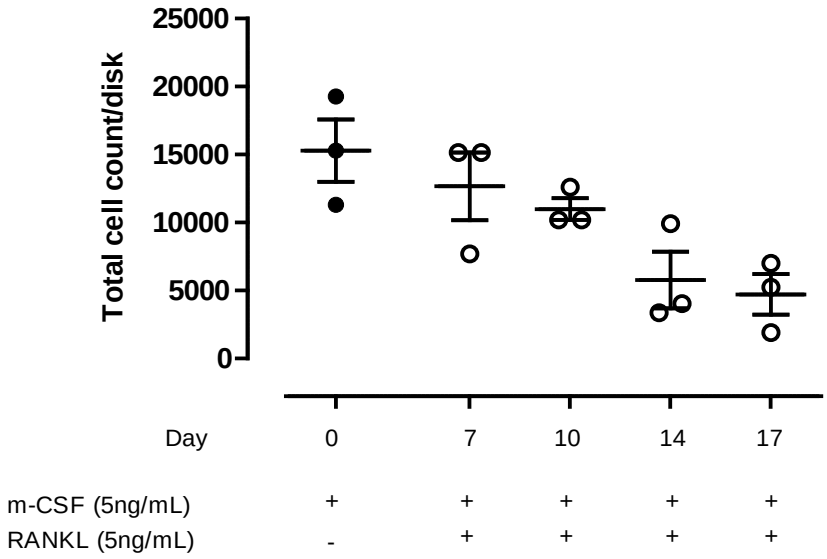

Figure 3. 3 - Total cell count from one donor reduces over a 17-day time-course. Total cell count was obtained through manual counts of cells adhered to each disk. Data was obtained from three replicate disks seeded with $CD14^{+ve}$ cells and cultured over the time-course of the assay. Total cell count reduced in equal decline from day 0 to day 17 where a minimum total count was obtained. Mean ± SEM is shown, statistical analysis was not done due to donor number=1; 3 replicate disks per donor.

3.3.4 The automated cell counting method was successfully validated

To ensure the accuracy and validity of the data yielded from the automated algorithm, 8 random images from the completed osteoclast assays were selected and run through manual and automated cell counts. From the initial comparison, a large degree of error was shown between these two methods reaching a maximum of 78% difference. From the automated method, each histogram bin obtained was analysed to determine whether its contents were objects (i.e. cells) or noise. Analysis showed that there were a vast number of objects always located within histogram bin 1 which was set at 0-100 pixels. From the analysis of the subplots, this bin was shown to be selecting noise (individual or small groups of pixels which were not cells) as objects, and recording these. Subsequently, total cell count increased and the percentage difference between manual counts and automated counts was 11.7% to 78.1%, an unacceptable value (Table 3.1).

Histogram bar 1 was thus removed from total cell counts, and a further comparison between manual cell count and automated cell count minus histogram bin 1 was conducted. A total percentage difference of 12.8% was found, which when compared to the total percentage difference of two manual counts (25.7%) showed no significant difference (Table 3.1). Automated total counts (minus histogram bar 1) were therefore obtained using this automated method and used for the remaining experiments within this thesis. For additional quality control, after every 40 images a manual cell count was performed (~10 images per experiment), where results had to fall within the acceptable percentage difference criteria.

Table 3. 1 - A comparison between manual and automated total cell counts.*8 randomly selected images were counted manually and using the automated algorithm (Disk 1-8) and total counts were compared. A comparison between two manual counts from two different analysts was also performed across five different randomly selected disks to give a baseline error percentage (Disks A-E).*

Disk	Total Cell Count (Manual)	Total Cell Count (Automated)	% Difference
1	3128	3819	-22.1
2	541	926	-71.2
3	1687	3004	-78.1
4	759	1038	-36.8
5	989	1147	-16.0
6	129	214	-65.9
7	48	77	-60.4
8	145	162	-11.7

Disk	Total Cell Count (Manual)	Total Cell Count (Automated: minus histogram bin 1)	% Difference
1	3128	2978	4.8
2	541	546	-0.9
3	1687	1639	2.8
4	759	679	10.5
5	989	936	5.4
6	129	132	-2.3
7	48	45	6.3
8	145	132	9.0

Disk	Total Cell Count (Manual 1)	Total Cell Count (Manual 2)	% Difference
A	655	674	-2.9
B	448	399	10.9
C	297	341	-14.8
D	290	283	2.4
E	417	389	6.7

3.3.5 A significant reduction in total cell count occurred after seven days culture in differentiation medium

Total cell count at day 0 was 14,043 ± 1,576 cells/disk, which after seven days culture in differentiation medium significantly reduced to 8,187 ± 5,671 cells/disk ($p \leq 0.01$). A further reduction from day 7 to day 10, and day 10 to day 14 was noted; 5,671 ± 817 cells/disk and 2,789 ± 413 cells/disk respectively, which corresponded with the decrease in cell density presented in the images. A reduction in total cell count was seen from day 14 to day 17 (1,716 ± 377 cells/disk) was believed to be due to cell senescence and death. For this reason all subsequent assays were only performed up until day 14 (Figure 3.4).

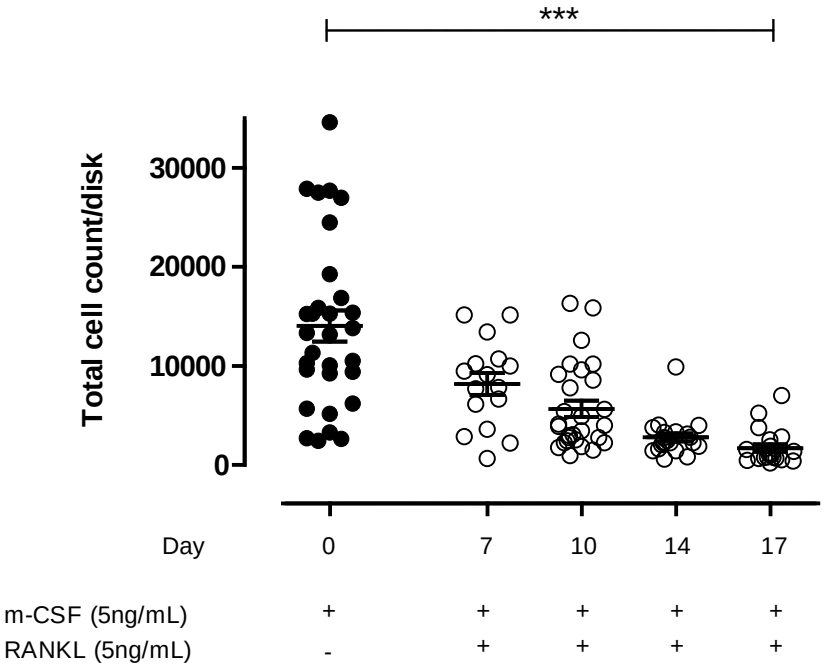

Figure 3. 4 - Total cell count over a 17-day time-course.. A significant reduction in total cell count was seen over the 17-day time-course after culture in differentiation medium. A substantial decrease was seen 7 days after supplementation with m-CSF and RANKL. At day 17, low cell counts were obtained suggesting cell senescence, therefore future assays terminated at day 14. Values were obtained from n=8 donors (3 disks per donor at each time-point) and mean ± SEM is shown. Statistical analysis was performed using a one-way ANOVA with a Bonferroni post-test. Significance *** refers to $p<0.001$.

3.3.6 The creation of an automated total counting algorithm substantially reduced analysis time and increased total cell count accuracy

Analysis time was reduced 10-fold from 100 to 9 hours per donor (n=1) when using the automated counting algorithm opposed to manual counts. The accuracy and reproducibility of results obtained also improved due to a lack of inter-analyst variability. However, the automated method did contain a major limitation by not deciphering $TRAP^{+ve}$ from $TRAP^{-ve}$ cells. This analysis of $TRAP^{+ve}$ cells and osteoclasts was therefore completed manually.

3.3.7 $TRAP^{+ve}$ cell counts significantly increased after seven days of culture in RANKL medium

After the addition of RANKL, $TRAP^{+ve}$ cell number was monitored across the time-course of the differentiation assay (Figure 3.5). A significant increase in $TRAP^{+ve}$ cell number from 0 ± 0 $TRAP^{+ve}$ cells/disk at day 0, to 2,266 ± 481 at day 7 ($p<0.0001$) was seen. After a further 4 days in culture (day 10), $TRAP^{+ve+}$ cell number increased to 4,982 ± 1162 cells/disk, supporting the presence of $TRAP^{+ve}$ cells in representative images in Figure 3.2. From day 10 a significant reduction occurred to day 14, resulting in 2,450 ± 424 cells/disk where cells had fused into larger multi-nucleated cells *i.e.* osteoclasts.

3.3.8 Osteoclast numbers peaked after 10 days of culture in differentiation medium

Osteoclasts form from the fusion of $TRAP^{+ve}$ mononuclear cells in the presence of m-CSF and RANKL. Osteoclasts significantly increased from day 0 to day 7 in m-CSF and RANKL cultures; 0 ± 0 osteoclasts/disk to 120 ± 80 osteoclasts/disk ($p<0.01$, Figure 3.6). A peak in osteoclast numbers was shown after ten days where osteoclast numbers reached 325 ± 71 osteoclasts/disk. After a further 4 days osteoclast number slightly decreased to 85 ± 43 osteoclasts/disk, but this was not significant, suggesting that at day 14 either $TRAP^{+ve}$ cells were fusing to form giant multinucleated cells, or were being lost through cellular senescence, reducing $TRAP^{+ve}$ cells.

3.3.9 Percentage osteoclastogenesis significantly increased in the presence of RANKL to a peak at day 10

The percentage of osteoclastogenesis at day 0 was 0% due to the absence of RANKL (Figure 3.7). In the presence of RANKL a significant increase in osteoclastogenesis across the 14-day time-course was found ($p<0.0001$). Reported here, the percentage of osteoclastogenesis was shown to increase to 0.8 ± 0.5% at day 7, to a peak of 2.3 ± 0.8% at day 10, after which it reduced to 2.0 ± 0.9%. This data confirmed the successful differentiation of the osteoclast but revealed no information regarding functional resorptive activity.

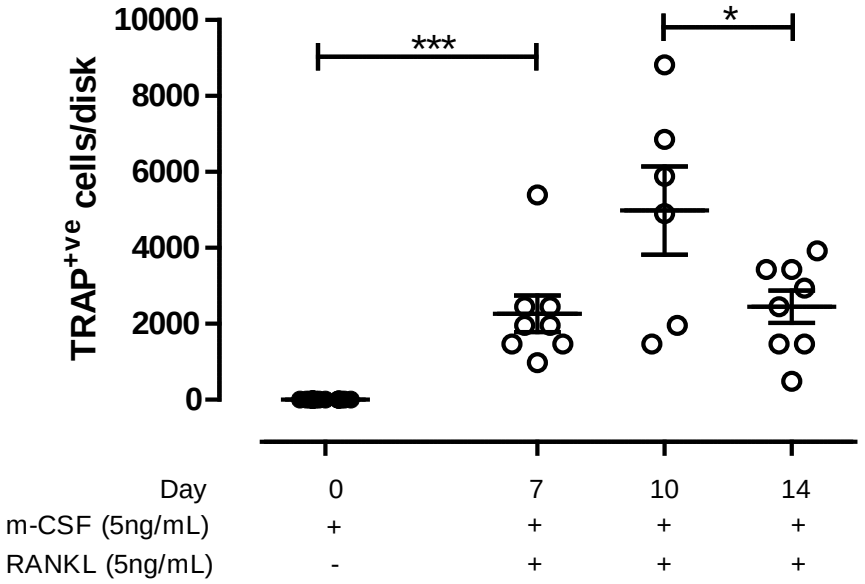

Figure 3. 5 - TRAP^{+ve} cell count significantly increased after seven days of culture in RANKL medium.. From Day 0, differentiation cultures were supplemented with m-CSF and RANKL. After 7 days of culture TRAP^{+ve} cells significantly increased and were shown to reach a peak number at day 10. A significant reduction in TRAP^{+ve} count then followed to day 14. Values were obtained from 8 donors (3 disks per donor per time-point, mean plotted) and the mean ± SEM is shown. Statistical analysis was performed using a one-way ANOVA with a Bonferroni post-test(between day 10 and 14) and a Student's t-test (between day 0 and 7 due to different culture medium). Significance * and *** refers to $p<0.05$ and $p<0.001$ respectively.

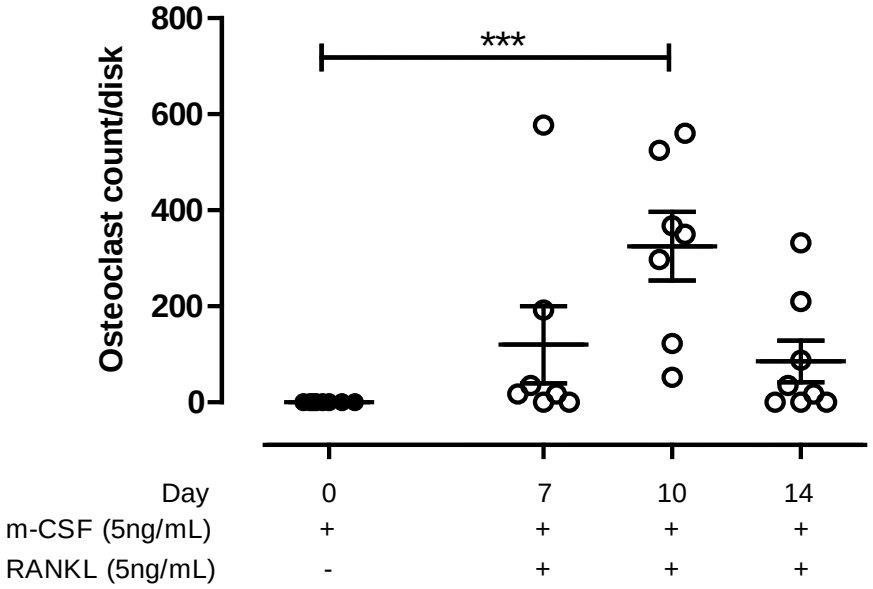

Figure 3. 6 - Osteoclast count significantly increased after seven days of culture in differentiation medium.Through the addition of RANKL, an increase in osteoclast count from day 0 to day 7 was seen. A significant increase in osteoclast number was found after day 10, following which a decline was noted. Values were obtained from n=8 donors (3 replicate disks per donor per time-point, mean plotted) and mean ± SEM shown. Statistical analysis was performed using a Student's t-test. Significance *** refers to $p<0.001$.

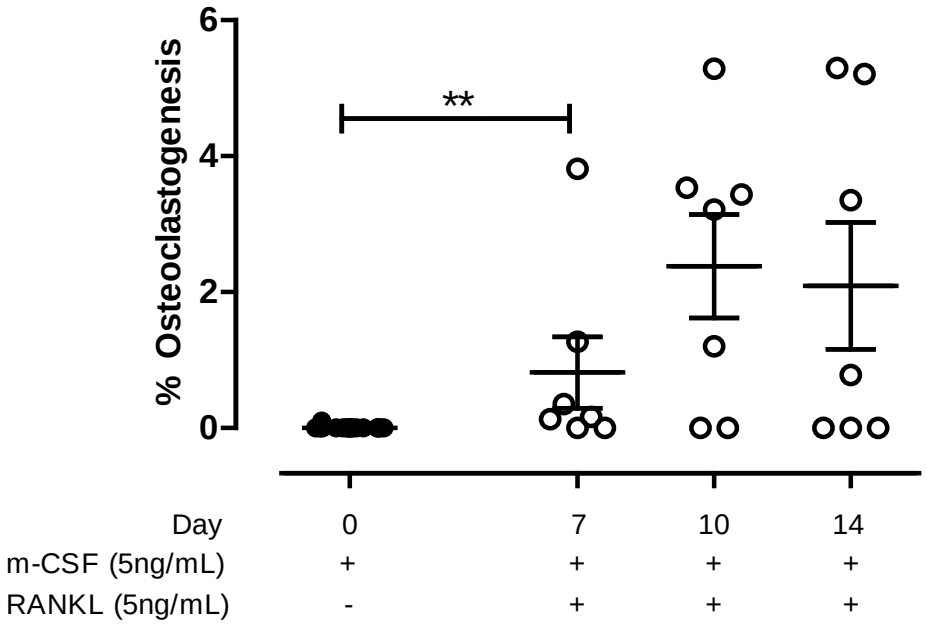

Figure 3. 7 - Percentage osteoclastogenesis significantly increased due to the addition of RANKL.After seven days of culture in differentiation medium a significant increase in percentage osteoclastogenesis was seen compared to day 0. This increase continued to day 10, where peak osteoclastogenesis was seen, further supporting previously reported increases in $TRAP^{+ve}$ and osteoclast counts. Following this a reduction in percentage osteoclastogenesis was noted at day 14. Values were obtained from n=8 donors (3 replicate disks per donor per time-point, mean plotted) and mean ± SEM shown. Statistical analysis was performed using a Student's t-test. Significance ** refers to $p<0.01$.

3.3.10 Novel analysis of 2D resorptive parameters by confocal microscopy showed no significant improvement in sensitivity or accuracy

A novel method of analysis was tested in this chapter with the aim to improve the sensitivity and accuracy of calculating total area resorbed (Figure 3.8). The traditional toluidine blue staining method was used to show an average of 3.3 ± 1.4% resorption from 12 individual images. Alongside this, confocal microscopy images of the same 12 disks were collected using a x20 lens. A slight increase in area resorbed was found using this confocal methodology due to increased resolution; 4.4 ± 1.0%, however no significant increase was found. Due to the highly labour-intensive and costly method of confocal microscopy, the traditional toluidine blue method was used to determine surface area eroded within subsequent chapters.

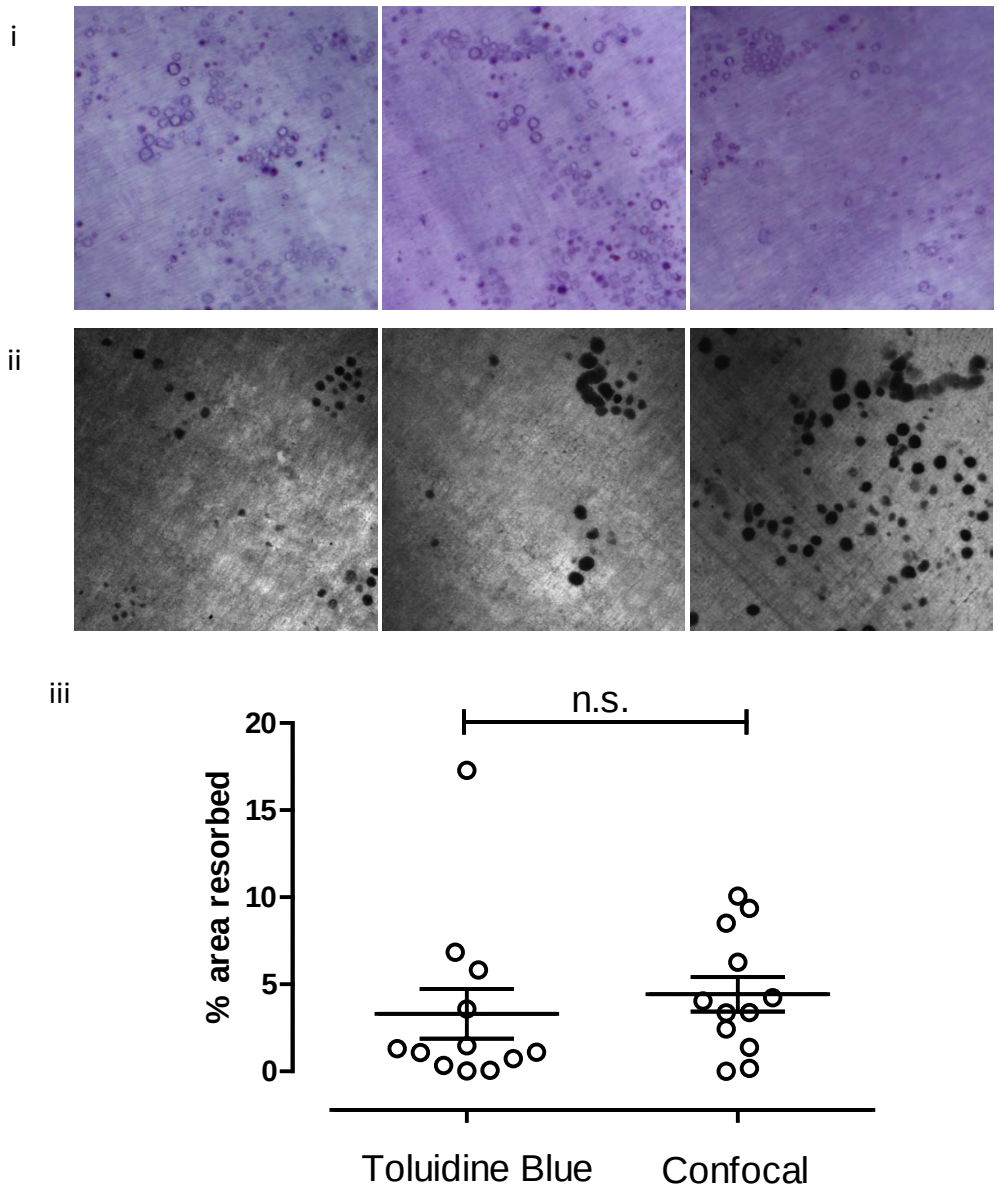

Figure 3. 8 - A novel analysis method for calculating percentage area resorbed.A comparison between traditional toluidine blue staining of disks (i) and x20 confocal data yielded from calcein stained disks (ii) harvested from human osteoclast differentiation assays at day 14. No significant increase in sensitivity for percentage area resorbed was shown using the x20 confocal analysis method when compared to traditional toluidine blue methodology (iii) (p= 0.5236). Values were obtained from 12 disks (duplicate disks from n=6 donors) and mean ± SEM is shown. Statistical analysis was performed using a Student's t-test. (for toluidine blue images 1 pixel = 0.48µm, for confocal images 1 pixel= 0.8µm).

3.3.11 Establishing the importance of CCL2, CCL3, CCL5, IL-6 and TNF-α inhuman osteoclast differentiation *in vitro*

To identify which cytokines and chemokines were expressed and secreted during the time-course of the osteoclast assay, supernatants were harvested and stored at -80^{o}C upon collection. Supernatants were then analysed via ELISA (R&D systems) for the presence of specific pro-inflammatory cytokines and chemokines. The cytokines IL-6 and TNF-α were measured due to their relationship and role in inflammatory arthritis and destructive bone diseases. The chemokines CCL3, CCL2 and CCL5 were also measured due to their significantly elevated concentrations in inflammatory and destructive bone diseases.

3.3.11.1 IL-6 was present in culture supernatants across the 14-day time-course of human osteoclast differentiation

IL-6 was identified in all supernatants across the time-course. Within m-CSF only cultures, 151.9 ± 56.31 pg/mL IL-6 was found at day 0, which decreased to 96.28 ± 39.63 pg/mL at day 3 and continued to decrease until day 14 where 52.16 ± 36.36 pg/mL IL-6 was found, (but not significantly; p=0.5949, Figure 3.9). In comparison, m-CSF and RANKL cultures showed a decrease from 61.24 ± 25.23 pg/mL at day 3 to 52.93 ± 14.76 pg/mL at day 7, followed by a slight increase in IL-6 concentration to 81.86 ± 30.36 pg/mL at day 10. A final decrease to 60.95 ± 24.24 pg/mL was then seen at day 14 (Figure 3.9).

Secondary to this, the amount of IL-6 secreted per cell was next assessed. A significant reduction in IL-6 secretion was shown across the time-course in m-CSF only cultures from 0.95 ± 0.37pg/mL at day 0 to 0.14 ± 0.11pg/mL at day 14 ($p<0.05$). In m-CSF and RANKL cultures IL-6 increased across the time-course (0.48 ± 0.17pg/mL at day 7 to 1.09 ± 0.58pg/mL at day 14) but not significantly. Peak IL-6 secretion per cell was shown around day 10 in m-CSF and RANKL cultures, which was simultaneous with peak osteoclast numbers.

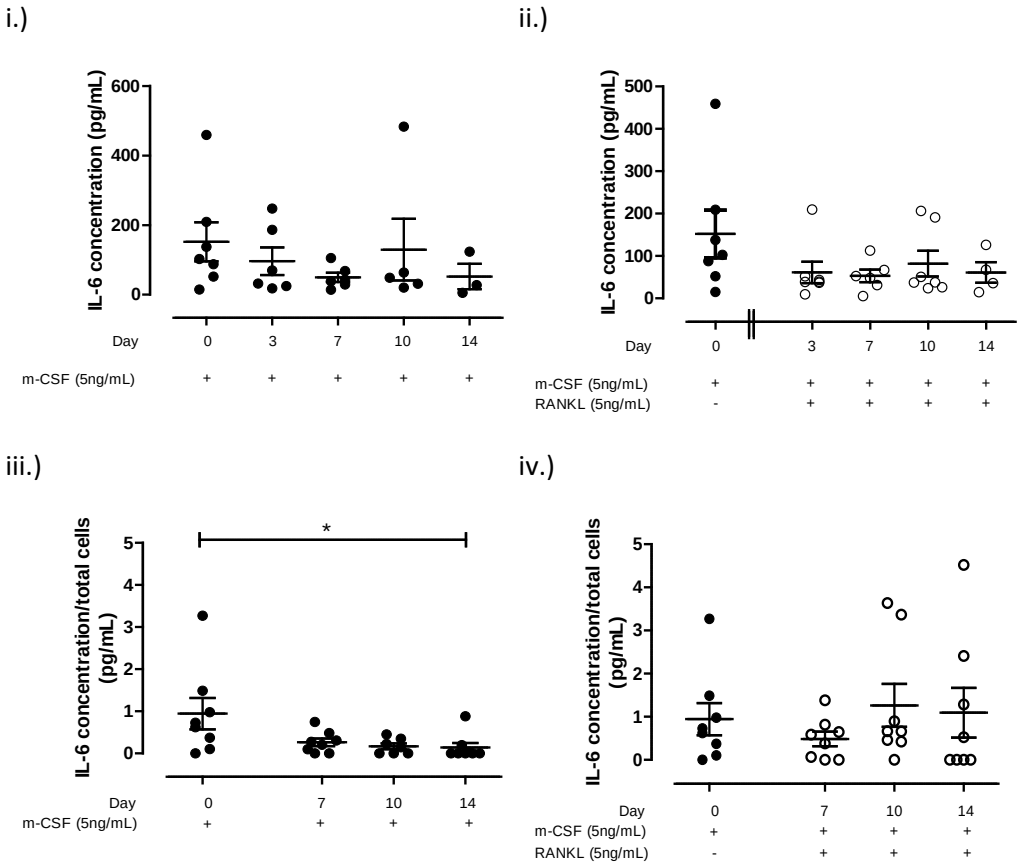

Figure 3. 9 - IL-6 secretion/cell increased in the presence of RANKL in osteoclast cultures.i.) IL-6in m-CSF only cultures reduced over the 14 day time-course but this was not significant (p=0.5949). ii.) After culture in m-CSF and RANKL, no significant increase in IL-6 concentration was quantified, but concentration levels were maintained across the time-course from day 3 to day 14. iii.) The secretion of IL-6 per cell was shown to significantly decrease over the 14 day time-course in m-CSF only supplemented cultures. iv.) In the presence of m-CSF and RANKL a slight increase of IL-6 secretion/cell at day 10 was seen, occurring at a comparable time to peak osteoclast number. Values plotted from n=8 donors (the mean from 3 disk replicates per donor per time-point is reported) and mean ± SEM is shown. Samples below the lower limit of quantification had no value recorded, explaining why some time-points do not have 8 replicates. Statistical analysis was performed using a ANOVA with a Bonferroni post-test. Significance * refers to $p<0.05$.

3.3.11.2 *TNF-α was not secreted directly from the osteoclast*

In cultures supplemented with m-CSF only, and m-CSF and RANKL, TNF-α was not detectable as results were found to be below the lower limit of quantification (15.6pg/mL).

3.3.11.3 *Levels of CCL5 were undetectable within human osteoclast culture supernatants*

CCL5 was found to be below the lower level of quantification (15.6pg/mL) in supernatants tested from all donors (n=8).

3.3.11.4 *CCL2 concentration significantly reduced in osteoclast culture supernatants*

CCL2 significantly decreased in m-CSF only cultures from 21.9 ± 2.3 ng/mL at day 0, to 13.9 ± 2.3ng/mL at day 7, and finally to 8.0 ± 3.8 ng/mL at day 14 ($p \leq 0.05$, Figure 3.10). In m-CSF and RANKL cultures, a significant reduction in CCL2 was also seen, where similar levels of CCL2 were shown; 18.6 ± 5.4 ng/mL at day 7, and 7.6 ± 2.2 ng/mL at day 14 ($p \leq 0.05$, Figure 3.10). The concentration of CCL2/cell showed a significant decrease in m-CSF only cultures but not in m-CSF and RANKL cultures.

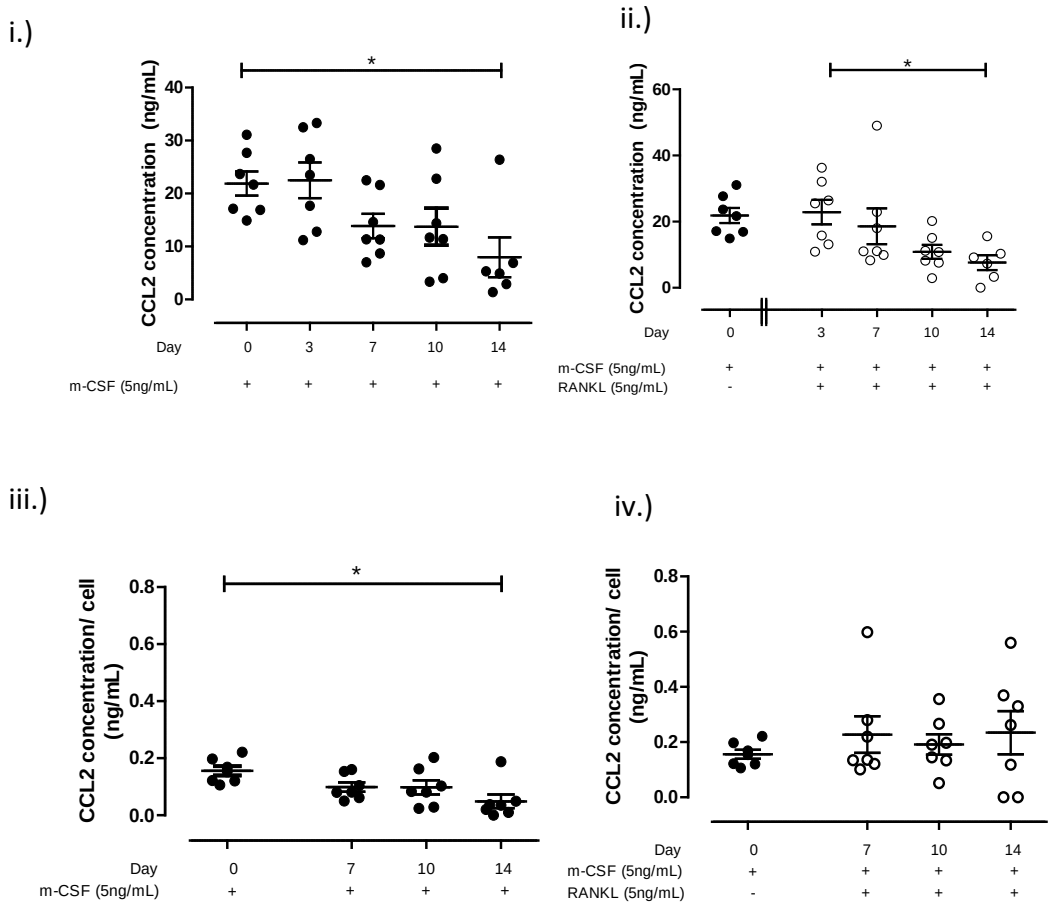

Figure 3. 10 - CCL2 was not directly secreted from the osteoclast in human *in vitro* osteoclast assays.. i.)CCL2 in m-CSF only cultures significantly reduced over the 14 day time-course. ii.) Through the supplementation of RANKL, a significant decrease in CCL2 concentration resulted over the time-course from day 3 to day 14. iii.) and iv.) CCL2 secretion/cell showed a significant reduction in m-CSF only conditions but not in differentiation cultures. Values plotted from n=8 donors (the mean from 3 disk replicates per donor per time-point is reported) and mean ± SEM is shown. Samples below the lower limit of quantification had no value recorded, explaining why some time-points do not have 8 replicates. Statistical analysis was performed using a ANOVA with a Bonferroni post-test. Significance * refers to $p<0.05$.

3.3.11.5 *CCL3 secretion per cell was shown to significantly increase after the addition of RANKL where a significant correlation between osteoclast number and CCL3 was shown*

m-CSF only cultures showed a concentration of CCL3 which was maintained across the 14-day time-course; at day 0 93.78 ± 23.03 pg/mL and at day 14 81.29 ± 25.73 pg/mL (Figure 3.11). Alternatively, CCL3 concentration in m-CSF and RANKL supplemented cultures at day 3 increased to 159.6 ± 21.22pg/mL from day 0, but this was not significant ($p=0.0580$) (Figure 3.11).The increase in CCL3 between day 0 and day 3 was noted to occur prior to peak osteoclast numbers as shown in Figure 3.6, and only occurred in m-CSF and RANKL cultures. After 7 days in m-CSF and RANKL cultures, CCL3 concentration decreased to 109.3 ± 13.86 pg/mL, before falling to 102.5 ± 32.23 pg/mL at day 10 and 87.52 ± 11.99 pg/mL at day 14.

The analysis of CCL3 secretion per cell showed no significant change in m-CSF only cultures; 0.76 ± 0.19pg/mL at day 0 and 0.51 ± 0.17pg/mL at day 14.In m-CSF and RANKL cultures a significant increase of CCL3 secretion per cell across the time-course was quantified ($p<0.05$). This coincided with increasing osteoclast numbers and thus a relationship between CCL3, RANKL and osteoclast number was postulated. No significant correlation between total cell count and CCL3 concentration was quantified, but a significant and positive relationship between osteoclast number and CCL3 concentration was present ($p\leq0.01$, $R=0.3221$); thus suggesting a role for CCL3 in RANKL-induced osteoclast differentiation.

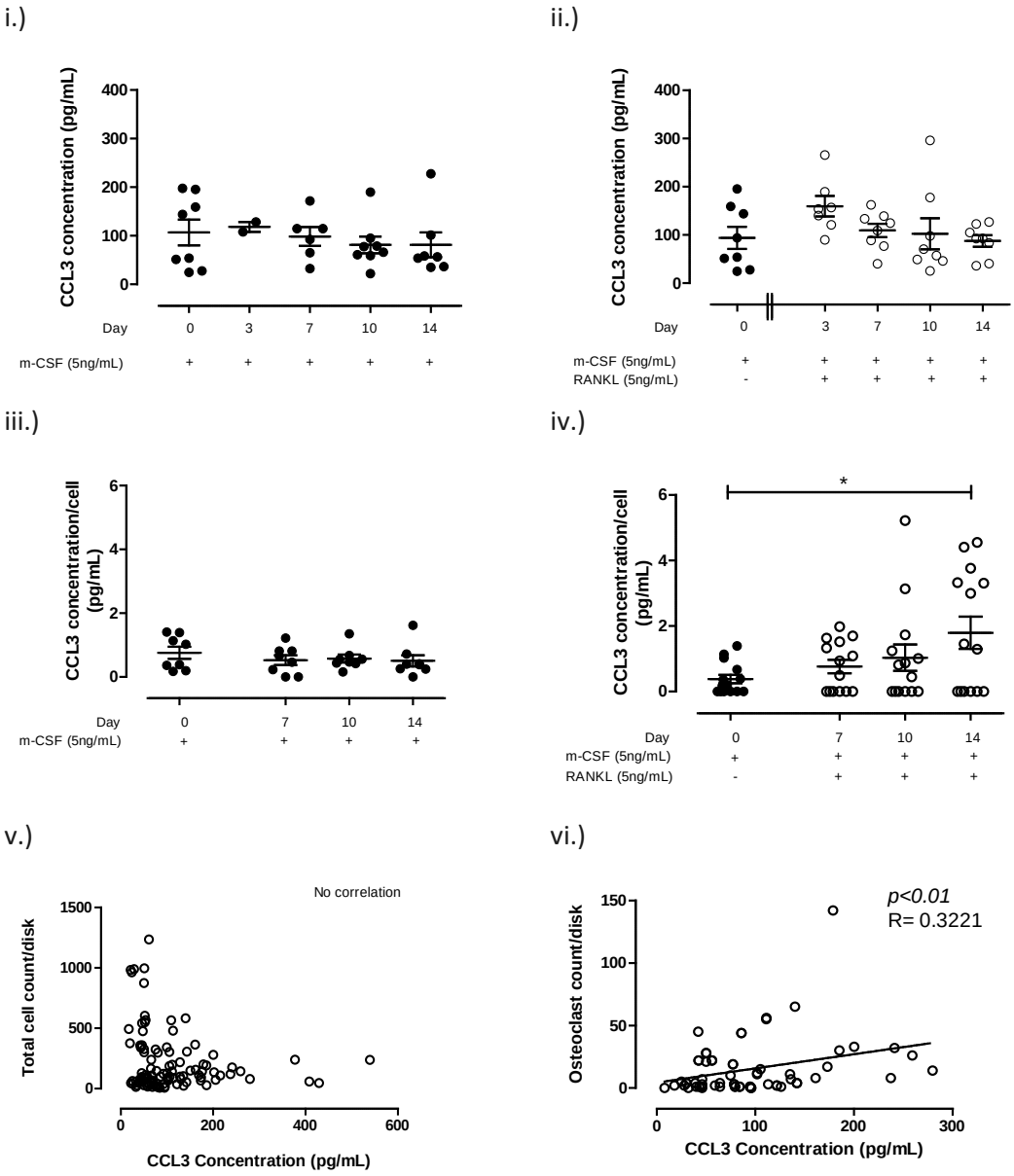

Figure 3. 11 - CCL3 secretion/cell significantly increased across 14 days in the presence of RANKL and was significantly correlated to osteoclast count..i.) CCL3 unchanged in m-CSF only medium. ii.) In m-CSF and RANKL cultures an increase in CCL3 occurred at day 3 (not significant),which declined to day 14. iii.) No significant changes in CCL3 concentration/cell were seen in m-CSF only cultures. iv.) In m-CSF and RANKL cultures a significant increase in CCL3 concentration/cell was seen. v.) and vi.) No correlation was found between total cell count and CCL3 concentration, but a significant, positive correlation was shown between osteoclast count/disk and CCL3 concentration ($p<0.01$, $R=0.3221$). Values plotted from n=8 donors (mean from 3 disks per donor per time-point reported). Mean ± SEM shown. Samples below quantification not shown. Statistical analysis; Student's t-test (day 0 and 14), one-way ANOVA (day 7 and 14) and Spearman's rank coefficient, * refers to $p<0.05$.

3.4 Discussion

A monoculture method was used to study the differentiation and activity of human osteoclasts *in vitro*. The monoculture method for studying human osteoclasts *in vitro* was already established in the Rheumatology Laboratory, but in this chapter was adapted to include a 7 day proliferation phase using 10ng/mL m-CSF. Supplementation of media with m-CSF enhanced osteoclast precursor proliferation in line with published methodologies that reported a range of 5-25ng/mL m-CSF in human osteoclast differentiation assays (*Hodge et al. 2011, Nicholson et al. 2000)*. Following this proliferation period, the differentiation phase was initiated (day 0) by supplementing cultures with RANKL containing medium (5ng/mL). In this chapter 5ng/mL RANKL led to quantifiable osteoclast numbers, which were sufficient for functional analyses. Approximately 2% of cells differentiated into osteoclasts at the termination of each assay (day 14). This yield was comparable, all-be-it higher, than levels (<1%) published by *Nicholson et al. (2000)*, and that reported by *Quinn et al. 1998, Udagawa et al. 2000* and *Han et al. 2000* where a broad range of 5 to 50ng/mL RANKL has been used.

The culture conditions chosen in this chapter supported an optimal 14 day differentiation period, which generated a reproducible and reliable method of osteoclast differentiation from $CD14^{+ve}$ monocultures. Day 14 was chosen as the end-point of the study due to a significant reduction in total cell count observed between day 14 and 17, which was attributed to osteoclast senescence and/or apoptosis. Although this observation was not further investigated, it does support the notion that the life-span of a differentiating osteoclast is limited to 2 weeks, where, after successful resorption, the cell becomes apoptotic, loses its adherence to bone, and is ingested by phagocytes (*Manolagas, 2000*). To confirm whether this also occurs in culture, markers of cellular apoptosis (e.g. Fas ligand and its receptor) could be assessed during the assay via flow cytometry (*Wu et al. 2005*).

Histological staining of ivory discs (used as the bone substrate) with haematoxylin and TRAP identified adherent osteoclast lineage and mature multi-nucleated osteoclasts on day 14 (*Oddie et al. 2000)*. The limitations of this method resulted in the development of novel methodologies, where confocal microscopy paired with

fluorescence-based TRAP stains (*i.e.* ELF97) quantified osteoclasts and monitored their movement (*Filgueira. 2004*). However, the prohibitive cost of this novel method and limited accessibility to confocal microscopes dictated that light microscopy was sufficient to detect $TRAP^{+ve}$ cells in line with the objectives of the chapter.

Following the use of traditional histological stains, total cell counts were performed manually. Cell counts for each assay took >130 hours to complete which protracted the time frame for obtaining results and limited the total number of assays processed at any time. Several cell counting methodologies were used for the quantification of cells in suspension (a haemocytometer, electrical gating and flow cytometry), but very few existed for counting cells fixed to the matrix on which they were grown (*Tzuret al. 2011, Bonetta 2005*). The main published methodology for counting adhered cells was recently described by *Ravi et al. (2014)* where stained cells were counted manually using a tag function in image processing software; ImagePro Plus. Such methodology matches that outlined in Chapter 2 Section 2.2.11. However, this method was time-consuming and prompted the creation of a novel, high-throughput automated algorithm for counting total adhered cells. Implementation of this automated method substantially reduced analysis time to 9 hours whilst maintaining the accuracy of manual counts.

During the creation of this algorithm, code for DCT-normalisation from previous illumination invariant facial recognition software was employed to overcome issues with inconsistent background lighting. The use of this innovative illumination invariant recognition algorithm was tested by *Leszczyński (2010)* where its inclusion significantly benefitted the verification of tested facial features. Using the same theory, the use of GUIs for high-throughput database searching was utilised by *Ciancanelli et al. (2015)* to find the binding sites of the transcription factor IRF7. It was therefore evident that such an application was pivotal to developing not only businesses involving security or surveillance, but also within a wide range of applications as far afield as in biology; one example being shown in this chapter.

Through the addition of the DCT-normalisation code, the automated, high-throughput counting algorithm was created and modified into a GUI. As described in this chapter this novel '6-click' process, took a maximum of 5 minutes to count adhered cells, before being turned into a completely automated script. This method was validated as it showed a comparable degree of accuracy in cell counts when compared to manual counts from two individual analysts. For this reason the method was taken forward as an accurate cell counting algorithm. The translational application of this automated method also meant that it could be used for object counting in many biological disciplines; leukocyte quantification in arthritic joints, nuclei counting in single cells, vacuole analysis etc.

After total counts were obtained, a RANKL dependent increase in $TRAP^{+ve}$ and osteoclast number was observed, confirming data previously reported and reviewed by *Quinn et al. (1998)*. The next task was to accurately determine and quantify the resorptive activity of the osteoclast. Traditionally toluidine blue was chosen over other methods such as scanning electron microscopy for the calculation of area resorbed, where it has long been documented that the addition of RANKL has a causative effect on an increase in osteoclastic resorption (*Sarma & Flanagan. 1996, Keller et al. 2012*). In this chapter a novel method for the analysis of confocal images showed no significant benefit in sensitivity over the traditional toluidine blue method. However, confocal images with higher resolution distinctly showed the presence of multiple erosions, but due to the following it was decieded the costs did not outweigh the benefits; lengthy acquisition times, sample mounting and equipment cost. Although this direct comparison between toluidine blue and confocal had not previously been published, the results for the quantification of area resorbed using confocal microscopy supports those of *Jeon et al. (2012)*. Jeon and colleagues (2012) used confocal microscopy to identify area of resorption pits over the time-course of a standard osteoclast assay. It was concluded that osteoclasts formed multiple smaller single pits at day 7, but by day 14 the fusion of multiple osteoclasts caused the appearance of larger areas of resorption.

Following on from this, culture supernatants were analysed to obtain surrogate soluble mediators of osteoclast differentiation. Several pro-inflammatory cytokines

were documented to play a role in destructive bone diseases including IL-1, IL-11, IL-15, IL-8, IL-17, TNF-α and IL-6 (*Roodman. 1999, Azuma et al. 2000, Goldring et al. 2002, Durand et al. 2013)*. All of these cytokines were shown to increase pre-osteoclast cell migration and fusion into mature osteoclasts, along with further effects on osteoclast resorptive ability, either in co-cultures or *in vivo*. Recently, the increased presence of one of these cytokines, IL-6, in erosive bone diseases has become a main area of interest. IL-6 is secreted from T cells, B cells and monocytes, and is significantly increased in RA patients where it correlates with bone destruction in arthritic joints and animal models (*Robak et al. 1998, Nowell et al. 2003, Mihara et al. 2012, Rose-John 2012*). Additionally, IL-6 was shown to increase in the presence of IL-1 and TNF-α, but its effects *in vitro* were variable and dependent upon culture methodology. The direct secretion of IL-6 from osteoclast differentiation cultures was assessed in this chapter where results showed IL-6 to slowly decrease across a 14 day time-course. A significant decrease in IL-6 concentration per cell in control cultures confirmed that the secretion was driven by a RANKL-mediated effect from $TRAP^{+ve}$ cells. The data in this chapter therefore indicated a role for IL-6 in osteoclast formation in monocultures, but a role in osteoclast-mediated resorption was not investigated.

The indirect effects of IL-6 on bone resorption have previously been reported as the autocrine/paracrine secretion of IL-6 was shown to enhanced bone resorption in bone marrow co-cultures from patients with Paget's disease (*Roodman et al, 1992*). More recently, an *in vivo* role of IL-6 trans-signalling was postulated from data published by *Tanaka et al. 2013* where treatment of murine arthritis with an anti-mouse IL-6R antibody led to attenuated osteoclast number and bone loss. To investigate this further, the paracrine and autocrine involvement of IL-6 trans-signalling in osteoclast differentiation, resorption and secretion of soluble mediators in monocultures will be assessed in Chapter 4.

In addition to IL-6, TNF-α was tested for but found at negligible levels in the supernatants from the osteoclast differentiation assays, suggesting no role in the direct differentiation of the osteoclast. This was a controversial finding due to previously published material that showed increases in osteoclastogenesis from the

secretion of TNF-α in co-cultures of human marrow cells and from TNF-α secreted from osteoblastic cells (*Roodman et al. 1999, Azuma et al. 2000*). The lack of detectable TNF-α described in this chapter was of particular note, as it provided evidence for the lack of TNF-α secretion direct from the osteoclast, possibly implying its redundancy in healthy osteoclastogenesis. This was important as TNF-α is known to be significantly elevated and partly responsible for detrimental pathology in bone destructive diseases (*Matsuno et al. 2002*).

In addition to these cytokines, a relationship between osteoclast formation and the inflammatory chemokines CCL9, CXCL12, CCL5, CCL2 and CCL3 has also been suggested where their increased presence has correlated to enhanced osteoclastogenesis and resorption (*Koch et al. 1992, Choi et al. 2000, Han et al. 2001, Yano et al. 2005, Pharoah et al. 2006, Iwamoto et al. 2008, Szekanecz et al. 2010, Vallet et al. 2011, Wintges et al. 2013*). These chemokines stimulate the migration of pre-osteoclasts and facilitate their fusion into osteoclasts. CCL5 was found at significantly elevated levels in erosive bone diseases such as JIA and RA (*Patel et al. 2001, Pharoah et al. 2006, Wintges et al. 2013*). This chapter indicated that CCL5 was not detected within osteoclast supernatants obtained from either monocultures or control assays. This concurs with data obtained in an *in vivo* model, whereby increased osteoclastogenesis and decreased bone formation was observed in CCL5 deficient mice (*Wintges et al. 2013*). Such data suggests a possible role for CCL5 in the inhibition of osteoclast differentiation, and thus, could explain the lack of CCL5 in our cultures.

In contrast to CCL5, CCL2 was detectable in supernatants harvested from m-CSF and RANKL cultures. Furthermore, a significant reduction in CCL2 was observed across the time-course. This supported previous data that showed a requirement for a minimal level of CCL2 for the expression of DC-STAMP, but that CCL2 levels did not significantly increase thereafter, indicating CCL2 was not secreted from the osteoclast (*Miyamoto et al. 2009)*. The CCL2 level quantified in this chapter may have originated from mononuclear cells present at day 0, and as these differentiated into $TRAP^{+ve}$ cells a corresponding reduction in CCL2 levels was observed. Alternatively, CCL2 may have been secreted from the osteoclast, but due

to the increasing acidic conditions caused by the active osteoclast, this acid sensitive chemokine could have reduced over-time due to its short half-life (*Zhang et al. 2009, Fan et al. 2011*). In the future, real time qPCR measuring the gene expression of CCL2, and CCL5, prior to their acidic degradation could confirm whether they are secreted.

Finally, a third chemokine CCL3 is found at elevated levels in arthritic diseases. No significant increase in CCL3 across the time-course of m-CSF and RANKL cultures was detected, but a significant increase in CCL3 concentration/cell was found, along with a significant, positive relationship with osteoclast count. This supports previous data obtained from co-cultures where CCL3 was concluded to be an osteoclastogenic differentiation factor (*Choi et al. 2000*). Along with this, the theory of CCL3 being able to withstand a low pH and maintain its functionality provides evidence for a role in the pathology of destructive bone diseases (*Choi et al. 2000* and *Han et al. 2001*). The concentration of CCL3 in this chapter was substantially lower than found in erosive bone diseases; RA-29ng/mL (synovial fluid), OA- 0.7ng/mL (synovial fluid), MM-1000pg/mL (bone marrow plasma) (*Choi et al. 2000, Komano et al. 2006, Pharoah et al. 2006, Vallet et al. 2011, Vangsness et al. 2011*). This suggests that the production of CCL3 from the osteoclast is either capable of being increased due to the inflammatory milieu of the joint, and/or secondary sources of this chemokine exist; macrophages, monocytes and fibroblasts.

Additional to the *in vitro* role of CCL3, in the last 20 years the *in vivo* role of CCL3 was investigated. The presence of significant quantities of CCL3 within the RA synovium was shown to induce the migration of $CD14^{+ve}$ and $CD16^{-ve}$ monocytes, thus linking CCL3 and bone erosions in arthritic diseases; RA, JIA, and OA (*Koch et al. 1994, Komano et al. 2006, Pharoah et al, 2006, Vangsness et al. 2011*). Furthermore, elevated levels of CCL3 were shown in another bone destructive disease, multiple myeloma (MM). In MM, *Choi et al. (2000)* and *Han et al. (2001),* showed the presence of CCL3 in myeloma patients, where serum was collected and supplemented into bone marrow cultures, which resulted in a significant increase in osteoclastogenesis. Furthermore, when these cultures where supplemented with a

neutralizing antibody to CCL3, osteoclast formation was significantly inhibited (*Choi et al. 2000, Han et al. 2001*). Alongside the effects of CCL3 on osteoclast differentiation, *Vallet et al. (2011)* proposed a dual mechanism of CCL3 in inhibiting osteoblast activity, which would therefore have led to the uncoupling of the osteoblast/osteoclast relationship further enhancing the pathology seen. In order to fully understand the role CCL3 directly exerts on osteoclast formation and resorption, further *in vitro* and *in vivo* experiments will be presented in Chapter 5.

As discussed above several studies have postulated a role for both IL-6 and CCL3 in erosive bone disorders both *in vitro* and *in vivo*, but there is a lack of research directly linking these mediators with the process of mononuclear differentiation into osteoclasts. For this reason the further investigation of IL-6 and CCL3 in direct osteoclast differentiation and in the functional resorptive ability of these cells will be continued in Chapter 4 and 5 respectively.

3.5 Conclusion

During the course of this chapter a reproducible and effective method for the differentiation of human osteoclasts from $CD14^{+ve}$ mononuclear cells was reported, which facilitated an accurate and improved assessment of mediators involved in direct osteoclastogenesis compared to co-cultures. In tandem, the creation of a novel, high-throughput automated algorithm for counting total cells was reported, alongside its validation for use in the established osteoclast assays. Its use in osteoclast assays provided a significant advantage over manual total counts due to the following reasons; robustness, lack of inter-analyst variability and high-throughput nature. As such multiple disks could be run per donor increasing experimental validity. In addition to total cell counts, the algorithm could also be used as a guide for counting osteoclast numbers manually, and provide a quick and easy method for calculating percentage osteoclastogenesis. Finally, through the analysis of harvested osteoclast assay culture supernatants, TNF-α and CCL5 were shown to have no role on osteoclast differentiation. CCL2, although present in supernatants, was not significantly altered in the presence of RANKL, suggesting limited effect on osteoclastogenesis. However, both IL-6 and CCL3 were increased in the presence of RANKL, suggesting an autocrine role of these two pro-inflammatory mediators in the differentiation and maturation of the human osteoclast. It was therefore concluded that IL-6 and CCL3 could be novel surrogate biomarkers of osteoclast differentiation, where further research distinguishing their impact on osteoclastogenesis and bone destructive diseases would be necessary.

Chapter 4:Assessing the importance of IL-6/sIL-6R signalling in RANKL-mediated human osteoclast differentiation and functional resorption *in vitro*

4.1 Introduction

Levels of IL-6 (60.95 ± 24.24 pg/mL) detected in supernatants from osteoclast differentiations assays in Chapter 3 indicate that IL-6 and/or the combination of IL-6 and sIL-6R (from here on termed IL-6/sIL-6R) have the capacity to regulate the biological responses in one or all of the following cell types; osteoclast precursor cells (e.g. monocytes and macrophages), $TRAP^{+ve}$ mononuclear cells and osteoclasts. A role of IL-6 in bone formation is well documented from early osteoblastogenesis and maturation through to osteocyte formation (*Johnson et al. 2014*). Comparatively, less is known about its role in osteoclastogenesis and bone destruction. Monocytes (osteoclast precursors) and macrophages express IL-6R and respond to direct stimulation by IL-6 via the classical signalling pathway; a regulatory/physiological pathway involved in resolution of immune response and cellular regeneration. Limited evidence of IL-6R expression on the osteoclast is available (Chapter 1 Section 1.3.2.2), therefore it is not clear whether the osteoclast can respond directly to IL-6 via classical signalling, or whether it relies on trans-signalling as described next (*Kotake et al. 1996, Grivennikov et al. 2009, Miyamoto et al. 2009*, *Jones, Scheller & Rose-John 2011*).

A soluble form of IL-6R (sIL-6R) enables non-IL-6R expressing cells to respond to IL-6 by forming an IL-6/sIL-6R complex, thus allowing IL-6 cell signalling in the presence of gp130; trans-signalling (Figure 4.1). sIL-6R has a similar affinity for IL-6 as IL-6R, and also prolongs IL-6 plasma half-life (*Oh, Revel& Chebath1996, Peters et al. 1996, Müller-Newenet al. 1998*). sIL-6R is formed by proteolytic cleavage of cell membrane bound IL-6R (primarily from neutrophils) by ADAM10 and ADAM17 (*Garbers et al. 2011*). An increase in ADAM17 is commonly found in an inflammatory state (IL-1 and TNF-α) in concordance with an increase in sIL-6R (resultant of elevated neutrophil apoptosis; *Garberset al. 2011*). The elevated presence IL-6 and sIL-6R, in addition to ADAMs leads to the expansion and recruitment of monocytes to areas of high concentration, therefore increasing the pool of osteoclast precursors, whilst also diverting the immune response away from a neutrophilic phenotype (apoptosis). Additionally, sIL-6R can be formed by differential mRNA splicing. A polymorphism in the IL-6R gene at the coding site for

proteolytic cleavage can change aspartic acid to alanine, and in 2013 this polymorphism was found to correlate with higher sIL-6R expression (*Kim et al. 2003*). However, the importance of the mechanism by which sIL-6R is generated is likely to alter within different diseases; i.e. reduced alternative splicing of sIL-6R is associated with RA (*Marinou et al. 2007*).

Evidence supporting a role of IL-6 trans-signalling in osteoclast formation was first reported in 1993 by *Tamura et al.* who showed a significant increase of osteoclast number in murine co-cultures containing bone marrow cells and osteoblasts, when stimulated with IL-6 (200ng/mL) and sIL-6R (500ng/mL). Furthermore, IL-6 and sIL-6R were unable to trigger a comparable agonistic response when applied to the co-culture system individually (*Tamura et al. 1993*). These data show that osteoclasts respond preferentially to IL-6/sIL-6R stimulation versus IL-6. However the co-culture method did not provide insight to the direct actions of IL-6 trans-signalling on osteoclast differentiation, but highlighted its indirect effects through a RANKL-dependent mechanism (Chapter 1). For example, in co-cultures IL-6 stimulates RANKL secretion from synovial T cells and stimulates STAT3 signalling in osteoblasts leading to RANKL secretion (*O'Brien et al. 1999, Hashizume et al. 2008*). Contestable data was however published in 2003 by *Kudo et al.* who concluded IL-6 trans-signalling exerted a RANKL-independent effect on osteoclast formation. In their study, a significant increase in multinucleated cells and resorption pits were found in cultures supplemented with m-CSF and IL-6/sIL-6R, compared to m-CSF and IL-6 alone (*Kudo et al. 2003*). Such data therefore suggested that IL-6 trans-signalling played a role in osteoclastogenesis and that RANKL was not essential for this differentiation. However, the use of $RANKL^{-/-}$ mice confirms the critical presence of RANKL for homeostatic osteoclastogenesis, where $RANKL^{-/-}$ mice develop severe osteopetrosis, decreased tooth eruption and defective leukocyte differentiation (P*ettit et al. 2001)*. The true physiological nature of multinucleated cells differentiated from cultures supplemented with m-CSF and IL-6/sIL-6R but not RANKL is therefore questionable, particularly as cell size and nucleus number were decreased (*Kudo et al. 2003*).

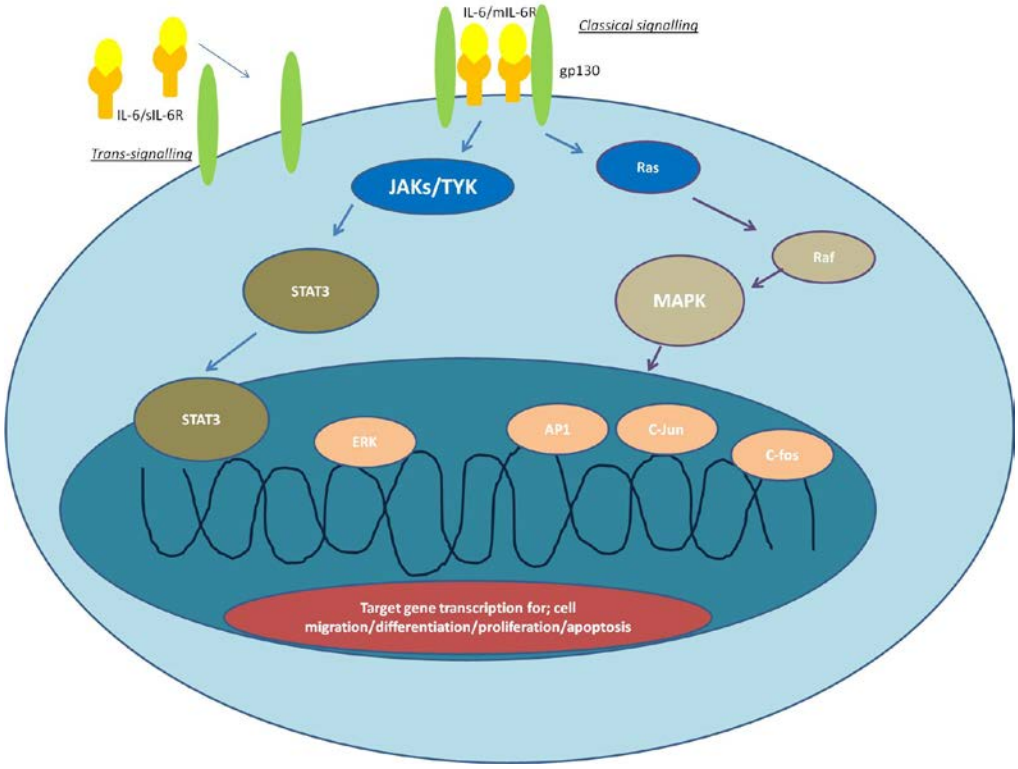

Figure 4. 1 - An illustration of extracellular IL-6 and sIL-6R activating IL-6 classical and IL-6 trans-signalling IL-6 can signal through two signalling pathways depending on whether IL-6R is expressed on the surface of the cell (*i.e.* monocytes/macrophages). Classical signalling results from IL-6 binding to membrane bound IL-6R (top right pathway) which stimulates the dimerization of gp130, which is ubiquitously expressed on cells. Cells which do not express IL-6R are still responsive to IL-6 though through the presence of soluble IL-6R (sIL-6R; released due to either proteolytic cleavage or alternative splicing) and cellular expression of gp130, termed trans-signalling (top left pathway). IL-6 and sIL-6R form a complex in the extracellular space which can then activate gp130 on the cells membrane. Once bound gp130 dimerizes and activates the JAK/STAT pathway leading to downstream STAT3 signalling and activation of transcription factors and osteoclast differentiation target genes.

Extensive literature was published supporting a role of IL-6 in osteoclast differentiation and bone erosions (as summarised in *Hashizume & Mihara 2011*). However the direct effect of the IL-6/sIL-6R complex upon monocyte differentiation into osteoclasts had not been established. In addition, the specific effect of IL-6 trans-signalling upon *in vitro* osteoclast formation and pathological bone resorption during inflammatory arthritis had not been evaluated. For this reason, studies in the following chapter will utilise sgp130-Fc (a kind gift from Prof Rose-John) as a research tool to block IL-6 trans-signalling in an *in vitro* system of human

osteoclastogenesis from $CD14^{+ve}$ mononuclear cells in the presence of RANKL. Sgp130-Fc is comprised of gp130's extracellular region joined to the Fc region of human IgG1 and readily binds to IL-6/sIL-6R complex, with a 10-fold higher affinity than natural sgp130 (*Jostock et al. 2001*). Additionally, sgp130-Fc specifically binds to the complex and thus only blocks trans-signalling, not classical signalling, where such a design was pivotal to the experiments in this chapter (*Jostock et al. 2001*). Sgp130-Fc will therefore be used to identify firstly any role IL-6 trans-signalling exerted in the direct differentiation of the osteoclast from $CD14^{+ve}$ mononuclear cells, and secondly, any role on mature osteoclast facilitated bone resorption, through the utilisation of both 2D and 3D methodology. These two parameters will be measured in three different 'models' of osteoclastogenesis; i.) a physiological model utilising sgp130-Fc to inhibit autocrine IL-6 trans-signalling, ii.) a model simulating the inflammatory milieu of an arthritic joint (*Nowell et al. 2003, Wong et al. 2006, Nowell et al. 2009*), and iii.) a model to distinguish the therapeutic potential of inhibiting IL-6 trans-signalling in osteoclastogenesis. Data collected will elucidate the importance of IL-6 trans- versus classical signalling in the pathological profile of bone destruction, and ultimately help understand signalling in destructive bone diseases, where the pathological inflammatory milieu of a joint is thought to be pivotal to resorption (both human: RA or MM, and murine: CIA or AIA; *Kotake et al. 1996, Maslinski et al. 2003, Nowell et al. 2003, Nowell et al. 2009, Jones, Scheller & Rose-John 2011*).

The aim of this chapter was to define the direct role of IL-6 trans-signalling on the physiological differentiation of $CD14^{+ve}$ mononuclear cells into osteoclasts stimulated by m-CSF and RANKL through the use of sgp130-Fc. HYPER-IL-6 was used to mimic the pathological inflammatory milieu of the joint and to establish the direct role of IL-6 trans-signalling on osteoclast formation and subsequent bone resorption. Supernatants collected from across the time-course were used to measure the role of IL-6 trans-signalling in modulating the secretion of osteoclast-associated chemokines (CCL2, CCL3, CCL5). Specifically the aims of this chapter were;

1. To determine the impact of basal IL-6 trans-signalling on the differentiation of human $CD14^{+ve}$ cells by measuring osteoclast formation, osteoclast-dependent bone resorption and osteoclast-related chemokines using sgp130-Fc as a tool to specifically block the pathway.

2. To simulate the pathological milieu of an arthritic joint using HYPER-IL-6 and monitor the resultant effects on osteoclast differentiation, resorption (overall &individually) and secretion of chemotactic proteins from $CD14^{+ve}$ mononuclear precursors and osteoclasts.

3. To assess the therapeutic potential of sgp130-Fc inhibiting HYPER-IL-6 induced osteoclastogenesis; thus evaluating its potential as a target for inhibiting enhanced osteoclast differentiation and resorption *in vitro*, highlighting potential translational applications.

4.2 Essential Methodology

The below diagrams highlight the essential methods used throughout this chapter. Full detail of all these methods can be found in their respective sections in Chapter 2.

- ***Osteoclast assay set up (Chapter 2 Sections 2.2.1 - 2.2.4)***

Condition	Number of Donors	Number of Replicate Disks per donor	Chapter Sections	Comments
m-CSF only	5	4	4.3.1	Mean values from the replicate disks of each donor plotted
m-CSF and sgp130-Fc	5	4		
m-CSF and RANKL	8	8		
m-CSF, RANKL and sgp130-FC	8	8		
m-CSF and RANKL	7	8	4.3.2	
m-CSF, RANKL and HYPER-IL-6 (10ng/mL)	7	8		
m-CSF and RANKL	1	4	4.3.2.2	
m-CSF, RANKL and HYPER-IL-6 (0.5ng/mL)	1	4		
m-CSF, RANKL and HYPER-IL-6 (1ng/mL)	1	4		
m-CSF, RANKL and HYPER-IL-6 (2.5ng/mL)	1	4		
m-CSF, RANKL and HYPER-IL-6 (5ng/mL)	1	4		
m-CSF and RANKL	8	4	4.3.2.3	
m-CSF, RANKL and HYPER-IL-6 (0.5ng/mL)	8	4		
m-CSF and RANKL	6	4	4.3.3	
m-CSF, RANKL, HYPER-IL-6 and sgp130-Fc	6	4		

-PBMCs isolated from healthy human whole blood via density centrifugation went through magnetic activated cell sorting to yield a pure suspension of $CD14^{+ve}$ monocytes (as illustrated).

- Disks were seeded with 3.2 x 10^6 cells and cultured with m-CSF alone (5ng/mL) or in combination with RANKL (5ng/mL). Culture supernatants collected and replenished every 3-4 days. Disks harvested at day 14.

Caption 3 - Isolation of human CD14+ve monocytes from peripheral blood. Human blood layered onto hisotpaque is centrifuged yielding peripheral blood mononuclear cells. CD14+ve monocytes isolated by magnetic activated cell sorting and 3.2 x 10^6 cells/mL are seeded onto ivory disks prior to culture in osteoclast proliferation/differentiation medium.

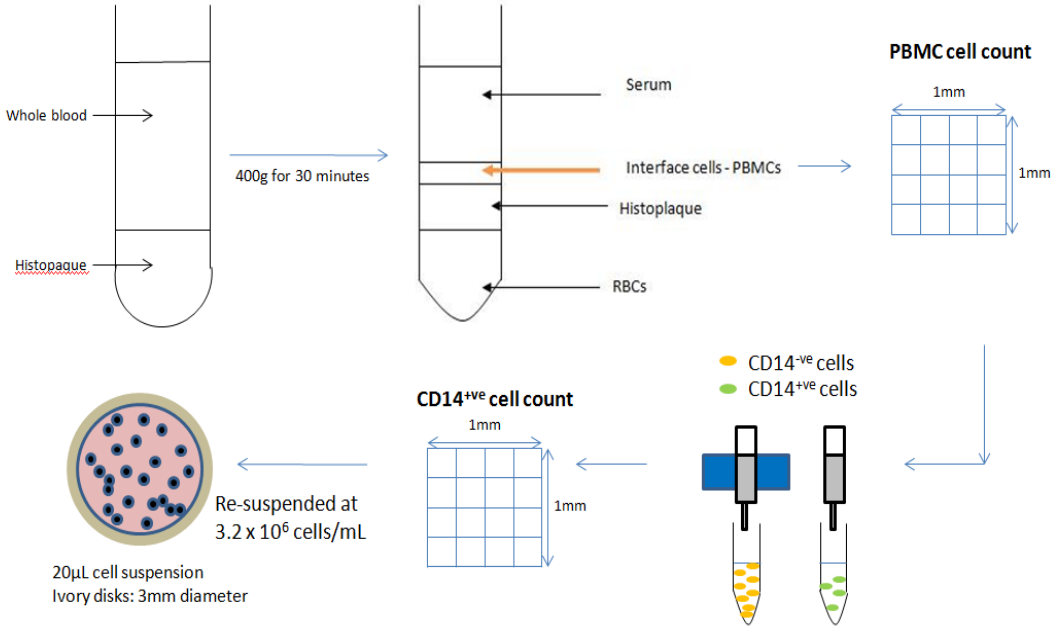

- ***Quantitative parameter assessment of the osteoclast assay***

-Disks harvested at day 14 were fixed with glutaraldehyde prior to staining with TRAP and haematoxylin to identify total cells and osteoclasts; quantified through MATLAB and manual counts. Following cell counts adhered cells were removed and disks stained with toluidine blue or calcein to facilitate quantification of resorbed area. Harvested supernatants were analysed by ELISA.

-In addition, individual pit parameters (area, perimeter, volume and depth) were imaged via confocal microscopy (x60) and quantified using MetaMorph. All of these assessments can be found in the diagram which follows.

Caption 4 - The osteoclast assay and functional analyses. Disks seeded with $CD14^{+ve}$ monocytes are cultured up to day 14 in the presence or absence of sgp130-Fc and/or HYPER-IL-6. Every 3-4 days disks and their supernatants were harvested and used for one of the following analyses; cell staining (TRAP and haematoxylin), area of resorption quantification (toluidine blue or calcein), confocal analysis of individual pit characteristics, and ELISA.

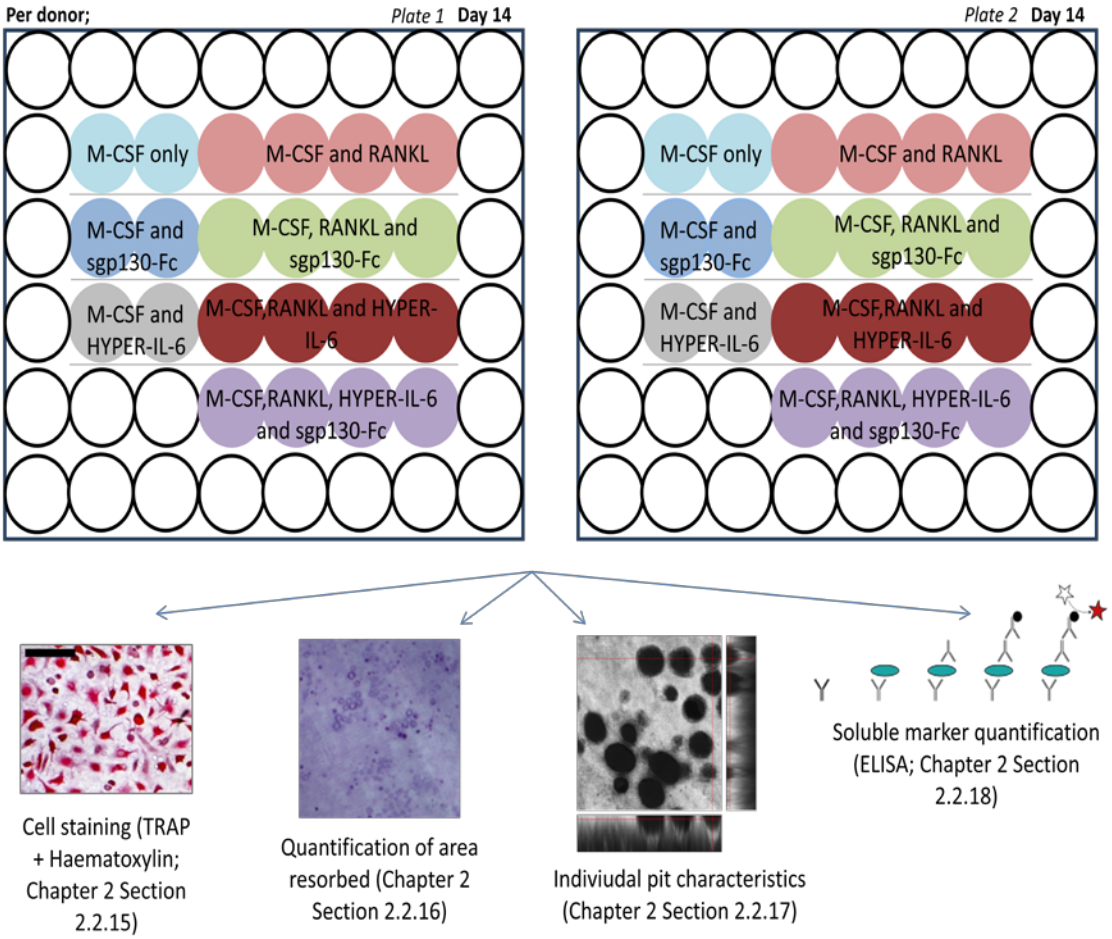

4.3 Results

In this section the impact IL-6 trans-signalling on osteoclastogenesis in the following models was assessed; a model of physiological osteoclast formation and functional resorption, a model simulating the inflammatory milieu of an arthritic joint, and a model to distinguish IL-6 trans-signalling as a therapeutic target.

4.3.1 Determining the impact of IL-6 trans-signalling in a model of physiological osteoclast formation and functional resorption

The potential impact of IL-6 trans-signalling upon the physiological process of bone resorption was studied *in vitro* by supplementing CD14+ve mononuclear cells with culture medium containing sgp130-Fc, m-CSF and RANKL. Osteoclastogenesis assays finished after 14 days at which point osteoclast number (by TRAP staining) and the area of resorbed bone substrate (by toluidine blue staining) were quantified. Markers of osteoclast differentiation (TRAP5b), resorption (CTX-1), pain and inflammation (NGF, CCL2, CCL3 and CCL5) were measured by ELISA over the time-course of each experiment.

4.3.1.1 Sgp130-Fc significantly reduced TRAP^{+ve} cell, osteoclast number and resorption of ivory disks

TRAP^{+ve} cell counts were significantly ($p \leq 0.05$) reduced by sgp130-Fc (donors: n =8, Figure 4.2 and Figure 4.3, i). A significant 30% reduction in osteoclast count was observed in assays supplemented with sgp130-Fc versus control containing m-CSF and RANKL (donors: n=8, Figure 4.3, ii, $p \leq 0.05$). Under non-differentiating conditions (m-CSF only) TRAP^{+ve} cells and osteoclasts were absent or diminutive in number on the cultured disks (donors n=5, Figure 4.2 and Figure 4.3, iii and iv).

The area of bone substrate resorbed was significantly reduced by sgp130-Fc (donors: n =8, 0.59 ± 0.16% of disk) compared to m-CSF + RANKL control cultures (donors: n =8, 1.09 ± 0.16%, Figure 4.4, $p \leq 0.05$). No resorption was detected in cultures containing m-CSF ± sgp130-Fc (donors: n =5, Figure 4.4). The resorbed surface of the ivory disks was observed and analysed by traditional light microscopy

and high resolution confocal microscopy. Due to a lower frequency of resorption pits (Figure 4.3) and the high objective used for confocal microscopy, a representative image of multiple resorption pits on sgp130-Fc treated disks was hard to acquire. However, fewer resorption pits were evident which were smaller in pit area, volume and depth as determined visually from x,y and z representation (Figure 4.5).

4.3.1.2 CTX-1 and TRAP5b unaffected by sgp130-Fc treatment

TRAP5b and CTX-1 were measured by ELISA on day 7 and 10. TRAP5b levels were comparable in m-CSF + RANKL cultures and m-CSF + RANKL + sgp130-Fc on day 7 (1.21 ± 0.90 and 1.26 ± 0.32 U/L) and day 10 (2.67 ± 0.85 and 1.22 ± 0.55 U/L; donors n=2, Figure 4.6, i). The 2-fold reduction in TRAP5b by sgp130-Fc on day 10 was not significant but supported the significant reduction in $TRAP^{+ve}$ cells and osteoclasts numbers observed (Figure 4.3).

CTX-1 was not significantly affected by sgp130-Fc treatment of $CD14^{+ve}$ cell cultures also containing m-CSF + RANKL (day 7 and day 10), but a 4-fold decrease was noted on day 10 in the presence of sgp130-Fc, which was absent on day 7 (donors n=2, Figure 4.6, ii).

4.3.1.3 NGF, CCL2, CCL3 or CCL5 secreted from osteoclast were unaffected by sgp130-Fc

NGF was not detected in any of the supernatants tested (donors n=5, Figure 4.7). The level of CCL2 and CCL3 in cultures containing m-CSF and RANKL was unaffected by sgp130-Fc (donors: n =5, Figure 4.7). The secretion of CCL5 by osteoclasts and $TRAP^{+ve}$ cells was low and variable (donors: n =5, Figure 4.7).

i.)

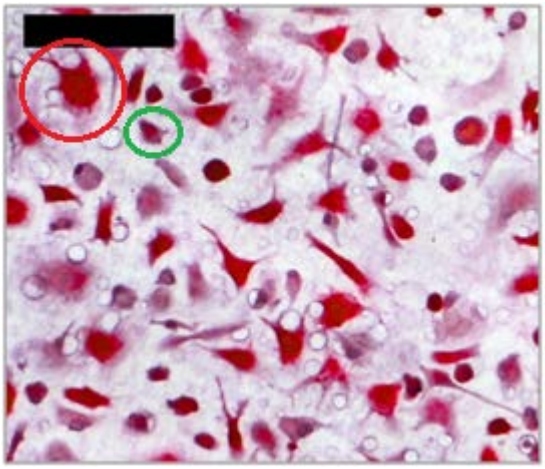

ii.)

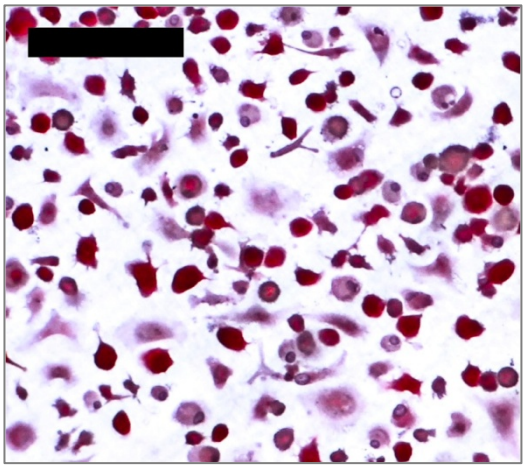

iii.)

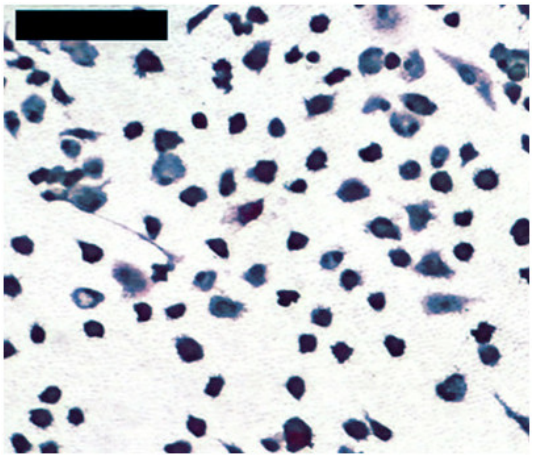

iv.)

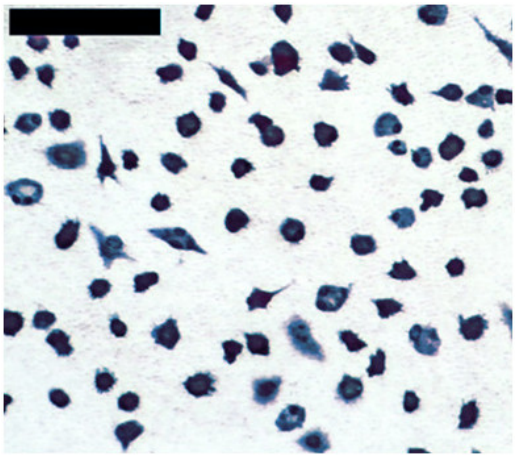

Figure 4. 2 - Representative images of osteoclast differentiation cultures supplemented with sgp130-Fc.Disks were cultured for 14 days in differentiation medium (m-CSF and RANKL) either supplemented with or without sgp130-Fc (500ng/mL)from n=8 donors. i.) In differentiation medium only cultures many $TRAP^{+ve}$ mononuclear (green circle) and multinuclear cells(red circle)were seen adhered to disks. Multiple resorption pits could also been seen across the disk. ii.) Through the supplementation of sgp130-Fc a substantial reduction in both $TRAP^{+ve}$ mononuclear and multinuclear cells was seen, and cell size also appeared reduced. Resorption pit number appeared reduced from differentiation cultures. iii.) Control cultures containing only m-CSF lacked $TRAP^{+ve}$ cells. iv.) Control cultures containing m-CSF and sgp130-Fc also lacked $TRAP^{+ve}$ cells. (Scale bar 100µm).

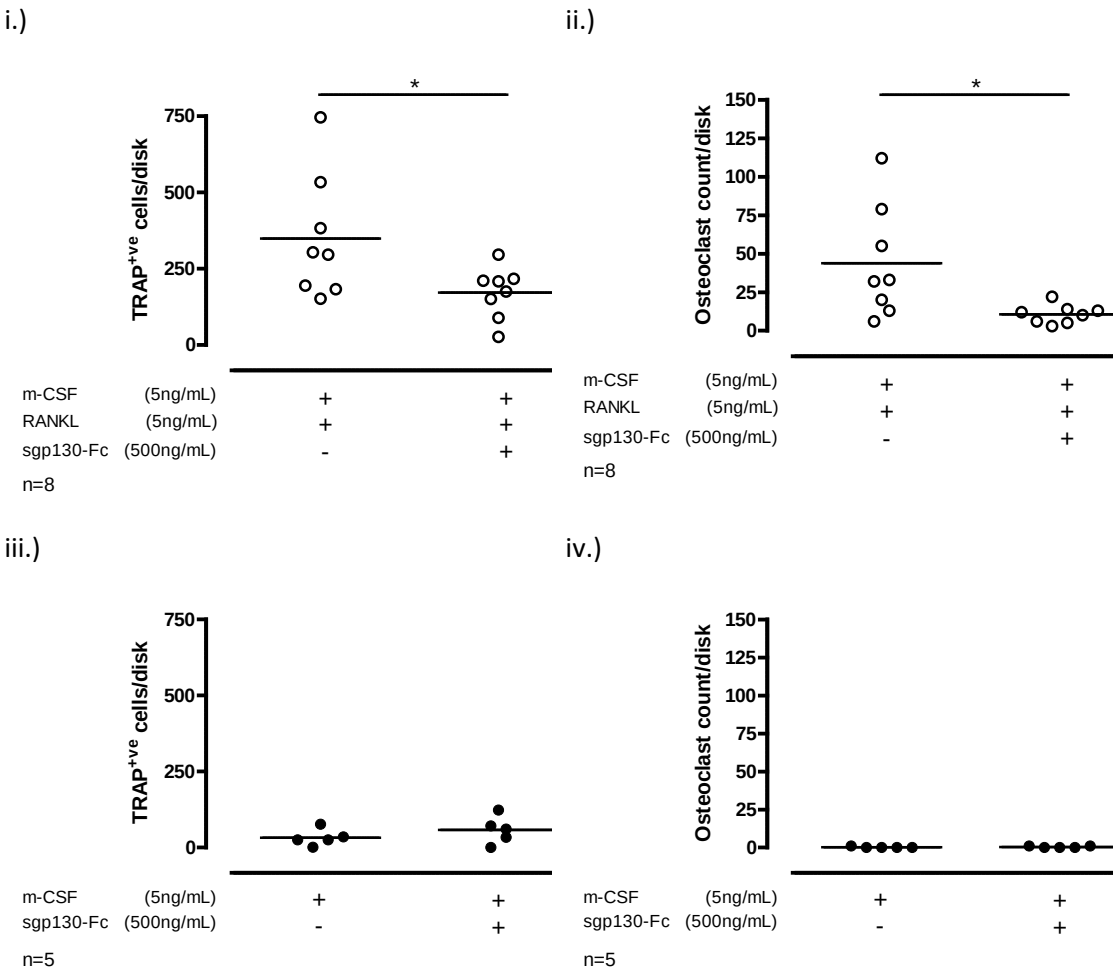

Figure 4. 3 - Sgp130-Fc significantly reduced TRAP^{+ve} mononuclear and multinuclear cell formation.Across the time-course of the osteoclast assay sgp130-Fc (500ng/mL) was added into cultures. After 14 days cells were still viable and disks were harvested and stained with haematoxylin and TRAP. i.) A significant reduction in TRAP^{+ve} cells resulted from sgp130-Fc supplementation(donors n=8; mean plotted from 8 disk replicates per donor). ii.) Osteoclast count significantly reduced in the presence of sgp130-Fc(donors n=8; mean plotted from 8 disk replicates per donor). iii.) and iv.) In m-CSF control cultures with/without the supplementation of sgp130-Fc, negligible TRAP^{+ve} cells and osteoclasts were counted(donors n=5; mean plotted from 4 disk replicates per donor). Mean ± S.E.M shown. Student's t-test was used to determine significance (* p≤0.05).

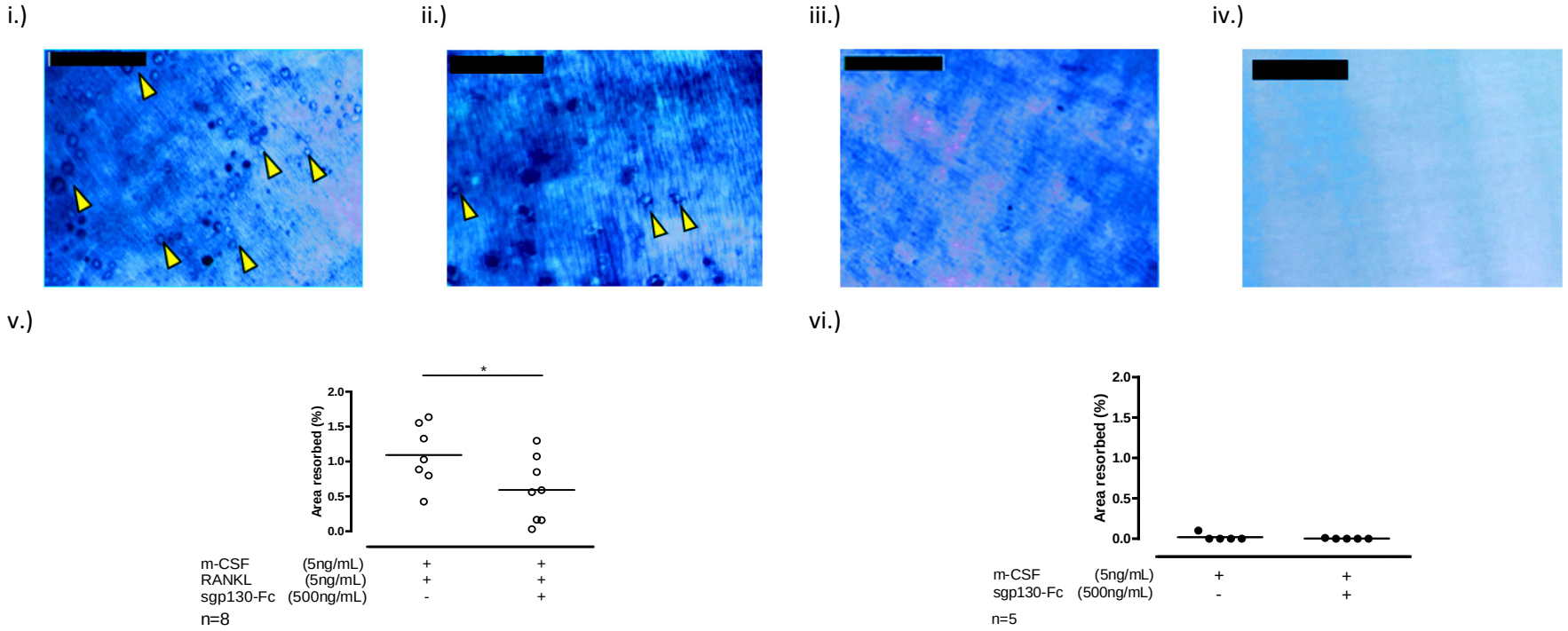

Figure 4. 4 - Sgp130-Fc significantly reduced total area resorbed in human osteoclast cultures.Following counts at day 14, disks were stained with toluidine blue. i.) M-CSF and RANKL cultures had multiple resorption pits (yellow arrows), but treatment with sgp130-Fc (ii) substantially reduced their number. iii.) and iv.) No resorption was found in m-CSF only cultures ± sgp130-Fc. v.) A significant reduction of total area resorbed in sgp130-Fc cultures was found compared to m-CSF and RANKL (donors n=8;mean plotted from 4 disks per donor,*p≤0.05*). vi.) No resorption was present in cultures lacking RANKL(donors n=5, mean plotted from 2 disks per donor). Mean ± S.E.M. reported, statistical significance assessed using Student's t-test (*p≤0.05). Scale bar = 250µm.

i.)

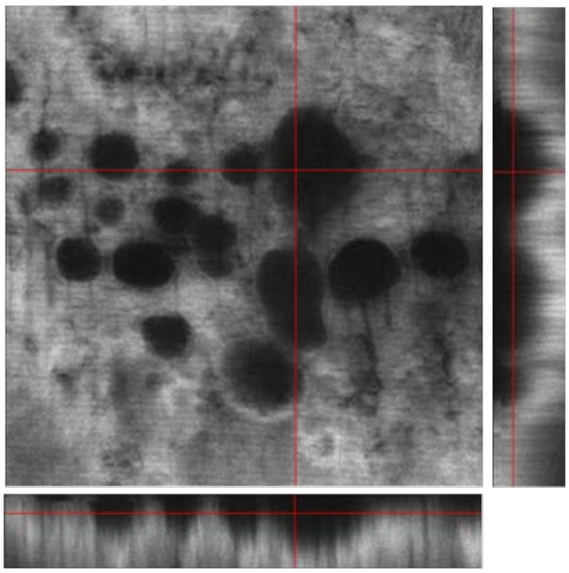

ii.)

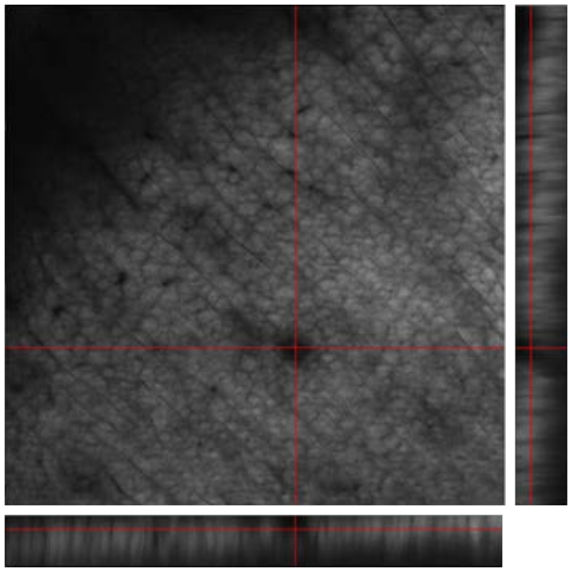

Figure 4. 5 - High resolution confocal microscopy revealed visually reduced resorption pit number and depth in sgp130-Fc supplemented human osteoclast cultures *in vitro*.Following toluidine blue staining and light microscopy, disks were bleached and stained in calcein prior to confocal imaging at x60. i.) Multiple resorption pits were evident across the surface of disks cultured in m-CSF and RANKL. ii.) Supplementation of sgp130-Fc into m-CSF and RANKL cultures yielded very few resorption pits (one pit visualised where lines intersect). Where imaged, resorption pits were smaller in diameter and depth compared to m-CSF and RANKL cultures.0.27µm = 1 pixel. (Statistical analysis was not preformed due to donor number =1).

i.)

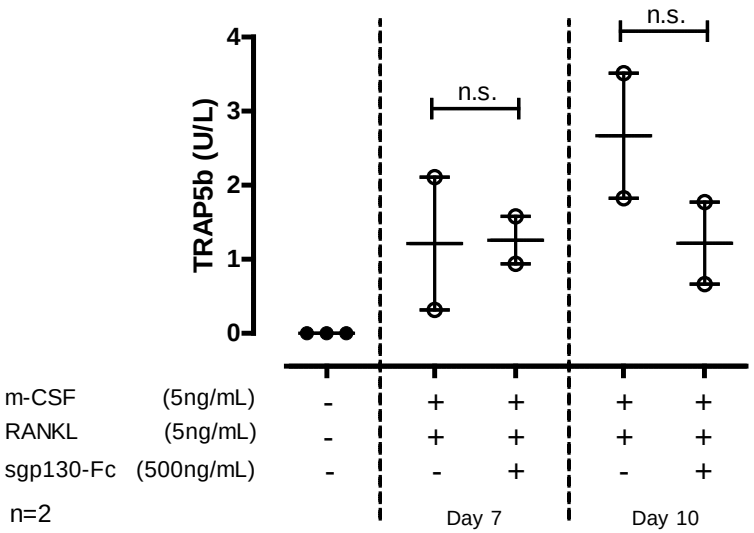

ii.)

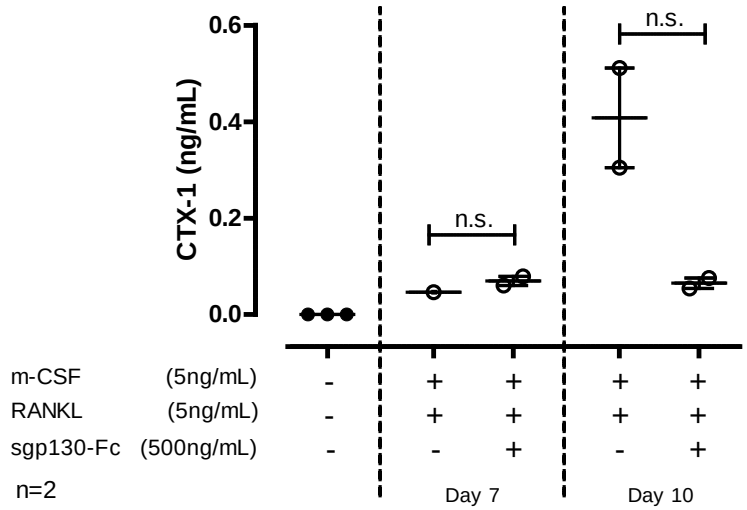

Figure 4. 6 - TRAP5b and CTX-1 levels decreased but not significantly in the supernatants of osteoclast differentiation cultures supplemented with sgp130-Fc.Soluble markers of resorption and osteoclast differentiation were assessed in the supernatants from osteoclast cultures(donors n=2; the mean of 8 replicate disks per donor was plotted). i.) A decrease in TRAP5b levels were found in cultures treated with sgp130-Fc compared to m-CSF and RANKL cultures. ii.) A similar decrease in CTX-1 levels were found in cultures treated with sgp130-Fc but this was not significant. Mean ± S.E.M shown, statistical analysis carried out using a Student's t-test.

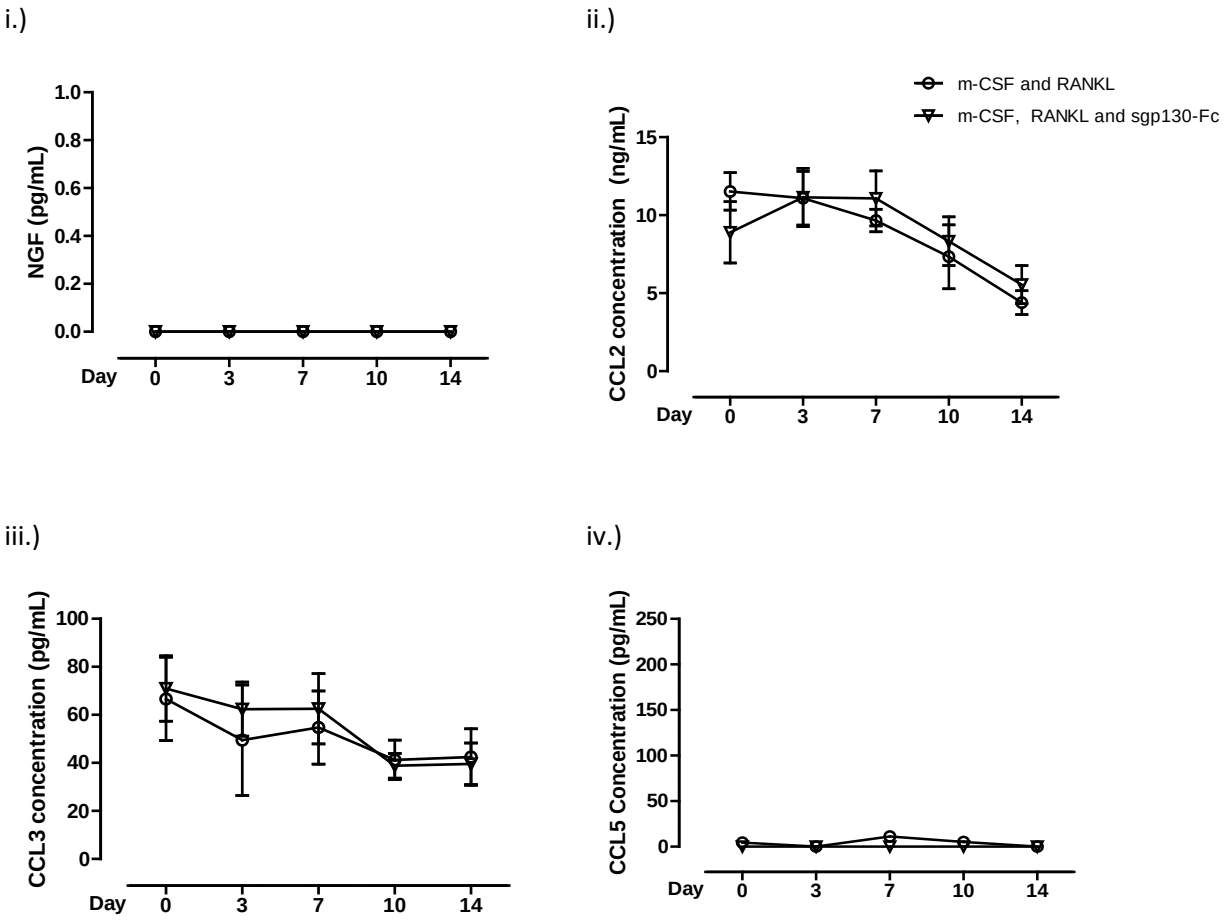

Figure 4. 7 - NGF, CCL2, CCL3 and CCL5 were not significantly altered by sgp130-Fc supplementation into osteoclast cultures.Harvested supernatants from osteoclast differentiation assays were analysed by ELISA for the presence of a pain mediator and inflammatory chemokines. i.) Negligible levels of NGF were reported in both m-CSF and RANKL cultures and those supplemented with sgp130-Fc (n=8 donors; mean plotted from 8 replicates per donor). ii.) and iii.) The secretion profiles of CCL2 and CCL3 from osteoclast cultures treated with sgp130-Fc matched that from m-CSF and RANKL cultures (n=8; mean plotted from 8 replicates per donor). iv.) The secretion of CCL5 was variable in cultures and although m-CSF and RANKL cultures showed elevated CCL5 levels compared to sgp130-Fc treated, this was not significant (n=8; mean plotted from 8 replicates per donor). Mean ± S.E.M shown and statistical analysis was carried out using a one way ANOVA.

4.3.2 Modelling IL-6/sIL-6 R joint inflammation to study osteoclastogenesis and bone resorption by IL-6 trans-signalling *in vitro*

Human osteoclast differentiation cultures, grown under standard conditions were supplemented with the IL-6 trans-signalling agonist HYPER-IL-6. HYPER-IL-6 was used to mimic the inflammatory milieu of a diseased joint and to establish the direct impact of IL-6/sIL-6R upon osteoclastogenesis (TRAP), resorption of a bone substrate (CTX-1) and soluble mediators of pain, inflammation and osteoclast formation (NGF, CCL3, CCL5 and CCL2).

4.3.2.1 HYPER-IL-6 (10ng/mL) reduced TRAP^{+ve} cell and osteoclast number without affecting bone resorption

Adherent cells on ivory disks were of a variable phenotype and surface coverage was reduced by HYPER-IL-6 (Figure 4.8). TRAP^{+ve} cells were significantly decreased by HYPER-IL-6 compared with m-CSF + RANKL only cultures (141 ± 26 to 292 ± 51 cells/disk; donors n=7,Figure 4.9, i, $p \leq 0.05$). A 3-fold reduction in osteoclast number was also noted but this was not significant (donors n=7, Figure 4.9, ii). Although the number of bone resorbing osteoclasts were reduced, no significant change at day 14 to the area of bone resorbed by HYPER-IL-6 was found (donors n=5, Figures 4.9).

i.)

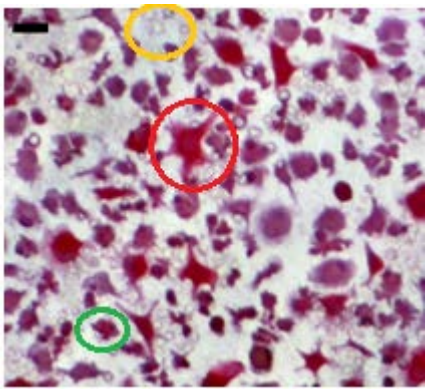

ii.)

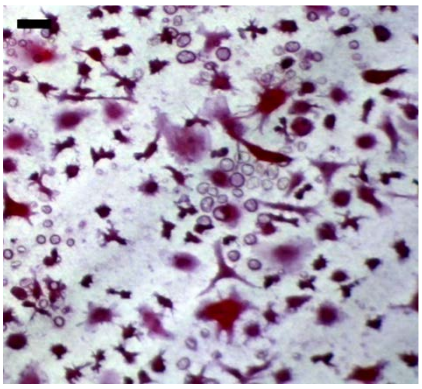

Figure 4. 8 - The addition of HYPER-IL-6 (10ng/mL) to osteoclast cultures altered the cellular phenotype of cells adhered to disks.Disks were treated with 10ng/mL HYPER-IL-6 for 14 days alongside those treated with m-CSF and RANKL. i.) Representative images of adhered TRAP^{+ve} mononuclear (green circle) and multinucleated osteoclasts (red circle) in differentiation cultures. Resorption pits were also seen across the disks (orange circle). ii.) Disks treated with 10ng/mL HYPER-IL-6 showed cells of altered phenotype, smaller size, and irregular shape, where fewer cells were found across the disk. Many resorption pits were visible across the disk. Scale bar equal to 50µm.

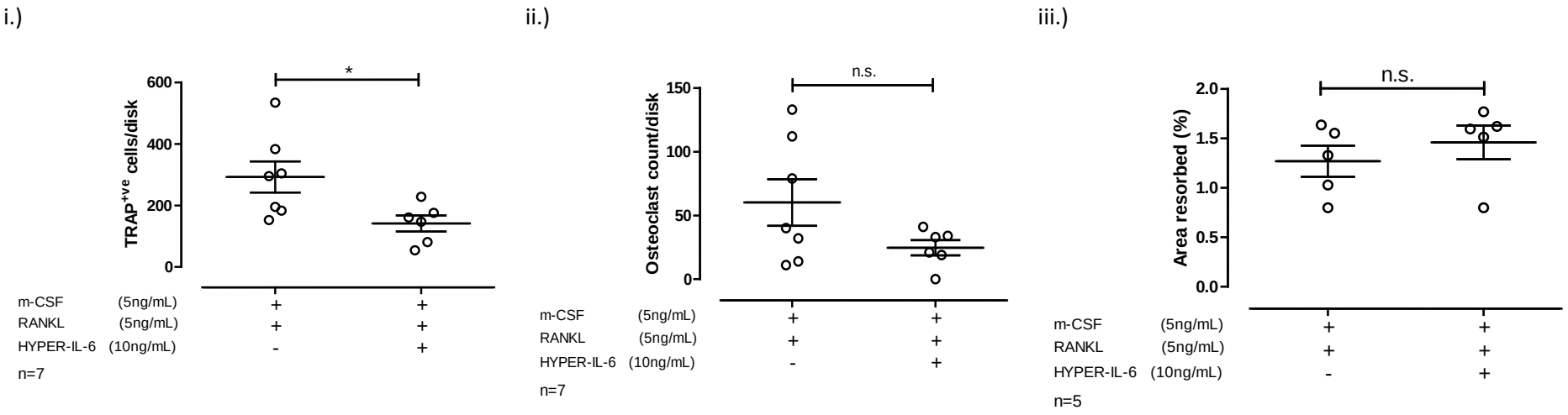

Figure 4. 9 - TRAP^{+ve} cells were significantly reduced in the presence of 10ng/mL HYPER-IL-6 but not osteoclast number.After 14 days of culture in an osteoclast assay ivory disks were harvested and stained for cell counts prior to cell removal enabling the quantification of area resorbed. i.) At 10ng/mL HYPER-IL-6 a significant decrease in TRAP^{+ve} cells from m-CSF and RANKL cultures was found(donors n=7; mean plotted from 8 replicates per donor). ii.) Osteoclast number remained unchanged with 10ng/mL HYPER-IL-6(donors n=7; mean plotted from 8 replicates per donor). iii.) Total area resorbed was comparable in m-CSF and RANKL cultures ± sgp130-Fc (data plotted from n=5 donors; mean represents 8 replicate disks). Mean ± S.E.M shown and statistical analysis was carried out using the Student's t-test (*p≤0.05).

4.3.2.2 Concentration dependent osteoclast differentiation and bone resorption by HYPER-IL-6

The concentration dependent differentiation of $CD14^{+ve}$ cells by HYPER-IL-6 (0.5ng/mL to 5ng/mL) in m-CSF + RANKL cultures was tested to further explain the lack of increase in osteoclast number in the presence of 10ng/mL HYPER-IL-6 despite the significant increase in $TRAP^{+ve}$ cells (Figure 4.8 and 4.9).The concentration range was tested on cells harvested from n=1 donor, where 4 disks per concentration were assessed. $TRAP^{+ve}$ cell numbers were highest on disks cultured in medium supplemented with 0.5ng/mL HYPER-IL-6 (1098 ± 346) versus m-CSF + RANKL cultures (380 ± 63, Figure 4.10 and 4.11). Osteoclast number was increased 3-fold by supplementing differentiation medium containing m-CSF + RANKL with HYPER-IL-6 (0.5ng/mL); osteoclast/disk= 245 ± 58 versus 74 ± 18 (Figure 4.11). The area of bone resorbed by osteoclasts was increased by HYPER-IL-6 (0.5ng/mL) in m-CSF + RANKL cultures; the percentage of the disk resorbed was 8.6 ± 2.3 versus 1.0 ± 0.2 (2 disks were assessed per concentration from n=1 donor, Figure 4.11).

4.3.2.3 HYPER-IL-6 increased bone resorption without affecting $TRAP^{+ve}$ or osteoclast counts

Subsequent assays (n=8 donors) were conducted in medium containing m-CSF + RANKL ± HYPER-IL-6 (0.5ng/mL) for a total of 14 days (Figure 4.12). Total cell count was reduced by HYPER-IL-6, from 4172 ± 1187 to 2284 ± 484 cells/disk; but this was not significant (Figure 4.13). $TRAP^{+ve}$ cell and osteoclast counts were reduced by HYPER-IL-6;although again not significantly (Figure 4.13). Bone resorption was quantified as a functional measure for osteoclasts, where the area of each disk resorbed was significantly increased by HYPER-IL-6 (6.91 ± 1.77 versus 2.54 ± 0.70% for m-CSF + RANKL); see Figure 4.13 ($p \leq 0.05$).

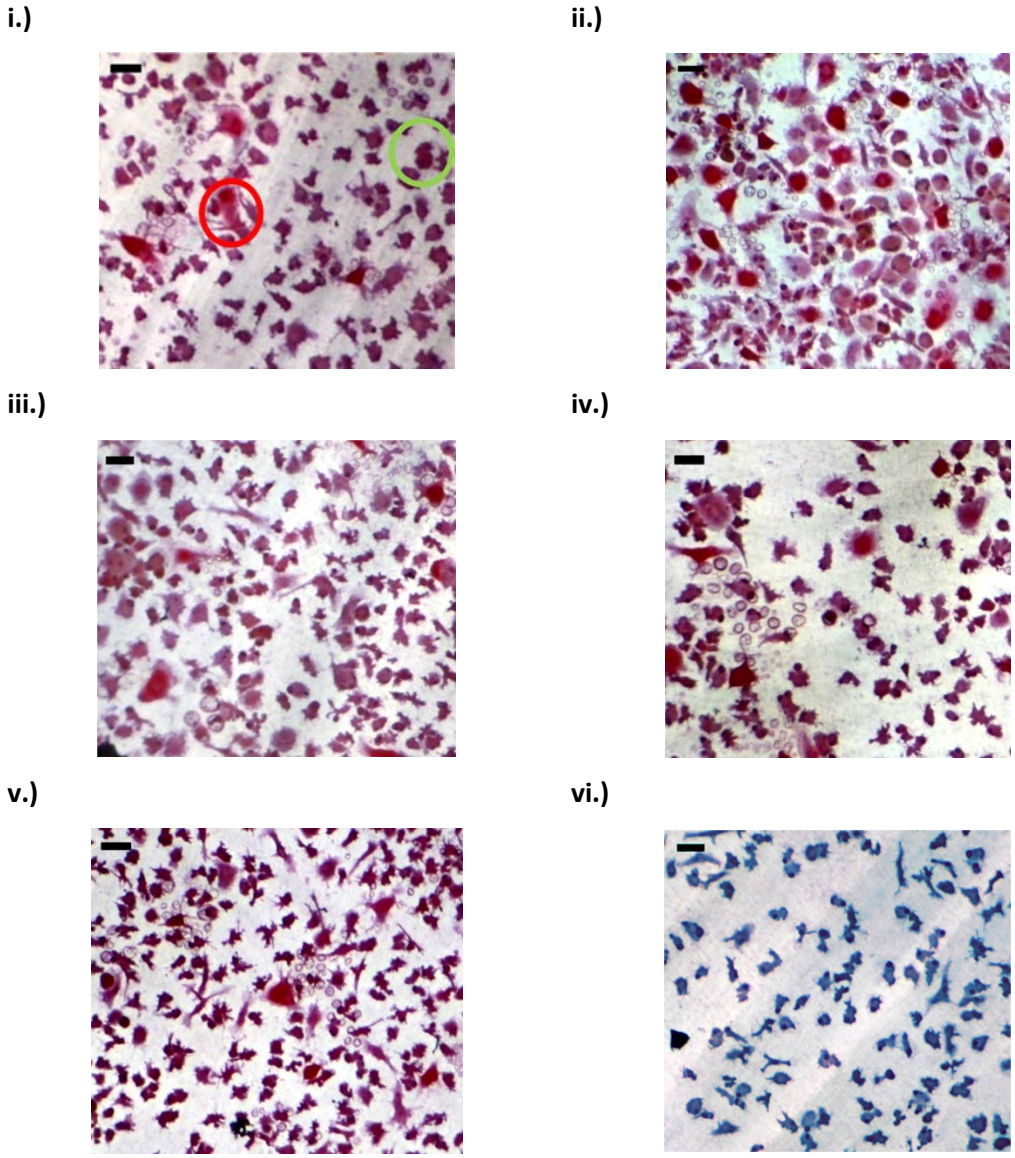

Figure 4. 10 - Representative day 14 images from osteoclast differentiation assays supplemented with HYPER-IL-6.. Over 14 days osteoclast assays were treated with a range of HYPER-IL-6. i.) In m-CSF and RANKL cultures TRAP^{+ve} mononuclear (green circles) and multinuclear cells (red circles) were adhered to ivory disks, in addition to multiple resorption pits. ii.) At 0.5ng/mL HYPER-IL-6, TRAP^{+ve} cells and resorption pits appeared increased compared to (i). iii.) In the presence of 1ng/mL HYPER-IL-6 TRAP^{+ve} cells were reduced from (i) with fewer resorption pits. iv.) At 2.5ng/mL HYPER-IL-6 cell number appeared reduced but TRAP^{+ve} cells and resorption pits were present compared to (i). v.) In the presence of 5ng/mL HYPER-IL-6 TRAP^{+ve} multinuclear cell number was reduced from (i). vi.) In m-CSF only cultures no TRAP^{+ve} cells were found. (Scale bar 50µm).

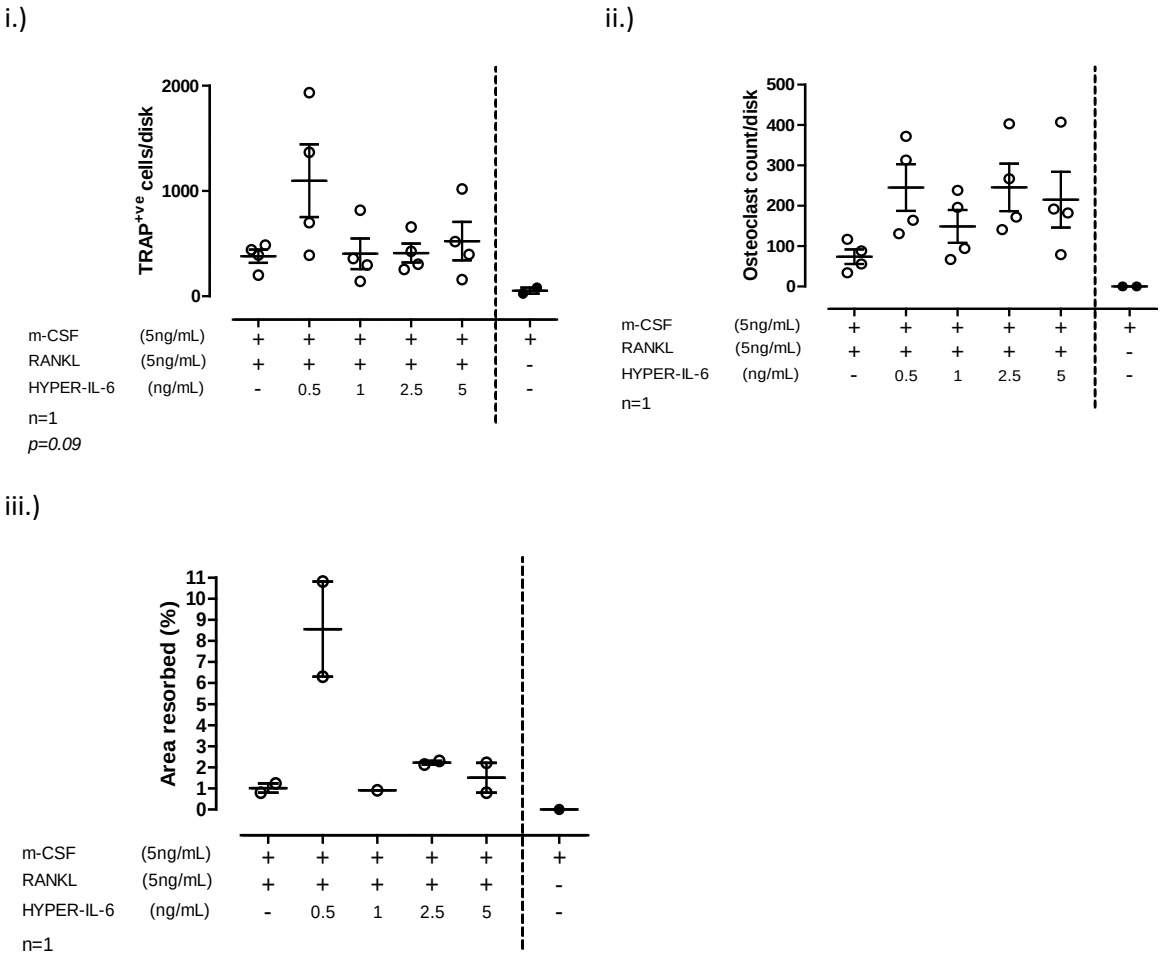

Figure 4. 11 - HYPER-IL-6 at 0.5ng/mL increased TRAP^{+ve} cell number, osteoclast count and total area resorbed.Harvested disks treated with a range of HYPER-IL-6 concentrations were stained and cell counts completed at day 14. i.) TRAP^{+ve} cell count peaked at 0.5ng/mL HYPER-IL-6 in osteoclast differentiation cultures. HYPER-IL-6 at 1ng/mL to 5ng/mL showed comparable TRAP^{+ve} cell numbers to differentiation cultures. ii.) Osteoclast number was found also to peak at 0.5ng/mL HYPER-IL-6, but osteoclastogenesis was still elevated in 1ng/mL-5ng/mL HYPER-IL-6 when compared to differentiation cultures. iii.) A substantial increase in area resorbed was shown in the presence of 0.5ng/mL HYPER-IL-6 when compared to differentiation cultures alone. Resorption in 1ng/mL- 5ng/mL HYPER-IL-6 was comparable to differentiation cultures. N=1 donor; 4 disks were assessed at each concentration from this one donor. No statistics carried out due to limited sample number. Data was reported as mean ± S.E.M.

i.) ii.)

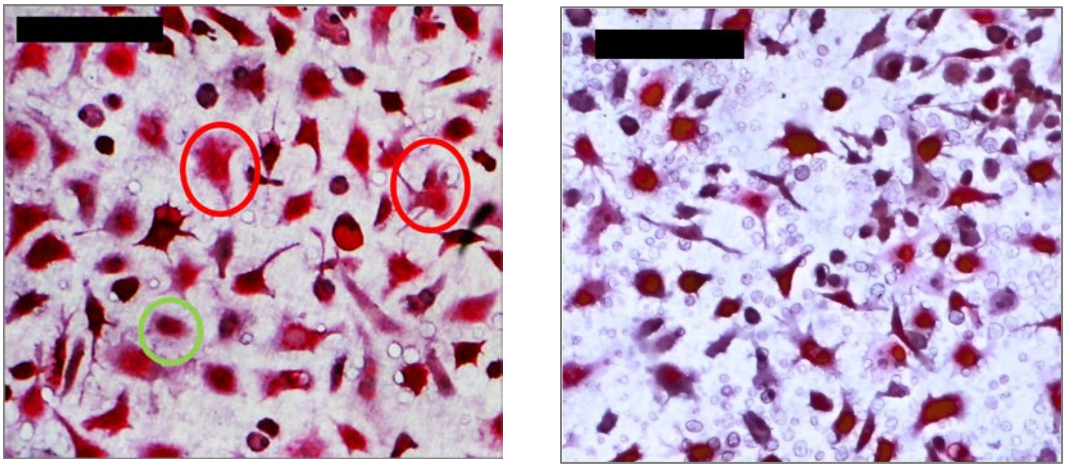

Figure 4. 12 - Cultures treated with 0.5ng/mL HYPER-IL-6 showed reduced TRAP^{+ve} cell numbers but increased bone resorption.The optimal dose of 0.5ng/mL HYPER-IL-6 was previously established and used over a 14 day culture period in the human osteoclast differentiation assay in n=8 donors (4 replicate disks were analysed for each donor at each time-point). i.) Many TRAP^{+ve} mononuclear (green circles) and multinuclear cells (red circles) were found adhered to the ivory disks at day 14 in m-CSF and RANKL cultures. ii.) Through the addition of 0.5ng/mL HYPER-IL-6, a reduction in TRAP^{+ve} cells were noted but substantial resorption pit formation across the disk was evident. (Scale bar 100um).

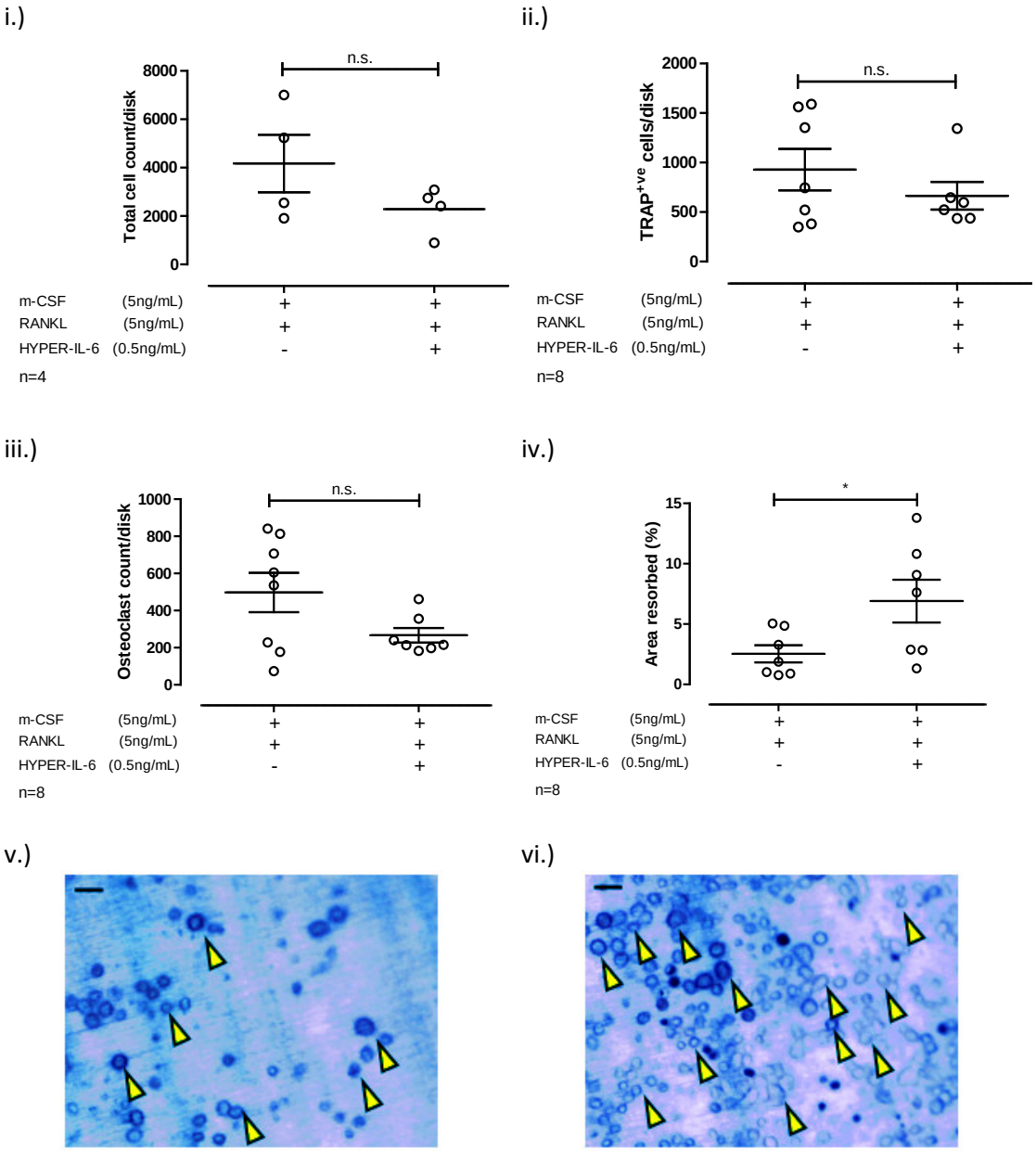

Figure 4. 13 - HYPER-IL-6 cultures showed no significant change in total cells, TRAP^{+ve} cells or osteoclast number, but area resorbed significantly increased at day 14.Cell counts and area resorbed were quantified from harvested disks. i., ii. and iii.) No significant change in total cell number, TRAP^{+ve} cell, or osteoclast number resulted from HYPER-IL-6 supplementation(n=4 donors (total cell count) and n=8 donors (TRAP and osteoclast); mean of 4 replicate disks per donor plotted). iv.) A significant increase in area resorbed resulted fromHYPER-IL-6 supplementation in m-CSF and RANKL cultures(n=8 donors; mean of 4 replicate disks plotted, *p≤0.05*). v.) Resorption pits in m-CSF and RANKL cultures reduced compared to HYPER-IL-6 cultures (vi.) where extensive resorption was shown. Mean ± S.E.M. shown and Student's t-test was performed (*p≤0.05).Scale bar 50µm.

4.3.2.4 HYPER-IL-6 increased resorption pit depth but not pit area

HYPER-IL-6 significantly enhanced bone resorption by osteoclasts. The impact of HYPER-IL-6 upon individual osteoclasts was next assessed by analysing individual pit parameters (area, depth and volume) using high resolution confocal microscopy.

Disks from one representative assay were imaged (m-CSF + RANKL versus m-CSF + RANKL + HYPER-IL-6). The surface area measurement for pits was comparable for m-CSF + RANKL (2518 ± 353.4 μm^2) versus m-CSF + RANKL +HYPER-IL-6 cultures (2148 ± 370.2 μm^2; Figure 4.14). Pit volume was increased by HYPER-IL-6 (1196 ± 257.4 versus 851.6 ± 212.6 μm^3 for M-CSF + RANKL; Figure 4.14) but not significantly. Pit depth was increased on disks from HYPER-IL-6 (12.32 ± 1.5 µm) versus m-CSF + RANKL cultures (6.304 ± 0.5µm; *p≤0.001*; Figure 4.14).

4.3.2.5 TRAP5b levels unaffected by HYPER-IL-6 but CTX-1 levels increased

TRAP5b was quantified on day 7 and 10 of the osteoclastogenesis assay. There was no significant difference in TRAP5b levels when m-CSF + RANKL ± HYPER-IL-6 were compared. CTX-1 was significantly increased by HYPER-IL-6 on day 7 (Figure 4.15, p≤0.05), but not on day 10 when compared to m-CSF and RANKL cultures.

4.3.2.6 CCL2, CCL3 and CCL5 secretion was not altered by HYPER-IL-6 in vitro

Supernatants from osteoclast cultures containing M-CSF + RANKL ± HYPER-IL-6 were replenished every 3-4 days. No NGF was detected in any of the supernatants collected over the 14 day time-course (data not presented). CCL2 and CCL3 production was unaffected by the inclusion of HYPER-IL-6 in the differentiation medium (Figure 4.16). CCL5 levels were low and highly variable (Figure 4.16).

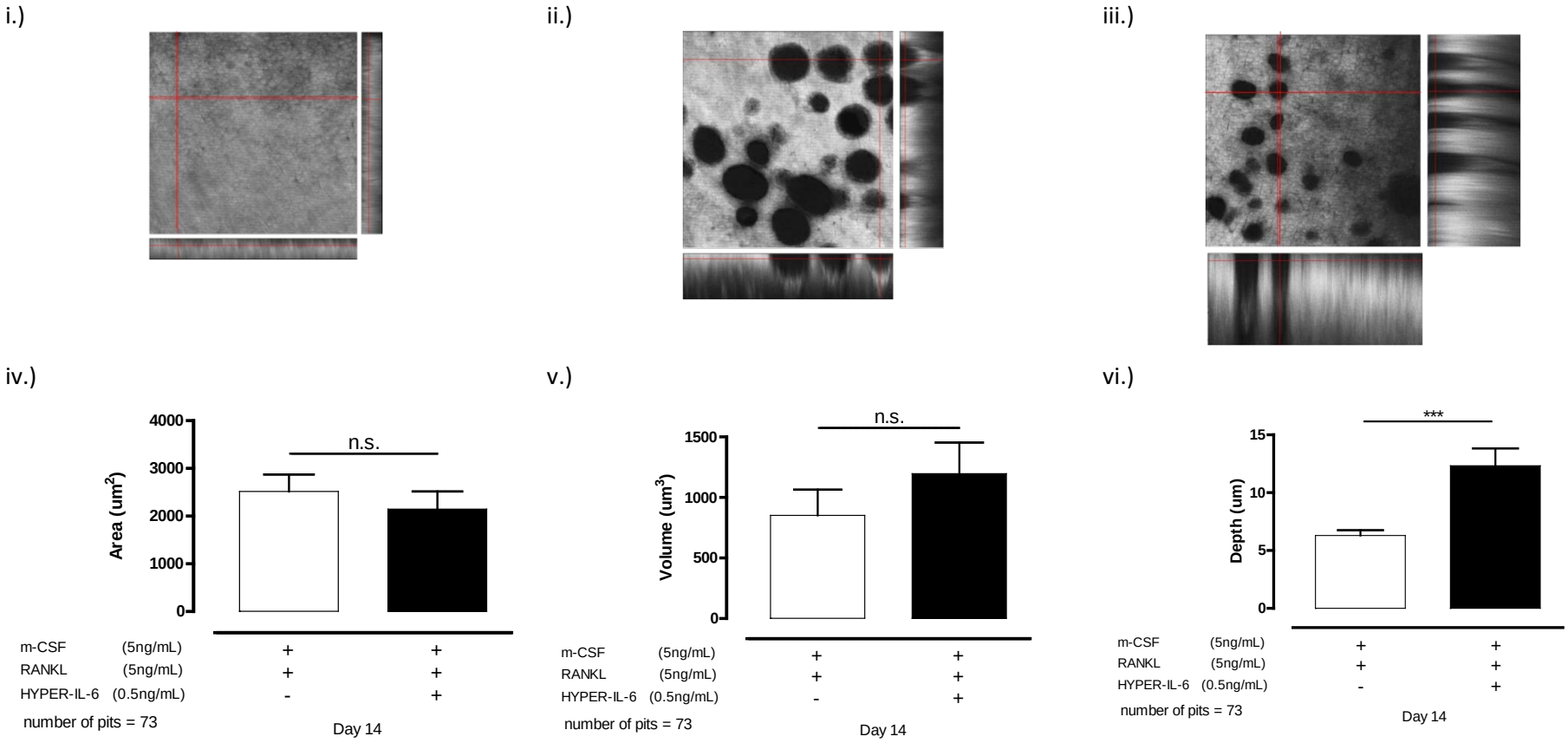

Figure 4. 14 - HYPER-IL-6 substantially increased resorption pit depth. 3-D data stacks were obtained using confocal microscopy for n=73 pits from 1 donor under m-CSF and RANKL cultures ± HYPER-IL-6. i.) m-CSF only cultures lacked resorption pits. ii.) In m-CSF and RANKL cultures multiple resorption pits with varying depths were seen compared to HYPER-IL-6 cultures (iii) with smaller pits and increased depth. iv. and v.) Surface area and pit volume did not significantly change.vi.) HYPER-IL-6 caused a significant increase in pit depth (*p≤0.001*). 0.27µm = 1 pixel. Statistics were carried out using a Student's t-test.

i.)

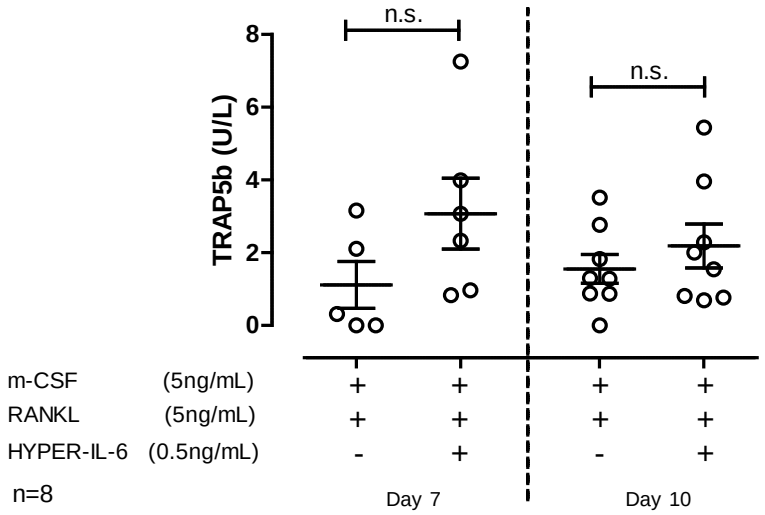

ii.)

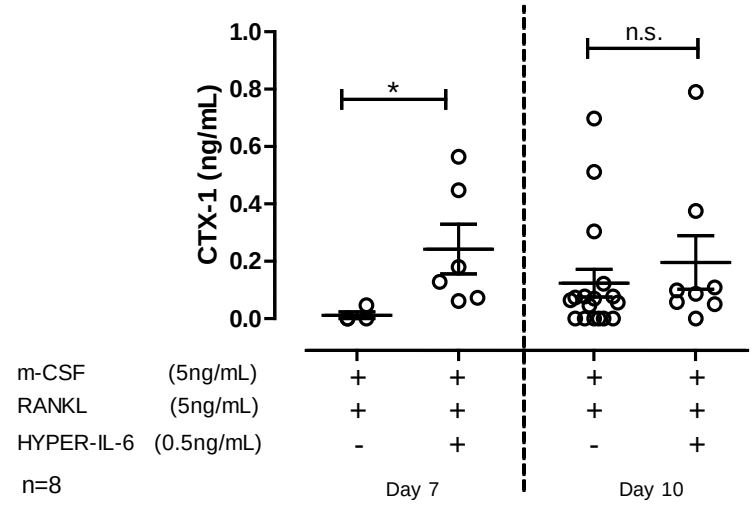

Figure 4. 15 - HYPER-IL-6 caused the significant early increase in CTX-1 levels at day 7.. Supernatants harvested from osteoclast differentiation assays were assessed for the presence of TRAP5b and CTX-1. i.) TRAP5b levels at day 7 and day 10 were not significantly changed in the presence of HYPER-IL-6 when compared to m-CSF and RANKL cultures. ii.) A significant early increase in CTX-1 levels was found at day 7 (*p≤0.05*), being indicative of the early activation of osteoclast resorptive activity in the presence of 0.5ng/mL HYPER-IL-6. At the later time-point of day 10 this increase was no longer significant. N=8 donors; mean plotted from 4 replicate disks per donor. Mean ± S.E.M. shown and statistical analysis carried out using Student's t-test (*p≤0.05).

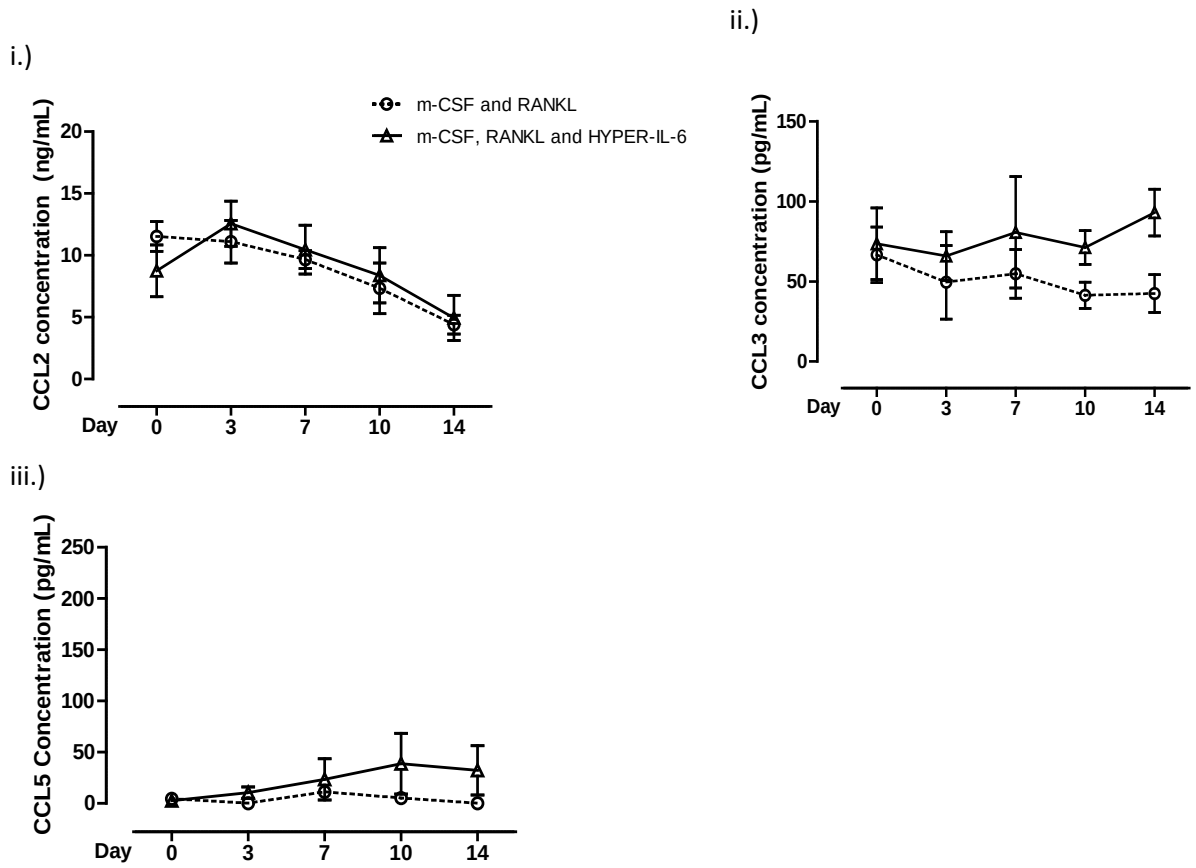

Figure 4. 16 - HYPER-IL-6 had no effect on the direct secretion of CCL2, CCL3 or CCL5 from the osteoclast.. The analysis of osteoclast assay supernatants by ELISA was carried out across the 14 day time-course. i.) and ii.) Both CCL2 and CCL3 secretion profiles were comparable in cultures treated with 0.5ng/mL HYPER-IL-6 and differentiation medium alone(mean plotted from n=8 donors per time-point; 4 replicate disks per donor were cultured). iii.) CCL5 levels were increased across the time-course in HYPER-IL-6 treated cultures compared to differentiation medium only, but this increase was variable and not significant(mean plotted from n=8 donors per time-point; 4 replicate disks per donor were cultured). Data reported at mean ± S.E.M. from n=8 donors per time-point (4 replicate disks per donor at each time-point). Statistical analysis was completed using a one way ANOVA.

4.3.3 Assessing the potential therapeutic benefit of blocking IL-6/sIL-6R signalling on bone *in vitro*

The potential therapeutic benefit of specific blockade of IL-6 trans-signalling on bone resorption was measured *in vitro.* HYPER-IL-6 was used as an agonist of osteoclastogenesis whilst sgp130-Fc was used to block IL-6 trans-signalling. Soluble markers of osteoclast differentiation (TRAP5b), resorption (CTX-1), pain and inflammation (NGF, CCL2, CCL3 and CCL5) were measured by ELISA.

4.3.3.1 The inhibition of HYPER-IL-6 induced bone resorption and soluble markers of osteoclast differentiation and resorption by sgp130-Fc

HYPER-IL-6 (0.5ng/mL) containing osteoclast cultures were treated with sgp130-Fc (500ng/mL) and both consequential osteoclast differentiation and bone resorption data were quantified *in vitro*. The number of $TRAP^{+ve}$ cells and osteoclasts (per disk) were comparable on disks from m-CSF + RANKL ± sgp130-Fc + HYPER-IL-6 (n=6 donors, Figures 4.17 and 4.18). However significant reductions in HYPER-IL-6-induced bone resorption by sgp130-Fc was noted (Figure 4.18, $p \leq 0.05$).

Sgp130-Fc addition to m-CSF + RANKL + HYPER-IL-6 cultures had no effect on TRAP5b or CTX-1 levels being comparable to m-CSF + RANKL cultures at both day 7 and day 10 (n=4 donors, Figure 4.19). NGF was not present in m-CSF + RANKL ± HYPER-IL-6 + sgp130-Fc cultures (data not shown). CCL2 was maintained at similar levels in all cultures until day 14, where a significant increase from 4.39 ± 0.76 to 12.49 ± 0.38ng/mL was found in cultures supplemented with m-CSF + RANKL ± HYPER-IL-6 + sgp130-Fc ($p \leq 0.001$; n=4 donors, Figure 4.20). CCL3 and CCL5 remained unchanged by the addition of m-CSF + RANKL ± HYPER-IL-6 + sgp130-Fc compared to m-CSF + RANKL cultures (n=4 donors, Figure 4.20).

i.) ii.)

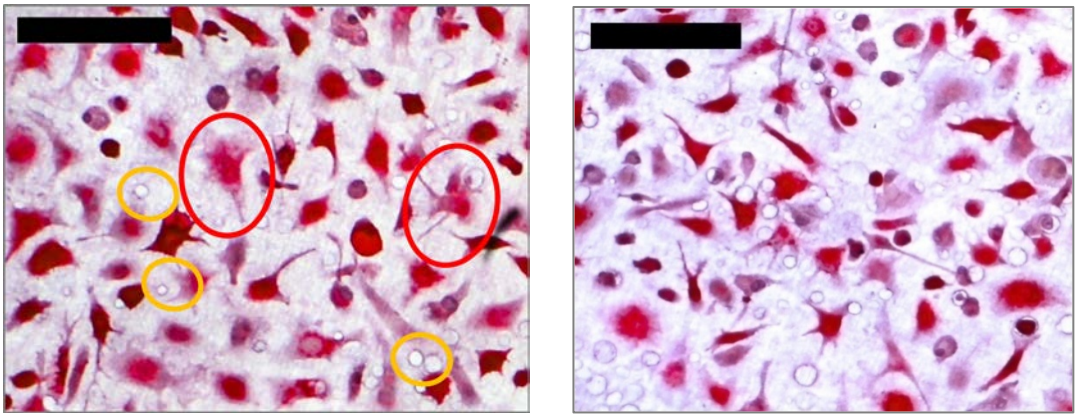

Figure 4. 17 - Supplementation of sgp130-Fc and HYPER-IL-6 into osteoclast cultures yielded comparable osteoclast numbers to differentiation cultures.. The addition of both sgp130-Fc and HYPER-IL-6 into osteoclast differentiation assays was carried out throughout the 14-day time-course. i.) Multiple $TRAP^{+ve}$ multinucleated osteoclasts(red circles) were found in differentiation cultures alongside the formation of many resorption pits (orange circles). ii.) In the presence of sgp130-Fc and HYPER-IL-6, $TRAP^{+ve}$ multinucleated cells and resorption pit number were comparable to those of differentiation cultures. (Scale bar 100um).

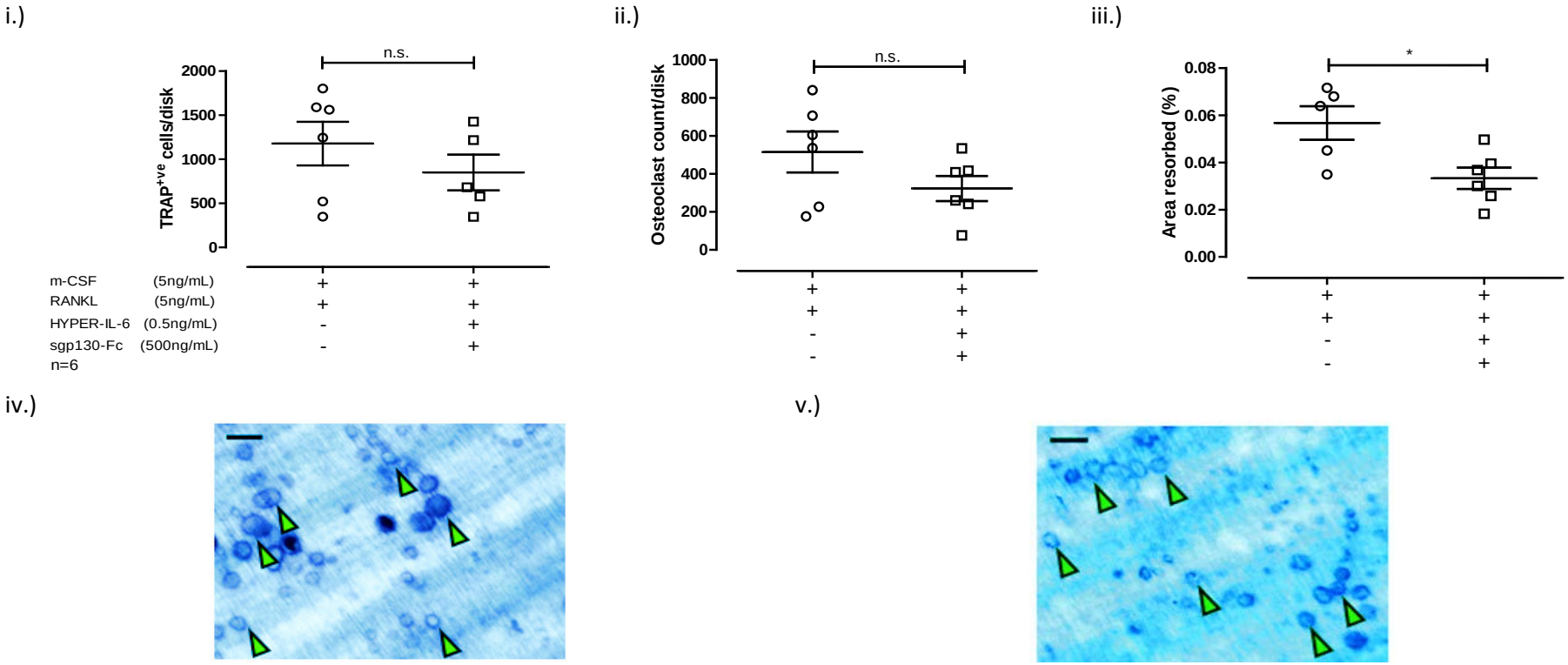

Figure 4. 18 - Sgp130-Fc and HYPER-IL-6 had no effect on TRAP^{+ve} or osteoclast number, but do significantly reduce resorption area.. Cell counts completed at day 14alongside area resorbed quantification. i.) and ii.) No significant change in TRAP^{+ve} cell or osteoclast count was found between m-CSF and RANKL ± sgp130-Fc + HYPER-IL-6. iii.) sgp130-Fc and HYPER-IL-6 supplemented cultures did however show a significant reduction in area resorbed (*p≤0.05*). iv. and v.) Representative images of resorption pits from m-CSF and RANKL ± sgp130-Fc + HYPER-IL-6 cultures. N=6 donors; 4 replicate disks per donor, mean plotted. Mean ± S.E.M. shown. Student's t-test performed (*$p \leq 0.05$). Scale bar 50µm.

i.)

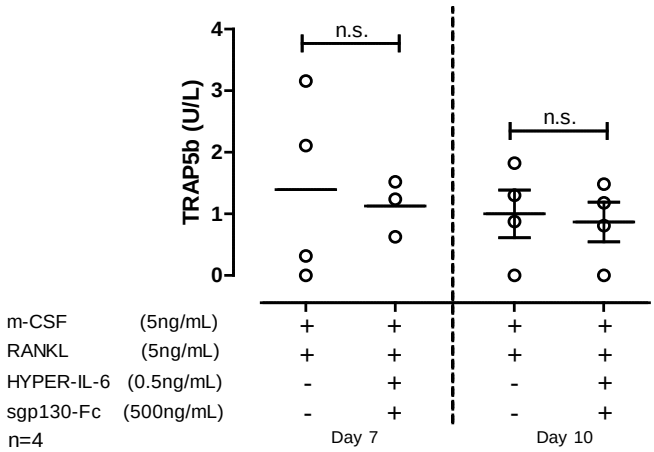

ii.)

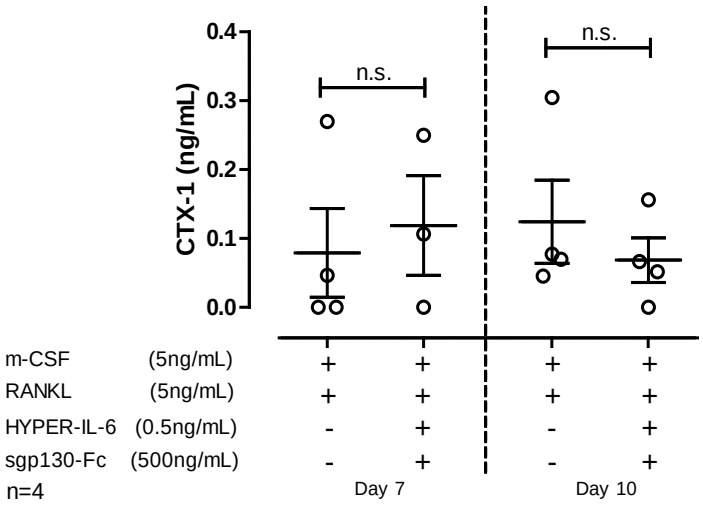

Figure 4. 19 - No significant changes in TRAP5b or CTX-1 were found in the supernatants of sgp130-Fc and HYPER-IL-6 supplemented cultures.. To help establish the effect of sgp130-FC and HYPER-IL-6 in combination on osteoclast differentiation and activity soluble levels of CTX-1 and TRAP5b were measured in harvested supernatants. i.) No significant change in TRAP5b levels over days 7 and 10 was noted either, suggested that osteoclast differentiation was not altered through the addition of sgp130-Fc and HYPER-IL-6. ii.) No significant change in CTX-1 levels were noted on day 7 or day 10, suggesting the degree of resorption in each of these cultures were comparable. N=4 donors; mean plotted from 4 replicate disks per donor. Mean ± S.E.M. shown and statistics were carried out using the Student's t-test.

i.)

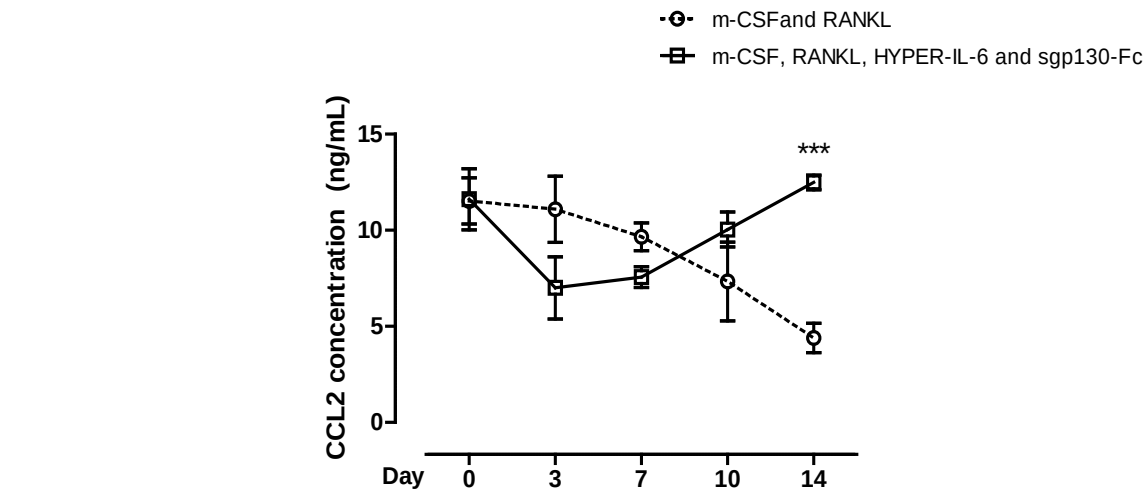

ii.)

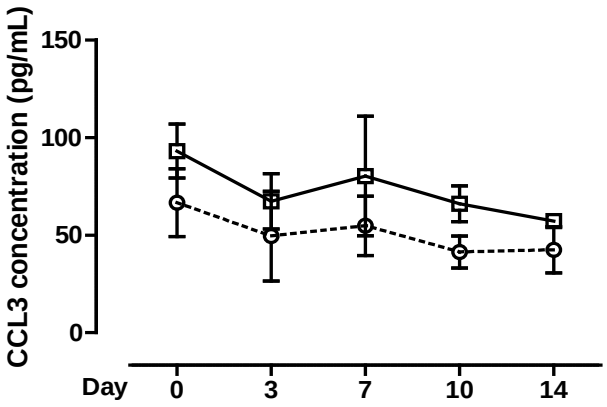

iii.)

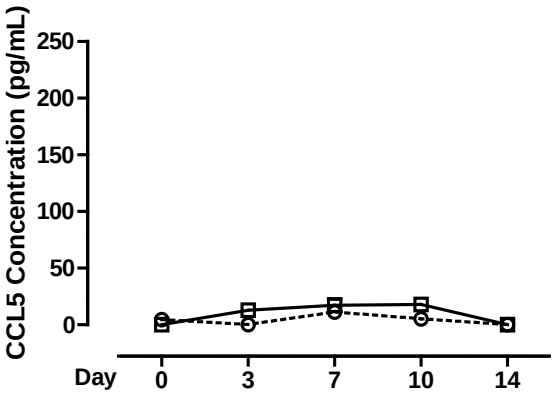

Figure 4. 20 - Supplementation of sgp13-Fc and HYPER-IL-6 into osteoclast differentiation cultures significantly increased CCL2 levels at day 14.. Following on from soluble markers of resorption and differentiation, the secretion of several chemokines were assessed in supernatants from n=6 donors where 4 replicate disks per donor were assessed. i.) Overall, no significant change in the secretion of CCL2 across the time-course was noted, but a significant increase was noted at day 14 in sgp130-Fc and HYPER-IL-6 treated cultures compared to differentiation medium cultures (*p≤0.001*). ii.) and iii.) The secretion profiles of CCL3 and CCL5 were comparable in sgp130-Fc and HYPER-IL-6 treated cultures when compared to differentiation cultures. Results were reported as mean ± S.E.M., where the mean from n=4 donors per time-point was plotted. Statistical analysis was performed using a one way ANOVA (all graphs) and a Student's t-test (concentrations at day 14 for CCL2; ***p≤0.001).

4.4 Discussion

An indirect relationship between IL-6 trans-signalling and increased osteoclastogenesis was first reported in 1993 by *Tamura et al.* but since has been reported in multiple cell systems through supplementation of IL-6 and sIL-6R into co-cultures of osteoblasts or bone marrow cells (*Tamura et al. 1993, Heinrich et al. 1998, Palmqvist et al. 2002*). The increased osteoclastogenesis resulted from IL-6 stimulated osteoblasts and T cells which secreted RANKL, thus indirectly increasing osteoclast differentiation (*Soysa et al. 2012*). The role of IL-6 trans-signalling in the process of osteoclastogenesis was further verified by the essential presence of both IL-6 and sIL-6R into cultures, and through the addition of anti-sIL-6R which reduced 'osteoclast-like multinucleated cells' (*Tamura et al. 1993*). Supporting this for the first time a direct link between IL-6 trans-signalling and osteoclastogenesis in m-CSF and RANKL supplemented $CD14^{+ve}$monocultures was identified in this chapter.

In our monocultures a basal level of IL-6 (Chapter 3, Section 3.3.11.1) was quantified in supernatants postulating a role of IL-6 signalling in osteoclastogenesis. Due to the clinical significance of increased IL-6 and its soluble receptor in destructive bone diseases (*Houssiau et al. 1988, Kyrtsonis et al. 1996, Keul et al. 1998*), and the debated existence of membrane bound IL-6R on the osteoclast (*Gao et al. 1998*), IL-6 trans-signalling was focussed upon. The inhibition of IL-6 trans-signalling, via addition of sgp130-Fc, resulted in a significant decrease in $TRAP^{+ve}$ cell number, osteoclasts and area resorbed. It was concluded that in our culture system IL-6 trans-signalling exerted a role in homeostatic osteoclastogenesis. Following this, a pathological role of increased IL-6 trans-signalling in osteoclastogenesis was investigated, mimicking the clinical aetiology of elevated IL-6 and sIL-6R in destructive bone diseases. The fusion protein HYPER-IL-6 was used initially at 10ng/mL, which induced a significant reduction in $TRAP^{+ve}$ cells yet comparable levels of resorption were reported after 14 days of culture. Such contradicting results suggested 10ng/mL HYPER-IL-6 stimulated the earlier differentiation of mononuclear cells into mature osteoclasts. If this were the case then it is conceivable that by day 14 $TRAP^{+ve}$ cells had lost adherence to the bone substrate, and only the eroded bone surface remained. This hypothesis may be tested by

obtaining cell counts every 3 days to establish whether HYPER-IL-6 had a stimulatory effect on osteoclast differentiation at 10ng/mL. Furthermore, to examine whether 10ng/ml HYPER-IL-6 was toxic to cultured cells, apoptotic cells could be quantified across the time-course using a TUNEL assay. Alternatively, a dose response relationship for HYPER-IL-6 could be examined by supplementing varying lower concentrations of HYPER-IL-6 into assays to prolong the life span of the differentiating cells. This was next tested.

A range of 0.5 - 5ng/mL HYPER-IL-6 was supplemented into disks cultured in m-CSF and RANKL (n=1 donor). This process provided preliminary data, which indicated 0.5ng/mL HYPER-IL-6 as the optimal concentration to carry out analysis at day 14; increased $TRAP^{+ve}$ cells, osteoclasts and resorption at day 14. Further supporting the selection of 0.5ng/mL HYPER-IL-6 the observed increased levels of TRAP5b and CTX-1 in harvested supernatants (day 7), suggested HYPER-IL-6 mediated an early increase in osteoclast differentiation.

From such preliminary data, 0.5ng/mL HYPER-IL-6 was taken forward for the true assessment of HYPER-IL-6 on osteoclastogenesis on a larger sample size (n=8 donors). Total cell count at day 14 was substantially attenuated in HYPER-IL-6 supplemented cultures when compared to m-CSF and RANKL alone, although this was not significant. A comparable number of $TRAP^{+ve}$ cells and osteoclasts were also quantified in both HYPER-IL-6 supplemented cultures and m-CSF and RANKL. However, HYPER-IL-6 induced a significant increase in the area of bone surface resorbed compared to m-CSF and RANKL cultures. Such data suggested an early role of HYPER-IL-6 in functional resorptive activity of the osteoclast. The quantification of CTX-1 also supported this suggestion where significantly increased levels were found at day 7 in HYPER-IL-6 supplemented m-CSF and RANKL cultures compared to m-CSF and RANKL alone, but were comparable at day 10. Collectively, the data described above indicates a role for HYPER-IL-6 in stimulating early osteoclast differentiation when compared to our control m-CSF and RANKL cultures.

Although the direct mechanisms behind the early increase in osteoclastogenesis was not established, several theories can be postulated when in context with previous publications. These theories span several stages of osteoclastogenesis including precursor cell proliferation, precursor cell migration, precursor cell fusion, TRAP^{+ve} cell adherence, the secretion of degradative products, osteoclast motility and osteoclast survival, and will be discussed next (outlined in Figure 21).

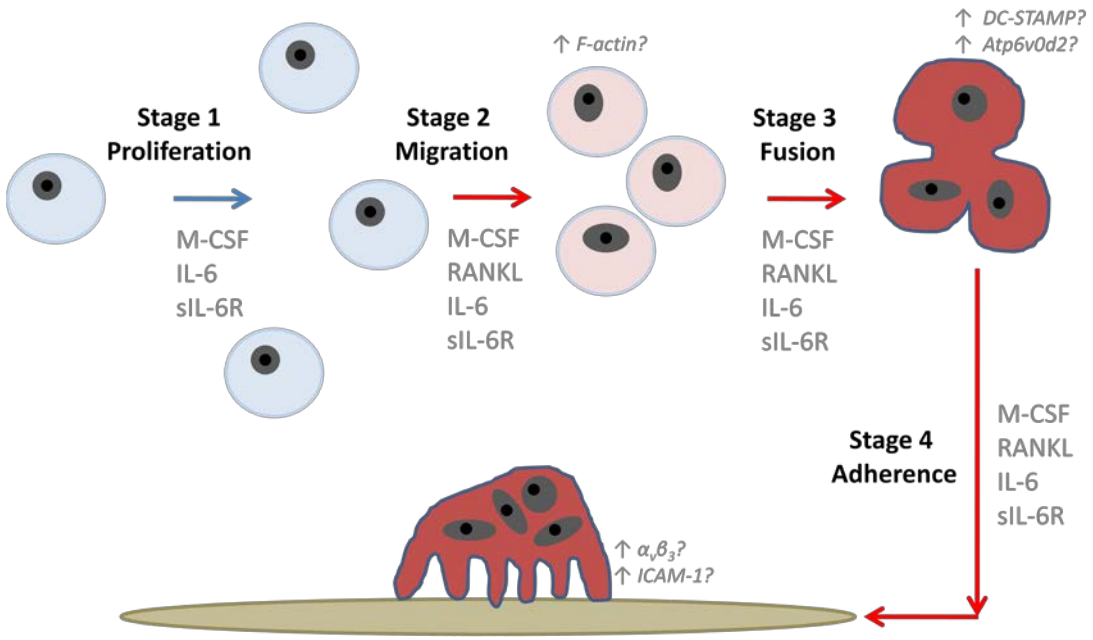

Figure 4. 21 - Postulated roles of IL-6 trans-signalling in early osteoclastogenesis.The combination of data presented in this thesis and that previously published has led to a number of postulated stages during osteoclast differentiation that IL-6/sIL-6R could influence. The following stages could be effected by IL-6 trans-signalling and the effective mediator is hypothesised in *italics* in the diagram; Stage 1 - mononuclear cell proliferation, Stage 2- mononuclear migration due to chemotaxis, Stage 3 - TRAP^{+ve} mononuclear cell fusion, Stage 4 - multinucleated TRAP^{+ve} cell adherence to bone.

The initial increase of osteoclastogenesis within our monocultures may have resulted from an increase in precursor cell proliferation and migration. In a study by *Jougasaki et al. 2010,* monocytes treated with IL-6 and sIL-6R showed enhanced cell movement, thus directly linking IL-6 trans-signalling to precursor cell migration. Further supporting this theory, gp130 was identified to have a role in monocyte migration, therefore linking this receptor to osteoclast precursors (*Johnson et al.*

2014). IL-6 trans-signalling could therefore have enabled the migration of osteoclast precursors, aiding them in creating cell-cell contact needed for cell fusion. Further experimental work assessing the migratory activity of the cells would be needed to distinguish whether IL-6 trans-signalling plays a role in osteoclast precursor proliferation and migration. Such work could include fluorescently tagging phalloidin in the cell and tracking the re-organisation and polymerisation of F-actin via confocal microscopy; especially over the first 72 hours (methodology utilised by *Campos et al. 2009*). Within this methodology an increased polymerisation would indicate enhanced cell migration, and therefore a greater chance of cell fusion.

Following this, an early increased chance of cell fusion may also have resulted in the decreased $TRAP^{+ve}$ cell number seen at day 14. The fusion proteins dendritic cell-specific transmembrane protein (DC-STAMP), integrins and Atp6v0d2 are the most common in osteoclast differentiation (*Kim et al. 2008, Miyamoto 2011, Oikawa et al. 2012, Soysa et al. 2012*, *Islam et al. 2014, Witwicka et al. 2015*). If IL-6 trans-signalling stimulated the early increase of these proteins, an increase in precursor cell fusion may have occurred. As illustrated in Section 4.2.2.3, there was no significant increase in $TRAP^{+ve}$ cell count, an early shift in peak $TRAP^{+ve}$ cell number could have been seen, which by day 14 had decreased to non-significant levels due to the limited precursor pool. Although no current research has investigated a relationship between IL-6 trans-signalling and the expression of fusion proteins, there have been reports of the effect of IL-6 alone. *Sanecka et al. (2011)* reported IL-6 secretion to be reduced from murine DC-$STAMP^{-/-}$ dendritic cells, therefore implying a role of DC-STAMP in IL-6 secretion. The relevance of this relationship is however questionable in relation to the osteoclast as dendritic cells express IL-6Rα; therefore observed effects may have resulted from classical and not trans-signalling (*Park et al. 2004*). Following this, IL-6 was reported to have no impact on DC-STAMP or Atp6v0d2 expression in osteoclast precursor cultures (*Teramachi et al. 2014*). Again, such negligible effects could be a direct result of sIL-6R being absent, limiting signalling to the classical IL-6 pathway and not trans-signalling. Overall,

further experimental work is essential to identifying and understanding the role of IL-6 trans-signalling in the expression of fusion proteins.

Subsequent to cell fusion resulting in multinucleated $TRAP^{+ve}$ cells, IL-6 trans-signalling could have also exerted a stimulatory effect on cell adherence to the bone substrate. This was highlighted by *Gado and colleagues (2000)* who reported a role of IL-6/sIL-6R in the elevated expression of adhesion proteins on the surface of bone marrow mononuclear cells in MM. IL-6 trans-signalling could therefore have increased the number of precursor cells capable of adherence to the bone substrate, and thus, impacted on osteoclast differentiation and fusion. Additional to this, IL-6 and sIL-6R secretions from apoptotic osteocytes are known to increase ICAM-1 resulting in increased osteoclast precursor recruitment, attachment and osteoclastogenesis (*Cheung et al. 2012)*. Furthermore, a link between IL-6 and $\alpha_v\beta_3$was also previously reported (*Antonov et al. 2011*), but it was thought that the $\alpha_v\beta_3$ stimulation caused NF-κβ signalling and which increased IL-6 secretion, and not vice versa. To determine the effect of IL-6 trans-signalling on the expression of attachment proteins their gene or protein expression could be quantified between day 0-7 of osteoclast differentiation within m-CSF and RANKL cultures supplemented with and without HYPER-IL-6.

The discussion points above yield speculation as to why the $TRAP^{+ve}$ cell count in sgp130-Fc supplemented cultures significantly reduced. It is believed that the above points are more critical to IL-6/sIL-6R associated osteoclast differentiation, rather than mature osteoclast activity, due to representative images showing a significant lack of $TRAP^{+ve}$ osteoclasts in sgp130-Fc cultures, suggesting sgp130-Fc inhibited osteoclastogenesis early on, and conversely HYPER-IL-6 stimulated the early differentiation of osteoclasts.

The significant increase in area resorbed could have resulted from two possible pathways. Firstly, IL-6 trans-signalling could have increased the number of differentiating osteoclasts due to increased precursor cell proliferation, migration and fusion, as discussed above. Collectively, these changes would result in an increased resorption, and/or IL-6 trans-signalling stimulated motility and survival of

mature osteoclasts, where a single osteoclast exerted a stronger resorptive phenotype. *In vivo* data has previously suggested a role for IL-6 in mature osteoclast motility, where in IL-$6^{-/-}$ mice the osteoclast motility was significantly reduced in joints subjected to antigen-induced arthritis (*Wong et al. 2006*). However, a definition between IL-6 classical and IL-6 trans-signalling was not made.

Following general osteoclast motility, a role of IL-6 trans-signalling on the secretion of resorptive enzymes from the osteoclast could also be postulated. Supporting this hypothesis is our finding that HYPER-IL-6 caused a significant increase in pit depth (compared to m-CSF and RANKL cultures), but had no effect on pit surface area or volume. As no increase in individual pit area was found, it is unlikely that IL-6/sIL-6R caused an increase in osteoclast cell size, and therefore had no further role in precursor cell fusion for giant multinucleated cells. The interpretation of pit depth data does exhibit one major limitation however; all data was obtained from one donor where multiple pits under each treatment condition were quantified. Increased sample number is therefore pivotal for reproducibility and reliability of this data to be proven and would need to be completed in future experiments (*N.B.* sample number was restricted due to time restraints). Despite this, preliminary data shows for the first time that IL-6/sIL-6R is linked to a significant increase in pit depth. Translationally, this data could have large diagnostic benefit, especially in patients with elevated IL-6 and/or sIL-6R, potentially allowing the classification of their disease phenotype (further discussed in Chapter 6). Furthermore, IL-6 trans-signalling has also been reported to attenuate new bone formation via a down-regulation of osteoblast activity and a decrease in secretion of OPG thus heightening bone destruction (*Gado et al. 2000*).

To our knowledge this is the first reported data of IL-6 trans-signalling significantly increasing resorption pit depth in a monoculture system, and suggests IL-6 trans-signalling to stimulate the enhanced secretion of degradative enzymes. In monocultures, no published data currently exists to identify IL-6 trans-signalling stimulating the secretion of resorptive enzymes (CATK, TRAP, MMP-2, -3, -9 and -13*etc.*) from the osteoclast, therefore making this a distinct area of research for the future. Interestingly, an association between CATK and IL-6 mRNA has been

reported due to the discovery that a response sequence to IL-6 fell within the 5'-untranslated region of CATK, and this was also true for TRAP, and once activated stimulates their secretion (*Reddy et al. 1995, Rood et al. 1997, Li and Chen 1999*, *Podgorski et al. 2009*). However, a recent report indicated a significant decrease in IL-6 secretion due to CATK inhibition, therefore suggesting IL-6 was resultant of CATK expression, and not vice versa (*Hussein et al. 2016*). Controversially, data reported from murine co-cultures showed unchanging CATK mRNA expression in the presence of IL-6, although cultures may have lacked sIL-6R preventing IL-6 trans-signalling (*Kamolmatyakul et al. 2001*).

IL-6 and sIL-6R have also been reported to induce the secretion of TRAP5b *Hashizume et al. (2008)* also reported IL-6 and sIL-6R to induce TRAP5b secretion, which could again have led to increased osteoclast differentiation. A controversial role of IL-6 also exists for MMP secretion, where it's been suggested to stimulate secretion of MMPs -1, -2, -3, -9 and -13 MMPs from synovial cells or murine calvarial cultures (*Kusano et al. 1998, Hashizume and Mihara 2009, Suzuki et al. 2010*). Such a mechanism could be explained by the individual actions of IL-6 classical signalling versus trans-signalling, but this is not well characterised and needs further investigation. As the specific pathway of IL-6 signalling was not confirmed in these experiments, inference of data is completed with caution. However, in murine calvarial cultures IL-6/sIL-6R complex enhanced MMP-2, -3, -9 and -13 secretion, showing direct relation to IL-6 trans-signalling, but the origin of secretion was unknown due to the use of co-cultures (*Kusano et al. 1998*). Furthermore, IL-6 trans-signalling was reported to increase RANKL signalling and therefore enhance MMP9 secretion from osteoclasts, thus, providing a direct link to IL-6 trans-signalling and osteoclast activity (*Sundaram et al. 2007*). To fully establish the effects of IL-6 trans-signalling on the resorptive enzyme secretion from the osteoclast an extensive amount of research needs to be completed including methodologies such as ELISAs (CTX-1), zymograms (MMPs), histological staining (of MMPs, TRAP) and protein quantification. Following this, knock-out models of enzymes (both *in vitro* and *in vivo*) found to be associated with IL-6 trans-

signalling in osteoclast cultures could be used to further define its role in direct osteoclast-mediated bone destruction.

An explanation for the observed increased in resorbed area can therefore be postulated from the results reported in this Chapter and from previous publications. However, what is still unknown is why a general decrease in $TRAP^{+ve}$ cell number resulted. It was reported that the downstream activation of phophoinositide-3 (PI3K) from IL-6 trans-signalling is an important anti-apoptotic mediator through phosphorylating B cell leukemia-2 (Bcl-2) and Bcl-2 associated death promoter (BAD), preventing their association (*Heinrich et al. 1998, Hirano et al. 2000*). Such a mechanism would therefore prolong cell survival, thus directly linking to IL-6 trans-signalling. However, as the osteoclasts primary function is to resorb bone, once its purpose has been fulfilled cell death may occur. For this reason it could be suggested that $TRAP^{+ve}$ cell number decreased at day 14 in HYPER-IL-6 cultures due to their extensive stimulation in the early stages of the osteoclast assay (day 1-7). By day 14 osteoclasts have lost adherence and senescence associated secretory phenotype (SASP) may have been activated following STAT1/STAT3 and p53 interaction (downstream of IL-6 trans-signalling; *Kojima et al. 2013*), meaning only resorption sites remain. Supporting this theory in our culture system supplemented with sgp130-Fc, the downstream activation of phophoinositide-3 (PI3K) from IL-6 trans-signalling would have been attenuated and cellular apoptosis would have increased. To prove such a theory the quantification of anti-apoptotic protein secretion from the osteoclast (RT-PCR) or a TUNEL assay would identify the importance of IL-6/sIL-6R in osteoclast apoptosis. $TRAP^{+ve}$ cell visualisation pre-day 14 (*i.e.* day 7) may reveal the optimal time-point of assay termination.

Data reported from cultures supplemented with HYPER-IL-6 or sgp130-Fc highlighted the importance of IL-6 trans-signalling in osteoclast formation and osteoclast-mediated bone destruction. Importantly, the supplementation of sgp130-Fc or HYPER-IL-6 into monocultures at day 0 was suggested as the rate-determining step of osteoclastogenesis (Figure 4.22).

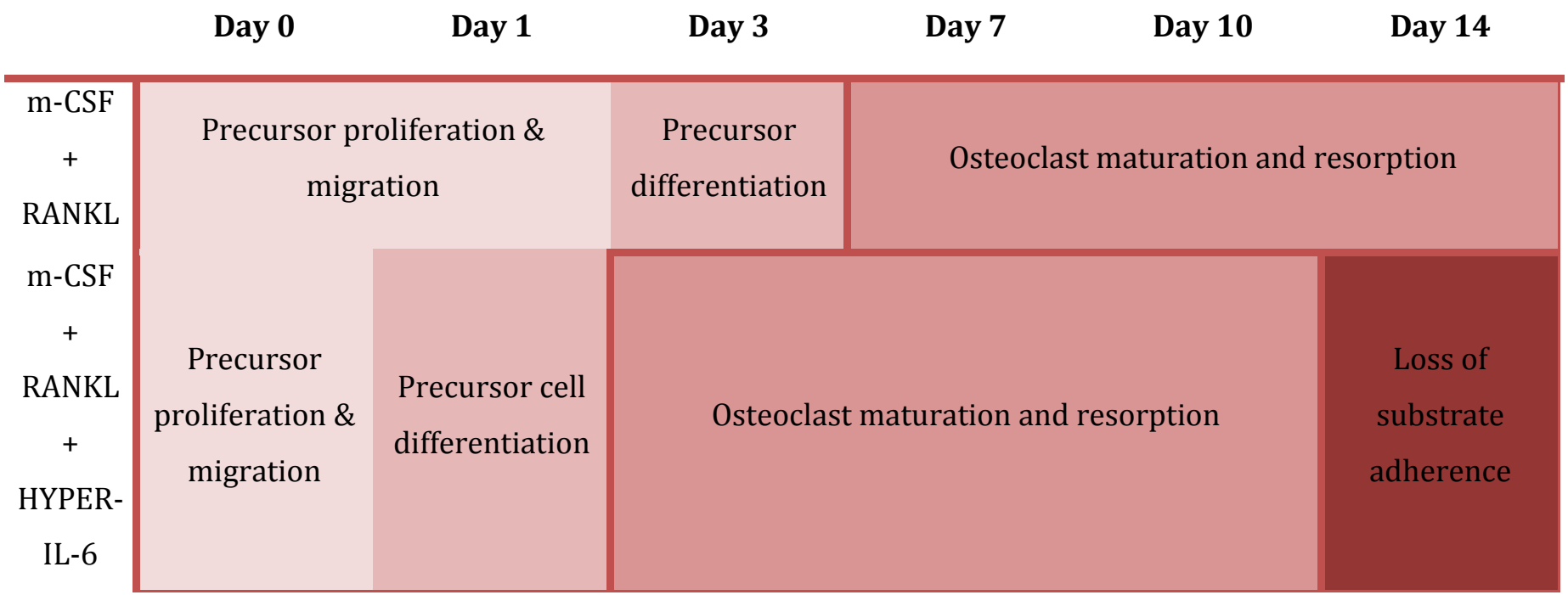

Figure 4. 22 - An illustration of the postulated shift exerted by HYPER-IL-6.. The addition of HYPER-IL-6 is thought to have stimulated an increase in osteoclast precursor cell proliferation, migration and differentiation within the first days of culture in the presence of RANKL. Subsequently peak osteoclast numbers were hypothesised to have occurred around day 7, where simultaneous increases in bone resorption and pit depth would have occurred (day 7 to 10). Following extensive resorption, mature osteoclasts are postulated to have lost adherence to the bone substrate, and therefore account for the decreased osteoclast number at day 14.

4.4.1 The effect of IL-6 trans-signalling on the secretion of chemotactic proteins

In addition to the proposed effects of IL-6 trans-signalling on osteoclastogenesis, it is thought that IL-6/sIL-6R may also affect the release of chemotactic proteins from differentiating cells and/or mature osteoclasts. The release of such chemotactic factors could thus exert additional effects on osteoclast differentiation/resorption and co-localised cells. Reported here, IL-6 concentration/cell increased over 14 days and could therefore suggest self-amplification (Chapter 3, Section 3.3.11.1). Similarly, an increase in gp130 transcription and cellular expression was reported in smooth muscle cells when stimulated through IL-6 trans-signalling (*Klouche et al. 1999)*, and it could be postulated that the same occurs in osteoclastogenesis. *In vivo* the hypothesised existence of an IL-6 trans-signalling induced amplification loop would result in severe bone destruction (*i.e.* the presence of such an amplification loop has been reported in smooth muscle cells by *Klouche et al. 1999*). In contrast, *in vitro*, the limited number of osteoclast pre-cursors would mean a decrease in $TRAP^{+ve}$ cell count would be observed despite the observed increase in bone area resorption, thus mimicking the results observed in this chapter.

This chapter demonstrates that both CCL2 and CCL3 secretion in osteoclast differentiation cultures were independent of IL-6 trans-signalling. This finding opposed that previously reported by Hu and colleagues *(2008),* who identified IL-6enhanced CCL2 secretion and stimulated *in vitro* monocyte migration. Similarly, and in contrast to the findings of this thesis, IL-6 and sIL-6R secretion from coronary obstructive pulmonary disease (COPD) patients was shown to significantly correlate to increased CCL3 (*Ravi et al. 2014*). However, the use of co-cultures within the previously published studies and pure cultures in this thesis may account for the observed differences in IL-6 mediated CCL2 and CCL3 secretion. Therefore, the data described within this chapter furthers knowledge in the field by showing elevated CCL2 and CCL3 secretion induced by IL-6 trans-signalling was not of osteoclast origin, and nor does it aid monocyte migration. The effects reported from these previous studies are therefore independent of IL-6 trans-signalling in the osteoclast

assay. However, it is likely that they have synergistic relationships in inflammation and leukocyte recruitment *in vivo*. Further experiments defining the role of CCL3 in osteoclastogenesis will be extensively reported in Chapter 5.

4.4.2 IL-6 as a pain mediator in pathological bone destruction

In addition to the postulated role of IL-6 trans-signalling in osteoclast differentiation and resorption pit formation, it has also been linked to bone associated pain. Crucially, IL-6 alone cannot sensitize nociceptors until sIL-6R is present, and mice lacking gp130 on nociceptors present with attenuated inflammatory algesia, thus further highlighting the role of IL-6 trans-signalling in nociception (*Obreja et al. 2002, Andratsch et al. 2009*). IL-6 trans-signalling in models of tissue inflammation and neuronal injury sensitizes transient receptor potential channel vanilloid (TRPV1) on DRG through gp130, leading to increased neuronal cell communication, induction of substance P, calcitonin gene-related peptide (CGRP) and galanin (*Murphy et al. 1999, De Jongh et al. 2003, Oberja et al. 2005, Andratsch et al. 2009*, *Scheller et al. 2011, Miguel, Kraychete& Nascimento. 2014*). As pain assessment was not a primary outcome of the experimental methodology, this was however not directly assessed. Despite this, a role of IL-6 trans-signalling in bone-associated pain will be discussed and put forward in relation to our findings.

The supplementation of the osteoclast assay with HYPER-IL-6 resulted in an increase in the area resorbed implying significantly elevated osteoclast activity, an increase bone acidification and dissolution of bone mineral through H^+ secretion [carbonic anhydrase; $H_2O + CO_2 \rightarrow HCO_3^- + H^+$] (*Gay & Mueller 1974, Lehenkari et al. 1998*). Subsequently, increased bone pain could result from an enhanced activation of acid-sensing neurones (TRPV1) alongside the release of neuropeptides (*i.e.* CGRP) which potentiate and translate noxious stimuli into pain (*Yoneda et al. 2011*). Although pain cannot be measured *in vitro*, harvested supernatants from across the time-course could have been assessed for pH to yield data regarding the H^+ content. Finally, any secondary effects of NGF, CCL2 and CCL3 as pain mediators were

thought minimal due to their concentrations either being unquantifiable (NGF) or unchanging (CCL2 and CCL3) after stimulation with HYPER-IL-6.

4.4.3 IL-6 trans-signalling as a potential therapeutic target in osteoclast-mediated diseases

In vivo IL-6 trans-signalling exerts a stimulatory role in bone destruction and associated pain, yet no direct evidence for its role on osteoclastogenesis has been reported, only from co-cultures. For the first time data reported in this chapter proved IL-6 trans-signalling to directly and significantly increase the resorptive capability of the osteoclast and lead to substantial bone resorption. Such data therefore presents IL-6 trans-signalling as a therapeutic target for the inhibition of bone destruction. Sgp130-Fc was used to assess the efficacy of targeting IL-6 trans-signalling to decrease bone destruction. Sgp130-Fc was shown to significantly decrease osteoclastic resorption, through reducing levels of osteoclastogenesis, TRAP5b and CTX-1 to levels comparable to m-CSF and RANKL cultures. Due to decreased osteoclast numbers in sgp130-Fc cultures an early role of IL-6 trans-signalling in osteoclast differentiation is again suggested. This further supports the hypothesised role of HYPER-IL-6. If IL-6 trans-signalling exerted negligible effect on osteoclast differentiation and primarily affected the activity of the mature osteoclast, equal numbers of osteoclast would be found in sgp130-Fc treated to m-CSF and RANKL only cultures.

The results presented in this chapter support and further the knowledge of IL-6's role in bone destruction, where previous data from IL-$6^{-/-}$ models have shown synergistic relationships between IL-6 and resorption. For example, the synergistic relationship between IL-6 and estrogen in bone destruction (*Poli et al. 1994*), and the importance of IL-6 in mononuclear cell proliferation (*Wong et al. 2006*). However, the importance of IL-6 trans-signalling to classical signalling in osteoclast differentiation was still unknown. IL-6 trans-signalling was first associated with osteoclastogenesis in a seminal *in vivo* study, whereby the treatment of murine CIA with sgp130-Fc resulted in significant reductions of arthritis severity (including inflammation, synovial hyperplasia, infiltration of leukocytes and joint destruction) and decreased disease progression (*Nowell et al. 2009*). Additional work from the

Rheumatology group at Cardiff University also suggested that the treatment of murine CIA with sgp130-Fc led to fewer $TRAP^{+ve}$ multinucleated cells in addition to reduced bone and cartilage erosions (*Smale,* unpublished). The data of Nowell and colleagues (2009) is strongly supported by our *in vitro* data, which provided definitive evidence for a role of IL-6 trans-signalling on direct osteoclastogenesis, thus, highlighting IL-6 trans-signalling as a novel therapeutic target.

The data presented here, in addition to the dual inhibitory functionality of sgp130-Fc on inflammation and bone erosion (*Nowell et al 2009*), illustrate the direct and indirect effects of IL-6 trans-signalling on osteoclastogenesis. Direct effects of attenuated IL-6 trans-signalling lead to reduced monocyte infiltration, migration and fusion resulting in decreased osteoclast pre-cursors. In addition, data reported in this chapter also suggests that sgp130-Fc significantly attenuates the secretion of resorptive enzymes, reducing visible bone erosions both *in vitro* (area of disk resorbed) and *in vivo* (CIA joint histology). Indirectly, sgp130-Fc prevents the secretion of osteoclast stimulating factors (*i.e.* RANKL) and chemotactic mediators (*i.e.* CCL2, CCL3 *etc*) from co-localised cells (T cells/stromal cells) further reducing osteoclast differentiation and favouring neutrophil differentiation and migration (*Rabe et al. 2008*). Although further research is needed, the data presented within this thesis points to a possible role for sgp130-Fc in the treatment for pain (*i.e.* attenuated hyperalgesia and hypersensitivity), and for controlling bone resorption associated with hormone imbalances (*i.e.* menopausal women). Thus possibly identifying novel therapeutic areas for an IL-6 based therapy.

The combined published data and that reported in this chapter therefore identifies the potential clinical use of sgp130-Fc. In addition to the pre-discussed effectiveness of this treatment, its use also has a major advantage over currently used methods due to its specificity for inhibiting IL-6 trans-signalling. Currently therapeutic strategies involve antibody antagonists to IL-6R (*i.e.* tocilizumab) which neutralise both membrane bound and soluble receptor, and have been clinically used in inflammatory diseases including RA where disease onset (*i.e.* decreased disease activity score) and pathology (*i.e.* C-reactive protein) are attenuated (*Yoshizake et al. 1998, Choy et al. 2002*). However, the lack of specificity results in

the global inhibition of IL-6 signalling, which could potentially exert negative side-effects on homeostatic leukocyte migration and function (*Mantovani, Kaplanski & Farnarier 2003, Weissenbach et al. 2004*).

The selective inhibition of IL-6 trans-signalling via sgp130-Fc shows increased efficacy and has increased potential for use as a therapeutic in the future treatment of destructive bone diseases. Alternatively, in the future small interfering RNA (siRNA) could be used as a therapy for enhanced IL-6 trans-signalling (*Whitehead et al. 2009*). sIL-6R gene expression could be targeted by siRNA thus preventing IL-6 trans-signalling through proteolytic cleavage, while unaltering membrane expression of IL-6R, therefore maintaining classical signalling. Precedence for this hypothesis was exhibited as siRNA targeting of IL-6 gene expression resulted in reduced signalling protein activation, cell expansion, interactions and survival (*Bharadwaj et al. 2011*). However, prior to the use of either of these methodologies, definitive evidence of IL-6 trans-signalling in osteoclastogenesis is essential. Therefore, further studies would include complete time-course concentration profiling of IL-6, sIL-6R and their complex to identify the time-points that IL-6 trans-signalling exerts its primary effects both *in vitro* and *in vivo*. Subsequently, effective concentration/dose ranges, dosage times and drug delivery routes would be distinguished, alongside a consideration of sgp130-Fc potency against alternative treatments of IL-6 inhibition.

4.5 Conclusion

The data presented within this chapter builds upon the published literature that suggested a role for IL-6 trans-signalling in co-cultures of osteoclasts (*Tamura et al. 1993, Heinrich et al. 1998* and *Palmqvist et al. 2002*). Specifically, our data identifies a novel, direct link between IL-6 trans-signalling and osteoclastogenesis in m-CSF and RANKL supplemented $CD14^{+ve}$ monocultures. Resorption pit characteristics were obtained from a confocal methodology developed in this thesis. A novel pathological role of IL-6 trans-signalling (illustrated via HYPER-IL-6) in enhanced osteoclast resorption was reported alongside increased resorption pit depth (a novel pathological outcome). Collectively, the data suggested that elevated IL-6 trans-signalling led to an early increase in osteoclast number, although this is yet to be proven.IL-6 trans-signalling was therefore presented as a therapeutic target in increased osteoclastogenesis *in vitro*, where supplementation with sgp130-Fc reduced osteoclast number and resorption to pre-established control levels. In conclusion, this chapter presents preliminary data for IL-6 trans-signalling as a therapeutic target in enhanced osteoclastogenesis, where further work investigating the translational impact of sgp130-Fc on *in vivo* osteoclastogenesis is key to its future pharmaceutical potential.

Chapter 5:Defining the role of C-C chemokine ligand 3 (CCL3) in osteoclast differentiation and functional resorptive activity *in vitro* and *in vivo*

5.1 Introduction

A novel role for CCL3 in osteoclast differentiation was postulated from the correlation of CCL3 and osteoclast number reported at the conclusion of Chapter 3. This chapter therefore aims to decipher the role CCL3 plays during the differentiation and functional resorptive activity of the osteoclast *in vitro*, and to elucidate whether this chemokine could be a therapeutic target *in vivo* for erosive bone diseases.

M-CSF and RANKL signalling induces the characteristic gene expression of mediators pivotal to osteoclast differentiation and function; TRAP, CATK and calcitonin receptor (CTR) (*Boyle, Simonet& Lacey2003)*. The third mediator OPG (natural decoy receptor of RANKL), inhibits osteoclast formation and maintains a healthy bone turnover system. Disruption of this equilibrium results in a diseased state where cytokines and chemokines exert pathological roles leading to dysregulation of bone homeostasis. In the last 15 years several inflammatory CXC- and CC-chemokines were reported to exert a role in osteoclastogenesis and functional resorption. CXC chemokines are involved in the chemotaxis of neutrophils and the process of angiogenesis, both of which maintain the diseased joint with a constant supply of nutrients and leukocytes via the newly formed vasculature. CXCL8, CXCL10, CXCL9 and CXCL12 are increased in synovial tissue (ST) and fluid (SF) of RA patients and are secreted from synovial macrophages and ST cells (*Koch 2005)*. CXCL5, CXCL1, CXCL7, CXCL6 are also found at increased levels in RA SF and ST but are commonly secreted from ST fibroblasts (*Koch 2005)*. CC- chemokines CCL2, CCL3, CCL5, and CCL20 are all elevated and causative in monocyte recruitment to ST and SF in RA, and are secreted from ST fibroblasts and macrophages (*Koch 2005)*. Several *in vitro* co-culture studies have monitored the effect of these chemokines on osteoclastogenesis. However, the direct role of chemokines on mononuclear cell differentiation into osteoclasts is hard to distinguish due to their secondary effects on co-cultured cells.

CCL3 is a chemokine of growing importance in destructive diseases (RA, OA, JIA and MM) where pathologically elevated osteoclastogenesis is reported (*Koch et al. 1994, Oba et al. 2005, Vangsness et al. 2011, Muller et al. 2015,*). Bone destruction

results from the secretion of matrix degrading proteins and the secretion of H^+ ions via proton pumps which together dissolve bone matrix. Importantly, CCL3 is stable at low pH, as in an eroded joint, further implicating this chemokine in osteoclastogenesis and increased bone resorption. The quantification of this increased bone resorption traditionally occurs through toluidine blue staining (*Massey & Flanagan 1999)*. Recent insight into two dimensional (2-D) analysis has yielded questions regarding its translocation to osteoclast activity, where 3D imaging is providing greater knowledge of the osteoclasts activity. One pioneer in the field, *Goldberg et al. (2012)*, published initial results of using 3-D imaging to quantify resorption, where it was concluded that area resorbed was deceptive due to altering volumes of pits dependent upon Rho GTPases in the osteoclast. In order to further our knowledge of the effect CCL3 has on osteoclastogenesis and define the 3-D characteristics of resorption the novel analysis method using z-stacks from laser-scanning confocal microscopy used in Chapter 4 will similarly be used.

A role of CCL3 has also been postulated in pain and inflammation due to significantly elevated levels in RA, OA, Arthus reaction, inflammatory bowel disease and chronic obstructive pulmonary disease (COPD), but the mechanistic action of this increase is still unknown (*Ajuebor et al. 2004, Yanaba et al. 2004, Szekanecz et al. 2010, Vangsness et al. 2011, Ravi et al. 2014)*. In these diseases, the significant increase in CCL3 was also found to be simultaneous with other pro-inflammatory cytokines and chemokines in the inflammatory milieu of the joint; IL-6, sIL-6R, CCL2 and CCL5 (*Chintalacharuvu et al. 2005, Koch 2005, Pharoah et al. 2006, Hashizume & Mihara 2011*). Published material states the effect of CCL3 on the co-expression of these mediators and significant enhancement on osteoclastogenesis in co-cultures and *in vivo* models (*Koch 2005, Oba et al. 2005, Nowell et al. 2009, Vangsness et al. 2011*). However, their direct effect on osteoclast differentiation and resorption remains elusive.

Published material describes a clear indirect role for CCL3 in disease pathology, inflammation and possibly pain, but no direct evidence for its role on osteoclastogenesis was shown. In this chapter, human *in vitro* monocultures will determine the role CCL3 exerts on osteoclast differentiation and on resorptive

activity. Additionally, through the use of *in vivo* methods, the effect of CCL3 on both 2D and 3D bone pathology and inflammation will be assessed. The hypothesis for this chapter is that CCL3 enhances osteoclast differentiation and resorption *in vitro* and *in vivo*. In order to address this hypothesis, the chapter proceeds with these following objectives:-

1.) To measure CCL3 by ELISA from cultures of human $CD14^{+ve}$ cells exposed to osteoclast-differentiation stimulating mediators, and to determine CCL3's role in osteoclastogenesis and bone degeneration using a neutralising antibody *in vitro*

2.) To investigate the presence of surrogate soluble markers of osteoclast differentiation (TRAP5B), resorption (CTX-1), pain and inflammation (NGF, CCL2, CCL3, CCL5, IL-6 and sIL-6R) by ELISA in osteoclast differentiation assays treated to anti-CCL3.

3.) To study the effect of CCL3 inhibition on bone pathology in an *in vivo* model of murine inflammatory arthritis

5.2 Essential Methodology

The below diagrams highlight the essential methods used throughout this chapter to obtain the reported results. Full detail of all these methods can be found in their respective sections as stated next to the diagrams.

- ***Osteoclast assays (Chapter 2 Sections 2.2.1 - 2.2.4)***

Condition	Number of Donors	Number of Replicate Disks per donor	Chapter Section	Comments
m-CSF only	4	4	5.3.1	Mean values from the replicate disks of each donor plotted
m-CSF and OPG (100ng/mL)	4	4		
m-CSF and RANKL	8	4		
m-CSF, RANKL and OPG (100ng/mL)	5	4		
m-CSF and RANKL	1	4	5.3.2.2	
m-CSF, RANKL and anti-CCL3 (2ng/mL)	1	4		
m-CSF, RANKL and anti-CCL3 (4ng/mL)	1	8		
m-CSF, RANKL and anti-CCL3 (8ng/mL)	1	8		
m-CSF only	4	2	5.3.2.3 to 5.3.2.5	
m-CSF and anti-CCL3 (8ng/mL)	5	2		
m-CSF and IgG1 (8ng/mL)	4	2		
m-CSF and RANKL	9	4		
m-CSF, RANKL and anti-CCL3 (8ng/mL)	9	4		
m-CSF, RANKL and IgG1 (8ng/mL)	4	4		
m-CSF only	9	2	5.3.4	
m-CSF and OPG (8ng/mL)	4	2		
m-CSF and RANKL	8	4		
m-CSF, RANKL and OPG (8ng/mL)	5	4		

-PBMCs isolated from healthy human whole blood via density centrifugation went through magnetic activated cell sorting to yield a pure suspension of $CD14^{+ve}$ monocytes (as illustrated).

- Disks were seeded with 3.2 x 10^6 cells and cultured with m-CSF alone (5ng/mL) or in combination with RANKL (5ng/mL). Culture supernatants collected and replenished every 3-4 days. Disks harvested at day 14.

Caption 5 - Isolation of human CD14+ve monocytes from peripheral blood. Human blood layered onto hisotpaque is centrifuged yielding peripheral blood mononuclear cells. CD14+ve monocytes isolated by magnetic activated cell sorting and 3.2 x 10^6 cells/mL are seeded onto ivory disks prior to culture in osteoclast proliferation/differentiation medium

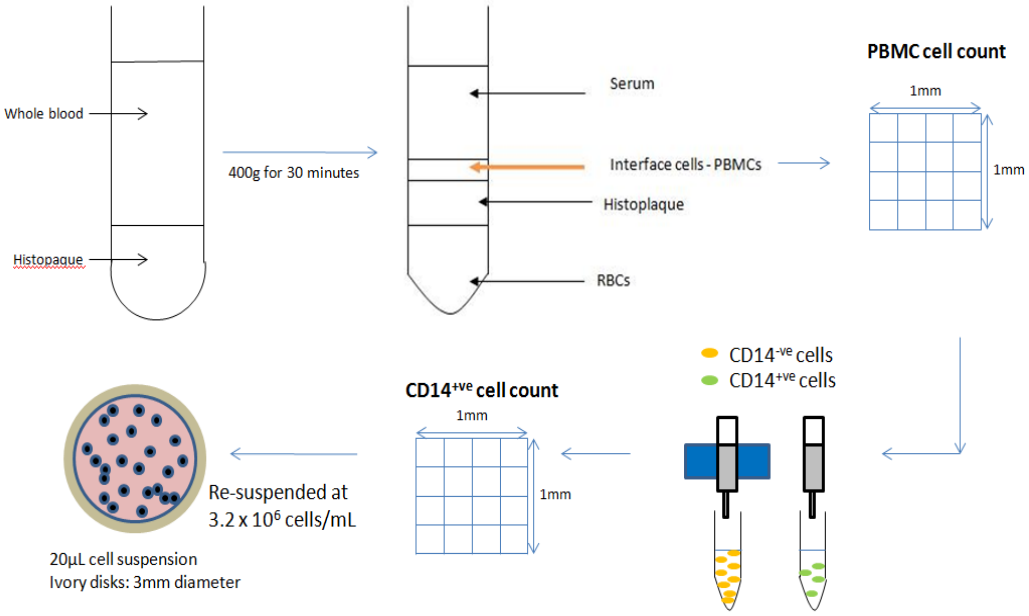

-Disks harvested at day 14 were fixed with glutaraldehyde prior to staining with TRAP and haematoxylin to identify total cells and osteoclasts; quantified through MATLAB and manual counts. Following cell counts adhered cells were removed and disks stained with toluidine blue or calcein to facilitate quantification of resorbed area. Harvested supernatants were analysed by ELISA.

-In addition, individual pit parameters (area, perimeter, volume and depth) were imaged via confocal microscopy (x60) and quantified using MetaMorph. All of these assessments can be found in the diagram which follows.

Caption 6 - The osteoclast assay and functional analyses. Disks seeded with $CD14^{+ve}$ monocytes are cultured up to day 14 in the presence or absence of anti-CCL3. Every 3-4 days disks and their supernatants were harvested and used for one of the following analyses; cell staining (TRAP and haematoxylin), area of resorption quantification (toluidine blue or calcein), confocal analysis of individual pit characteristics, and ELISA.

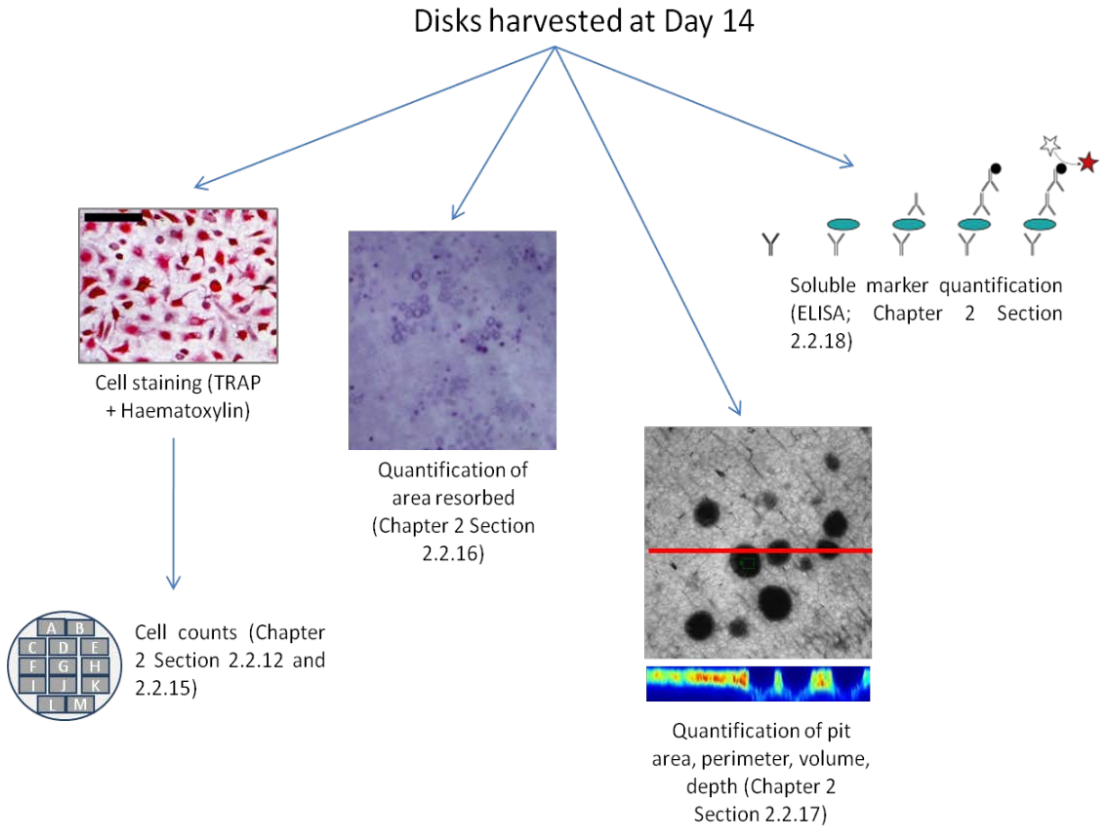

- ***CIA (Chapter 2 Section 2.2.19)***

-Male DBA-1 mice (n=12) were equally divided into two groups; a control IgG1 group (n=6) and an anti-CCL3 group (n=6).

-Mice were injected i.d. at day 0 with 2 x 50µL CFA containing 2mg/mL collagen. A booster i.d. injection of 2 x 50µL CFA + collagen was given at day 21. At day 21 the IgG1 control group received 100µL i.p. injection of IgG1 antibody (5mg/kg), and the anti-CCL3 group received an i.p. injection of anti-CCL3 (5mg/kg). Mice received an additional 5 doses every other day prior to being culled on day 29. Paw diameter was assessed every day alongside arthritis severity (clinical score); each paw was scored from 1 to 4 (see Chapter 2 Section 2.2.19 for details).An overview is presented below.

Caption 7 - Murine CIA induction and treatment with anti-CCL3. Mice were injected at day 0 with CFA + collagen, and were given a booster injection at day 21. On day 21 mice were divided into two treatment groups, one receiving anti-CCL3 and one receiving control isotype IgG Ab. Mice were monitored every day for paw swelling and arthritis severity. An additional 5 doses were given to mice on alternate days, and on day 29 mice were culled.

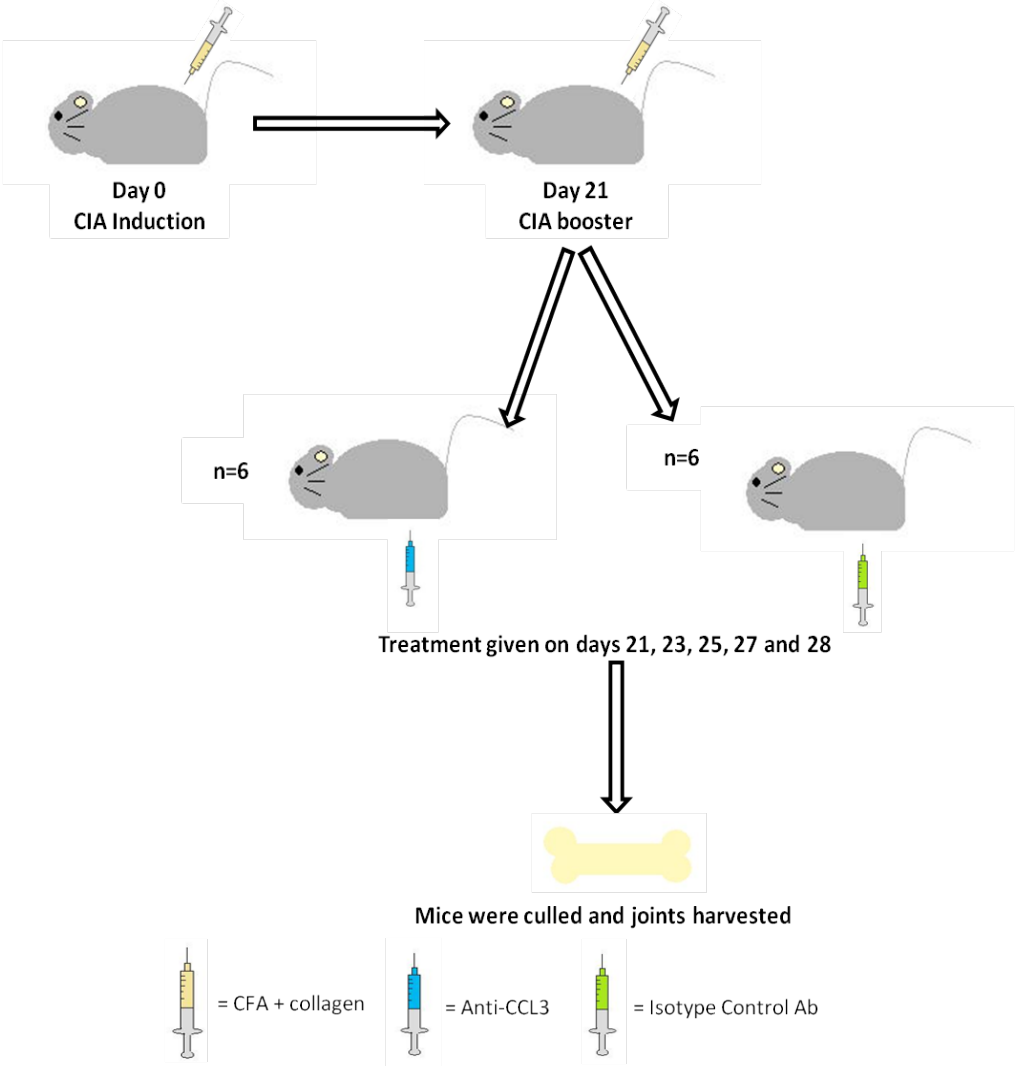

-Mice were culled on day 29 and joint tissues from both fore- and hind-limbs were harvested. Shoulder joints were fixed in 10% neutral buffered formalin solution for 24 hours at room temperature and then placed into 70% alcohol for 2 weeks. Knee and ankle joints were fixed and stored in 70% alcohol.

- ***Joint assessment (Chapter 2 Sections 2.2.20- 2.2.27)***

-Radiographs of forepaws and hind paws were acquired and assessed for erosions in 12 joints (Chapter 2 Section 2.2.21). 3D reconstructions of murine hind paws were obtained from µCT (Chapter 2 Section 2.2.22).

-Post imaging murine forepaws were decalcified in EDTA over 3 weeks. Joints were then embedded in paraffin wax ready for histological assessment. Sections of 7µm thickness were cut and stained with TRAP and haematoxylin facilitating cell counts. Each section was assessed for arthritic index (inflammatory infiltration, joint exudate, synovial hyperplasia and bone erosion) and osteoclast numbers (n=6 for each treatment group; left and right forepaws assessed). A summary is presented below;

Caption 8 - Methodologies for the analysis of bone destruction. Mice were culled on day 29 and their hind paws and forepaws harvested. All paws were examined by x-ray to yield a radiographic erosive score. Hind paws were imaged by µCT for erosions and forepaws were embedded in wax and assessed histologically for $TRAP^{+ve}$ cells and an arthritic index.

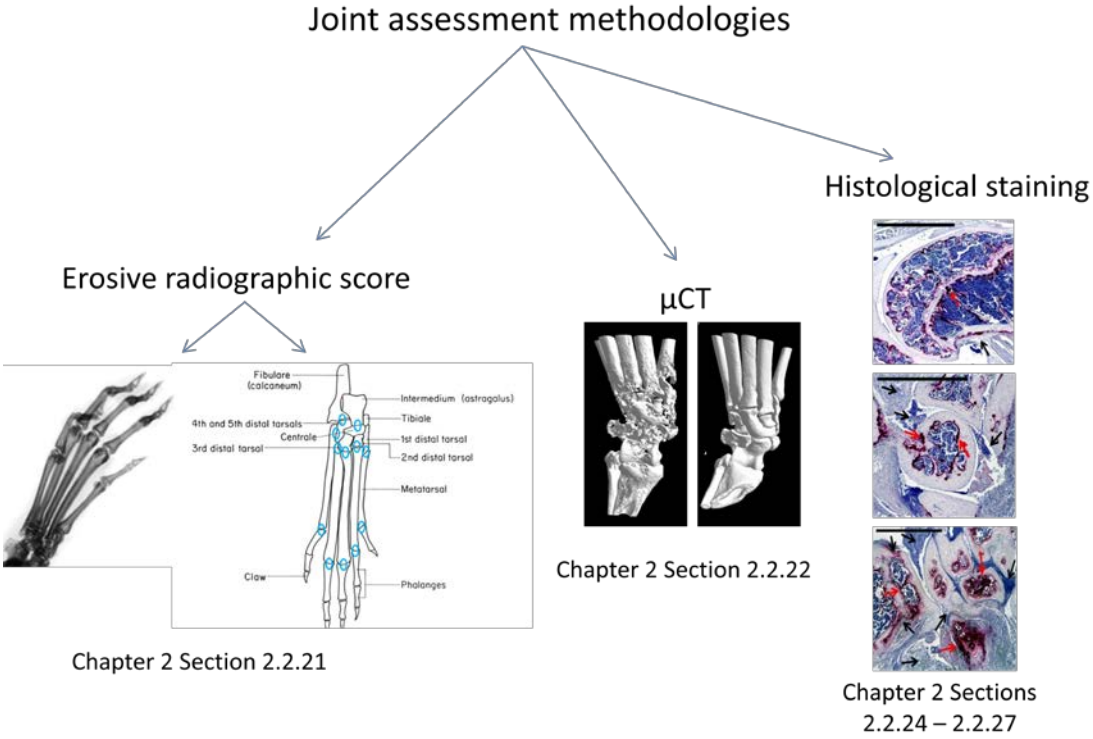

5.3 Results

In this chapter the role of CCL3 in osteoclast formation and associated resorption was investigated both *in vitro* and *in vivo*. Initial experiments using OPG, the decoy receptor of RANKL, at a previously published concentration of 100ng/mL, established whether our *in vitro* osteoclastogenesis assay was sensitive enough to show significant inhibition of osteoclast formation. Following this, the osteoclast assay was used to determine the role of CCL3 in osteoclast differentiation and bone degradation both in m-CSF and RANKL cultures and in the presence of a neutralising antibody to CCL3 *in vitro*. Supernatants were collected every 3-4 days and disks were harvested and fixed. Haematoxylin and TRAP stains were used to visualise nuclei and differentiating osteoclasts. Cell counts were reported as cells/disk ($28mm^2$) and given as the mean ± S.E.M. Secondary markers of osteoclast differentiation (TRAP5b) and bone resorption (CTX-1) were quantified. TRAP concentrations were quantified on day 7 (the optimal time-point established in Chapter 3 Section 3.2.7 where a significant increase in TRAP cell number is first quantified) and CTX-1 concentrations were quantified on day 10 (the optimal time-point established in Chapter 4 Section 4.3.1.2 due to negligible levels at day 7). In addition, surrogate soluble mediators of pain (NGF, CCL2, CCL3, IL-6) and inflammation (CCL2, CCL3, CCL5, IL-6 and sIL-6R) were measured in human osteoclast differentiation cultures across the 14-day time-course *in vitro*. Anti-CCL3 was then tested as an experimental treatment for prevention of bone destruction in a murine *in vivo* model of collagen-induced arthritis (CIA) using radiological and histological analyses.

5.3.1 OPG significantly inhibits osteoclastogenesis in m-CSF and RANKL supplemented cultures

The supplementation of osteoclast differentiation cultures with 100ng/mL OPG significantly reduced $TRAP^{+ve}$ cells (87 ± 10) compared to m-CSF and RANKL cultures (536 ± 146; $p \leq 0.05$, Figure 5.1 and 5.2), with a similar profile of reduction for osteoclast number (OPG: 5 ± 2, m-CSF and RANKL: 299 ± 84; $p \leq 0.05$, Figure 5.1 and 5.2). The corresponding area of resorption was also significantly reduced in the

presence of OPG (0.14 ± 0.01%) compared to m-CSF and RANKL cultures (1.98 ± 0.56%; Figure 5.5 and 5.6, $p \leq 0.05$).

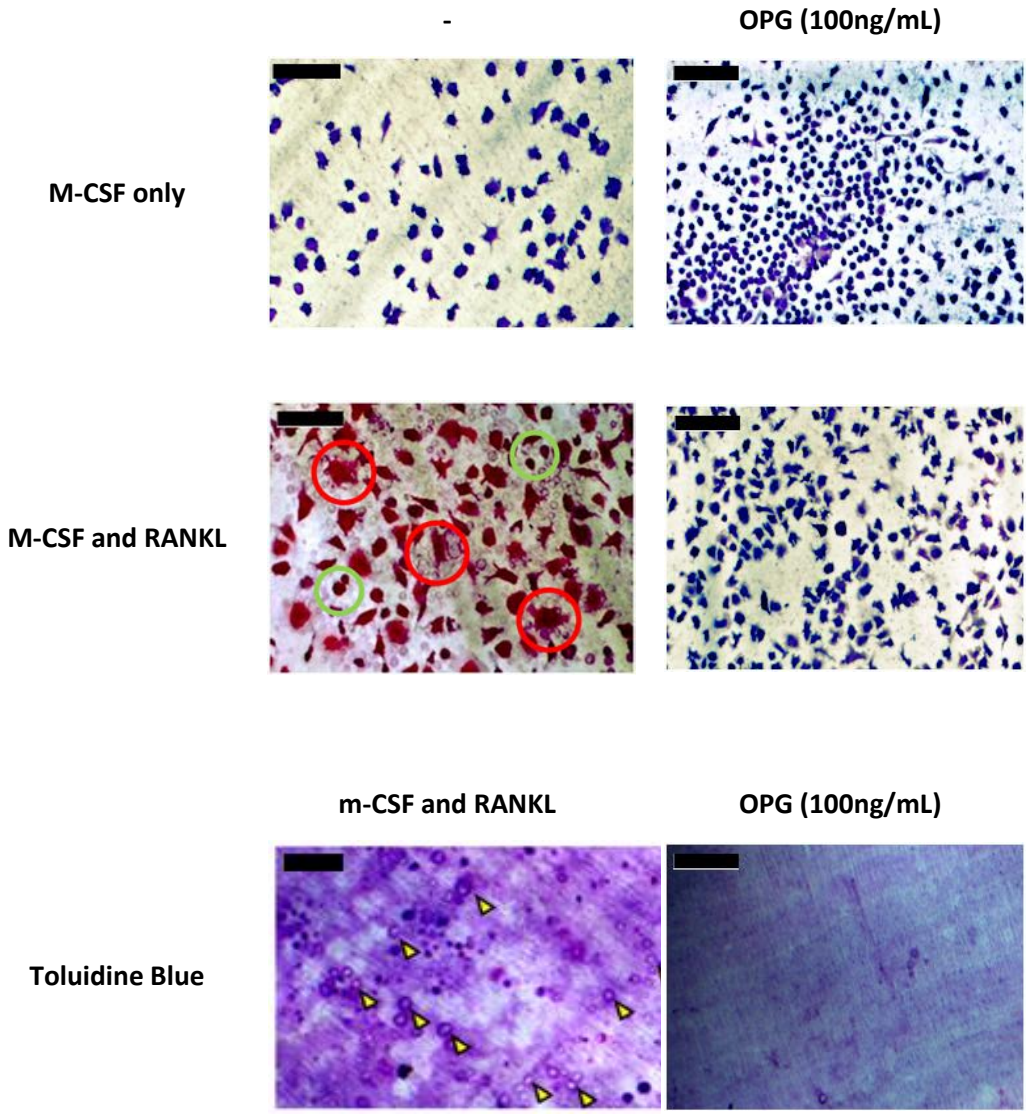

Figure 5. 1 - Supplementation of OPG into m-CSF and RANKL cultures visually reduced TRAP^{+ve} cell and osteoclast number.TRAP^{+ve} cells (green circles)and osteoclasts(red circles) were visualised at high numbers in cultures supplemented with m-CSF and RANKL. The addition of OPG resulted in a remarkable decrease in TRAP^{+ve} cells and osteoclasts seen, along with a visual reduction in cell size. In m-CSF control cultures no TRAP^{+ve} cells or osteoclasts were seen. Toluidine blue imaging showed the clear presentation of multiple resorption pits (yellow arrows)in m-CSF and RANKL cultures, but through the addition of OPG areas of resorption were negligible. Scale bar 50µm.

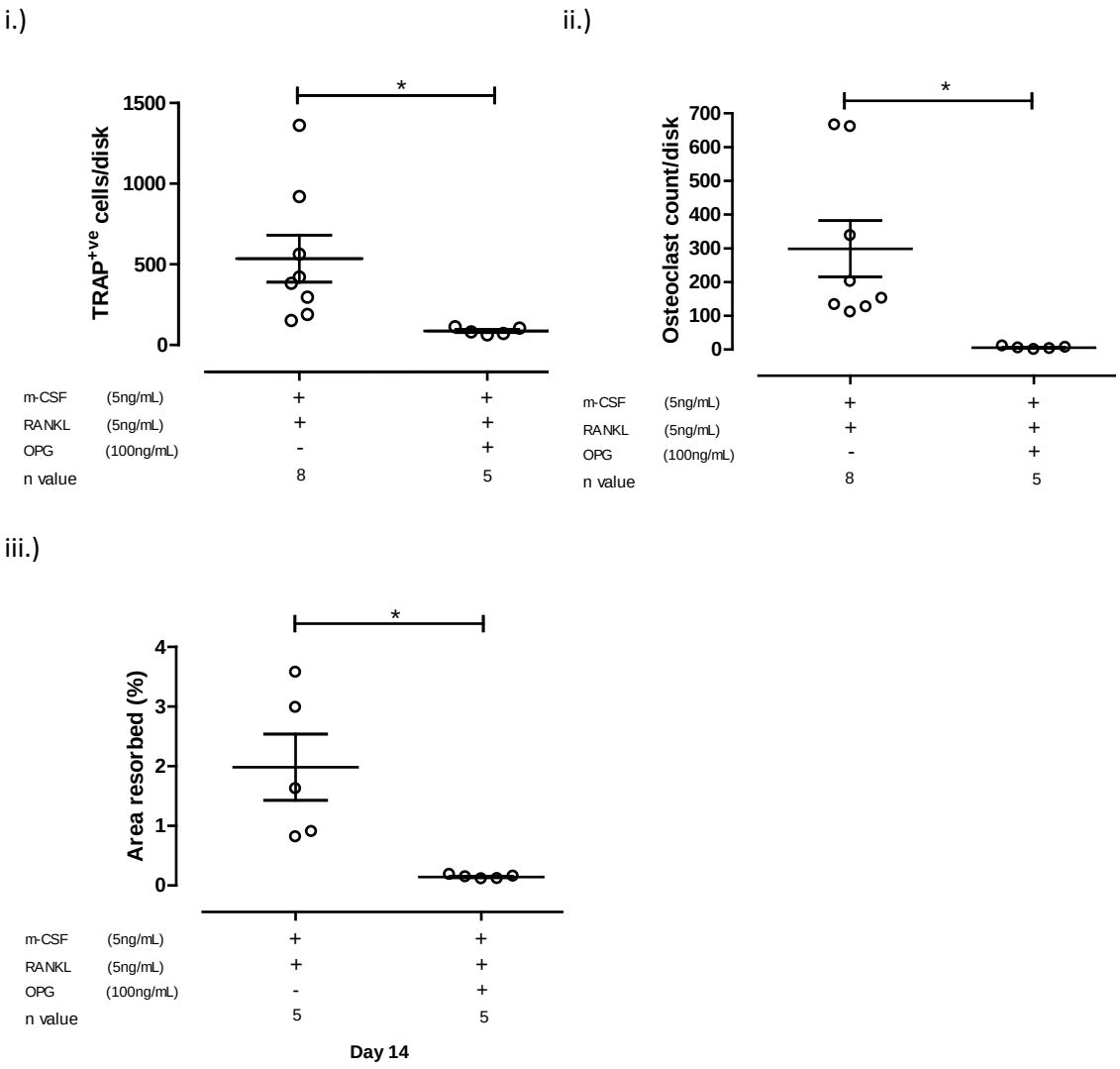

Figure 5. 2 - OPG supplementation significantly reduces osteoclast formation and functional resorptive activity.. After 14 days of culture in m-CSF and RANKL ± OPG (100ng/mL) cultured disks were harvested, fixed and stained to obtain TRAP^{+ve} and osteoclast counts. Post counts, cells were removed and disks were stained with toluidine blue for quantification of resorption. i. and ii.) m-CSF, RANKL + OPG showed significantly reduced TRAP^{+ve} and osteoclast counts (both $p \leq 0.05$). iii.) Supplementation of OPG caused a significant reduction in area resorbed compared to m-CSF and RANKL ($p \leq 0.05$). N= 8 donors for m-CSF and RANKL cultures; mean of 4 replicate disks plotted. N=5 donors for m-CSF, RANKL + OPG cultures; mean of 4 replicates per donor plotted. Statistical analysis using a Student's t-test was performed. Mean ± SEM data values were reported.

5.3.2 Determining the direct effect of CCL3 in human osteoclast differentiation and bone resorption *in vitro*

The direct effect of CCL3 in osteoclast differentiation and bone resorption *in vitro* was investigated due to its significant correlation with osteoclastogenesis in Chapter 3. Precursor cells were differentiated into osteoclasts in the presence of m-CSF and RANKL over 14 days where maximum osteoclast differentiation and resorption had occurred (Chapter 3.3.7 and 3.3.8). In destructive bone diseases a complicated milieu of pro-inflammatory cytokines are present in the joint, potentially masking the direct role of CCL3 in osteoclastogenesis. To understand the role of CCL3 in human osteoclast formation and resorption, a neutralising antibody to CCL3 was added to osteoclast cultures and its effect on osteoclast number (TRAP staining) and resorbed area (toluidine blue) measured at day 14. 3D confocal imaging of resorption pits was paired with novel analysis methodology to distinguish the direct effect of CCL3 in morphological pit characteristics including depth and volume.

5.3.2.1 CCL3 secretion by osteoclasts significantly increases in the presence of RANKL in vitro

CCL3 concentration at baseline (Day 0) was 93 ± 26pg/mL and after 24 hours remained unchanged in proliferation medium (89 ± 12pg/mL) but decreased in m-CSF and RANKL cultures (56 ± 6pg/mL). In m-CSF and RANKL cultures, a significant increase to 162 ± 24pg/mL was reported after 7 days ($p \leq 0.05$, Figure 5.3), which coincided with the significant increase in $TRAP^{+ve}$ cells (Chapter 3 Section 3.3.7).

5.3.2.2 Concentration dependent decreases in $TRAP^{+ve}$ mononuclear and multinucleated cells results from anti-CCL3 treatment in vitro

Osteoclast number significantly reduced in a concentration dependent-manner in the presence of 2-8ng/mL anti-CCL3 ($p \leq 0.01$), where comparative reductions were noted at both 4- and 8ng/mL. Greater reproducibility was seen at 8ng/mL as there was a decreased data range. A power calculation proved a 5-fold reduction in 'n

number' using 8ng/mL anti-CCL3 compared to 4ng/mL anti-CCL3. Total cell count was comparable between both concentrations highlighting unaffected precursor cell expansion; 10347 ± 501 versus 9167 ± 702 (Figure 5.4). Subsequent differentiation assays with increased n number were therefore run with the supplementation of 8ng/mL anti-CCL3 to determine the impact of CCL3 in osteoclast formation and resorption. No $TRAP^{+ve}$ osteoclasts were observed in m-CSF cultures.

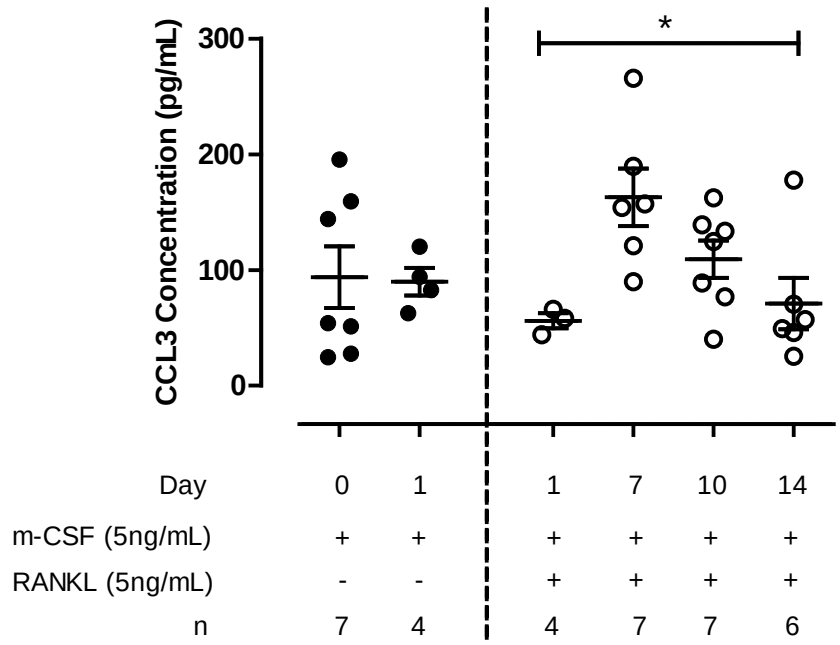

Figure 5. 3 - RANKL induces a significant early increase in CCL3 in monocultures.. Proliferation cultures at day 0, were either supplemented with m-CSF only or m-CSF and RANKL. Control m-CSF cultures showed no difference in CCL3 concentration after 24 hours. Differentiation cultures however showed an initial reduction in CCL3 after 24 hours which was followed by a significant increase to day 7 ($p \leq 0.05$). A gradual decline in CCL3 then followed from day 7 to day 14 when assays were terminated. N=7 donors (apart from day 1 conditions where n=4 donors), means from 4 disks per time-point were plotted. Statistical analysis using a One-Way ANOVA was performed between m-CSF and RANKL culture time-points, and mean ± SEM data values are reported.

i.)

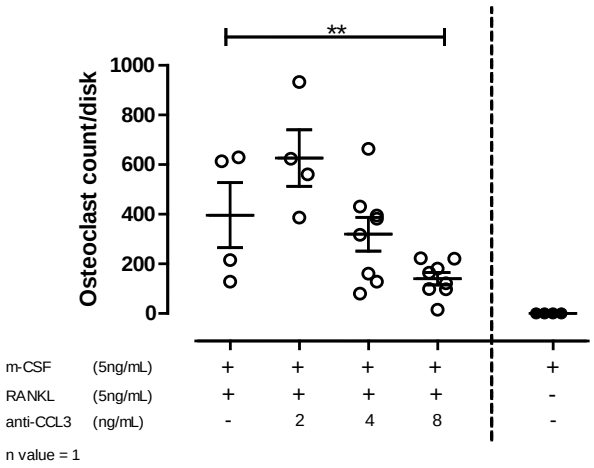

ii.)

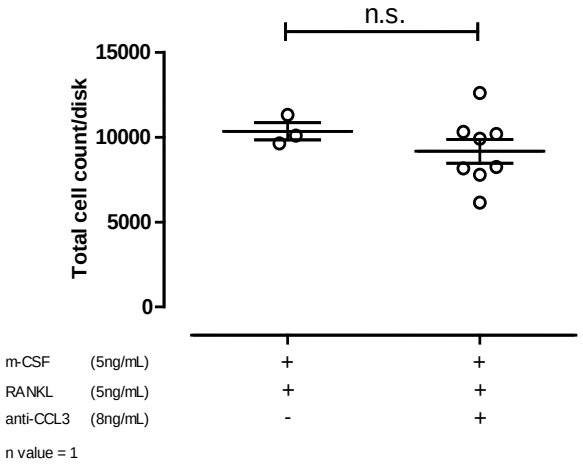

Figure 5. 4 - the addition of anti-CCL3 into human osteoclast differentiation cultures resulted in a significant dose-dependent reduction in osteoclast number.Osteoclast differentiation assays were treated with anti-CCL3 Ab from 0-8ng/mL from day 0. Assays were terminated at day 14 when disks were harvested, fixed and stained with TRAP and haematoxylin. i.) A significant reduction in osteoclast count (*p≤0.01*) was seen across the concentration range of anti-CCL3 Ab. In control cultures supplemented only with m-CSF, osteoclast number was negligible. ii.) Total cell number was shown at comparable levels in differentiation cultures and those supplemented with 8ng/mL anti-CCL3. Data reported in this Figure was obtained from n=1 donor; minimum number of 4 replicate disks per treatment condition. Statistical analysis using a one-way ANOVA was performed (** = *p≤0.01*), and mean ± SEM data values were reported.

5.3.2.3 *Supplementation of 8ng/mL anti-CCL3 into differentiation cultures significantly reduced osteoclast count at day 14*

$TRAP^{+ve}$ cell number was comparable in osteoclast cultures treated with m-CSF and RANKL in the absence and presence of anti-CCL3; 536 ± 146 and 555 ± 195 respectively (Figure 5.5 and 5.6, i). However, osteoclast number was independent to $TRAP^{+ve}$ cells and significantly reduced in the presence of anti-CCL3 compared to m-CSF and RANKL; 113 ± 41 opposed to 299 ± 84 respectively ($p \leq 0.05$, Figure 5.6, ii). In m-CSF and RANKL cultures treated with an isotype control antibody, $TRAP^{+ve}$ cells and osteoclast counts were unchanged, thus proving the importance of CCL3 specifically in osteoclast formation (n=4, Figure 5.6, iii and iv). $TRAP^{+ve}$ cells and osteoclasts were absent m-CSF only cultures and m-CSF in combination with anti-CCL3 or IgG (Figure 5.6, v and vi).

5.3.2.4 *The addition of anti-CCL3 into differentiation cultures significantly reduced the area of resorption after 14 days of culture*

Harvested disks from m-CSF and RANKL cultures exhibited 1.5 ± 0.4% resorption across the disk surface. Through anti-CCL3 supplementation, a significant 3-fold reduction in the area of resorption across the disk to 0.4 ± 0.1 % ($p \leq 0.05$) resulted(Figure 5.7 and 5.8). m-CSF and RANKL cultures in combination with IgG showed comparable levels of resorption; 0.6 ± 0.1 % and 0.7 ± 0.1 % respectively. m-CSF alone or in combination with anti-CCL3 or IgG did not produced resorption (Figure 5.8).

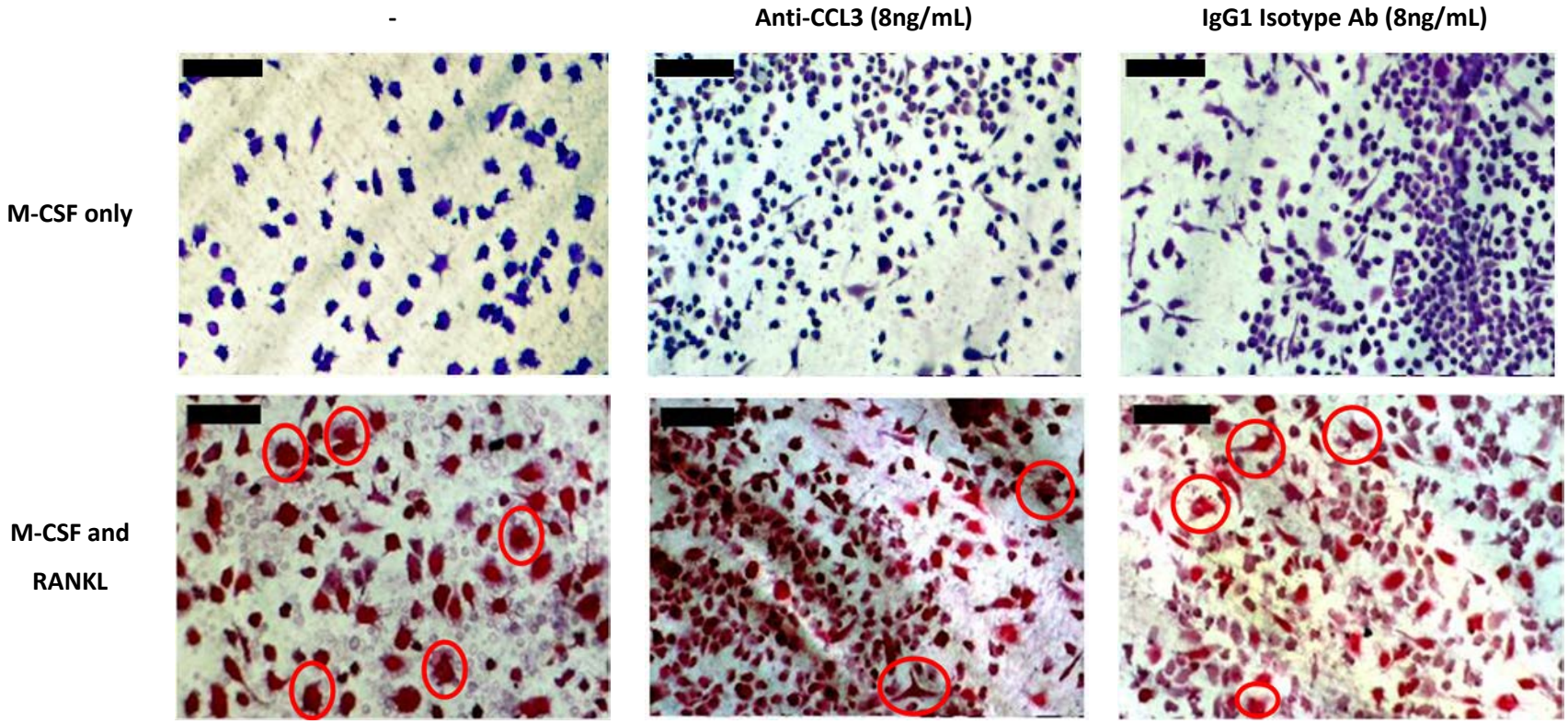

Figure 5. 5 - Neutralisation of CCL3 (anti-CCL3 8ng/mL) in m-CSF and RANKL cultures reduced osteoclast number.Human osteoclast cultures were treated for 14 days withanti-CCL3 and/or ± isotype control IgG1. Anti-CCL3 caused a visual reduction in osteoclast number(red circles) to m-CSF and RANKL cultures. Osteoclast number in isotype control cultures were comparable to m-CSF and RANKL cultures. No $TRAP^{+ve}$ cells were found in m-CSF only cultures. Scale bar 50µm.

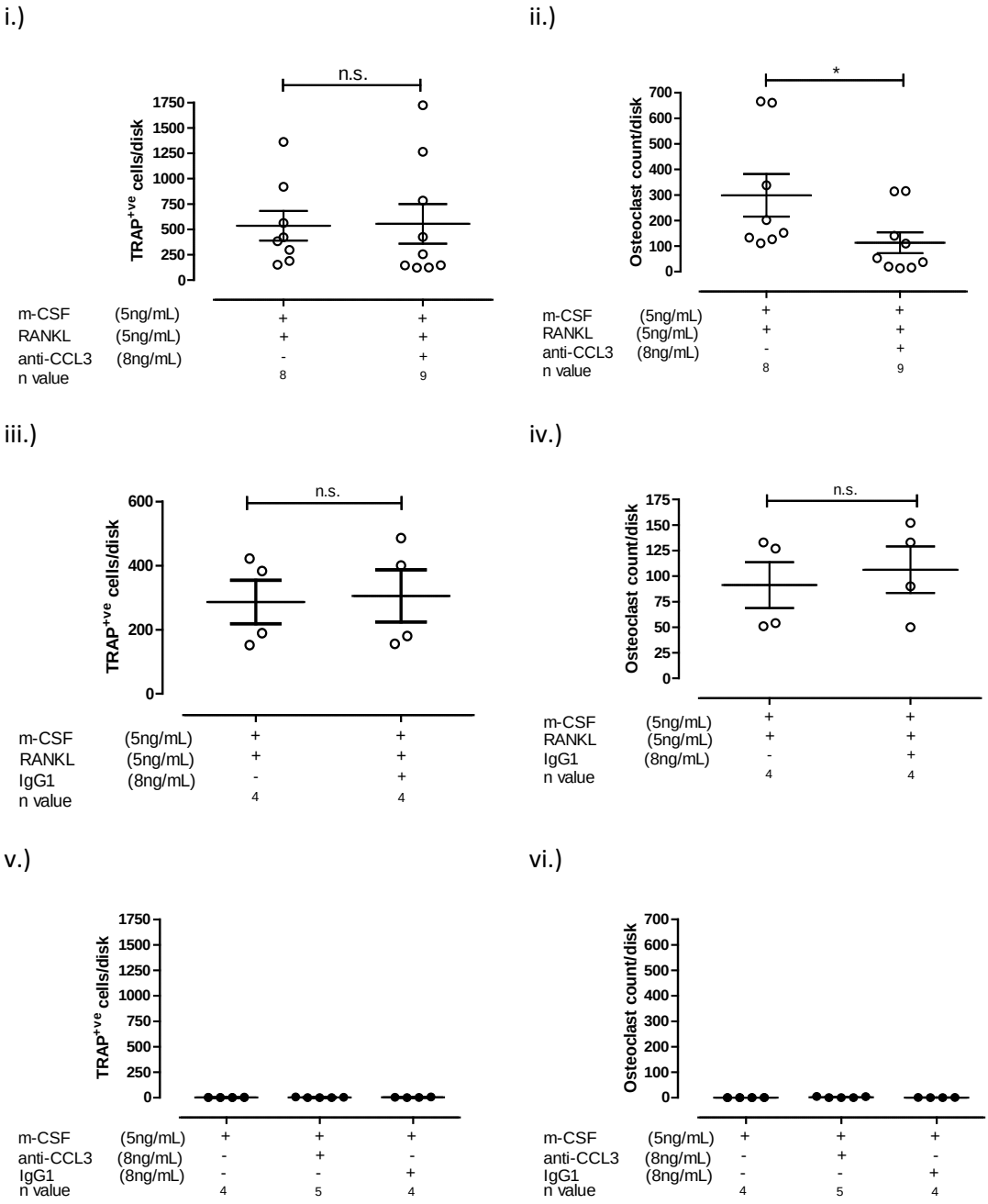

Figure 5. 6 - Neutralisation of CCL3 (8ng/mL) significantly decreased osteoclast number.Osteoclast assays ± anti-CCL3 or IgG1 were run to day 14 where disks were harvested, fixed and stained. i.) $TRAP^{+ve}$ cells were comparable in m-CSF and RANKL cultures ± anti-CCL3. ii.) Osteoclast count significantly decreased in the presence of anti-CCL3 (*p≤0.05*). iii.) and iv.) $TRAP^{+ve}$ cell and osteoclast number were comparable in m-CSF and RANKL ± IgG1 cultures(n=4 donors; 4 replicate disks per donor, mean plotted). v.) and vi.) No $TRAP^{+ve}$ cells or osteoclasts were found in the absence of RANKL. For m-CSF and RANKL ± anti-CCL3 n=9 donors; 4 replicate disks per donor, mean plotted. Statistical analysis using a Student's t-test (* = *p≤0.05*). Mean ± SEM data.

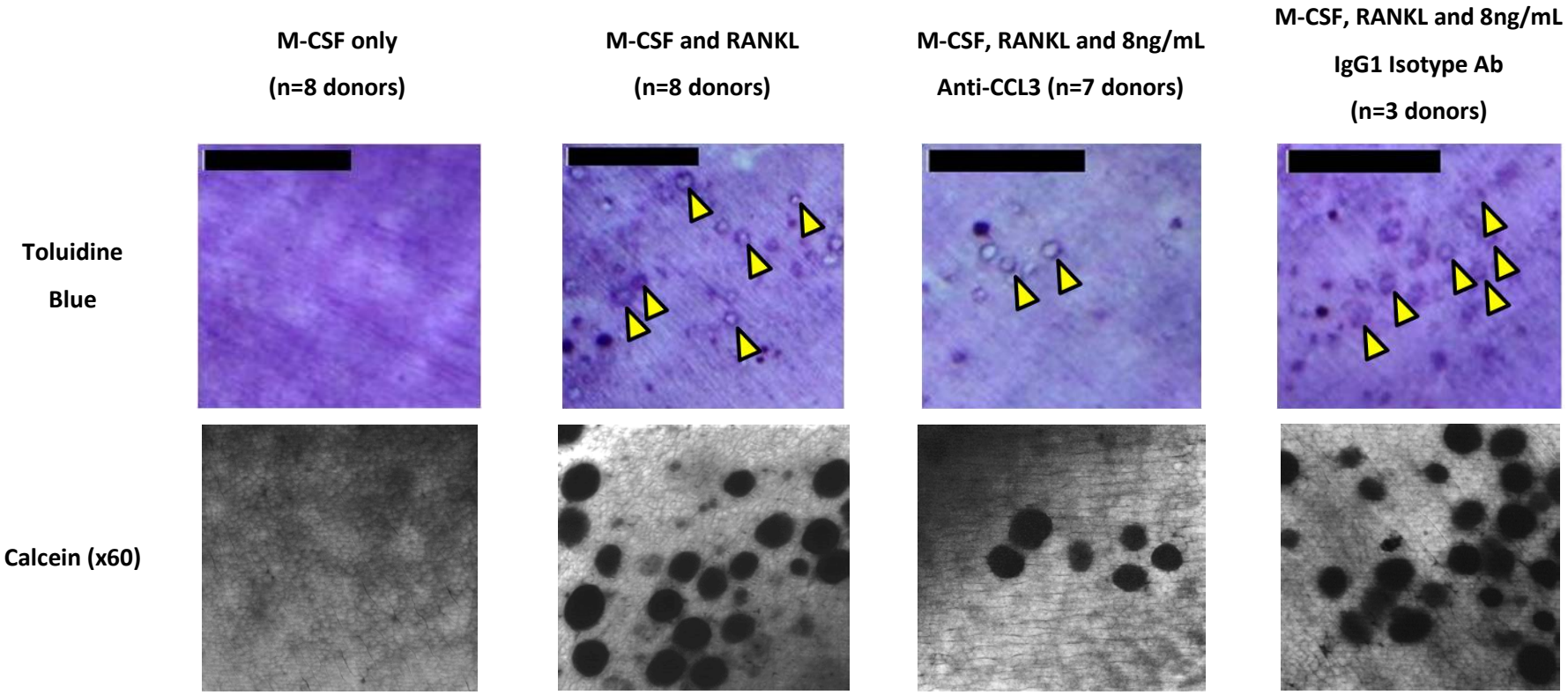

Figure 5. 7 - Resorption pit number was visually reduced after neutralisation of CCL3 in m-CSF and RANKL cultures.At day 14 disks were harvested from osteoclast assays and adherent cells were removed, stained with toluidine blue or calcein, and imaged by light or confocal microscopy. M-CSF ± anti-CCL3 or IgG1 showed no resorption. M-CSF and RANKL cultures showed extensive resorption, which was shown to reduce in the presence of anti-CCL3 but not IgG1.Toluidine blue scale bar=50µm, confocal images 1 pixel = 0.27µm.

i.)

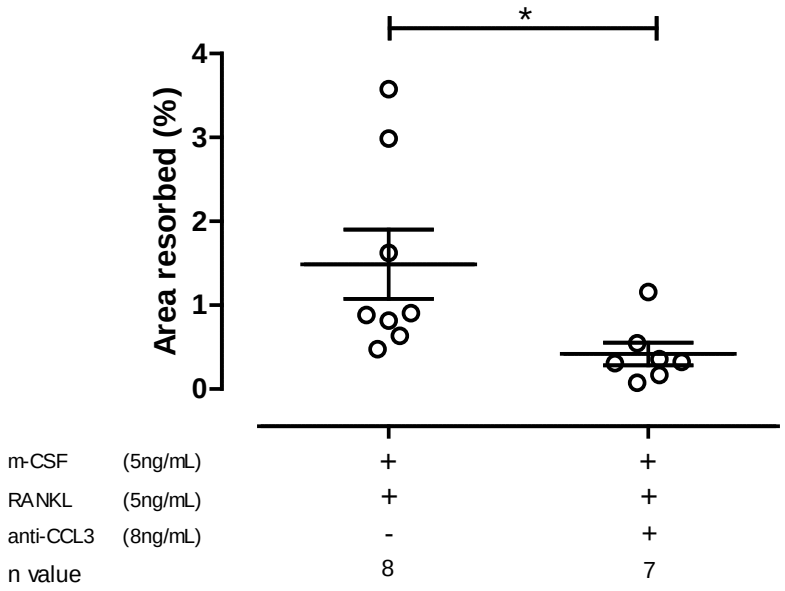

ii.)

iii.)

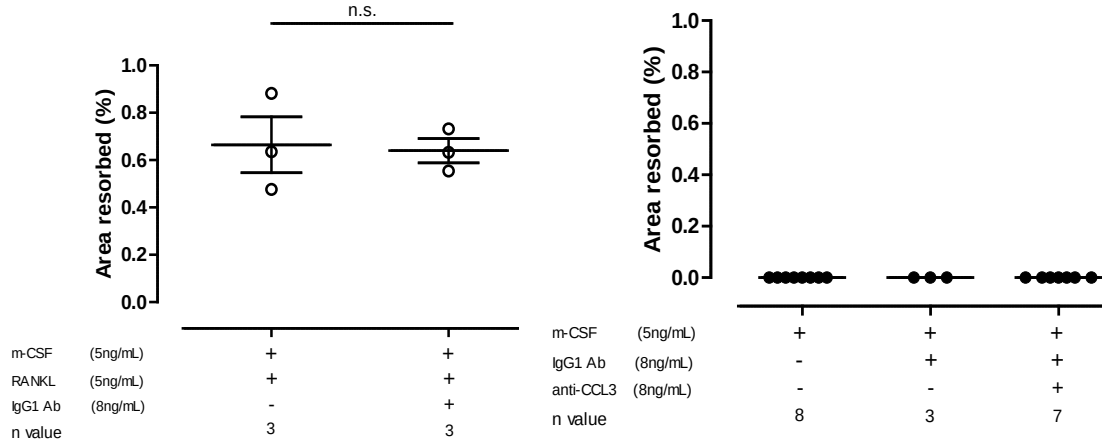

Figure 5. 8 - Neutralisation of CCL3 in m-CSF and RANKL cultures led to a significant reduction in area resorbed at day 14.Disks were harvested at day 14 of the osteoclast assay. Adhered cells were removed and disks stained with toluidine blue prior to quantification of resorbed area. i.) Anti-CCL3 supplementation into m-CSF and RANKL caused a significant decrease in area resorbed % compared to m-CSF and RANKL cultures (*p≤0.05*, n=8 donors; 2 replicate disks per donor, mean plotted).ii. and iii.) Differentiation cultures treated with isotype control Ab (minimum of n=3 donors; 2 replicate disks per donor, mean plotted) or cultures without RANKL showed no significant difference to matched controls. Student's t-test performed (* = *p≤0.05*). Mean ± SEM shown.

5.3.2.5 *Anti-CCL3 did not significantly affect the depth and volume of resorption pits*

Resorption pit number across the disk was significantly reduced in the presence of anti-CCL3 (Section 5.3.2.4) but the individual parameters of each pit were still unknown (*i.e.* area, volume and depth). Such individual pit parameters are thought to be result of 'stationary resorption', where the osteoclast has tightly adhered to the bone substrate forming a sealing zone and creating a contained space in which degradative enzymes are released. To assess whether stationary resorption is altered in the presence of anti-CCL3, confocal microscopy was used to create XY and XZ image stacks. 3D reconstructions of eroded bone surfaces were then made from these image stacks which allowed assessment of individual pit parameters.

Average pit area (1963 ± 414 versus 1988 ± 341) and perimeter (188 ± 16 compared to 187 ± 9) were comparable in m-CSF and RANKL versus m-CSF, RANKL and anti-CCL3 cultures (n=6 donors). Pit depth (7.1 ± 0.9µm versus 6.7 ± 0.6µm)and pit volume (527.3 ± 90.9µm3 versus 573.9 ± 90.0µm^3) in m-CSF and RANKL cultures with and without anti-CCL3 were also comparable.

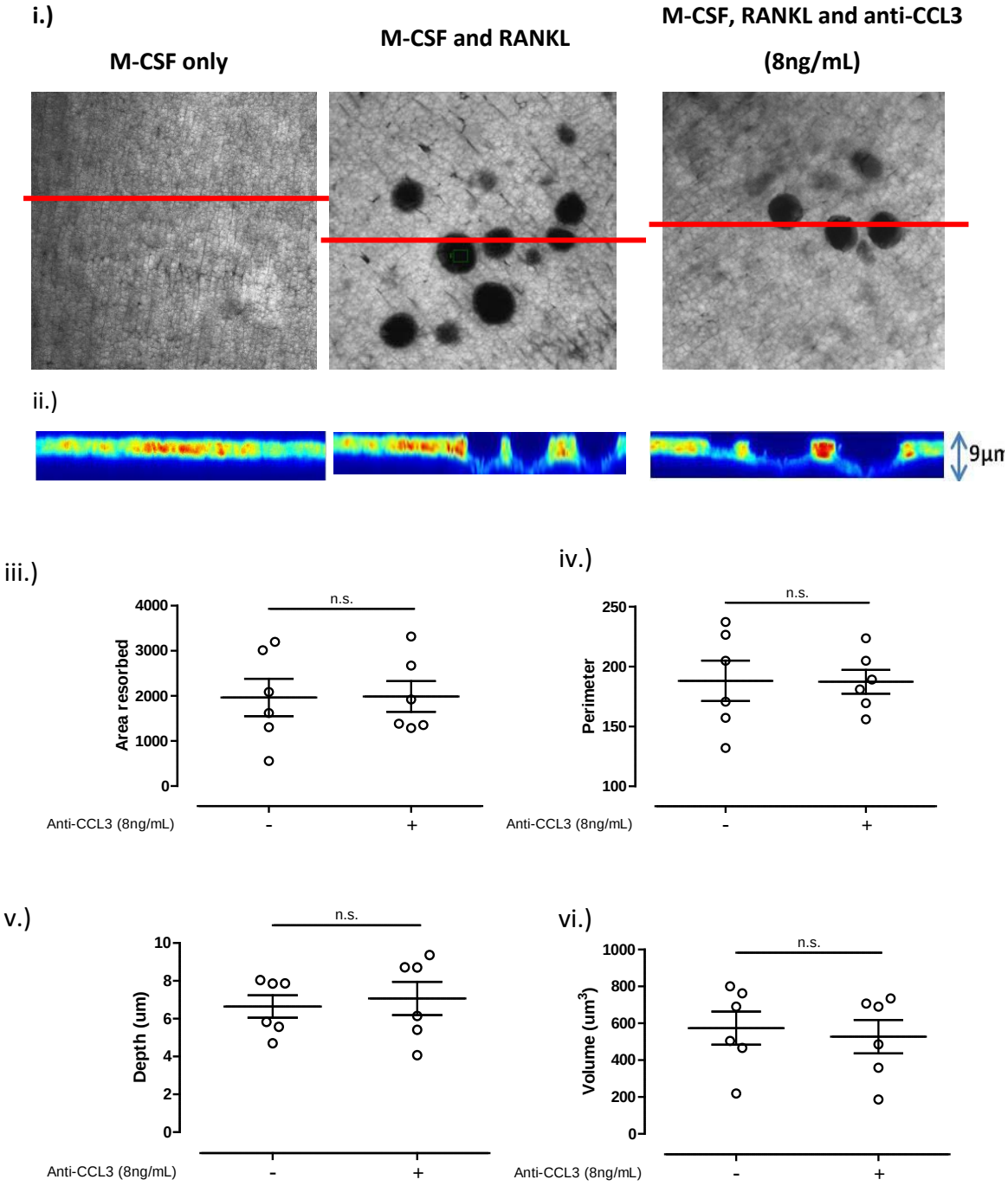

Figure 5. 9 - CCL3 has no effect on resorption pit characteristics.The three-dimensional analysis of resorption pits from confocal imaging at x60 yielded XY images showcasing the presence of pits (i).XZ slices (red lines) facilitated the visualisation of pit depth (ii). Individual pit characteristics in m-CSF, RANKL and anti-CCL3 cultures showed no significant differences in pit area, perimeter, depth or volume to m-CSF and RANKL cultures (iii – vi respectively; n=6 donors; 2 disks per donor imaged, 10 images per disk quantified, mean plotted). 0.27µm = 1 pixel. Statistical analysis using a Student's t-test was performed. Mean ± SEM data shown.

5.3.3 Quantifying the presence of selected indirect markers of osteoclast function, pain and inflammation

Due to the postulated direct role of CCL3 in osteoclast formation from Sections 5.3.2.3 and 5.3.2.4, secondary markers of osteoclast differentiation (TRAP5b) and resorption (CTX-1), were measured at day 7 and day 10 to provide additional evidence for a biological role of CCL3 in osteoclastogenesis. Levels of NGF, CCL2, CCL5, IL-6 and sIL-6R were also quantified in supernatants harvested from across the OC assay time-course by ELISA to assess any relationship CCL3 may have with pain and inflammation markers.

5.3.3.1 Soluble marker of osteoclast differentiation, TRAP5b, and resorptive function, CTX-1, were not significantly reduced by anti-CCL3

TRAP5b was significantly elevated in m-CSF and RANKL differentiation versus non-differentiating (m-CSF only) cultures; 1.37 ± 0.28 versus 0.19 ± 0.09 U/L (*p≤0.01,* Figure 5.10). TRAP5b was not altered by anti-CCL3 (1.43 ± 0.43 U/L) in differentiation cultures.

CTX-1 increased in m-CSF and RANKL cultures compared to m-CSF only, but this was not significant (0ng/mL to 0.14 ± 0.06ng/mL respectively). In the presence of anti-CCL3, CTX-1 from m-CSF and RANKL cultures was reduced but not significantly. CTX-1 levels were at the lower limit detection sensitivity for the assay.

5.3.3.2 Establishing the effect of anti-CCL3 on the secretion of indirect markers of pain and inflammation (CCL2, CCL5, IL-6 and sIL-6R) from human osteoclast differentiation cultures in vitro

CCL2 was produced at high levels comparable in m-CSF alone cultures and m-CSF and anti-CCL3 treated cultures. Supplementation of cultures with RANKL caused CCL2 levels to decrease gradually from day 0 to day 14 (41 ± 19 to 19 ± 5ng/mL). Comparable expression was found in m-CSF, RANKL and anti-CCL3 cultures. CCL5

was only measured in five assays as levels were consistently lower than the detection limit of the ELISA (Figure 5.11).

sIL-6R from m-CSF cultures in the presence and absence of anti-CCL3 slowly declined across the time-course; 63 ± 28 to 28 ± 13pg/mL. The supplementation of RANKL into these cultures yielded comparable levels of sIL-6R, as did the addition of anti-CCL3. The secretion of IL-6 across the time-course matched that of sIL-6R. In m-CSF only and m-CSF with anti-CCL3, IL-6 was comparable and gradually declined; 144 ± 113 (day 0) to 49 ± 35pg/mL (day 14). In cultures supplemented further with RANKL, a similar declining profile of secretion was reported; 73 ± 22 (day 0) to 42 ± 24pg/mL (day 14), which again was unaffected in the presence of anti-CCL3; 52 ± 14 (day 0) to 20 ± 18pg/mL (day 14, Figure 5.12).

i.)

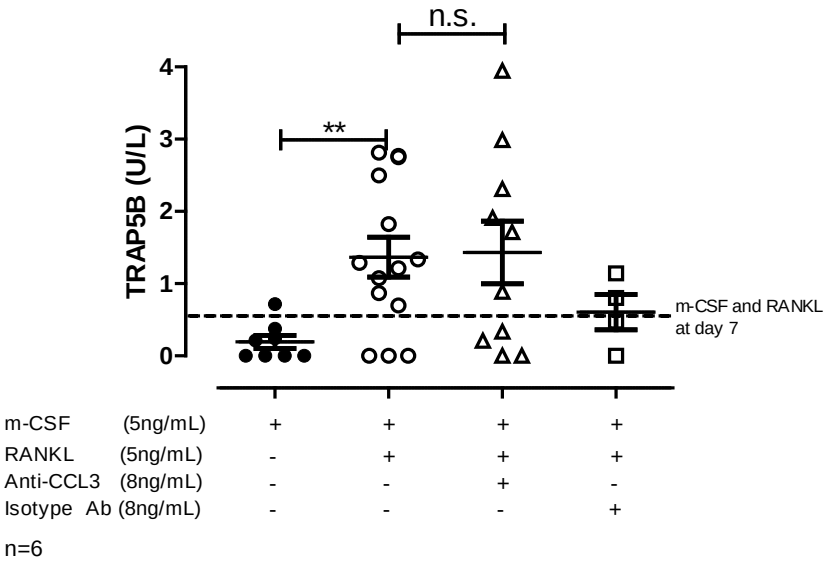

ii.)

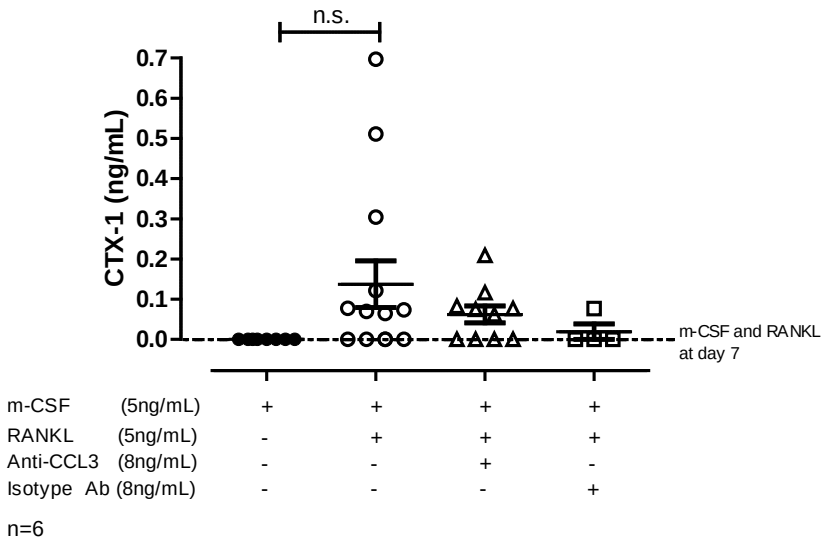

Figure 5. 10 - CTX-1 and TRAP5b secretion at day 10 increased in the presence of RANKL but anti-CCL3 had no further effect on their levels.Supernatants from osteoclast differentiation assays were collected at day 10 and analysed by ELISA for CTX-1 and TRAP5b. i.) Soluble TRAP5b significantly increased in m-CSF and RANKL cultures compared to m-CSF only cultures (*p≤0.01*), but was not affected through CCL3 neutralisation in m-CSF and RANKL cultures. ii.) CTX-1 increased in m-CSF and RANKL cultures compared to m-CSF only but this was not significant. Anti-CCL3 treatment caused a decrease in CTX-1 levels, as did IgG1, but this was not significant. m-CSF and RANKL ± anti-CCL3; N=6 donors, 2 replicate disks per treatment condition, mean plotted.IgG1 control; N=4 donors, 2 replicate disks, mean plotted. Statistical analysis using a Student's t-test was performed (** = *p≤0.01*). Mean ± SEM data reported.

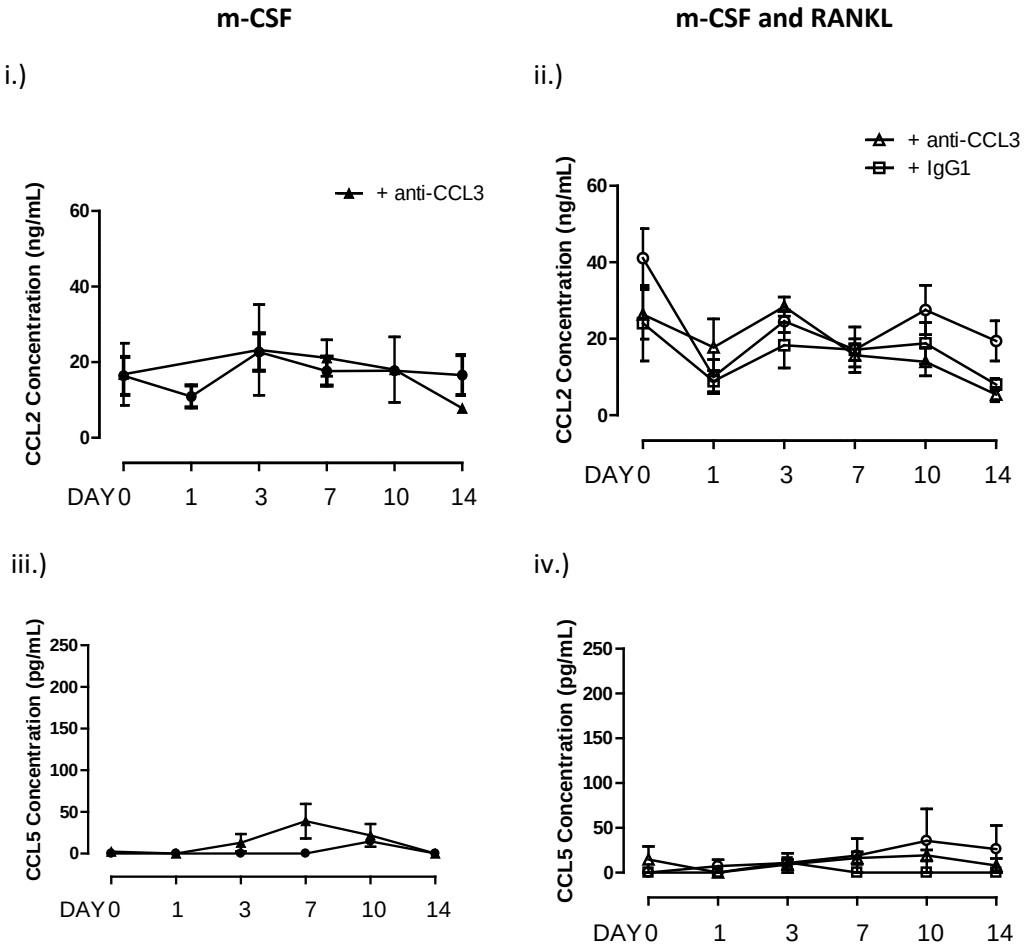

Figure 5. 11 - Soluble inflammatory chemokines in anti-CCL3 treated osteoclast cultures were not significantly reduced compared to controls. Supernatants from across a 14-day osteoclast differentiation assay were collected and analysed for soluble mediators of inflammation via ELISA. i.) CCL2 showed no significant difference across a 14-day time-course in m-CSF only and m-CSF + anti-CCL3 cultures. ii.) CCL2 concentrations in m-CSF and RANKL cultures across the 14-day time-course were unaltered in the presence of anti-CCL3 or IgG1. . iii.) CCL5 in m-CSF only cultures were negligible until day 10 (n=1 donor; 4 replicate measurements per donor, mean of donor plotted ± S.E.M.). iv.) CCL5 in m-CSF and RANKL cultures ± anti-CCL3 or IgG1 increased from day 0 to day 10, but this was not significant. For m-CSF ± anti-CCL3; n=4 donors, 4 replicate measurements per donor, mean of all donors plotted ± S.E.M.). For m-CSF, RANKL ± anti-CCL3;n=9 donors, 4 replicate measurements per donor, mean of all donors plotted ± S.E.M. Statistical analysis using a one-way ANOVA was performed. Mean ± SEM reported. *N.B.* no sample exists for m-CSF and anti-CCL3 cultures at day 1 due to analyst error.

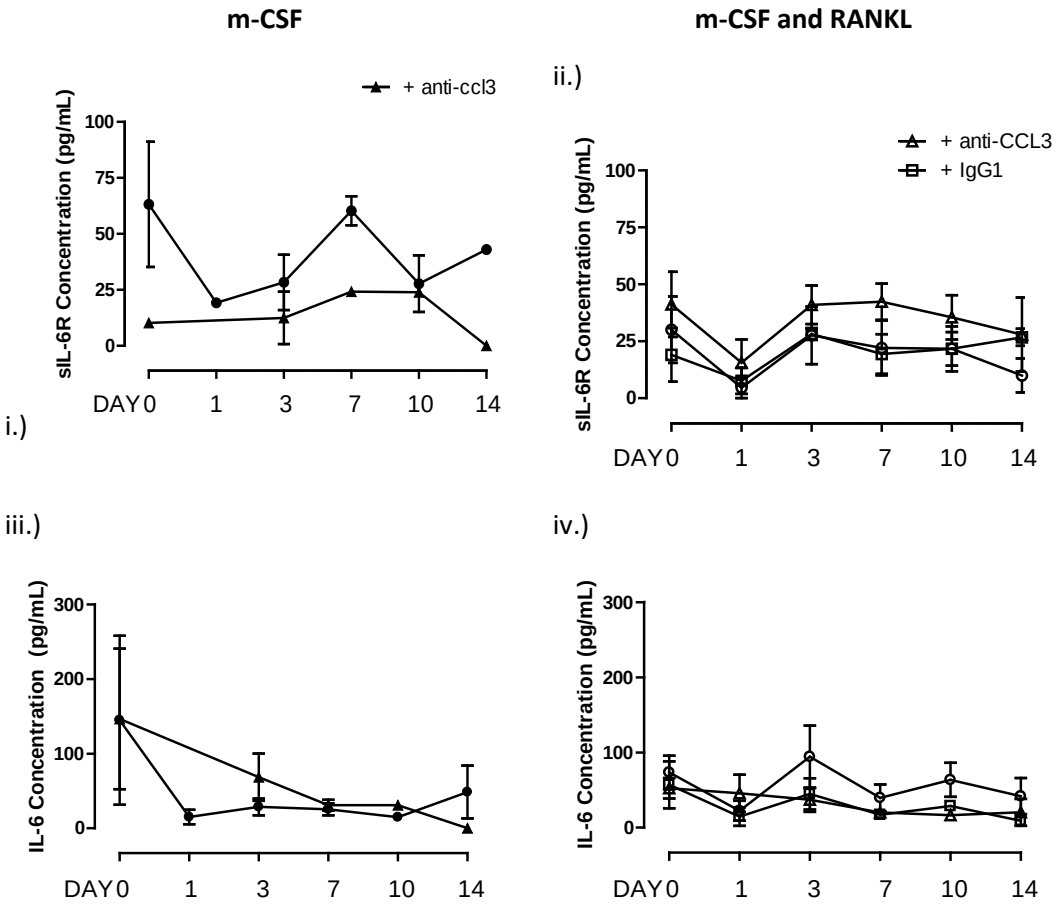

Figure 5. 12 - Soluble inflammatory cytokines in anti-CCL3 treated osteoclast cultures were not significantly altered compared to controls. Across the 14-day osteoclast differentiation assay collected supernatants were analysed for soluble inflammatory cytokines using ELISA. i.) and ii.) A biphasic response of sIL6R in m-CSF only cultures was ameliorated through the supplementation of RANKL. In cultures supplemented with anti-CCL3 or isotype control, sIL-6R was comparable to m-CSF and RANKL cultures. iii.) and iv.) IL-6 concentration was shown to decrease across the time-course in m-CSF only ± anti-CCL3. In m-CSF and RANKL cultures alone or in combination with anti-CCL3 or IgG1, the profile of IL-6 was unchanged. For m-CSF ± anti-CCL3; n=4 donors, 4 replicate measurements per donor, mean of all donors plotted ± S.E.M.). For m-CSF, RANKL ± anti-CCL3;n=9 donors, 4 replicate measurements per donor, mean of all donors plotted ± S.E.M. Statistical analysis using a one-way ANOVA was performed. Means ± SEM reported. *N.B.* no sample exists for m-CSF and anti-CCL3 cultures at day 1 due to analyst error.

5.3.4 Comparing the potency of anti-CCL3 compared to OPG in the inhibition of osteoclast formation and function

Data reported showed a clear role for CCL3 in driving osteoclast differentiation and subsequently a role in the resorption of bone-substrate. Next the comparative efficacy of anti-CCL3 versus an established inhibitor of osteoclastogenesis (OPG) was tested. OPG or anti-CCL3 was investigated at 8ng/mL per culture well. Cell counts and bone substrate resorbed were measured on day 14 whilst soluble markers of osteoclast differentiation (TRAP5B), bone resorption (CTX-1; measured on day 10), and pain (NGF, CCL2, CCL3, IL-6) and inflammation (CCL2, CCL3, CCL5, IL-6 and sIL-6R) were quantified by ELISA across the time-course.

5.3.4.1 The addition of OPG into osteoclast differentiation cultures significantly reduced osteoclast number and bone substrate resorption after 14 days

OPG reduced the number of $TRAP^{+ve}$ cells (246 ± 84) and significantly decreased osteoclasts (21 ± 9) counted per disk compared to m-CSF and RANKL cultures (536 ± 146 and 299 ± 84 respectively; $p \leq 0.05$). $TRAP^{+ve}$ cells and osteoclast numbers were comparable in OPG and anti-CCL3 treated cultures (Figure 5.13 and Figure 5.14). OPG prevented resorption of ivory and images were comparable with those from m-CSF only cultures (Figure 5.15). OPG and anti-CCL3 had equivalent potency in this regard (n=3, Figure 5.16).

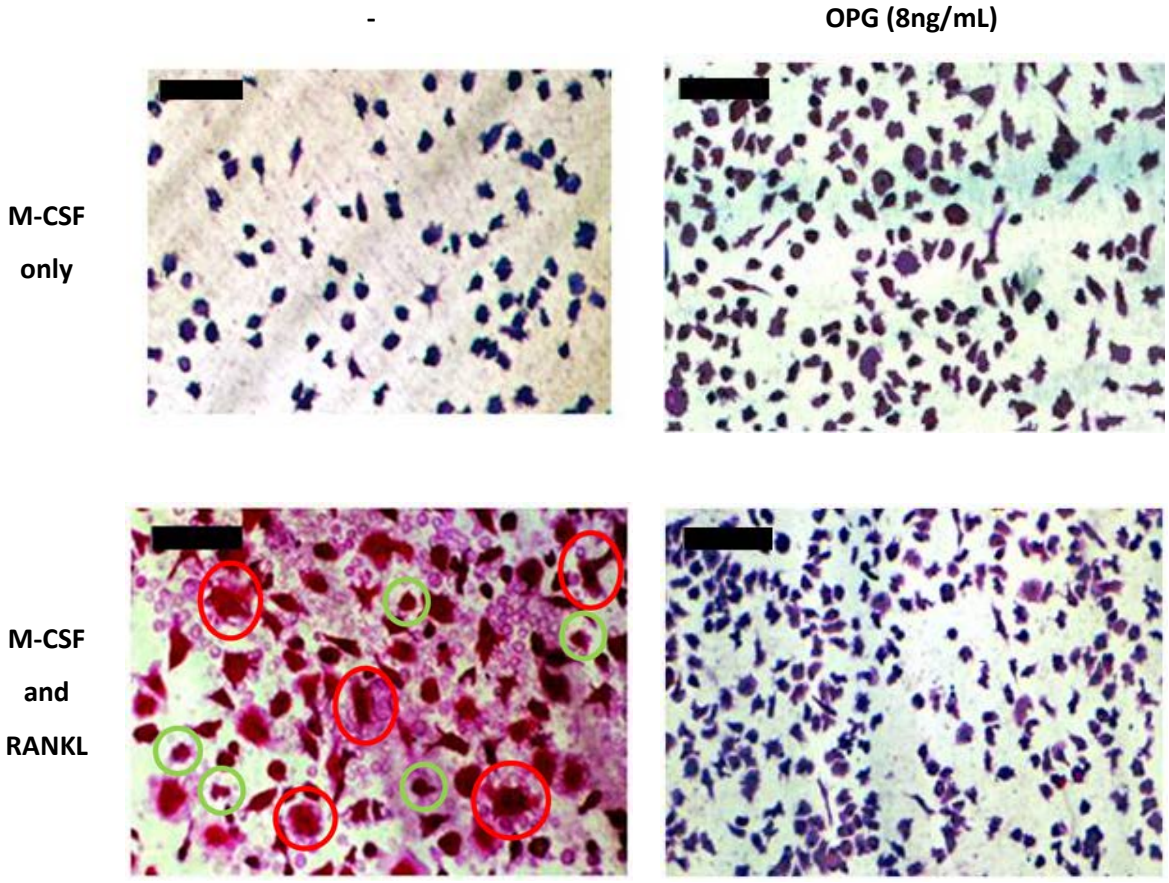

Figure 5. 13 - M-CSF and RANKL cultures supplemented with OPG showed an extensive decrease in TRAP^{+ve} cells and osteoclasts adhered to disks.M-CSF and RANKL cultures alone showed the presence of TRAP^{+ve} cells (green circles) and osteoclasts (red circles) in high numbers across the disk. Through the addition of OPG a remarkable decrease in TRAP^{+ve} cells and osteoclasts were seen, along with a visual reduction in cell size. In m-CSF control cultures no TRAP^{+ve} cells or osteoclasts were seen. Scale bar 50µm.

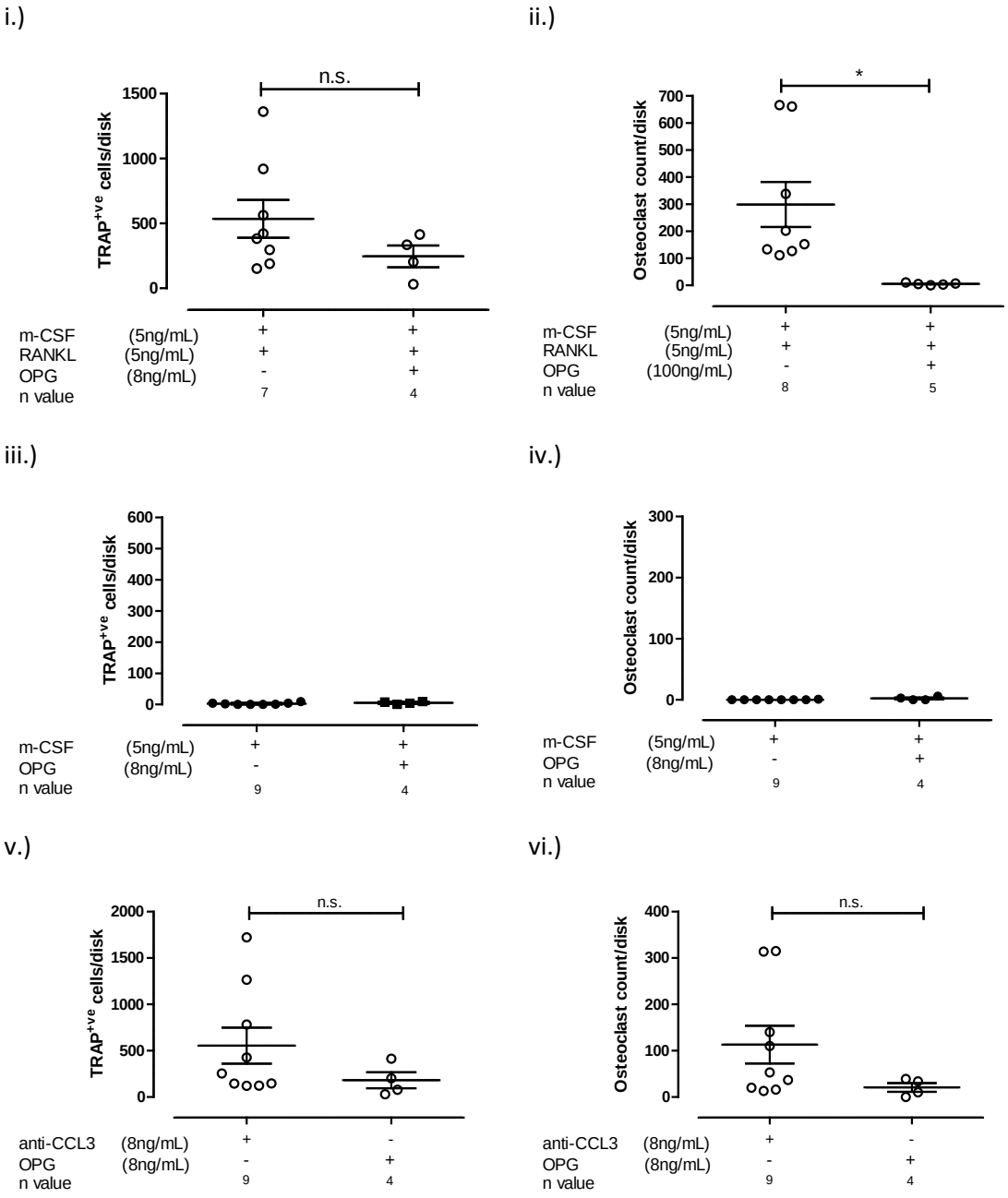

Figure 5. 14 - OPG (8ng/mL) significantly reduced osteoclast number in m-CSF and RANKL cultures.Osteoclast assays were supplemented with 8ng/mL OPG over a 14 day time-course (m-CSF and RANKL cultures; n=8 donors, 4 replicate disks per donor, m-CSF, RANKL + OPG; n=5, 4 replicate disks per donor; mean per donor plotted). At day 14 disks were harvested and stained. i.) OPG reduced $TRAP^{+ve}$ cell count but not significantly compared to m-CSF and RANKL cultures. ii.) OPG significantly reduced osteoclast count compared to m-CSF and RANKL (*p≤0.05*). iii. and iv.) M-CSF cultures ± OPG showed no significant increase in $TRAP^{+ve}$ cells or osteoclast count. v. and vi.) OPG had no effect on $TRAP^{+ve}$ cell or osteoclast number compared to m-CSF and RANKL cultures + anti-CCL3. Student's t-test was performed(* = *p≤0.05*). Mean ± SEM data reported.

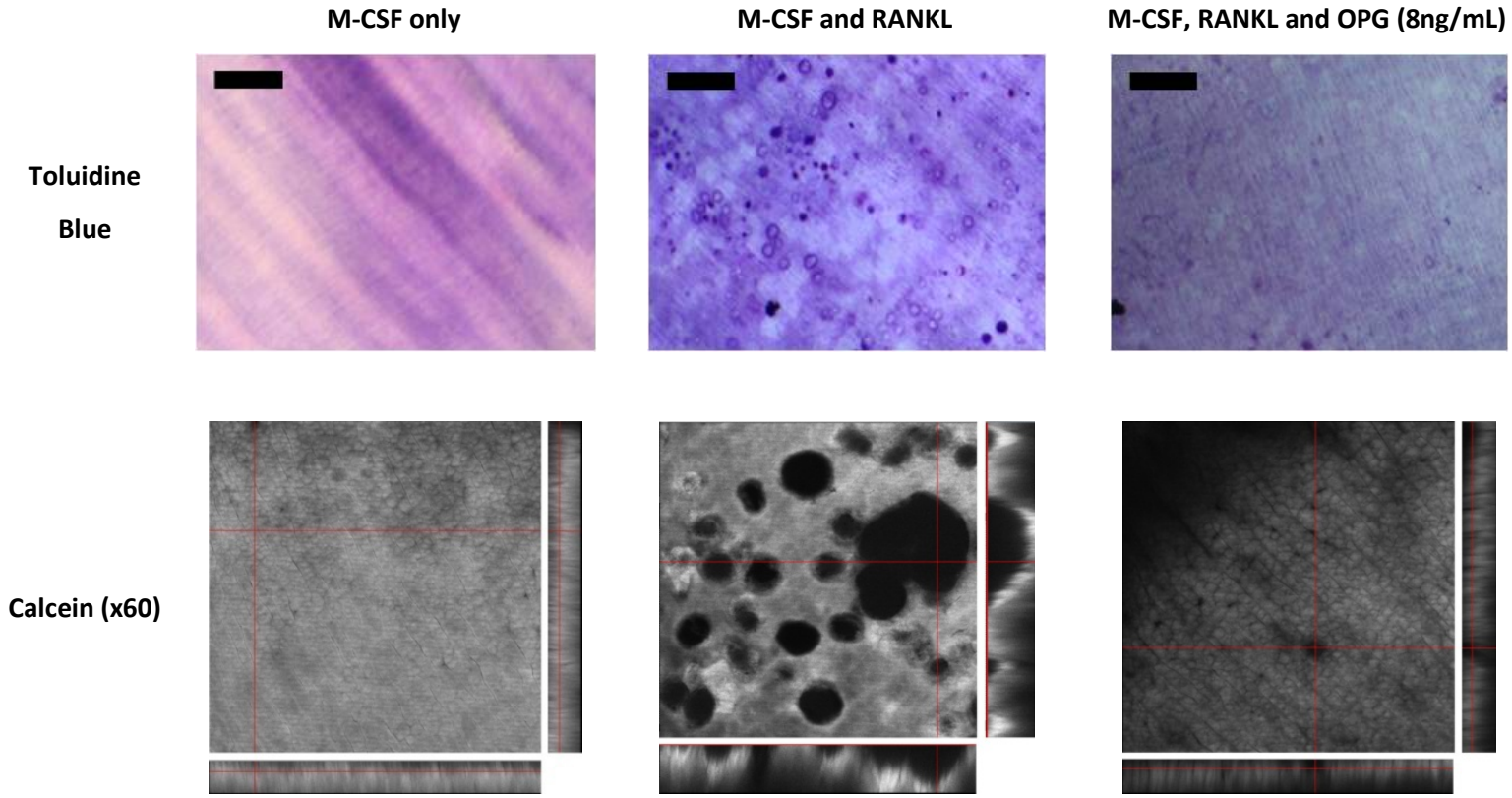

Figure 5. 15 - OPG (8ng/mL) substantially reduced the appearance of resorption pits in human osteoclast differentiation assays.. Osteoclast assays ± OPG were cultured to day 14. At assay termination disks were harvested, adhered cells removed, and disks were stained with toluidine blue or calcein prior to imaging with light or confocal microscopy. Resorption pits were only visibly present in m-CSF and RANKL cultures without OPG. Toluidine blue scale bar= 50µm, confocal images 1 pixel =0.27µm.

i.)

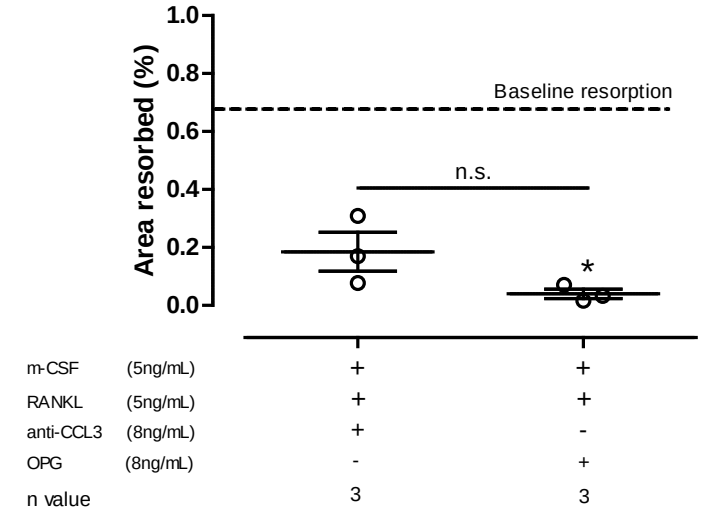

ii.)

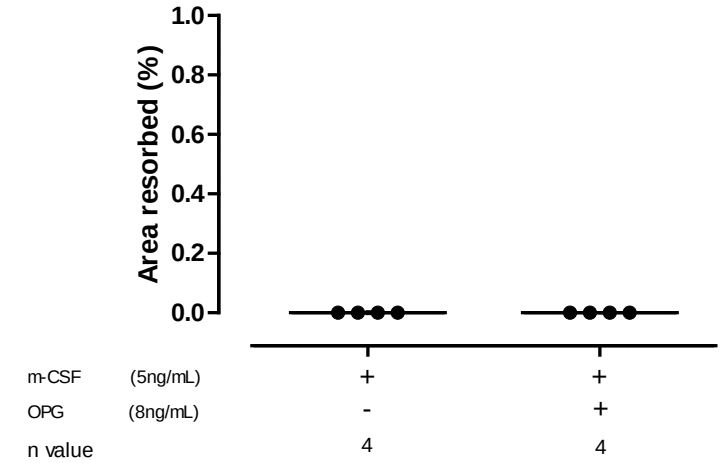

Figure 5. 16 - OPG (8ng/mL) significantly reduced area resorbed at day 14 when supplemented into osteoclast differentiation cultures.Disks from osteoclast assays were harvested at day 14, cells removed, and were stained with toluidine blue prior to facilitate the quantification of area resorbed. i.) A significant decrease in percentage area resorbed was found between m-CSF and RANKL cultures and those supplemented with OPG (*p≤0.05*; n=3 donors, 2 replicate disks per donor, means plotted). No significant difference was reported between anti-CCL3 and OPG supplemented differentiation cultures. ii.) Resorption was absent in RANKL-deficient cultures(n=4 donors; 2 replicates per donor, mean plotted). Statistical analysis using a Student's t-test (* = *p≤0.05*). Mean ± SEM reported.

5.3.4.2 *OPG supplementation had no significant effect on the secreted soluble mediators of osteoclast differentiation (TRAP5b) and bone resorption (CTX-1)*

OPG had no effect on TRAP5b levels when compared to m-CSF and RANKL differentiation cultures; 1.42 ± 0.12 versus 1.37 ± 0.28 U/L (Figure 5.17). CTX-1 levels from m-CSF and RANKL cultures reduced in the presence of OPG, although not significantly; 0.14 ± 0.06 to 0.01 ± 0.01 ng/mL. Again, CTX-1 levels were at the lower limit of detection.

5.3.4.3 *The addition of OPG in human osteoclast differentiation cultures reduced inflammation mediators (CCL2, CCL3, CCL5, sIL-6R and IL-6) to levels comparable to m-CSF only cultures*

Although high levels of CCL2 were found its secretion was comparable from m-CSF alone or m-CSF and RANKL cultures in the presence of OPG (Figure 5.18, i and ii). CCL3 secretion from m-CSF cultures in the presence or absence of OPG yielded comparable concentration profiles.CCL3 in m-CSF and RANKL cultures increased from day 0 to day 1 (63 ± 15 to 184 ± 59pg/mL), which was absent in the additional presence of OPG (40 ± 3 to 40 ± 8pg/mL; Figure 5.22, iii and iv). CCL5 was again found to be below the lower limit of detection in n=7 assays, where in n=1 minimal levels were detected in all cultures (Figure 5.18, v and vi).

In the presence and absence of OPG, comparable declining profiles of sIL-6R expression were found in m-CSF alone, and m-CSF and RANKL cultures; in m-CSF and RANKL averaging 30 ± 15 (day 0) to 10 ± 7pg/mL (day 14; Figure 5.19, i and ii). Similar results were shown for IL-6 concentrations in m-CSF only and m-CSF and RANKL cultures in the presence or absence of OPG; in m-CSF and RANKL averaging 73 ± 22 (day 0) to 42 ± 24pg/mL (day 14; Figure 5.19, iii and iv).

i.)

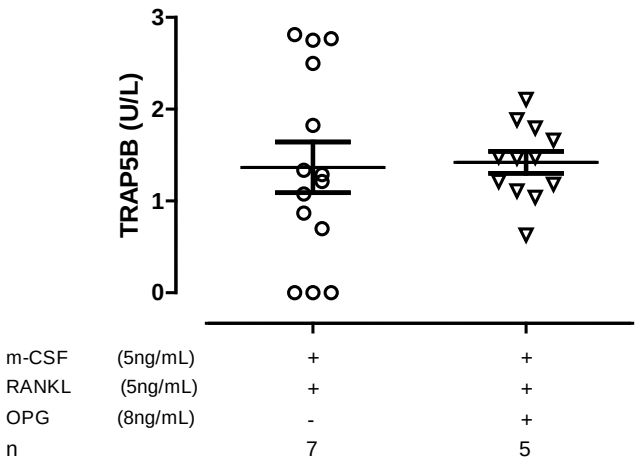

ii.)

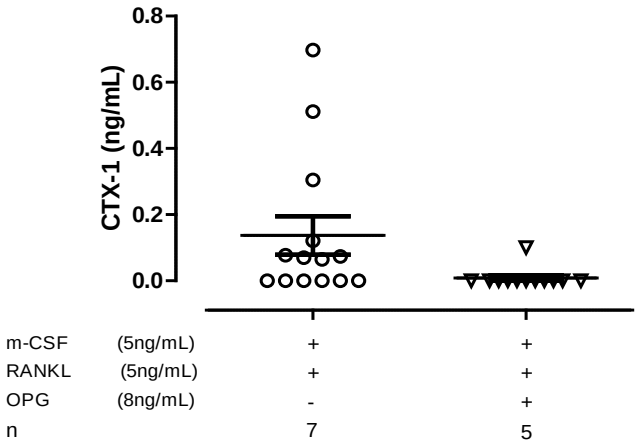

Figure 5. 17 - TRAP5b and CTX-1 decreased but not significantly in the presence of OPG (8ng/mL).Supernatants from osteoclast differentiation assays were collected at day 10 and were analysed by ELISA for the presence of CTX-1 and TRAP5b. i.) Soluble TRAP5b from OPG treated differentiation cultures was comparable to differentiation cultures at day 10. ii.) OPG supplementation of m-CSF and RANKL cultures decreased CTX-1 levels but not significantly. M-CSF and RANKL;N=7 donors, mean from 2 replicate disks per donor plotted. M-CSF, RANKL + OPG;N=5 donors, mean from 2 replicate disks per donor plotted. Statistical analysis using a Student's t-test was performed. Mean ± SEM reported.

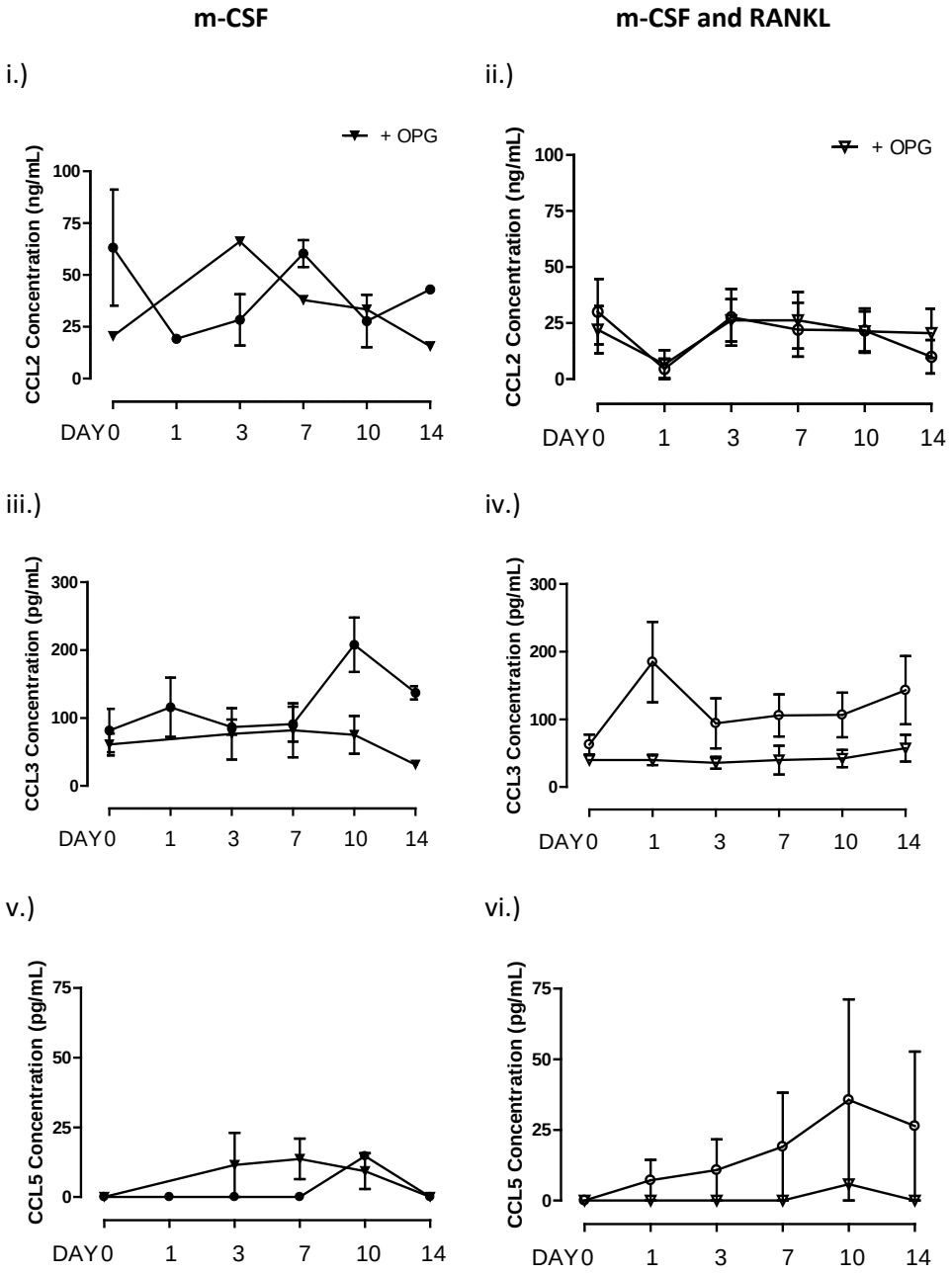

Figure 5. 18 - Soluble chemokine inflammatory marker CCL3 was reduced in OPG treated osteoclast cultures.Supernatants across the time-course of osteoclast assays were collected and analysed via ELISA. i. and ii.) CCL2 secretion was comparable within all treatment conditions. iii. and iv.) CCL3 in m-CSF and RANKL assays increased at day 1 and thus slowly declined to day 14. OPG treated cultures showed baseline levels from day 0 to 14. v. and vi.) CCL5 increased in m-CSF and RANKL cultures but negligible levels were found in OPG. No sample existed for m-CSF and OPG cultures at day 1. M-CSF and RANKL; N=7 donors, 2 replicate disks per donor. M-CSF, RANKL + OPG;N=5 donors, 2 replicate disks per donor. Means of all donors plotted ± SEM reported. One-way ANOVA preformed.

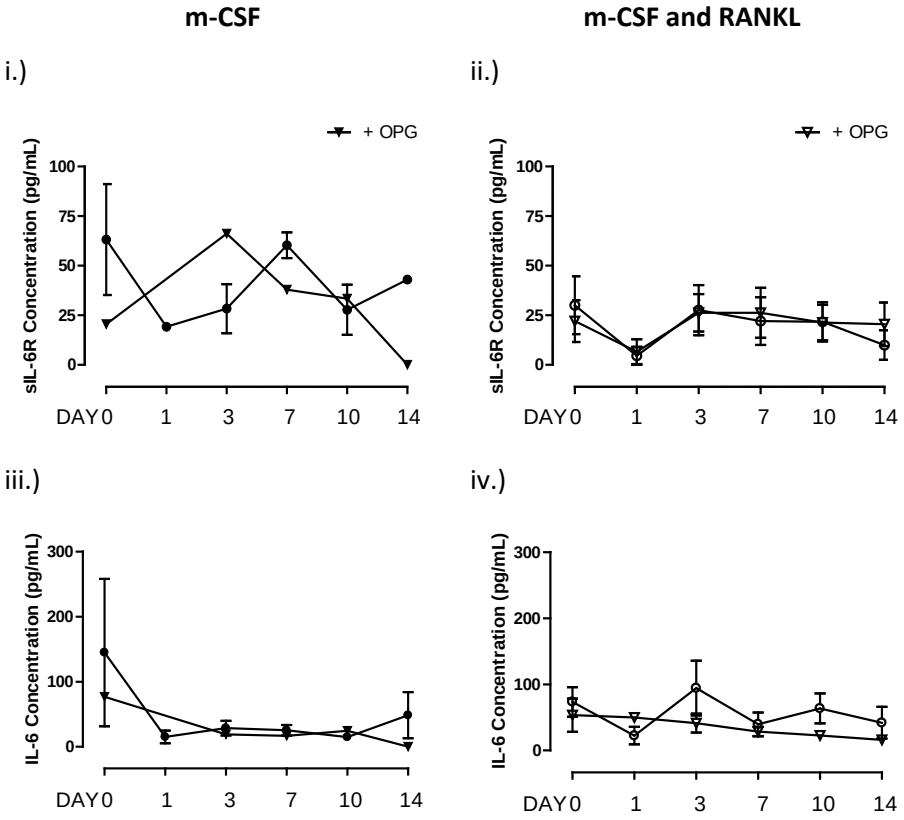

Figure 5. 19 - Soluble cytokine inflammatory markers in OPG cultures were not significantly different to osteoclast control cultures.Supernatants across the time-course of osteoclast assays were collected and analysed via ELISA. i. and ii.) sIL-6R in m-CSF only and m-CSF and RANKL cultures ± OPG were not significantly altered. iii. and iv.) IL-6 concentration was comparable in m-CSF only cultures ± OPG, and within m-CSF and RANKL ± OPG. No sample existed for m-CSF and OPG cultures at day 1. M-CSF and RANKL; N=7 donors, 2 replicate disks per donor. M-CSF, RANKL + OPG;N=5 donors, 2 replicate disks per donor. Means of all donors plotted ± SEM reported. One-way ANOVA preformed.

5.3.5 Determining the impact of inhibiting CCL3 on bone pathology and inflammation in a murine model of CIA

The inhibitory effect of anti-CCL3 on bone resorption *in vitro* was established in Section 5.3.2 and its therapeutic potential suggested in Section 5.3.4. Next the effectiveness of this strategy *in vivo* was tested in the murine model of collagen induced arthritis (CIA). *Brand, Latham & Rosloniec (2007)* reported the use and application of this model for RA, where mice were immunized with CFA and type II collagen on day 0 and by day 21 show the first clinical signs of arthritis (erythema and swelling of the meta-tarsals/tarsals/ankle joint). In this respect, the murine model of inflammatory arthritis (CIA) was established and treatment ensued with either anti-CCL3 or a paired isotype control antibody (IgG1). Mice received five treatment doses of either anti-CCL3 or isotype control by intraperitoneal injection on alternate days. The same dose of each treatment was given to each mouse. Dose was calculated from the average murine weight and previously reported CCL3 concentrations in murine plasma (*Kasama et al. 1995*). The experiment ended on day 29 when joints were harvested for 3D imaging (micro-CT) and histology (haematoxylin and TRAP staining).

5.3.5.1 The treatment of murine CIA with anti-CCL3 had no effect on clinical score

Anti-CCL3 exerted diminutive impact upon CIA-associated inflammation, by clinical score (5 ± 2) and paw diameter measurements (2.4 ± 0.2mm), versus mice treated with the isotype control Ab (6 ± 2 and 2.4 ± 0.1mm; Figure 5.20).

5.3.5.2 In anti-CCL3 treated mice a significant reduction in radiological erosive score in hind paws and forepaws were found

Radiological assessment of erosions in the tarsals, meta-tarsals and phalanges joints of the hind paw were carried out to show the *in vivo* effect of anti-CCL3 on the resorptive activity of the osteoclast. A significant 2-fold decrease in the number of erosions per hind paw in anti-CCL3 treated mice compared to isotype mice was

proven (*p≤0.01,* Figure 5.21*)*. Similarly, treatment with anti-CCL3 yielded a significant 2-fold reduction in forepaw erosions compared to isotype controls; 1.50 ± 0.44 compared to 2.91 ± 0.49 (*p≤0.05,* Figure 5.22). Using micro-CT extensive bone degradation was seen in hind paw reconstructions, where anti-CCL3 had a protective effect on joint architecture; specifically in the tarsal joints (Figure 5.23).

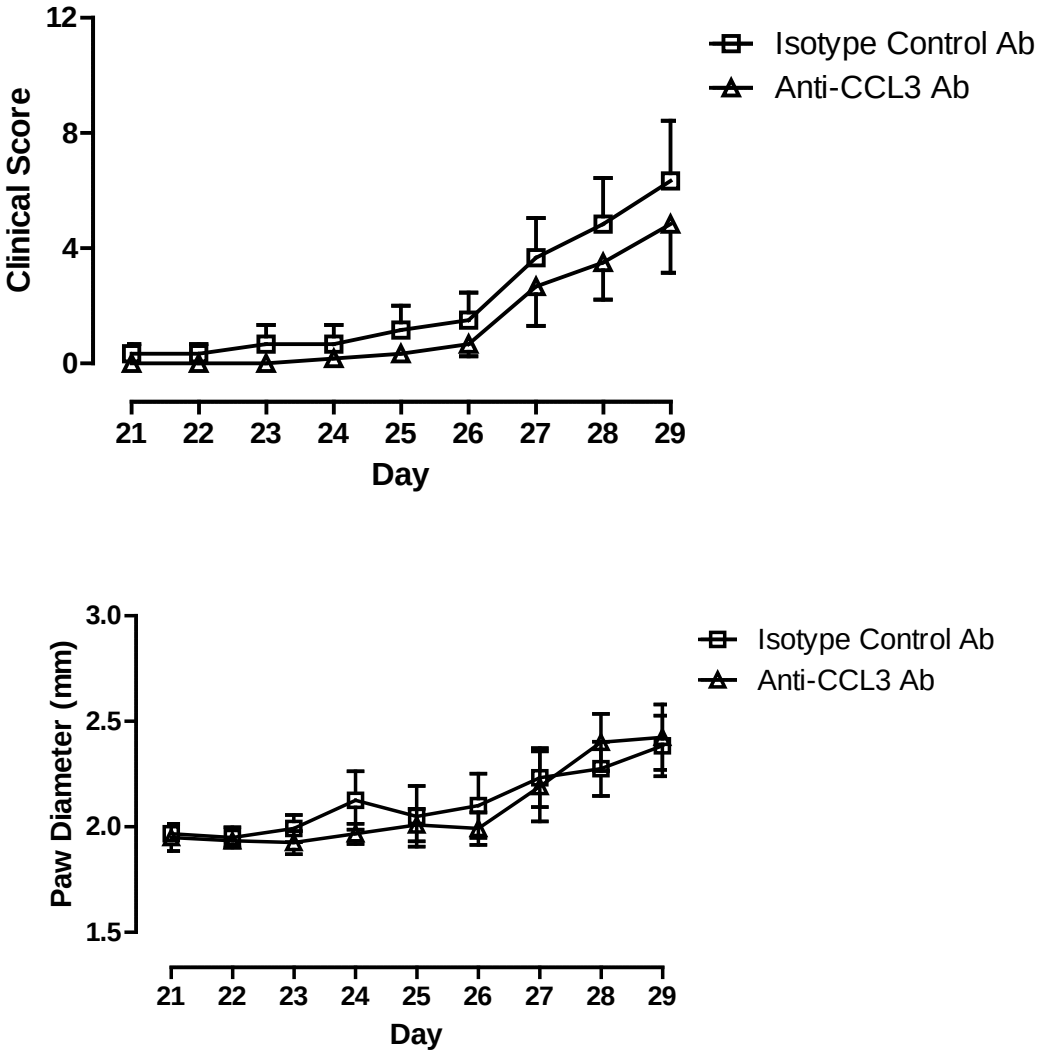

Figure 5. 20 - The *in vivo* treatment of mice with anti-CCL3 had no significant effect on the progression of CIA.Anti-CCL3 or isotype control Ab was given to a murine model of CIA on alternate days. The injection of anti-CCL3 had no significant impact on the clinical score of mice compared to isotype controls (n=6 per group). No significant difference was noted between treatment groups for paw diameter. Statistical analysis using a two way ANOVA was performed, and means ± SEM data values were reported.

Hind paws

Isotype Control

IgG2A (5 mg/kg)

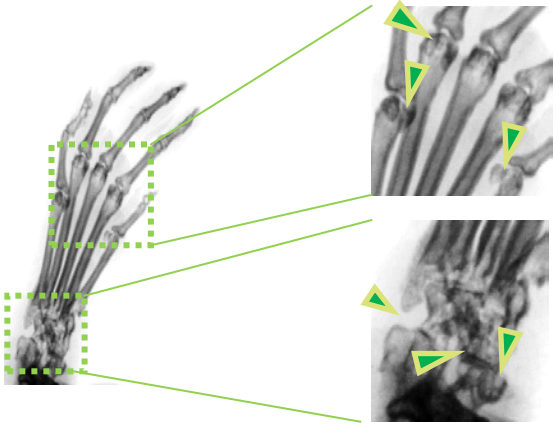

i.)

Anti-CCL3 (5mg/kg)

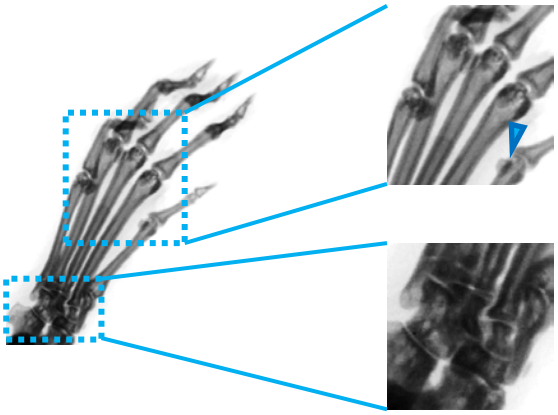

ii.)

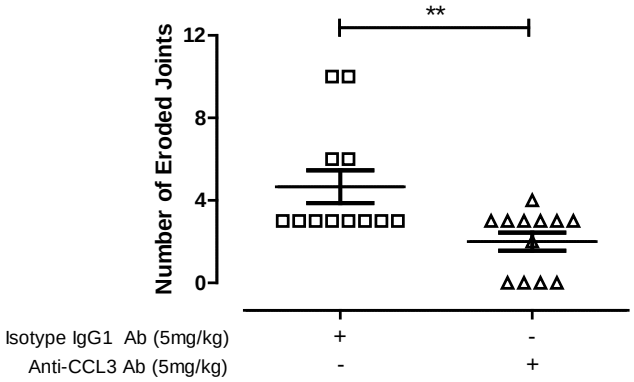

Figure 5. 21 - Radiological erosions in hind paws were significantly reduced in animals treated with anti-CCL3 compared to isotype controls.i.)Representative x-rays of hind paws from CIA mice treated with either anti-CCL3 or isotype control were acquired. ii.) A significant reduction in the number of eroded joints was found in hind paws from mice treated with anti-CCL3 compared to isotype controls (*p≤0.01,* n=6 mice per group; left and right hind paw assessed). Arrows indicate radiological erosions. Statistical analysis using a Student's t-test was performed(** = *p≤0.01*), and means ± SEM data values were reported.

Forepaws

i.)

Isotype Control

IgG2A (5 mg/kg)

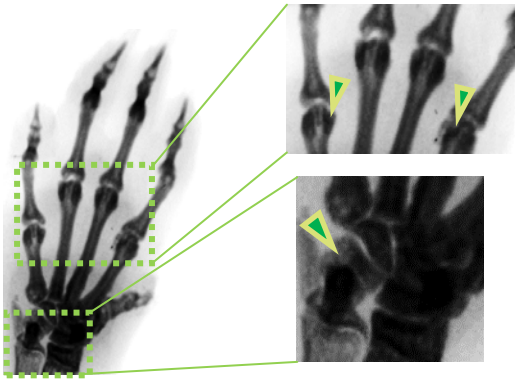

Anti-CCL3

(5mg/kg)

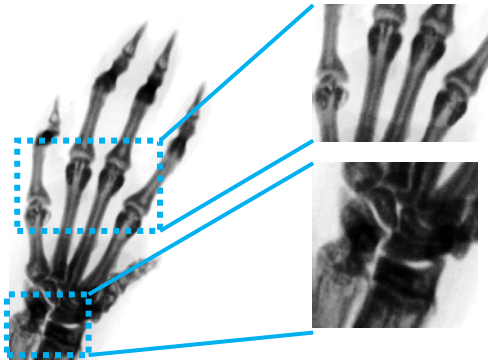

ii.)

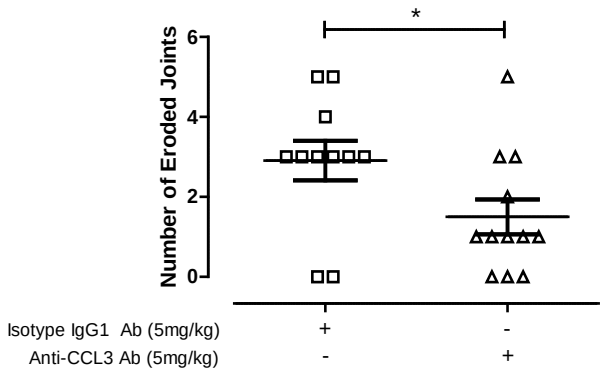

Figure 5. 22 - Radiological erosions in forepaws were significantly reduced in animals treated with anti-CCL3 compared to isotype controls.i.)Representative x-rays of forepaws from anti-CCL3 or isotype control Ab treated CIA mice were acquired. ii.) The number of eroded joints in the forepaw was significantly reduced in the presence of anti-CCL3 compared to isotype controls (*p≤0.05,* n=6 mice per group; left and right forepaw assessed). Arrows indicate radiological erosions. Statistical analysis using a Student's t-test was performed(* = *p≤0.05*), and means ± SEM data values were reported.

Isotype Ab Anti-CCL3 Ab

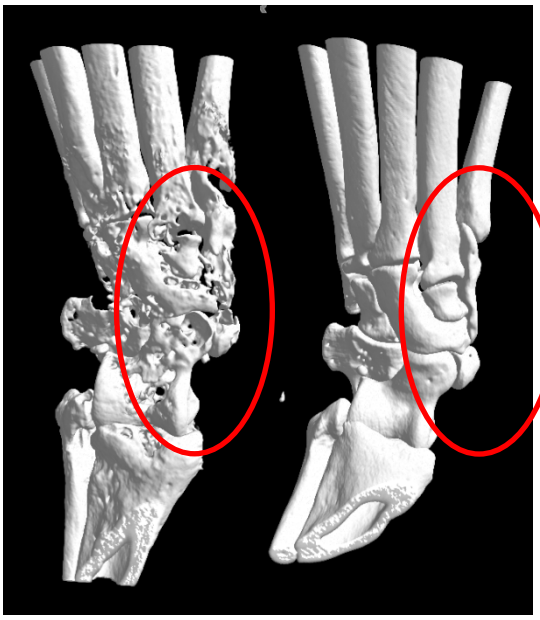

Figure 5. 23 - Micro-CT reconstructions illustrated the substantial protective effect of anti-CCL3 treatment on joint structureA reconstruction of the hind paw of an isotype treated mouse (n=1) and an anti-CCL3 treated mouse (n=1) shows the clear substantial differences in eroded bones of the tarsals. Anti-CCL3 treated mice appear protected from the erosive behaviour.

5.3.5.3 *Arthritis index was significantly reduced in the distal joints of anti-CCL3 treated mice*

Forepaws fixed in formalin were sectioned and stained with haematoxylin and TRAP facilitating assessment of inflammatory infiltrate, synovial hyperplasia, pannus formation and bone destruction, leading to the arthritic index (A.I.; composed of inflammatory and degenerative score). Inflammatory cell infiltration and synovial hyperplasia were comparable in shoulder joints from isotype and anti-CCL3 treated mice (A.I. 3.8 ± 0.6 versus 2.3 ± 0.4) and minimal cartilage/bone loss was present. Further analysis of the shoulder joint showed no significant difference in inflammatory (isotype: 2.9 ± 0.6, anti-CCL3: 1.9 ± 0.5) or degenerative score (isotype: 0.8 ± 0.2, anti-CCL3: 0.4 ± 0.2). Extensive TRAP staining was seen in the humerus growth plate in both treatment groups, highlighting the location of osteoclasts (Figure 5.24, i and ii, arrows).

The A.I. of the elbow was significantly reduced in anti-CCL3 treated mice compared to isotype controls; 4.9 ± 0.6 versus 2.7 ± 0.7 (Figure 5.25, $p \geq 0.05$). The inflammatory score was not significantly different in the forearm and elbow joint; 3.8 ± 0.4 versus 2.4 ± 0.6, but adipocytes had been displaced by infiltrating cells in both groups, along with an increase in exudate fibrin deposits in isotype treated mice but not anti-CCL3. TRAP staining was localised to the epiphysis in isotype controls, but was negligible in anti-CCL3 mice (Figure 5.24, iii and iv, arrows). The degenerative score for the elbow in anti-CCL3 animals compared to controls was significantly reduced; 1.1 ± 0.3 versus 0.4 ± 0.2 (Figure 5.25, $p \geq 0.01$).

A.I. of the wrist significantly decreased in the presence of anti-CCL3; 6.8 ± 0.6 versus 3.8 ± 0.36 (Figure 5.25, $p \geq 0.01$). Infiltrating immune cells were visibly enhanced in both adipose tissue and exudate of isotype controls, along with hyperplasia and bone erosions. A 1.8-fold significant decrease in inflammatory score from the wrist was reported after treatment with anti-CCL3; 5.3 ± 0.5 versus 2.9 ± 0.6 (Figure 5.25, $p \geq 0.01$). Inflammatory cell infiltration into surrounding tissues was evident in isotype joints, seen by 'creeping' over bone surface, but infiltration into the exudates was minimal (Figure 5.24, v and vi, arrows). The presence of TRAP was greatly increased in the radius and carpals of isotype animals, but anti-CCL3 mice

appeared protected with minimal TRAP presence or bone erosions. Degenerative scores for anti-CCL3 treated mice were significantly reduced from isotype controls; 1.5 ± 0.2 versus 0.9 ± 0.2 (Figure 5.25, *p≥0.05*).

5.3.5.4 Anti-CCL3 treatment of CIA significantly reduced histological osteoclast counts compared to isotype controls

In the shoulder joint no significant change in osteoclast number was found between isotype groups and those treated with anti-CCL3; 34 ± 7 versus 30 ± 5 osteoclasts (Figure 5.26, i). In the distal elbow joint, a significant reduction in osteoclast number was seen in anti-CCL3 treated mice; 18 ± 7 versus 4 ± 2 osteoclasts (*p≥0.05,* Figure 5.26). A significant decrease in osteoclast number was also found in the wrist joint of anti-CCL3 treated mice compared to isotype controls; 62 ± 21 versus 18 ± 4 osteoclasts (Figure 5.26, iii, *p≥0.05*). Overall, the *in vivo* data reported here proves that the significant reduction in bone degradation was due to significantly reduced osteoclast formation and resorptive activity, and further supports *in vitro* data.

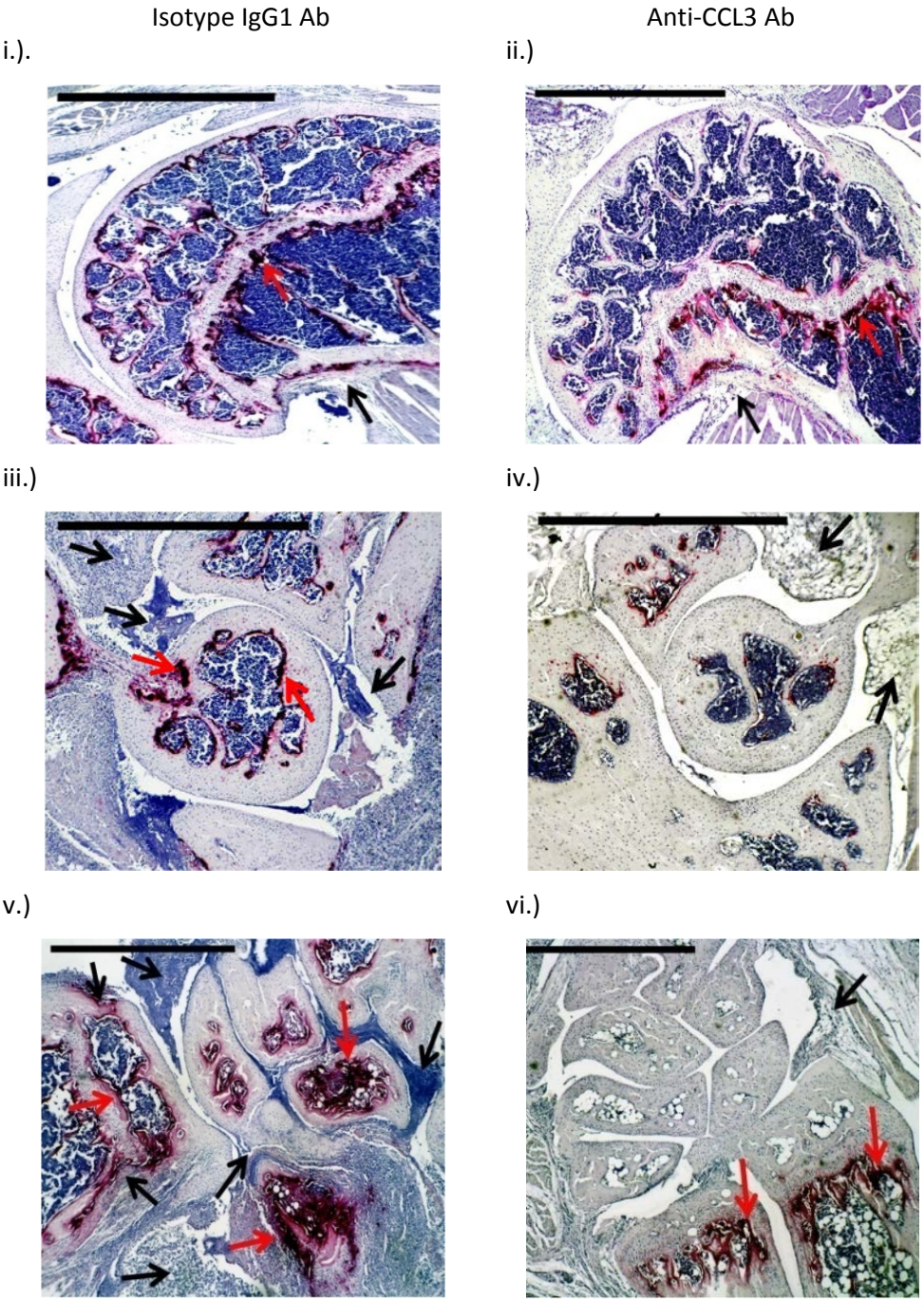

Figure 5. 24 - Enhanced TRAP staining was visualised in isotype control treated mice compared to anti-CCL3 treated.CIA-induced mice were treated with 5 doses of isotype IgG1 Ab (n=6) or anti-CCL3 Ab(n=6) prior to being culled on day 29. i + ii.) TRAP (red arrows) was evident in the humerus' epiphysis and growth plate in IgG1 treated mice, but only in the growth plate of anti-CCL3. iii. + iv.) TRAP localised in the elbow epiphysis of IgG1 mice but was absent in anti-CCL3 mice. v +vi.) Radial epiphysis showed extensive localisation of TRAP in carpals of IgG1 controls, compared to anti-CCL3 mice. Inflammatory infiltration, hyperplasia and resorption were seen in both treatment groups, but an extensive phenotype in the carpals of isotype mice were reported (black arrows). Scale bar 1mm.

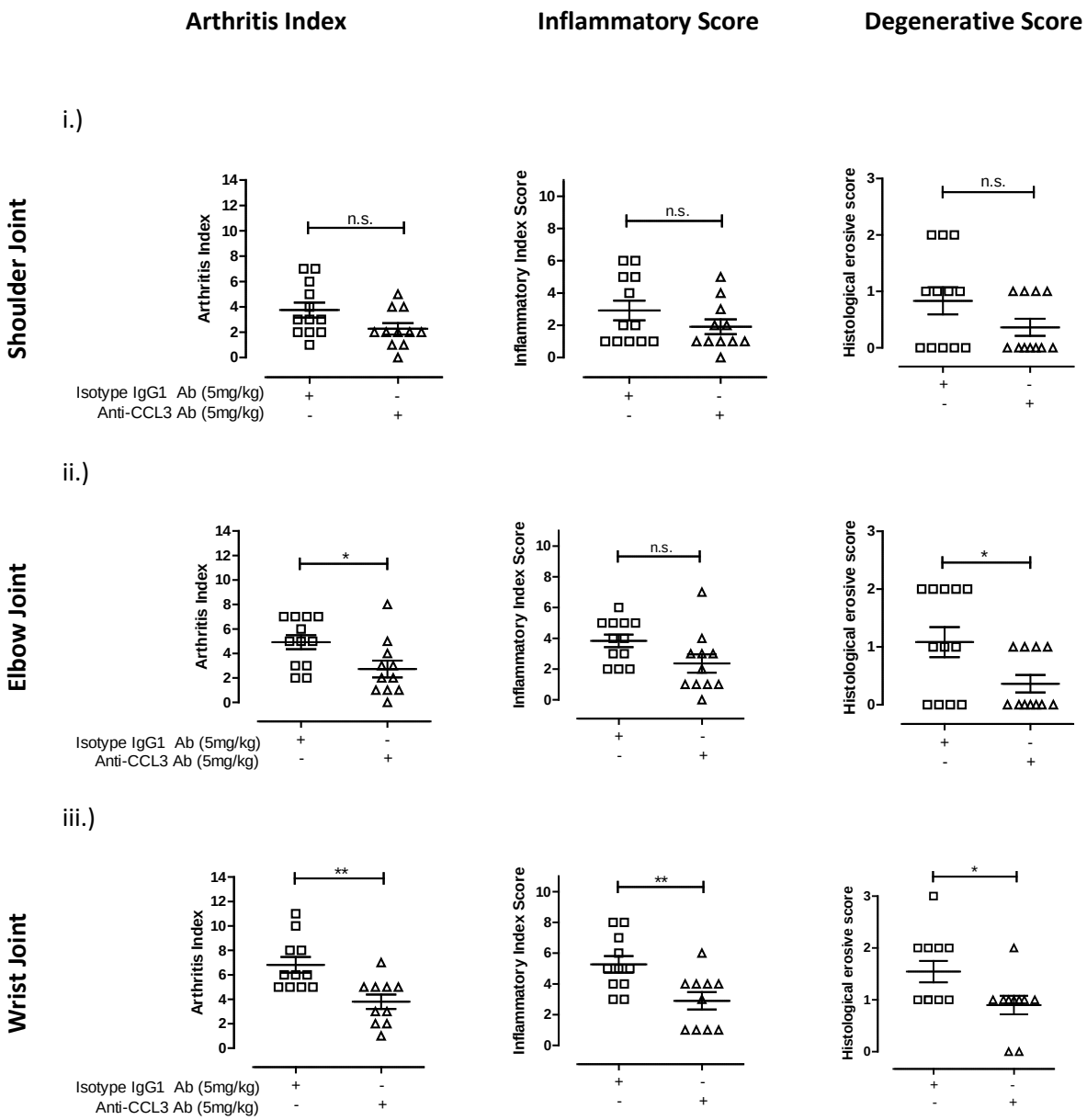

Figure 5. 25 - Anti-CCL3 treatment of CIA significantly reduced histological erosive scores in the elbow and wrist joints.Fore-arm sections were assessed for an inflammatory index score; subsynovial inflammation, synovial exudate and synovial hyperplasia/pannus formation, and erosive score. Addition of these scores resulted in the arthritis index (A.I.). i.) No significant difference in A.I. of isotype control mice and anti-CCL3 was seen in the shoulder joint. ii.) A.I. significantly reduced in the elbow joint after anti-CCL3 treatment (*p≥0.05*), but no change in inflammatory index resulted. A significant decrease in erosive score compared to anti-CCL3was found (*p≥0.05*). iii.) Anti-CCL3 significantly decreased the wrist A.I. (*p≥0.01*), which resulted from a significant reduction in inflammatory index and erosive score (*p≥0.01* and *p≥0.05*).N=6 mice per group, left and right forepaw assessed. Statistical analysis using a Student's t-test performed. Mean ± SEM data reported.

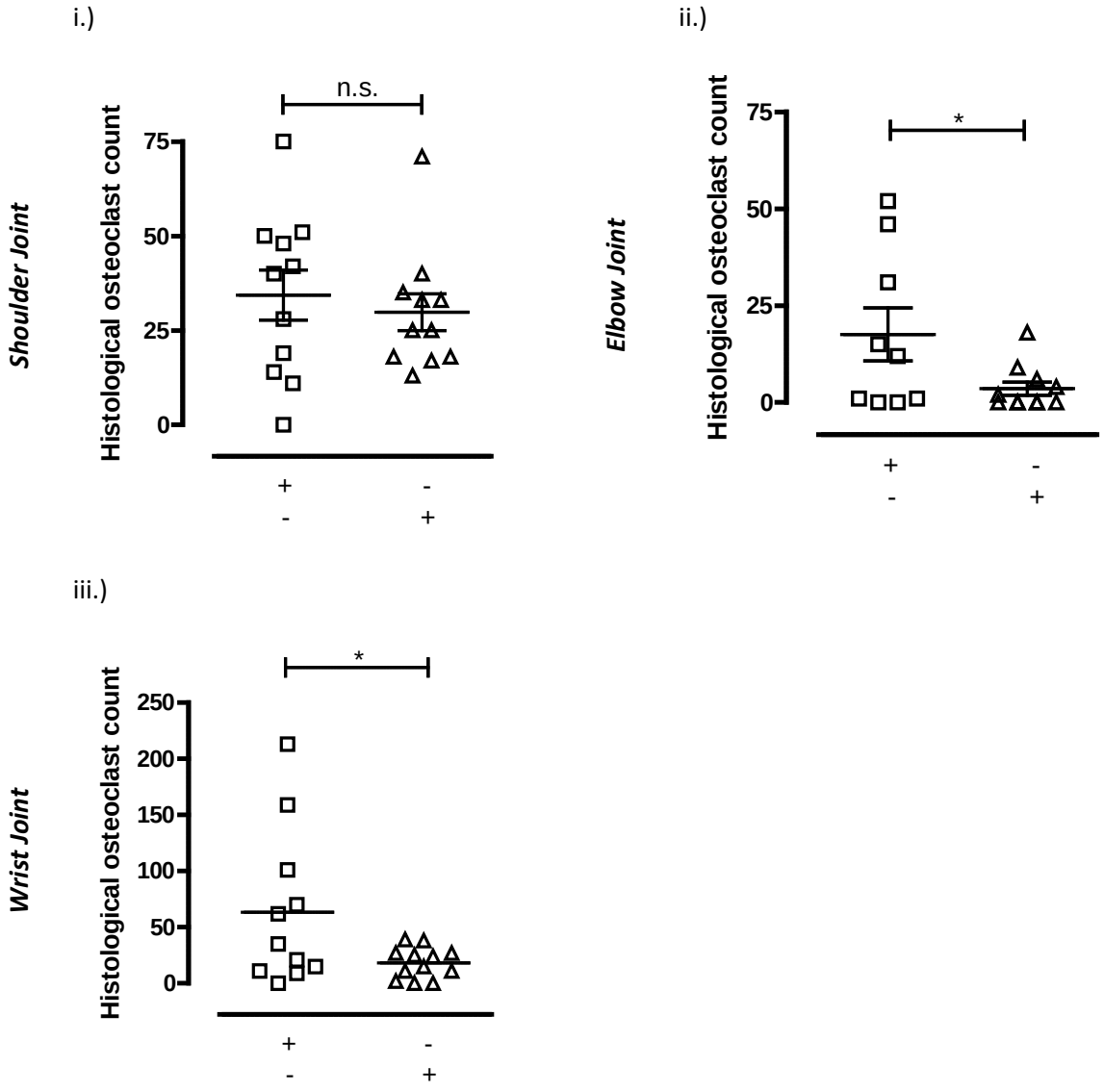

Figure 5. 26 - Osteoclast number significantly reduced in the elbow and wrist joints of anti-CCL3 treated mice.Following the histological analysis of fore-arm sections from mice treated with isotype or anti-CCL3 the presence of $TRAP^{+ve}$ osteoclasts was assessed per section. i.) Osteoclast number was unchanged in the shoulder joint of anti-CCL3 and isotype control treated mice. ii.) A significant reduction in osteoclast number in the elbow joints of anti-CCL3 mice compared to isotype controls resulted (*p≥0.05*). iii.) In wrists joints a significant decrease in osteoclast count resulted through anti-CCL3 treatment when compared to isotype control treated mice (*p≥0.05*). N=6 mice per group, left and right forepaw assessed. Statistical analysis using a Student's t-test was performed, and means ± SEM data values were reported.

5.4 Discussion

Increased CCL3 has been linked to enhanced osteoclastogenesis and bone resorption in both murine and human bone marrow cultures (*Tak et al. 1997, Toh et al. 2004, Szekanecz et al. 2010, Takano et al. 2014*). In this chapter a novel role of CCL3 in osteoclastogenesis was suggested from its significant early increase after RANKL stimulation. Neutralisation of CCL3 caused a significant attenuation of osteoclast number and resorption to similar levels as OPG in $CD14^{+ve}$ monocultures. Such *in vitro* data therefore postulates CCL3 as a novel therapeutic target in diseases characterised by extensive bone destruction, such as experimental inflammatory arthritis (CIA). In summary, the data presented in this chapter identifies a novel biomarker in destructive bone diseases with potential therapeutic benefits. The contextualisation of the above results and their impact on the clinical aspect of bone diseases will next be discussed.

5.4.1 CCL3 synergistically increased osteoclast formation in the presence of RANKL signalling

This chapter reports a novel role of CCL3 in mediating a significant increase in early osteoclastogenesis, which was linked to osteoclast formation and bone resorption. Furthermore, experiments investigating the effect of neutralising CCL3 on osteoclastogenesis reported a clear role of CCL3 in osteoclast differentiation ($TRAP^{+ve}$ cells and osteoclast counts), rather than the resorptive potential of the osteoclast (individual pit area, depth and volume data).

Although the mechanisms through which CCL3 aided osteoclast differentiation were not investigated, several theories could be postulated when considering the conclusions of previously published studies where CCL3 has been reported as RANKL dependent. Data reported in this chapter concurs with the previously reported RANKL-mediated increase in CCL3 in both mononuclear cell assays (24 hours post RANKL; *Koch et al. 1994*) and RAW264 osteoclast precursors (48 hours post RANKL; *Ishida et al. 2006*). More recently, addition of CCL3 into $CD14^{+ve}$ monocyte cultures was reported to increase osteoclast differentiation (*Dapunt et*

al. 2014). Collectively, the above studies suggest a common RANKL-mediated increase in CCL3 levels, allowing a crossover in RANKL signalling and CCL3 expression to be postulated (*Koch et al. 1994, Ishida et al. 2006, Dapunt et al. 2014*). Although both RANKL and CCL3 activate their own independent receptors (RANK - TRAFs and CCR1- GPCR respectively), the transcription and translation of downstream signalling proteins (NFATc1, AKT, MAPK and JNK)from each pathway could be intersected (*Lentzsch et al. 2003, Mueller & Strange 2004, Blair et al. 2005, Wada et al. 2006, Heinemann et al. 2011*).

Specifically, RANK activates TRAF6 which localises to its cytoplasmic region activating c-Src (leading to PI3K and Akt), NF-κβ, MAP kinases (JNK) and extracellular signal-related kinases (ERK1/2). Such activation results in the nuclear relocalisation of transcription factors (NFATc1, c-fos, P.U.1, AP.1, c-Jun) and the phosphorylation of STAT1 leading to the transduction of osteoclast related genes (DC-STAMP, Atp6v0d2, CATK, MMP9 and TRAP; *Galibert et al. 1998, Blair et al. 2005, Wada et al. 2006*). Comparatively, CCR1 activates MAPK and ERK1/2, but in a similar mechanism increases Akt through c-Src. The activation and relocation of NF-κβ, JNK, NFATc1, AP.1 to the nucleus results leading to enhanced NFATc1, MAPK, JNK and osteoclast related gene expression (DC-STAMP, Atp6v0d2, CATK, TRAP, integrins, vitronectin and calcitonin (*Jimi et al. 1999, Kukita et al. 2004, Mueller& Strange 2004, Kim et al. 2005, Wada et al. 2006, Xing et al. 2012*). Interestingly, CCR1 expression was observed to be increased on marrow cells cultured in RANKL (*Yu et al. 2004*) and from studies using RAW264 cells increased CCR1 was reported following NFATc1 activation (*Ishida et al. 2006*). Therefore, we can hypothesis that RANKL increased CCR1 expression on $CD14^{+ve}$ monocytes in our cultures, thus increasing cellular responsiveness to CCR1 ligands and increasing cell migration. The resultant and combined elevated expression of NFATc1, MAPK and JNK from both RANKL and CCL3 signalling would therefore offer one possible mechanism for the synergistic generation of osteoclast precursors.

Furthering current knowledge, in this chapter anti-CCL3 significantly reduced osteoclast number but had no effect on $TRAP^{+ve}$ cell count or supernatant-associated levels of TRAP5b. RANKL-RANK signalling could therefore be dominant

over CCL3-CCR1 signalling. Alternatively, it could be thought of as independent from RANKL-RANK signalling, but with similar effects on rate-determining steps of osteoclastogenesis; pre-cursor cell migration and fusion (*Takayanagi et al. 2002, Cassady et al. 2003, Ikeda et al. 2004, Partington et al. 2004,Sharma et al. 2007,Dapunt et al. 2014).* In contradiction*, Albuquerque et al. (2013)* showed CCL3 essential for murine TRAP expression. However, this difference could be explained by the use of a global CCL3 knockout model *in vivo* that resulted in a reduction of T cell and osteoblast mediated RANKL secretion, thus decreasing $TRAP^{+ve}$cell counts (*Yu et al. 2004, Castellino et al. 2006*, *Harvey & Kaymakcalan 2010, Dapunt et al. 2014*).

5.4.2 CCL3 in precursor cell migration

This chapter illustrates an important role of CCL3 in osteoclastogenesis. One such mechanism whereby CCL3 could mediate these effects is on precursor cell migration. Although not directly studied in this thesis, in 2004 *Yu et al.* reported enhanced precursor cell migration in the presence of CCL3 and RANKL. *Ishida et al.* (*2006*) further commented upon the global role of CCR1 ligands on osteoclast precursor cell migration, where a disruption of CCR1 signalling through receptor antagonism or inhibition resulted in decreased osteoclast number. In 2013 the mechanism behind decreased cell migration was established by *Gilliland et al. (2013),* where CCR1 signalling lead to increased F-actin polymerisation, thus meaning an attenuated CCR1 stimulation would result in decreased migration and motility. Secondary to the effects of anti-CCL3 on cell migration, migratory chemokines including CCL2 were unlikely to exert cell migration (as shown in this chapter), where *Mizutani et al. (2009)*and *Ishii et al. (2010)* showed CCL2 and CCL5 to have no effect on pre-cursor cell migration in the absence or presence of RANKL.

Alongside precursor cell migration, cell fusion into multi-nucleated giant cells could also present itself as a rate-determining step in osteoclastogenesis. The fusion proteins DC-STAMP and Atp6v0d2 (H^+-ATPase V0 domain) both play critical roles in cell-cell fusion and are downstream signalling proteins from NFATc1 activation

(*Kukita et al. 2004, Lee et al. 2006*, *Kim et al. 2008*). Although not established within this chapter, a pivotal finding showed CCL3 to have no effect on DC-STAMP expression, but again did enhance osteoclast formation (*Kukita et al. 2004*). It is therefore suggested that the effects of CCL3 on osteoclast differentiation were independent from the expression of the fusion protein DC-STAMP.

The role of Atp6v0d2 in osteoclast formation was studied in a global knock-out mouse, where decreased bone resorption but increased bone formation was found (*Lee et al. 2006)*. TRAP5b levels in Atp6v0d2$^{-/-}$ mice remained unchanged to controls (*Lee et al. 2006*). Comparably, TRAP5b was also unchanged in osteoclast cultures treated with anti-CCL3, despite a significant reduction in osteoclast number. Further data provided by *Lee et al. (2006)* showed a 5-fold reduction in ADAM-8 and -12from Atp6v0d2$^{-/-}$cultures, where osteoclast number could not be rescued by ADAM -8 and -12 supplementation (*Lee et al. 2006*). Additionally, CCR1$^{-/-}$ mice expressed decreased NFATc1 and Atp6v0d2, implicating CCR1 ligands (e.g. CCL3) in the expression and function of Atp6v0d2 (*Hoshino et al. 2010*). A potential *in vitro* role of CCL3 in Atp6v0d2- mediated cell fusion could therefore be postulated.

Further experimental work would be necessary to establish the role of Atp6v0d2 in osteoclastogenesis. Through gene disruption and gene depletion *in vivo,* knowledge of the importance and interplay between Atp6v0d2 and CCR1 signalling in osteoclastogenesis could be established. The experimental design would need to be carefully considered to ensure the essential expression of NFATc1, MAPK and JNK; *i.e.* NFATc1 knock-out is lethal mid-gestation (*Abdul-Sater et al. 2012*). *In vitro*, the molecular and protein expression of Atp6v0d2 could be quantified through western blot analysis, PCR or immunohistochemical staining. Disks would need to be harvested along with culture supernatants at earlier time-points (2-, 4-, 8-, 10-, 12-, 24-, 48- hours post RANKL supplementation) to identify when CCL3 exerts its primary effect on osteoclastogenesis and if this effects Atp6v0d2 expression. The pathways through which m-CSF, RANKL and CCL3 effect cellular responses, and the stages at which osteoclast differentiation could be affected, are defined in Figure

5.27. Note that CCL3/CCR5 signalling is negligible in osteoclastogenesis as previously reported by *Doodes et al. (2009)*and *Lebre et al. (2011)*.

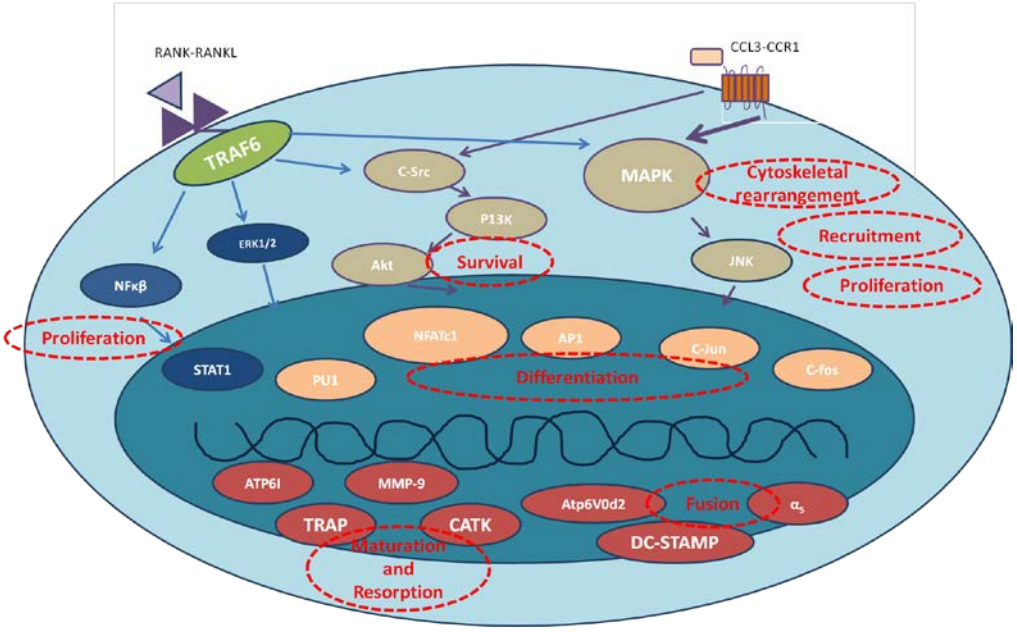

Figure 5. 27 - A schematic of RANKL-RANK and CCL3-CCR1 signalling pathways and their possible paths of interaction.RANKL binds to RANK on the surface on the cell and causes a cascade of intracellular signals. Initially, TNF-receptor associated factors (TRAFs) localise to the cytoplasmic domain of RANK which leads to c-Src, NF-κβ and MAP kinase activation (*Galibert et al. 1998, Blair et al. 2005* and *Wada et al. 2006*). Alternatively, CCL3 signals through its G protein coupled receptor CCR1 which directly activates downstream signalling molecules including MAP kinases, ERK1/2 and c-Src (*Mueller & Strange 2004*). In both pathways the activation of these proteins leads to transcription factor relocation to the nucleus and the transduction of osteoclastic genes; DC-STAMP, Atp6v0d2, CATK, MMPs, TRAP, which typify differentiating osteoclasts. Highlighted in red are areas of osteoclastogenesis that may be affected.

5.4.3 CCL3 exerts negligible effects on mature osteoclast resorptive function

Following on from studying the effects of CCL3 on osteoclastogenesis, the effect of CCL3 on the resorptive capability of the osteoclast was assessed. The neutralisation of CCL3 significantly reduced the total area of bone resorbed over the 14 day differentiation period, but no significant change in individual pit characteristics (pit area, volume and depth) were found. These data suggested that there was no effect of anti-CCL3 on resorption variables such as the motility of mature

osteoclasts, their attachment to bone surfaces, or the secretion of degradative enzymes.

However, CCL3 has been linked to the migration of mature osteoclasts differentiated in the presence of RANKL from murine RAW264 cells, where its presence caused a 2-fold increase in osteoclast motility after 24-hours (*Yu et al. 2004*). Neutralisation of anti-CCL3 was therefore suggested to reduce osteoclast motility, thus resulting in decreased resorption from active osteoclasts. This theory could be examined by fluorescently tagging F-actin (FITC-phalloidin; *Wilson et al. 2009*) and monitoring the osteoclasts motility rates across the disks surface.

Secondary to osteoclast motility, an effect of anti-CCL3 on reducing osteoclast attachment to bone substrate may also have occurred. Integrin $\alpha_v\beta_3$ expressed by the osteoclast is used for adherence to vitronectin, osteopontin and bone sialoprotein (*Horton 1997*, *Duong et al. 1999)*. α_v expression is downstream of NFATc1 implicating this integrin in RANK and CCR1 signalling, where CCR1 inhibition has shown decreased $\alpha_v\beta_3$ (*Ishida et al. 2006, Lin et al. 2013*). Subsequently, the neutralization of CCL3 in m-CSF and RANKL cultures could reduce α_v through reducing NFATc1, thus reducing osteoclast attachment. Opposing data has however been reported by Yu and colleagues (2004), who observed that CCL3 had no effect on osteoclast attachment, although they did not quantify the molecular expression of $\alpha_v\beta_3$ integrins. To further define the role of CCL3 on osteoclast attachment the expression of α_v integrins and the profile of NFATc1would need to be monitored at the molecular and protein level (qPCR).

Finally, in addition to osteoclast motility and attachment, CCL3 may also have affected the secretion of resorptive enzymes from the osteoclast. However, from data reported in this chapter the effect of CCL3 on resorptive enzyme secretion is thought to be minimal as there were no differences in the pit areas and depths between cultures with and without anti-CCL3. The data reported here supports that of *Yu et al. (2004)* who used an *in vitro* model of osteoclastogenesis which showed CCL3 to have no effect on the ability of a mature osteoclast to form resorption pits. Subsequently, the significant reduction in bone resorption reported

in this chapter is thought to be a secondary effect of significantly attenuated osteoclast number, rather than a direct effect of CCL3 on resorption. Supporting this *Ishii et al. (2010)* reported CCL3 to be down-regulated following the differentiation of mononuclear cells into osteoclasts, suggesting CCL3 signalling was no longer pivotal to mature osteoclast function *in vitro*.

However, a postulated peripheral role of CCL3 on *in vivo* osteoclastogenesis can be suggested from the associated role of increased CCL3 in bone diseases characterized by enhanced bone resorption (*Choi et al. 2000, Repeke et al. 2010, Vallet et al. 2011*). Using $CCL3^{-/-}$ mice CCL3 has been reported to have no effect on the secretion of resorptive enzymes including CATK (bone resorptive) and MMP-13 (cartilage destructive), from the osteoclast (*Albuquerque Taddei et al. 2013, Kikuta & Ishii 2013*). Additionally, their secretion was unaffected by Met-RANTES, a CCR1 antagonist, thus confirming these enzymes act independently of CCR1 signalling. In addition MMP-9 is also involved in joint destruction, where CCL3 has been found to stimulate its secretion in lung metastasis models from mononuclear cells and macrophages, however MMP-9 secretion from the osteoclast due to CCL3 remains unknown (*Yang et al. 2006, Wu et al. 2008).* To definitively prove the importance of CCL3 on the direct secretion of resorptive enzymes further experiments are needed where MMP presence and activity could be assessed using zymography (*Leeman et al. 2002, Hu et al. 2010, Franco et al. 2011, Chellaiah & Ma 2013*).

5.4.4 CCL3 inhibition potency *vs.* established osteoclast inhibitor *in vitro*

Data reported throughout this chapter therefore support the utilisation of anti-CCL3 as therapeutic against enhanced bone resorption. Prior to assessing the efficacy of anti-CCL3 in inhibiting osteoclast formation *in vivo*, the potency of osteoclast inhibition in the presence of anti-CCL3 compared to the known inhibitor OPG was assessed *in vitro* (*Udagawa et al. 2000, Irie et al. 2007*). The importance of OPG was previously reported as secretion increased after peak osteoclast differentiation, preventing extensive osteoclastogenesis (*Irie et al. 2007*). Published data states OPG supplementation into co-cultures of osteoblasts and bone marrow

cells completely inhibited osteoclast differentiation, maturation and survival, along with the blockade of substrate resorption (*Jimi et al. 1999)*.

For the first time, data reported in this chapter shows anti-CCL3 to have the same potency as OPG in inhibition of osteoclast formation in human $CD14^{+ve}$ osteoclast monocultures supplemented with m-CSF and RANKL. An increased sample number however would be needed to prove reproducibility of this comparison. Of pivotal importance, in cultures supplemented with OPG substantially reduced levels of CCL3, but not CCL2, CCL5, IL-6 and sIL-6R levels were found. Further evidence was therefore provided for involvement of CCL3 in the stimulation of early osteoclast formation by a RANKL-dependent pathway, thus providing a rationale for the use of anti-CCL3 as a therapeutic in destructive bone disease.

Initial experiments using anti-CCL3 as a therapeutic in models of destructive bone disease (*i.e.* arthritis, ovariectomized mice or cancer models) would be needed for proof of concept (*Kameda et al. 1997, Bord et al. 2003, Oursler 2003, McClung et al. 2006, Cummings et al. 2009, Pierroz et al. 2010, Yasuda et al. 2013*). If the neutralisation of CCL3 results in significantly attenuated bone destruction, the potency of such a treatment would next be assessed against current therapeutics; *i.e.* Denosumab, where a benefit *vs.* cost model could be established. In theory anti-CCL3 exerts several benefits over Denosumab, firstly that Denosumab is only functional in the presence of RANKL; if given after RANK activation, osteoclast differentiation and resorption still occur. Secondly, that determining Denosumab doses capable of inhibiting pathologically- enhanced bone resorption without disrupting bone homeostatic balance is difficult. For example, *Bargman et al. (2012)* treated mice with varying doses of OPG-Fc and found it could result in both osteopetrosis and osteoporosis. Although RANK signalling still occurs after anti-CCL3 treatment, research has shown significantly decreased motility and differentiation of pre- and mature osteoclasts (*Yu et al. 2004*). Osteopetrosis and osteoporosis are unlikely to occur with anti-CCL3 due to the redundancy of the chemokine system. However, this is, at the same time, a disadvantage of a therapy such as anti-CCL3: additional chemokines (CCL2 and CCL5) may increase and

enhance osteoclastogenesis in the absence of CCL3 *in vivo* through indirect RANKL secretion (*Ishii et al. 2010*).

Not only may anti-CCL3 attenuate bone destruction, it may also lead to a reduction in pain. The active secretion of protons creates an acidic environment leading to dissolution of bone mineral. Hyperalgesia may also arise from the acidic environment, as suggested by Nagae and colleagues (2006), where CFA injected into hind paws of mice led to an increase in acid-sensing ion channel (ASIC) and transient receptor potential vanilloid 1 (TRPV1) mRNA in dorsal root ganglions (DRGs). Thus, through anti-CCL3 attenuating bone destruction, a reduction of hyper-algesia may also result. Furthermore, the expression of TRPV1 on DRG was shown to be co-expressed with CCR1 (CCL3 receptor) on >85% of neurons, where CCL3 caused a 3-fold increase in TRPV1 sensitivity (*Zhang et al. 2005*). This pivotal finding provides the first mechanistic evidence for increased sensitization and pain in the presence of CCL3. A finding further supported by the identification of an endogenous self-amplification loop for CCL3 in microglial cells led to elevated CCL3 mRNA and enhanced NFAT signalling (*Kataoka et al. 2009*).

The prevalence of pain may also have resulted from the receptor, CCR1, and the ligand, CCL3. CCR1 inhibition has resulted in significant reductions of pain-like behaviour in animal models of hyperalgesia (*Lewis et al. 2014*). However, CCR1 is the receptor for many chemokines and therefore it could be the lack of CCL5, CCL7 or CCL23 signalling through CCR1 that has caused the decrease in pain. For example, CCL2 is linked to heightened pain perceptions in pelvic pain syndrome, where its neutralization has led to significant attenuation of pain-like behaviour (*Quick et al. 2012*). Commonly, mRNA levels of CCL2 and CCL3 increase simultaneously as in sciatic nerve injury models, therefore suggesting an ambiguous, dual neuro-inflammatory role of these chemokines (*Kiguchi et al. 2013*). However, in relation to osteoclast-associated pain, the impact of CCL2 is thought minimal due to unchanging levels in the presence of RANKL +/- anti-CCL3 from our *in vitro* cultures. To prove the importance of CCL3 in destructive bone pain further *in vitro* osteoclast differentiation assays are needed to quantify alternative pain mediator secretions (bradykinin, prostaglandin E2 etc.) in order to

establish possible pain pathways. The effects of anti-CCL3 on such pathways could then be assessed using an *in vivo* model of inflammatory arthritis (*e.g.* CIA) with behavioural testing prior to and post anti-CCL3 treatment.

5.4.5 CCL3 as a potential therapeutic target *in vitro*

To distinguish whether our significant reduction in osteoclast number and area resorbed *in vitro* was translated *in vivo,* the role of CCL3 was assessed in a murine model of inflammatory arthritis; CIA. *Kasama et al. (1995)* first reported the importance of CCL3 in the murine model of CIA where increasing concentrations of CCL3 over the induction time-course were found. A similar increasing profile was recorded within *in vitro* experiments reported in this chapter, together implying a role of CCL3 in the instigation and progression of CIA directed by the osteoclast. Following the quantification of CCL3 *in vivo*, *Kasama et al.* (*1995)* immunized animals with a CCL3-directed antibody which led to a reduction in disease presentation. The data reported in this chapter contradicts such a reduction, where no significant decrease in macroscopic scores of inflammation (clinical score and paw diameter) were reported. Although not fully understood, such differences may have resulted from variations in CIA induction and time-course (*i.e.* CIA was assessed for 29 days in this chapter versus 68 days in *Kasama et al. 1995*).

Following the assessment of anti-CCL3 on macroscopic pathologies associated with CIA, microscopic changes were assessed due to the novel findings of this thesis suggesting a role of CCL3 on osteoclastogenesis (see chapter 5.3.2.3). Radiological data showed a significant reduction of joint erosions in both fore- and hind paws of anti-CCL3 treated mice compared to controls, along with a visual improvement of hind paw joint structure by micro-CT imaging. Due to slow fixation methods hind paws were used for micro-CT analysis whilst forepaws were fixed quickly and used for histological analysis. Furthermore, forepaw analysis showed a significant reduction in degenerative score and osteoclast number in the presence of anti-CCL3 in the distal joints. This data therefore led to the novel finding that CCL3 was

involved in osteoclastogenesis *in vivo*, thus translating our data from *in vitro* studies into a more complex model of osteoclast differentiation.

To definitiely prove the importance of CCL3 in oteoclastogenesis and in turn CIA severity, additional experiments would be essential. Primarily, sample size would need to be increased alongside the repeition of this experiment to ensure that the effects seen within this chapter were not due to chance and are reproducible. During these additional stage 1 experiments a CCL3 concentration profile over the course of CIA induction would be quantified, similar to that which *Kasama et al. (1995)*. From this profile, a tailored dose range of anti-CCL3 could then be used in stage 2 experiments to assess the minimum effective dose and maximum tolerated dose concentrations (due to side effects or lethality). In addition the C_{max} and T_{max} could be identified to understand the absorption and removal of the compound. Additionally, in stage 2 experiments the dosing frequency and method of drug delivery would need to assessed, whilst maintaining compliance with Home Office and Project License regulations, to distinguish optimal treatment periods. Post stage 2 maximal beneficial effects of anti-CCL3 treatment in CIA development should therefore be known, where it may be concluded that an increased dose of anti-CCL3 could significantly reduce macroscopic inflammatory scores.

Alternative routes of CCL3 inhibition may also be preferred to administering anti-CCL3 such as ligand knock-out models or receptor antagonists/inhibitors. *Chintalacharuvu et al. (2005)* reported the importance of CCL3 in CIA by showing a significant reduction in inflammatory components in a $CCL3^{-/-}$ murine model. Whilst providing data which was contrary to that found in this chapter with anti-CCL3 treatment, differences may have resulted from complete knock-out of CCL3 versus its neutralisation (which may have only be partial due to dosing). The completion of stage 2 experiments as outlined above are pivotal to further insight into this finding to establish whether macroscopic pathologies of CIA can ever be inhibited by anti-CCL3 treatment. If, however a significant reduction of macroscopic pathologies does not result, anti-CCL3 may have altered the phenotype or density of infiltrating cells into the joint. For example, from the monocyte, macrophage, T cell and/or neutrophil phenotype which is typified by CIA, and this could be

assessed by FACS or immunohistochemistry (*Tak et al. 1997, Ramos et al. 2005, Xue et al. 2007, Szekanecz et al. 2010, Jonker et al. 2013, Shi et al. 2015*).

The significant reduction in osteoclast number and joint erosions did however support previous data reported by *Kondo et al. (2011)* who showed $CCL3^{-/-}$ and $CCR1^{-/-}$ mice to have attenuated leukocyte migration, osteoclast differentiation and joint erosions compared to $CCR5^{-/-}$ and wild-type mice. Together with data reported in this chapter (both *in vitro* and *in vivo)*, CCR1 is supported as the main receptor for CCL3-induced pathology in bone resorption, and therefore again presents itself as a potential therapeutic target. Initial use of a CCR1 antagonist, UCB35625, was shown to inhibit leukocyte chemotaxis, and could therefore potentially decrease osteoclast precursor cell migration (*Sabroe et al. 2000*). Following this, CCR1 antagonist, BX471, specifically inhibited signal transduction and osteoclastogenesis even after CCL3 stimulation (*Oba et al. 2005*). The CCR1 antagonist J-113863 which was given to mice with CIA also decreased inflammatory and destructive bone scores, alongside reducing leukocyte migration to joints (*Amat et al. 2006*). Furthermore, the CCR1 inhibitor MLN3897 also led to decreased cell interactions attenuating cell growth and survival through inhibition of Akt signalling (*Vallet et al. 2007*). It could thus be concluded that when combined with novel *in vitro* and *in vivo* data reported in this chapter, the antagonism of CCR1-CCL3 signalling reduced mature osteoclast formation, likely due to the inhibition of mononuclear cell migration, fusion and interaction. The impact of this novel therapeutic target will be further discussed in context with human diseases in Chapter 6, the General Discussion.

5.5 Conclusion

This chapter has identified and discussed a novel role of CCL3 in early osteoclast differentiation. Specifically, a RANKL-dependent, significant increase in CCL3 secretion occurred after 24-hours, exerting a significant role in early osteoclast differentiation *in vitro*. The neutralisation of CCL3 by an anti-CCL3 antibody *in vitro,* significantly attenuated osteoclast number and area resorbed to levels seen in OPG treated cultures. Individual resorption pit parameters were not significantly altered after CCL3 neutralisation, suggesting CCL3 has a role in osteoclast differentiation but not in osteoclastic resorption. The significant decrease of CCL3 in OPG supplemented cultures supports a RANKL-dependent action. In addition, the results reported in this chapter were contextualised in terms of pathological pain associated with bone destructive diseases, and a strong link between CCL3 and pain was postulated. The treatment of our reported murine model of CIA with anti-CCL3 led to significantly reduced radiological erosive scores and histological analysis showed significantly reduced osteoclast counts in distal joints. In conclusion, CCL3 neutralization was shown to be beneficial both *in vitro* and *in vivo* for the attenuation of osteoclastogenesis and protection of joints from osteolysis. Taken together, the data reported in this chapter and that previously published, implicates CCL3 in the development, progression and pain associated with destructive bone diseases. Further work establishing dose ranges is pivotal to establishing whether this therapeutic would be effective in reducing inflammatory pathologies in humans, and nociception.

Chapter 6:General Discussion

This thesis reports novel data on the role of IL-6 trans-signalling and CCL3 in osteoclast-mediated bone destruction supporting their published roles in inflammatory disease pathology (*Tamura et al. 1993, Schluger & Rom 1997, Ajuebor et al. 2004, Gabay 2006, Pharoah et al. 2006, Tanaka et al. 2014*). The importance of IL-6 trans-signalling and CCL3 is commonly reported in terms of inflammation, but data regarding their role in joint destruction is beginning to emerge as discussed in the previous chapters. However, the methodologies of co-cultures or receptor knock-out models are commonly reported in published studies which leave ambiguity as to the initiator of osteoclastogenesis and subsequent resorption (*i.e.* indirect effects of co-cultured cells on osteoclastogenesis). For example, co-cultures of bone marrow cells were used by *Choi et al. 2000* where CCL3 was reported as an osteogenic factor. All data reported in this thesis was obtained from the *in vitro* monoculture methodology established in Chapter 3: $CD14^{+ve}$ monocytes cultured on ivory in the presence of m-CSF and RANKL. At least 6 donors were used for each treatment condition, with multiple disk replicates per donor per condition. This robust methodology increased data integrity and validity over that previously reported from studies using cell co-cultures on glass (*Hirayama et al. 2002, Peruzzi et al. 2012*). Quantification of cytokines in culture supernatants allowed direct association with postulated osteoclastogenesis biomarkers.

Data presented in Chapter 3 also defined a novel computational algorithm for cell visualization and counting which was validated to provide high-throughput data analysis. The development of this algorithm vastly reduced analysis time (10-fold i comparison to conventional methods), thus enabling greater replicate numbers per donor under each treatment condition, further increasing data validity through reproducibility. The use of this algorithm could be wide-spread following further validation; *i.e.* pit number or surface area quantification, nuclei counting per cell, or tracking cellular migration in combination with imaging modalities (*Kramer et al. 2013*). The development of a processing algorithm for confocal images also led to quantitative resorption pit area and depth measurements where early changes in 3D resorptive characteristics were detected. This was reported as a pivotal finding in understanding the impact of pro-inflammatory stimuli on bone resorption.

Similar methodologies have been reported by *Soysa et al. (2009*) and *Goldberg et al.* (*2012*) who have all shown differences in osteoclast nuclei number, surface area and 'resorption cavity locations' respectively, but not in the presence of inflammatory mediators.

The application of the above methods in Chapters 4 and 5 yielded novel data about IL-6 trans-signalling and CCL3. Stimulated IL-6 trans-signalling lead to significantly increased osteoclast number. Preliminary data suggested a IL-6 trans-signalling to also significantly enhance individual osteoclast resorption in terms of pit depth, which could be inhibited through sgp130-Fc. At the conclusion of Chapter 5, CCL3 was shown as significantly increased in the presence of RANKL and was suggested to exert an early role in osteoclast fusion and differentiation, where its neutralization significantly reduced bone resorption both *in vitro* and *in vivo*. Such data therefore supports therapeutics designed to inhibit IL-6 trans-signalling and CCL3.

6.2 The dual importance of IL-6 trans-signalling in bone destruction and inflammation

IL-6/sIL-6R is one of the main pathogenic instigators of chronic inflammation and plays a major role in inflammatory arthritis (*Romas et al. 1996*). IL-6 is a pleiotropic cytokine affecting leukocytes, hepatocytes, bone cells and personal well-being, resulting in inflammation, increased hepcidin (anaemia), altered bone homeostasis and fatigue respectively (*Madhok et al. 1993, Nemeth et al. 2004, Benedetti et al. 2006,Davis et al. 2008*). IL-6 activates both inflammatory and resorptive pathologies and has thus been termed a 'keystone' cytokine in arthritis, osteoporosis, systemic lupus erythematosus, Castleman's disease, psoriasis and encephalomyelitis (*Grossman et al. 1989, Yoshizaki et al. 1989, Eugster et al. 2001, Ripley et al. 2005, Hunter and Jones 2015*). In Chapter 4 evidence was provided for a role of IL-6 trans-signalling in direct osteoclast formation and resorption, postulated to be resultant of the expression and activation of gp130 on the osteoclasts membrane (*Johnson et al. 2015*). Furthermore, an association between

RANK and IL-6 has also been reported by *Tsangari et al. (2004)* where IL-6 inhibition reduced RANK on precursor cells decreasing osteoclastogenesis, postulating an association with the autocrine up-regulation of RANK.

IL-6 trans-signalling is thus postulated as pivotal in bone destructive diseases such as the arthritides (*i.e.* RA, JIA psoriatic arthritis), periodontitis and MM (*Urashima et al. 1996, Robak et al. 1998, Elkayam et al. 2000, Peake et al. 2006, Hienz., Paliwa& Ivanovski2015*). In chronic inflammation sIL-6R (resultant of proteolytic cleavage and alternative splicing primarily from neutrophils) and IL-6 are elevated in synovial fluid, serum and plasma resulting in leukocyte chemotaxis, infiltration, hyperplasia, cytokine secretion, proteolytic enzyme secretion and osteoclast differentiation (*Srirangan & Choy 2010, Lamas et al. 2013*). In periodontitis the accumulation of leukocytes at periodontal lesions results from enhanced IL-6 which further stimulates the secretion of pro-osteoclastogenic cytokines (*i.e.* RANKL) from nearby cells (*i.e.* osteoblasts via PGE2 synthesis) and decreased anti-osteoclastogenic cytokines (*i.e.* OPG), which together enhance resorption (Chapter 4; *Dayer & Choy 2010, Hosokawa et al. 2014, Feng et al. 2017*). Similarly, in MM IL-6 supports plasma cell proliferation, differentiation, secretion of lytic enzymes and is thought to attenuate apoptosis leading to increased bone lesions (*Lauta 2003*). The development of therapeutics inhibiting IL-6 trans-signalling would therefore be beneficial in multiple clinical diseases which present with inflammation and/or bone destruction.

Unfortunately no such therapeutics are currently available to man, highlighting a novel area of drug development. It is hoped that novel treatments specifically blocking IL-6 trans-signalling will replicate and further improve on current therapeutics such as tocilizumab (anti-IL-6R) which has been shown to decrease disease pathology (*Sigaux et al. 2017*). The inhibition of IL-6 trans-signalling is preferable over treatment with tocilizumab due to its specific targeting of trans-signalling and not classical (*Wong et al. 2006, Axmann et al. 2009, Jones et al 2011*). Preliminary data supporting the progression of sgp130-Fc as a has been shown in animal models (*i.e.* RA, cancer, peritonitis, bowel diseases and atherosclerosis) where sgp130-Fc substantially reduced chronic-inflammation (*Atreya et al. 2000,*

Nowell et al. 2003, Becker et al. 2004, Bollrath et al. 2009, Nowell et al. 2009, Schuett et al. 2012). In addition, sgp130-Fc decreases the IL-6/sIL-6R complex half-life and aids its clearance, thereby further reducing IL-6 trans-signalling (*Peters et al. 1996,Jones et al. 2011*). Treatment with epigallocatechin-3-gallate (EGCG) has also been shown to increase endogneous sgp130 and thus decrease IL-6 trans-signalling (*Ahmed et al. 2008)*. However, further work assessing the reproducibility of such data and the validity of the findings in human diseases is needed.

Alongside the importance of IL-6 trans-signalling in chronic inflammation and bone destruction, IL-6 trans-signalling is significantly elevated in cardiovascular diseases, a common co-morbidity of arthritis, due to decreased inhibition by endogenous sgp130 (*Voskuyl et al. 2006, Naranjo et al. 2008, Kawashiri et al. 2011, Klimek et al. 2014*). Support for the use of sgp130-Fc therapy in atherosclerosis has been reported where inflammatory monocyte infiltration and plaque formation are reduced (*Pardali et al. 2012, Schuett et al. 2012*). The therapeutic targeting of IL-6 trans-signalling would therefore be beneficial in the treatment of primary and secondary diseases of chronic inflammation, thus enhancing drug efficacy and ultimately the quality of patient life.

Despite such promising data, initial experiments assessing the therapeutic potential of inhibiting IL-6 trans-signalling on osteoclastogenesis and resorption are still needed *in vivo* to determine the translation of *in vitro* data from Chapter 4. For example; treatment of CIA with sgp130-Fc where skeletal changes are monitored *in vivo* by quantification of bone turnover (*i.e.* IVIS and radiographs across disease duration), in addition to post mortem whole body imaging (*i.e.* µCT and radiographs) and histology (*i.e.* TRAP staining) assessing cell counts (inflammatory and osteoclasts) and bone erosions (*Schneider et al. 2005*). If the assessments of bone destruction are significantly reduced, evidence would be provided for dual functionality of sgp130-Fc in the inhibition of bone resorption and inflammation, exerting a significant advantage over current pharmaceuticals which globally knock-out IL-6 signalling. The dosing frequency and concentration of sgp130-Fc would require optimisation, and a comparison with alternative therapeutics (receptor and ligand synthetic antagonists/agonists or intracellular signalling inhibitors) would be

essential to ensure maximum drug efficacy and marketability. Furthermore, immunological differences and differing drug metabolism between rodent and man may pose difficulities and thus will require careful consideration. A cost-benefit analysis of inhibiting global IL-6 (*i.e.* tocilizumab or sirukumab) to IL-6 trans-signalling specifically would also be pivotal in marketing such a therapeutic, alongside highlighting an important area of further research.

6.3 The clinical relevance of CCL3

The neutralization of CCL3 was also postulated as a therapeutic for destructive bone diseases (Chapter 5 Section 5.3.5). CCL3 is clinically elevated in arthritis, asthma, lymphocytic leukaemia, multiple myeloma, retinal inflammation/degeneration, neuropathological diseases, osteomyelitis, breast and lung cancer (*Scheven et al. 1999, Wolf et al. 2003, Bièche et al. 2004*, *Pharoah et al. 2006, Geppert et al. 2010, Tregoning et al. 2010, Jehs et al. 2011, Sivina et al. 2011, Bandinelli et al. 2012*, *Chang et al. 2013, Dapunt et al. 2014, Mittal et al. 2014, Tsirakis et al. 2014, Kohno et al. 2014*). Research currently shows CCL3 foremost effects leukocyte migration (primarily monocytes) linking it to chronic inflammation and osteoclastogenesis, whilst also exerting a regulatory role in haematopoietic stem cell proliferation which, when uncontrolled, results in leukemogenesis and lymphoma (*Baba & Mukaida 2014, Takahashi et al. 2015*).

The implications of CCL3 neutralization have already been reported in leukocyte associated diseases including Wallerian degeneration, psoriasis and multiple myeloma, where anti-CCL3 reduced myelin breakdown and clearance by macrophages, regulated FOXP3 T_{regs} and decreased osteoclastogenesis and adhesion of myeloma-stromal cells respectively (*Oba et al. 2005, Perrin et al. 2005, Bolzoni et al. 2013, Chen et al. 2013*). The development of a therapeutic capable of inhibiting CCL3 would also be advantageous in the treatment of CCL3-induced fever where the common cyclooxygenase inhibitor ibuprofen is ineffective (*Minano et al. 1990, Melo Soares et al. 2006*). Furthermore, CCL3 has also been reported as

significant in the pathogenesis of asthma through eosinophil recruitment, thus its inhibition could additionally aid asthmatic patients (*Phillips et al. 2003*).

In addition to an inflammatory role, CCL3 is also emerging as an important mediator in destructive bone diseases, where its elevated presence at osteolytic sites has been reported, alongside its effect on *in vivo* bone resorption through global knock-out models (*Takano et al. 2014*). The global knock out of CCL3 resulted in a significant reduction in arthritic score and an attenuation in osteoclast differentiation and joint erosions in CIA and AIA mice respectivley (*Chintalacharuvu et al. 2005, Kondo et al. 2011).* In conjunction with the exerted role of CCL3 in osteoclastogenesis, a dual pathogenic mechanism of the inhibition of osteoblast function has been reported. CCL3 significantly decreased bone mineralisation and osteocalcin release in MM stromal cell cultures due to increased ERK signalling and down-regulation of osterix (*Vallet et al. 2011*). The data reported by *Vallet et al. (2011)* highlighting CCL3 as a pathogenic instigator of bone destruction supported and furthered the findings of *Hoshino et al. (2010)* where $CCR1^{-/-}$ mice presented with elevated osteoblast transcription factors (Runx2 and Atf4) and bone proteins (osteopontin and osteonectin), but reduced osteoclast size and number.

Furthermore osteoclasts from $CCR1^{-/-}$ mice to exhibited attenuated RANK expression, thus reducing RANKL-RANK interaction (*Hoshino et al. 2010*). From the data reported in Chapter 5 (Section 5.3.2.1) CCL3 was postulated as RANKL-dependent and was shown to exert a similar efficacy on osteoclastogenesis inhibition as the RANKL decoy receptor, OPG (Chapter 5 Section 5.3.4). Such data therefore supported the work of *Hoshino et al. (2010)* and the *in vivo* therapeutic use of anti-CCL3 in animal models. The therapeutic use of anti-CCL3 over OPG would be advantageous, firstly as homeostatic bone turnover would not be altered by anti-CCL3 (*i.e.* basal RANKL-induced osteoclastogenesis unaffected), and secondly due to the redundancy of the chemokine system where non-pathological chemotaxis from co-stimulating chemokines would still prevail. Additional benefits of neutralizing CCL3 may also arise after further testing assessing dosage and frequency of anti-CCL3 treatment where reduced leukocyte migration may present as 'anti-inflammatory' effects in addition to anti-resorptive.

The therapeutic potential of inhibiting CCL3 could therefore exert a major advantage in bone destructive diseases. Of additional interest is a novel chemokine receptor termed GPR15/BOB which was located on PBMCs from RA patients (*Cartwright et al. 2014*). Although the ligands of this receptor are not yet identified it has a known similarity to CCR5, an additional CCL3 receptor. GPR15/BOB could therefore be used in the pathogenesis of RA through CCL3 signalling, and could present itself as a novel therapeutic target. However, extensive research must be carried out prior to this being confirmed.

A positive correlation between CCL3 and mental health diseases (Alzheimer's disease, schizophrenia and depressive disorders) has also been reported (*Merendino et al. 2004, Simon et al. 2008, Geppert et al. 2010, Marksteiner et al. 2011, Reale et al. 2011*). *Ascoli and colleagues (2016)* reported increased CCL3 mRNA in bipolar patients that causes shift in macrophages expression, favouring M1 macrophages (CCL3 and IL-6 secreting), and subsequently affecting neuronal development (disputed by *Nakatani et al. 2006, Teixeira et al. 2008, Brietzke et al. 2009*). The presentation of mental health disorders (*i.e.* anxiety) has also been linked to RA (*Watad et al. 2017*). It has been postulated that both social (*i.e.* the patients mental attitude to coping with RA) and biological (*i.e.* increased CCL3) factors impact patient quality of life. Thus an additional subset of diseases which could benefit from the development of a novel anti-CCL3 therapeutic is presented.

6.4 IL-6 trans-signalling and CCL3 as novel therapeutic targets

The relevance of both IL-6 trans-signalling and CCL3 in destructive and inflammatory bone disease has therefore been discussed, alongside some common and novel therapeutics currently used. Although current therapies (both conventional and biological DMARDs) alleviate arthritic symptoms for the majority of patients, there still remain patients who are unresponsive and thus the need for novel therapeutics development exists (*Kim et al. 2015*). In addition, evidence is emerging questioning the long term therapeutic use of biological DMARDs such as

tocilizumab due to their associated adverse effects of significantly elevating serum total cholesterol, high-density lipoprotein cholesterol, low-density lipoprotein cholesterol and apolipoproteins 1-and 2 in RA (*Kawashiri et al. 2011)*.

The clinical relevance of developing an inhibitor to both IL-6 trans-signalling and CCL3 is clear from the above discussions. However, the effectiveness of these treatments alone on *in vivo* osteoclastogenesis and bone destruction has yet to be established. On reflection of *in vitro* data in Chapters 4 and 5, inhibition of IL-6 trans-signalling by sgp130-Fc was postulated to significantly reduce resorptive activity, and anti-CCL3 to significantly attenuate osteoclast differentiation, with a consideration that increased dose may reduce inflammation. However, due to the redundancy of the chemokine system a significant reduction on inflammation may never result. Thus it could be hypothesised that anti-CCL3 could be given therapeutically to attenuate osteoclast fusion and differentiation, in tandem with an IL-6 trans-signalling inhibitor to decrease mature osteoclast resorptive activity, thus reducing bone destruction via two mechanisms. As both mediators also exert comparable stimuli for cell motility, monocyte migration would consequentially decrease (*Clahsen & Schaper 2008*). Moreover, secondary effects of inhibiting IL-6 trans-signalling would be beneficial in decreasing associated inflammation (*Scheller et al. 2011*). The efficacy and tolerance between two drugs and their interaction pathways would however need to be assessed in order to distinguish any synergistic relationship. Safety testing assessing the production of ADAs would also be pivotal in determining the fate of such therapeutics to avoid immunogenicity complications (such tests would also need to be completed for each independently if they were to be developed).

Alongside the inhibition of inflammation and pathology, a reduction in pain perception may also occur, as increased concentrations of both have been linked to hyperalgesia in knee replacement patients (*Tomankova et al. 2014*). IL-6 trans-signalling sensitizes nociceptors and TRPV1 channels on DRG leading to increased neuronal cell communication (*Murphy et al. 1999, Obreja et al. 2002, De Jongh et al. 2003, Miguel, Kraychete & Nascimento. 2014*). CCR1 (receptor to CCL3) is co-expressed with TRPV1 on DRG where CCL3 stimulation causes a 3-fold increase in

sensitivity and maintains neuronal viability potentiating hyperalgesia and nociception (*Brenneman et al. 1999, Zhang et al. 2005*). The further characterization of the combined and independent effects of CCL3 and IL-6/sIl-6R complex on nociception would need to be established first *in vitro*; *i.e.* through the treatment of cerebral cortical cells and cortical astrocytes (feeder cells) with IL-6/sIL-6R, sgp130-Fc, CCL3 and/or anti-CCL3. The quantification of neuronal survival and activation would then ensue. If successful, such treatments may also be test in behavioural animal models prior to their additional use as potential analgesics.

6.5 Novel biomarkers of destructive bone diseases

Current biomarkers fail to detect the early progression of arthritic diseases thus highlighting the need for novel markers. Recent research has postulated the use of calprotectin as a biomarker of RA, where a significant correlation to disease activity (CRP and auto-antibodies) and ultrasound score were reported (*Soliman et al. 2016*). Although valuable in the prognosis of RA, the use of calprotectin as a biomarker still focuses upon the inflammatory side of the arthritides (inflammatory marker correlations and soft tissue ultrasound), and not on the dual importance of bone destruction. The need for a novel biomarker of destructive bone diseases is therefore still fundamental for the early classification of disease.

Research supporting the use of CCL3 as a biomarker was previously reported by *Takahashi et al. (2015)*, in a model of diffuse large B cell lymphoma, where the secretion of CCL3 from malignant B cells was indicative of B cell receptor activation and lymphoma diagnosis. Although not in a model of destructive bone disease, the use of CCL3 as a biomarker was shown to predict disease progression. From data reported in Chapters 4 and 5 showing IL-6 trans-signalling and CCL3 as important early mediators in osteoclast differentiation (*i.e.* increased precursor cell migration, proliferation and $TRAP^{+ve}$ cell fusion), it is postulated that IL-6/sIL-6R complex and CCL3 could be used as novel biomarkers of destructive bone diseases.

Assessment of endogenous IL-6/sIL-6R and CCL3 concentrations could be performed alongside common tests for the diagnosis of arthritis (*i.e.* complete

blood count, urine, blood biochemistry, rheumatoid factor), where serum or joint aspirates could be collected from patients and analyzed by automated ELISA (*i.e.* Randox Evidence Biochip Array). A comparison of results against a 'normal range' could determine the likeliness of destructive or inflammatory disease phenotype (*Richie & Francis 2003*). For example; a patient presenting with increased IL-6/sIL-6R and CCL3 is likely to suffer from an aggressive destructive bone phenotype (correlation with osteoclastogenesis and resorption), opposed to a patient with increased TNF-α and rheumatoid factor, who is likely to have an inflammatory disease phenotype with minimal bone destruction. A schematic of this is presented in Figure 6.1. Further work defining pathogenic ranges would be needed, but the following have already been published and could be used for guidance: >20.3 ng/mL CCL3 in synovial fluid indicative of destructive bone phenotypes, >55.2pg/mL CCL3 in plasma, >5pg/mL IL-6 or >41ng/mL sIL-6R in serum (*Robak et al. 1998, Pharoah et al. 2006,Takahashi et al. 2015*, *Palma et al. 2016*).

Through the identification of novel biomarkers, the prediction of early disease phenotype could have a significant impact on the following: specific therapeutics patients receive, early commencement of treatments, prevention of severe pathology (both inflammatory and destructive), maintaining joint functionality, decreasing hyperalgesia, reducing side effects of 'blanket drugs' (*i.e.* nausea after methotrexate), reducing cost to NHS (*i.e.* multiple drug treatments), and finally, increasing the patient's quality of life.

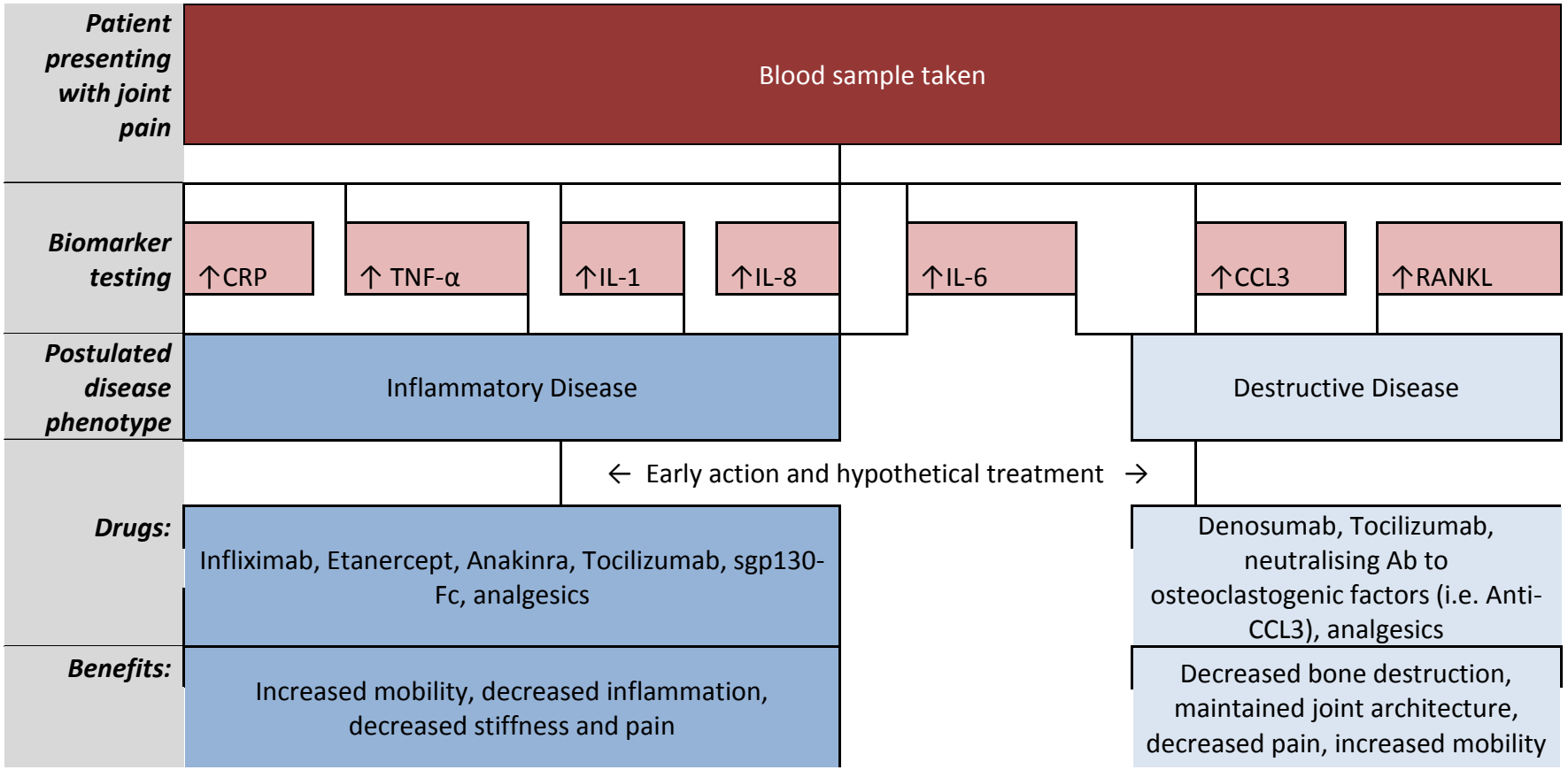

Figure 6. 1 - A flow diagram illustrating the theory behind the early diagnosis of inflammatory and destructive bone diseases, in addition to the postulated specific therapeutics which could be developed to prevent disease progression.

6.6 Conclusion

In conclusion, results reported in this thesis present novel data from imaging and analysis methodologies for the identification of specific pro-inflammatory mediators involved in enhanced osteoclast activity. Specifically, both IL-6 trans-signalling and CCL3 are reported as important early mediators of osteoclast differentiation with clear effects on bone resorption. Further experimental work using both *in vivo* animal models and arthritic patient samples will be necessary to fully elucidate the mechanisms and importance of IL-6 trans-signalling and CCL3 in destructive bone diseases. IL-6 trans-signalling and CCL3 could become novel therapeutic targets and/or biomarkers of disease activity.

Chapter 7: References

Abdul-sater Z. et al. (2012) Two Heterozygous Mutations in NFATC1 in a Patient with Tricuspid Atresia. PLOS One 7: 1–12.

Abe Y. et al. (2015) Inhibitory effect of bisphosphonate on osteoclast function contributes to improved skeletal pain in ovariectomized mice. J Bone Miner Metab 33: 125–134.

Ahmed S. et al. (2008) Epigallocatechin-3-gallate inhibits IL-6 synthesis and suppresses transsignaling by enhancing soluble gp130 production. PNAS 105: 14692-14697.

Ajuebor M.N., Kunkel S.L. & Hogaboam C.M. (2004) The role of CCL3 / macrophage inflammatory protein-1 a in experimental colitis. *European Journal of Pharmacology*, 497: 343–349.

Albuquerque De S.R. et al.(2013) The effect of CCL3 and CCR1 in bone remodeling induced by mechanical loading during orthodontic tooth movement in mice. Bone 52: 259–267.

Amat M. et al. (2006) Pharmacological blockade of CCR1 ameliorates murine arthritis and alters cytokine networks in vivo. British Journal of Pharmacology 149: 666–675.

Anandarajah A.P. et al. (2008) The effect of etanercept on osteoclast precursor frequency and enhancing bone marrow oedema in patients with psoriatic arthritis. Ann Rheum Dis 67: 296–301.

Anderson L.C. & Rao R.D. (2001) Intereukin-6 and nerve growth factor levels in peripheral nerve and crainstem after trigeminal nerve injury in the rat. Archives of Oral Biology 46: 633-640.

Andratsch M. et al. (2009) A Key Role for gp130 Expressed on Peripheral Sensory Nerves in Pathological Pain. The Journal of Neuroscience 29: 13473–13483.

Andrews N.A. (2008) Denosumab and the Treatment of Rheumatoid Arthritis : In an Occupied Field , Where Will a RANKL Inhibitor Fit In? International Bone & Mineral Society 5: 351–356.

Antonov A.S. et al. (2011) αVβ3 Integrin Regulates Macrophage Inflammatory Responses via PI3 Kinase/Akt-Dependent NF-κB Activation. J Cell Physiol. 226: 469–476.

Atreya R. et al. (2000) Blockade of interleukin 6 trans signalling suppresses T-cell resistance against apoptosis in chronic intestinal inflammation: Evidence in Chron disease and experimental colitis in vivo. Nature Medicine 6: 583 - 588.

Axmann R. et al. (2009) Inhibition of Interleukin-6 Receptor Directly Blocks Osteoclast Formation In Vitro and In Vivo. Arthritis & Rheumatism 60: 2747–2756.

Azuma Y. et al. (2000) Tumour Necrosis Factor-α Induces Differentiation of Bone

Resorption by Osteoclasts. J. Biol. Chem. 275: 4858-4864.

Baba T. & Mukaida N.(2014) Role of macrophage inflammatory protein (MIP) -1 α / CCL3 in leukemogenesis. Molecular and Cellular Oncology1: e29899-1 - e29899-5.

Bandinelli F. et al. (2012) CCL2 , CCL3 and CCL5 chemokines in systemic sclerosis : the correlation with SSc clinical features and the effect of prostaglandin E1 treatment. Clinical and Experimental Rheumatology 30: s44-49.

Bargman R. et al. (2012) High- and low-dose OPG–Fc cause osteopetrosis-like changes in infant mice. Pediatric Research 72: 495–501.

Becker C. et al. (2004) TGF-β suprresses tumour progression in colon cancer by inhibition of IL-6 trans-signalling. Immunity, 21: 491-501.

Bendele A. et al. (1999) Animal Models of Arthritis : Relevance to Human Disease *. Toxicologic Pathology 27: 134–142.

Benedetti F.D. et al. (2006) Impaired skeletal development in interleukin-6 transgenic mice. Arthritis & Rhuematism 54: 3551-3563.

Berg van den Wim B (2009) Lessons from animal models of arthritis over the past decade. Arthritis Research & Therapy 11: 250.

BertoliniD.R. et al. (1986) Stimulation of bone resorption and inhibition of bone formation in vitro by human tumour necrosis factors. Nature 319: 516-518.

Besson J.M. (1999) The neurobiology of pain. The Lancet 353: 1610-1615.

Bharadwaj U. et al. (2011) Mesothelin overexpression promotes autocrine IL-6 / sIL-6R trans-signaling to stimulate pancreatic cancer cell proliferation. Carcinogenesis 32: 1013–1024.

Bièche I. et al. (2004) Molecular profiling of inflammatory breast cancer: Identification of a poor-prognosis gene expression signature. Clinical Cancer Research 10: 6789-6795.

Blair H.C., Robinson L.J. & Zaidi M. (2005) Osteoclast signalling pathways. Biochemical and Biophysical Research Communications 328: 728–738.

Bollrath J. et al. (2009) gp130-mediated STAT3 activation in enterocytes regulates cell survival and cell-cycle progression during colitis-associated tumorigenesis. Cancer Cell 15: 91-102.

Bolzoni M. et al. (2013) Immunomodulatory drugs lenalidomide and pomalidomide inhibit multiple myeloma-induced osteoclast formation and the RANKL / OPG ratio in the myeloma microenvironment targeting the expression of adhesion molecules. Experimental Hematology 41: 387–397.

Bonetta L. et al. (2005) Flow cytometry smaller and better. Nature Methods 2: 785-795.

Bord S. et al. (2003) The effects of estrogen on osteoprotegerin , RANKL , and estrogen receptor expression in human osteoblasts. Bone32: 136–141.

Boyce B.F., Schwarz E.M.& Xing, L. (2006). Osteoclast precursors: cytokine-stimulated immunomodulators of inflammatory bone diesase. Curr Opin Rheumatol 18:427-432.

Boyle W.J., Simonet W.S. & Lacey D.L. (2003) Osteoclast differentiation and activation. Nature 423: 337-342.

Bozec A. et al. (2008) Osteoclast size is controlled by Fra-2 through LIF/LIF-receptor signalling and hypoxia.Nature Letters 454: 221–226.

Brackertz D., Mitchell G.F. & Mackay I.R. (1977) Antigen-induced arthritis in mice.Arthritis & Rheumatism 20: 841-850.

Brand D.D., Latham K.A. & Rosloniec E.F. (2007). Collagen-induced arthritis. Nature Protocols 2: 1269–1275.

Braun J. et al. (1999) Low secretion of tumor necrosis factor-α, but no other th1 or th2 cytokines, by peripheral blood mononuclear cells correlates with chronicity in reactive arthritis. Arthritis & Rhuematism 42: 2039-2044.

Brenneman D.E. et al. (1999) VIP and D -ala-peptide T-amide release chemokines which prevent HIV-1 GP120-induced neuronal death. Brain Research 838:27–36.

Brietzke E. et al. (2009) Brain , Behavior , and Immunity Abnormalities in serum chemokine levels in euthymic patients with Bipolar Disorder. Brain, Behavior and Immunity23:1079–1082.

Briscoe, J. et al., 1996. JAKs, STATs and signal transduction in response to the interferons and other cytokines. *Phil. Trans. R. Soc. Lond.*, 351, pp.167–171.

Bune, A.J., Hayman, A.R. & Evans, M.J., 2001. Mice lacking tartrate-resistant acid phosphatase (Acp 5) have disordered macrophage in ¯ ammatory responses and reduced clearance of the pathogen , Staphylococcus aureus. *Immunology*, (Acp 5).

Caetano-lopes J., Canhão H. & Fonseca J.E. (2007) Osteoblasts and bone formation. Acta Reumatólogica Portuguesa 32:103-110.

Campos S.B. et al.(2009) Cytokine-induced F-actin reorganization in endothelial cells involves RhoA activation. Am J Physiol Renal Physiol296: F487–F495.

Cartwright A. et al. (2014) Cytokine Orphan receptor GPR15 / BOB is up-regulated in rheumatoid arthritis. Cytokine 67: 53–59.

Cassidy A.I. et al. (2003) Regulation of the murine TRACP gene promoter. Journal of Bone and Mineral Research 18: 1901- 1904.

Castellino F. et al. (2006) Chemokines enhance immunity by guiding naive $CD8^+$ T

cells to $CD4^+$ T cell-dendritic cell interaction. Nature 440: 890-895.

Chailurkit L. et al. (2001) Biochemical Markers of Bone Turnover and Response of Bone Mineral Density to Intervention in Early Postmenopausal Women : An Experience in a Clinical Laboratory. Clinical Chemistry 47:1083–1088.

Chang D.H. et al. (2013) The Effect of Lung Cancer on Cytokine Expression in Peripheral Blood Mononuclear Cells. PLOS One 8: e64456.

Chellaiah M.A. & Ma T. (2013). Membrane Localization of Membrane Type 1 Matrix Metalloproteinase by CD44 Regulates the Activation of Pro-Matrix Metalloproteinase 9 in Osteoclasts. BioMed Research International 2013: 1-13.

Chen Q. et al. (2001) Testosterne inhibits osteoclast formation stimulated by parathyroid hormone through androgen receptor. FEBS Letters 491: 91-93.

Cheng J. et al.(2011) Interleukin-4 Inhibits RANKL-Induced NFATc1 Expression Via STAT6: A Novel Mechanism Mediating its Blockade of Osteoclastogenesis. J Cell Biochem 112: 3385-3392.

Chenu C. et al. (1988) Transforming growth factor 13 inhibits formation of osteoclast-like cells in long-term human marrow cultures. Proc. Natl. Acad. Sci. 85: 5683–5687.

Cheung W., Simmons C.A. & You L. (2012) Osteocyte apoptosis regulates osteoclast precursor adhesion via osteocytic IL-6 secretion and endothelial ICAM-1 expression. Bone 50: 104–110.

Chintalacharuvu S.R. et al. (2005) An essential role for CCL3 in the development of collagen antibody-induced arthritis. Immunology Letters 100: 202–204.

Choi S.J. et al. (2000) Macrophage inflammatory protein 1-alpha is a potential osteoclast stimulatory factor in multiple myeloma. Blood. 96: 671-675.

Choi S.J. et al.(2001) Antisense inhibition of macrophage inflammatory protein 1- α blocks bone destruction in a model of myeloma bone disease.J. Clin. Invest.108: 833–1841.

Choy E.H.S. et al. (2002) Therapeutic Benefit of Blocking Interleukin-6 Activity With an Anti – Interleukin-6 Receptor Monoclonal Antibody in Rheumatoid Arthritis. Arthritis & Rheumatism 46: 3143–3150.

Chubb S.A.P. (2012) Measurement of C-terminal telopeptide of type I collagen (CTX) in serum. Clinical Biochemistry 45: 928–935.

Ciancanelli M.J. et al. (2015) Life-threatening influenza and impaired interferon amplifcation in humna IRF7 deficiency. Science 348: 448-453.

Clahsen T. & Schaper F. (2008) Interleukin-6 acts in the fashion of a classicla chemokine on monocyte cells by inducing integrin activation, cell adhesion, actin polymerization, chemotaxis, and transmigration. J Leukoc. Biol. 84: 1-9.

Cook M.J. (1965) The anatomy of the laboratory mouse. Academic Press, M.R.C. Laboratory Animals Centre, Elsevier.

Copp D.H. et al. (1962) Evidence for Calcitonin- A new hormone from the parathyroid that lowers blood calcium. The Endocrine Society 70: 638- 649.

Coppieters K. et al. (2006) Formatted Anti – Tumor Necrosis Factor-α VHH Proteins Derived From Camelids Show Superior Potency and Targeting to Inflamed Joints in a Murine Model of Collagen-Induced Arthritis. Arthritis & Rheumatism 54: 1856–1866.

Coxon F.P. (2012) Chapter 25 - Fluorescence Imaging of Osteoclasts Using Confocal Microscopy. Bone Research Protocols, Methods in Molecular Biology 816.

Cromartie W.J. et al. (1977) Arthritis in rats after systemic injection of streptococcal cells or cell walls. The Journal of Experimental Medicine 146: 1585–1602.

Crook, T. & Warwick, D., 2011. Avoiding fusion in wrist arthritis. *The Journal of Bone and Joint Surgery*, pp.4–8.

Cummings S.R. et al. (2009) Denosumab for prevention of fractures in postmenopausal women with osteoporosis. N Engl Med 361:756-65.

Cunha, F. et al., 2007. The pattern of immune cell infiltration in chromoblastomycosis : involvement of macrophage inflammatory protein-1 alpha / CCL3 and fungi persistence . *Rev. Inst. Med. trop.*, (October 2015).

Danks L. et al. (2002) Synovial macrophage-osteoclast differentiation in inflammatory arthritis. Ann Rheum Dis 61: 916–921.

Dapunt U. et al. (2014) The Macrophage Inflammatory Proteins MIP1α (CCL3) and MIP2α (CXCL2) in Implant-Associated Osteomyelitis : Linking Inflammation to Bone Degradation.Mediators of Inflammation 2014; 1-10.

Davis M.C. et al. (2008) chronic stress and regulation of cellular markers of inflammation in rheumatoid arthritis: Implications for fatigue. Brain Behav Immun. 22:24-32.

Davies J. et al. (1989) the osteoclast functional antigen, implicated in the regulation of bone resorption, is biochemically related to the vitronectin receptor. The Journal of Cell Biology 109: 1817-1826.

Dawson J.K. et al. (2001) Fibrosing alveolitis in patients with rheumatoid arthritis as assessed by high resolution computed tomography, chest radiography and pulmonary function tests. Thorax 56: 622-627.

De Jongh R.F. et al. (2003) The role of Interleukin-6 in nociception and pain. Anesthesia & Analgesia 96:1096-1103.

Dinser R. (2008) Animal models for arthritis. Best Practice & Research Clinical Rheumatology 22: 253–267.

Døhn U.M. et al. (2006) Are bone erosions detected by magnetic resonance imaging and ultrasonography true erosions? A comparison with computed tomography in rheumatoid arthritis metacarpophalangeal joints. Arthritis Research & Therapy 8: 1-9.

Doodes P.D. et al. (2009) CCR5 Is Involved in Resolution of Inflammation in Proteoglycan-Induced Arthritis. Arthritis & Rheumatism 60: 2945–2953.

Doyle F.H., Banks L.M. & Pennock J.M. (1980) Radiological observations on bone resorption in Paget's disease. Arthritis and Rheumatism 23: 1205-1214.

Ducy P. et al.(1997) Osf2 / Cbfa1 : A Transcriptional Activator of Osteoblast Differentiation. Cell 89: 747–754.

Dumonde D.C. & Glynn L.E. (1961) The production of arthritis in rabbits by an immunological reaction to fibrin. British Journal of Experimental Pathology 43: 373-383

Duong L.T. & Rodan G.A. (1999) The role of integrins in osteoclast function. Journal of Bone Mineral Metabolism. 17: 1-6.

Duong L.T. et al. (2000) Integrins and signaling in osteoclast function. Matrix Biology 19: 97-105.

Durand M. et al. (2013) Monocytes from patients with osteoarthritis display increased osteoclastogenesis and bone resorption. Arthritis & Rheumatism 65: 148-158.

Eder J. (1997) Tumour necrosis factor-α and interleukin 1 signalling : do MAPKK kinases connect it all? Trends in Pharmacological Sciences 18: 319–322.

Elder C.J. & Bishop N.J. (2014) Rickets. Lancet383: 1665–1676.

Elkayam O. et al. (2000) Serum levels of IL-10, IL-6, IL-1ra, and sIL-2R in patients iwth psoriatic arthritis. Rheumatol Int 19: 101-105.

Enzerink A. et al. (2009) Clustering of fibroblasts induces proinflammatory chemokine secretion promoting leukocyte migration. Molecular Immunology 46: 1787–1795.

Fan J. et al. (2011) Chemokine Transcripts as Targets of the RNA-Binding Protein HuR in Human Airway Epithelium. The Journal of Immunology, 186: 2482-2494.

Feng W. et al. (2017) combination of IL-6 and sIL-6R differentially regaulte varying levels of RANKL-induced osteoclastogenesis through NF-κβ ERK and JNK signalling pathways. Nature Scientific Reports 7: 41411.

Filgueira L. (2004) Fluorescence-based staining for tartrate-resistant acidic phosphotase (TRAP) in osteoclasts combined with other fluorescent dyes and protocols. Jounral of Histochemistry & Cytochemistry 52: 411-414.

Finnegan A. et al. (1999) Proteoglycan (Aggrecan)-Induced Arthritis in BALB/c Mice

Is a Th1-Type Disease Regulated by Th2 Cytokines. The Journal of Immunology 163: 5383-5390.

Firestein G.S. et al. (1994) Synovial interleukin-1 receptor antagonist and interleukin- 1 balance in rheumatoid arthritis. Arhtritis & Rheumatism 37: 644-652.

Fleischmann R.M. et al. (2006) Safety of extended treatment with anakinra in patients with rheumatoid arthritis. Ann Rheum Dis 65: 1006–1012.

Franco G.C.N. et al. (2012) Inhibition of matrix metalloproteinase-9 activity by Doxycycline ameliorates RANK ligand-induced osteoclast differentiation in vitro and in vivo. Exp Cell Res 317: 1454–1464.

Gabay C. (2006) Interleukin-6 nd chronic inflammation. Arthritis Research & Therapy 8: S3.

Gado K. et al.(2000) Role of interleukin-6 in the pathogenesis of multiple myeloma. Cell Biology International 24: 195–209.

Galibert L. et al. (1998) The Involvement of Multiple Tumor Necrosis Factor Receptor (TNFR) -associated Factors in the Signaling Mechanisms of Receptor Activator of NF-κB, a Member of the TNFR Superfamily*. The Journal of Biological Chemistry 273: 34120–34127.

Galicia J.C. et al. (2004) Polymorphisms in the IL-6 receptor (IL-6R) gene: strong evidence that serum levels of soluble IL-6R area genetically influenced. Genes and Immunity 5: 513-516.

Gao Y. et al. (1998) Expression of IL-6 receptor and sgp130 in mouse bone marrow cells during osteoclast differentiation. Bone 22: 487-493.

Garbers C. et al. (2001) Species specificity of ADAM10 and ADAM17 proteins in interleukin-6 (IL-6) trans-signaling and novel role of ADAM10 in inducible IL-6 receptor shedding. the Journal of Biological Chemistry 286: 14804-14811.

Gay C.V. & Mueller W.J. (1973) Carbonic anhydrase and osteoclasts: Localization by labeled inhibitor autoradiography. Science 183: 432-434.

Geppert A.M. et al. (2010) CCL3 correlates with the number of mood disturbances and personality changes in patients with Alzheimer's disease. Psychiatry Research 176: 261-264.

Gengenbacher M. et al. (2007) Infliximab inhibits bone resorption by circulating osteoclast precursor cells in patients with rheumatoid arthritis and ankylosing spondylitis. Ann Rheum Dis 67: 620-624.

Genovese M.C. et al. (2008). Interleukin-6 Receptor Inhibition With Tocilizumab Reduces Disease Activity in Rheumatoid Arthritis With Inadequate Response to Disease-Modifying Antirheumatic Drugs. Arthritis & Rheumatism 58: 2968–2980.

Gilliland C.T. et al. (2013) The chemokine receptor CCR1 is constitutively active , which leads to G protein-independent, β-arrestin-mediated internalization*. The Journal of Biological Chemistry 288: 32194-32210.

Goldberg S.R. et al. (2012) A 3D scanning confocal imaging method measures pit volume and captures the role of Rac in osteoclast function. Bone 51: 145–152.

Goldring S.R. & Gravallese E.M.(2000). Pathogenesis of bone erosions in rheumatoid arthritis. Current Opinion in Rheumatology 12:195-199.

Gravestein L.A. &Borst J.(1998). Tumor necrosis factor receptor family members in the immune system. Immunology 10: 423-434.

Grevers L.C. et al. (2011) S100A8 Enhances Osteoclastic Bone Resorption In Vitro Through Activation of Toll-like Receptor 4. Arthritis & Rheumatism 63: 1365–1375.

Grigoriadis A.E. et al. (1994) c-Fos: a key regulaotr of osteoclast-macrophage lineage determination and bone remodelling. Science 266: 443-448.

Grivennikov S. et al.(2009). IL-6 and STAT3 are required for survival of intestinal epithelial cells and development of colitis associated cancer. Cancer Cell 15: 103–113.

Grossman R.M. et al. (1989) Interleukin 6 is expressed in high levels in psoriatic skin and stimulates proliferation of cultured human keratinocytes. Proc. Natl. Acad. Sci. 86: 6367-6371.

Halleen J.M. et al. (1999) Intracellular fragmentation of bone resorption products by reactive oxygen species generated by osteolcastic tartrate-resistant acid phosphatase. The Jounral of Biological Chemistry 274: 22907-22910.

Halleen J.M. et al. (2000) Tartrate-Resistant Acid Phosphatase 5b : A Novel Serum Marker of Bone Resorption*. Journal of Bone and Mineral Research 15: 1337–1345.

Han X. et al. (2000) CD47, a Ligand for the Macrophage Fusion Receptor, Participates in Macrophage Multinucleation *. The Journal of Biological Chemistry 275: 37984–37992.

Han J-H. et al. (2001) Macrophage inflammatory protein-1α is an osteoclastogenic factor in myeloma that is dependent of receptor activator of nuclear factor κβ ligand. Blood 97: 3349-3353.

Hargreaves K.M. et al. (1988) Bradykinin is increased during acute and chronic inflammation: therapeutic implications. Clin Pharmacol Ther 44:613-621.

Harvey B.P. & Kaymakcalan Z. (2010) RANKL expression in human T-lymphocytes requires cooperative signaling through the T-cell receptor and adhesion molecule CD2. Journal of Translational Medicine 8: O4.

Hashizume M., Hayakawa N. & Mihara M.(2008) IL-6 trans-signalling directly

induces RANKL on fibroblast-like synovial cells and is involved in RANKL induction by TNF-α and IL-17. Rheumatology 47: 1635–1640.

Hashizume M. & Mihara M. (2009). Desirable effect of combination therapy with high molecular weight hyaluronate and NSAIDs on MMP production. Osteoarthritis and Cartilage17: 1513–1518.

Hashizume M. & Mihara M. (2011) The Roles of Interleukin-6 in the Pathogenesis of Rheumatoid Arthritis. Arthritis 2011: 1-8.

Heinemann C. et al. (2011) Development of an osteoblast / osteoclast co-culture derived by human bone marrow stromal cells and human monocytes for biomaterials testing. European Cells and Materials 21: 80-93.

Heinrich P.C. et al. (1998) Interleukin-6-type cytokine signalling through the gp130 / Jak / STAT pathway. Biochem. J. 334: 297–314.

Hee Jeon et al. (2012) Quantification of temporal changes in 3D osteoclastic resorption pit using confocal laser scanning microscopy. Tissue Engineering and Regenerative Medicine 9: 29-35.

Helfrich M.H. & Ralston S.H. (2012) Bone Research Protocols. Springer Protocols (Methods in Molecular Biology) 816: 1-643.

Heymann D. et al. (1998) Oncostatin m stimulates macrophage-polykaryon formation in long-term human bone-marrow cultures. Cytokine 10: 98–109.

Hienz S.A., Paliwal S. & Ivanovski S. (2015) Mechanisms of bone reosrption in periodontitis. Journal of Immunology Research 2015: 615486.

Hill P.A. et al. (1998) The Cellular Actions of Interleukin-11 on Bone Resorption in Vitro. Endocrinology 139: 1564–1572.

Hirano T., Ishihara K. & Hibi M.(2000) Roles of STAT3 in mediating the cell growth , di erentiation and survival signals relayed through the IL-6 family of cytokine receptors. Oncogene 19: 2548–2556.

Hirayama T. et al. (2002) Osteoclast formation and activity in the pathogenesis of osteoporosis in rheumatoid arthritis. Rheumatology 41: 1232–1239.

Hitchon C.A. & El-gabalawy H.S.(2011) The Synovium in Rheumatoid Arthritis. The Open Rheumatology Journal 5: 107–114.

Hodge J.M. et al. (2011) M-CSF potently augments RANKL-induced resorption activation in mature human osteoclasts. PLOS one 6: e21462.

Holmdahl R. et al. (1992) Arthritis induced in rats with adjuvant oil is a genetically restricted, dependent autoimmune disease. Immunology 76: 197–202.

Hopkins S.J.& Meager A. (1988) Cytokines in synovial fluid : The presence of tumour necrosis factor and interferon. Clin. exp. Immunol. 73: 88–92.

HortonM. A. (1997) The αvβ3 Integrin "Vitronectin Receptor." Int. J. Biochem. Cell Biol.29: 721-725.

Horwood N.J. et al. (2001) IL-12 Alone and in Synergy with IL-18 Inhibits Osteoclast Formation In Vitro. The Journal of Immunology 166: 4915-4921.

Hoshino A. et al. (2010) Deficiency of Chemokine Receptor CCR1 Causes Osteopenia Due to Impaired Functions of Osteoclasts and Osteoblasts*.The Journal of Biological Chemistry 285; 28826–28837.

Hosokawa Y. et al. (2014) IL-6 trans-signalling enahnces CCL20 production from IL-1β-stimulated human periodontal ligament cells. Inflammation 37: 381-386.

Houssiau F.A. et al. (1988) Interleukin-6 in synovial fluid and serum of patients with rheuamtoid arthritis and other inflammatory arthritides. Arthritis and Rheumatism 31: 784-788.

Hu X. & Beeton C. (2010) Detection of Functional Matrix Metalloproteinases by Zymography. Journal of Visualized Experiments 45: e2445.

Hu Y. et al. (2008) IFN- γ and STAT1 Arrest Monocyte Migration and Modulate RAC/CDC42 Pathways. The Journal of Immunology 180: 8057-8065.

Huang H. et al. (2006) Induction of c-fos and NFATc1 during RANKL-stimulated osteoclast differentiation is mediatred by the p38 signaling pathway. Biochemical and Biophysical Research Communications 351: 99-105.

Hunter C.A. & Jones S.A. (2015) IL-6 as a keystone cytokine in health and disease.Nature Immunology 16: 448-457.

Hussein H. et al. (2016) Cathepsin K inhibition renders equine bone marrow nucleated cells hypo-responsive to LPS and unmethylated CpG stimulation *in vitro*. Comparative Immunology, Microbiology and Infectious Diseases 45: 40-47.

Ichikawa S. et al. (2016) Radiographic quantifications of joint space narrowing progression by computer-based approach using temporal subtraction in rheumatoid wrist. British Journal of Radiology 89: 20150403.

Ikeda F. et al. (2004) Critical roles of c-Jun signaling in regulation of NFAT family and RANKL-regulated osteoclast differentiation. J. Clin. Invest.114: 475–484.

Irie A. et al. (2007) Heparin enhances osteoclastic bone resorption by inhibiting osteoprotegerin activity. Bone 41: 165–174.

Ishii T. et al. (2010) Control of Osteoclast Precursor Migration : A Novel Point of Control for Osteoclastogenesis and Bone Homeostasis. IBMS BoneKey 7: 279–286.

Ishida N. et al. (2006) CCR1 acts downsteram of NFAT2 in osteoclastogenesis and enhances cell migration. Journal of Bone and Mineral Research 21: 48-57.

Ishimi Y. et al. (1990) IL-6 is produced by osteoblasts and induces bone resorption. The Journal of Immunology 145: 3297-3303.

Islam R. et al. (2014) Pin1 Regulates Osteoclast Fusion Through Suppression of the Master Regulator of Cell Fusion DC-STAMP. Journal of Celluar Physiology 229: 2166–2174.

Iwamoto T. et al. (2008) Molecular aspects of rheumatoid arthritis: chemokines in the joints of patients. FEBS Journal 275: 448-4455.

Issekutz A.C. et al. (1994) The role of tumour necrosis factor-alpha and IL-1 in polymorphonuclear leucocyte and T lymphocyte recruitment to joint inflammation in adjuvant arthritis. Clin Exp Immunol 97: 26–32.

James I.E. et al. (1999) Development and Characterization of a Human In Vitro Resorption Assay : Demonstration of Utility Using Novel Antiresorptive Agents. Journal of Bone and Mineral Research 14: 1562–1569.

Jehs T. et al. (2011). Astrocytoma cells upregulate expression of pro-inflammatory cytokines after co-culture with activated peripheral blood mononuclear cells. Acta Pathologica, Microbiologica et Immunologica Scandinavica 119: 551–561.

Jeon O.H. et al. (2012) Quantification of temporal changes in 3D osteoclastic resorption pit using confocal laser scanning microscopy. Tissue Engineering and Regenerative Medicine 9: 29-35.

Jilka R.L. (2003) Biology of the Basic Multicellular Unit and the pathophysiology of Osteoporosis. Med Pediatr Oncol 41: 182-185.

Jimi E. et al. (1999) Interleukin 1 Induces Multinucleation and Bone-Resorbing Activity of Osteoclasts in the Absence of Osteoblasts / Stromal Cells. Experimental Cell Research 247: 84–93.

Jimi E. et al. (1999) Osteoclast differentiation factor acts as a multifunctional regulator in murine osteoclast differentiation and function. The Journal of Immunology 163:434-442.

Jobke B. et al. (2014) Bisphosphonate-osteoclasts : Changes in osteoclast morphology and function induced by antiresorptive nitrogen-containing bisphosphonate treatment in osteoporosis patients. Bone 59: 37–43.

Johnson R.W. et al. (2014) The primary function of gp130 Signaling in osteoblasts is to maintain bone formation and strengthrather than promote osteoclast formaiton. Journal of Bone and Mineral Research 29: 1492–1505.

Johnson R.W. et al. (2015) Glycoprotein 130 (gp130)/interleukin-6 (IL-6) signalling in osteoclasts promotes bone formation in periosteal and trabecular bone. Bone 81: 343-351.

Jones S.J., Arora M. & Boyde A. (1995) The Rate of Osteoclastic Destruction of Calcified Tissues Is Inversely Proportional to Mineral Density. Calcified Tissue

International 56: 554-558.

Jones S.A., Scheller J. & Rose-John S. (2011) Therapeutic strategies for the clinical blockade of IL-6 / gp130 signaling. J. Clin. Invest. 121: 3375-3383.

Jongh De R.F. et al.(2003) The Role of Interleukin-6 in Nociception and Pain. Anesthesia & Analgesics 96: 1096–1103.

Jonker M. et al. (2013) Comparative analysis of inflammatory infiltrates in collagen-induced arthritis , kidney graft rejection and delayed-type hypersensitivity in non-human primates. Inflamm. Res. 62: 181–194.

Joosten L.A.B. et al. (2009) Inflammatory arthritis in caspase-1 gene deficient mice: Contribution of proteinase 3 for caspase-1-independent production of bioactive IL-1β. Arthritis & Rhuematology 60: 3651-3662.

Jostock T. et al. (2001) Soluble gp130 is the natural inhibitor of soluble interleukin-6 receptor transsignaling responses. Eur. J. Biochem. 268: 160-167.

Jougasaki M. et al. (2010) Statins suppress interleukin-6-induced monocyte chemo-attractant protein-1 by inhibiting Janus kinase / signal transducers and activators of transcription pathways in human vascular endothelial cells. British Journal of Pharmacology 159: 1294–1303.

Kaji H. et al. (1996) Prostaglandin E_2 stimulates osteoclast-like cell formation and bone-resorbing activty via osteoblasts: role of cAMP-dependent protein kinase. Jounral of Bone and Mineral Research 11: 62-71.

Kameda T. et al. (1997) Estrogen inhibits bone resorption by directly inducing apoptosis of the bone-resorbing osteoclasts. J. Exp. Med. 186: 489-495.

Kamolmatyakull, S., Chen, W. & Lil, Y., 2001. Interferon-γ down-regulates gene expression of cathepsin K in osteoclasts and inhibits osteoclast formation. J Dent Res. 80: 351-355.

Kanazawa I. (2015) Osteocalcin as a hormone regulating glucose metabolism. World J. Diabetes 6: 1345–1354.

Kannan K., Ortmann R.A. & Kimpel D. (2005) Animal models of rheumatoid arthritis and their relevance to human disease. Pathophysiology 12: 167–181.

Kasama T. et al. (1995) Interleukin-10 Expression and Chemokine Regulation During the Evolution of Murine Type 11 Collagen-induced Arthritis. J. Clin. Invest. 95: 2868-2876.

Kataoka A. et al. (2009) Activation of P2X7 receptors induces CCL3 production in microglial cells through transcription facto NFAT. Journal of Neurochemistry 108: 115–125.

Kawashiri S. et al. (2011) Effects of the anti-interleukin-6 receptor antibody, tocilizumab, on serum lipid levels in patients with rheumatoid arthritis. Rheumatol Int. 31: 451-456.

Keller J. et al. (2012) Divergent resorbability and effects on osteoclast formation of commonly used bone substitutes in a human *in vitro*-assay. PLOS One 7: e46757.

Kempeni J.(1999) Preliminary results of early clinical trials with the fully human anti-TNF monoclonal antibody D2E7. Ann Rheum Dis 58: I70–72.

Keophiphath M. et al. (2010) CCL5 promotes macrophage recruitment and survival in human adipose tissue. Arterioscler Thromb Vasc Biol 30: 39-45.

Keul R. et al. (1998) A possible role for soluble IL-6 receptor in the pathogenesis of systemic onset juvenile chronic arthritis. Cytokine 10: 729-734.

Kiguchi N. et al. (2013) Cytokine Epigenetic upregulation of CCL2 and CCL3 via histone modifications in infiltrating macrophages after peripheral nerve injury. Cytokine64: 666–672.

Kikuta J. et al. (2013) Sphingosine-1-phosphate-mediated osteoclast precursor monocyte migration is a critical point of control in antibone-resorptive action of active vitamin D. PNAS 110: 7009–7013.

Kikuta J. & Ishii M.(2013) Osteoclast migration, differentiation and function: novel therapeutic targets for rheumatic diseases. Rheumatology 52: 226–234.

Kim L.H. et al. (2003) Identification of Novel SNPs in the Interleukin 6 Receptor Gene (IL6R). Wiley-Liss 601: 1–6.

Kim M.S., Day C.J. & Morrison N.A. (2005) MCP-1 Is Induced by Receptor Activator of Nuclear Factor-κB Ligand, Promotes Human Osteoclast Fusion, and Rescues Granulocyte Macrophage Colony-stimulating Factor Suppression of Osteoclast Formation *. The Journal of Biological Chemistry, 280: 16163–16169.

Kim K. et al. (2008) NFATc1 induces osteoclast fusion via up-regulation of Atp6v0d2 and the dendritic cell-specific transmembrane protein (DC-STAMP). Molecular Endocrinology 22: 176-185.

Kim T. et al. (2010) ATP6v0d2 deficiency increases bone mass , but does not influence ovariectomy-induced bone loss. Biochemical and Biophysical Research Communications 403; 73–78.

Kim G.W. et al. (2015) IL-6 inhibitors for treatment of rheumatoid arthritis: Past, present, and future. Archives of Pharmacal Research 38: 575–584.

Kinne R.W., Stuhlmuller B.& Burmester G. R.(2007) Cells of the synovium in rheumatoid arthritis: Macrophages. Arthritis Research & Therapy 9: 1–16.

Kishimoto T. et al. (1995) Interleukin-6 Family of Cytokines and gp130. The Journal of The American Society of Hematology 86: 1243–1254.

Kitaura H. et al. (2002) Effect of IL-12 on TNF- α -Mediated Osteoclast Formation in Bone Marrow Cells: Apoptosis Mediated by Fas/Fas Ligand Interaction. The Journal of Immunology 169: 4732-4738.

Kitaura H. et al. (2014) Effect of Cytokines on Osteoclast Formation and Bone Resorption during Mechanical Force Loading of the Periodontal Membrane. The Scientific World Journal 2014: 617032.

Klein D.C. & Raisz L.G. (1970) Prostaglandins: Stimulation of Bone Resorption in Tissue Culture. Endocrinology 86: 1436–1440.

Klimek E. et al. (2014) Blood Monocyte Subsets and Selected Cardiovascular Risk Markers in Rheumatoid Arthritis of Short Duration in relation to Disease Activity. BioMed Research International 2014: 736853.

Klouche M. et al. (1999) Novel Path to Activation of Vascular Smooth Muscle Cells: Up-Regulation of gp130 Creates an Autocrine Activation Loop by IL-6 and Its Soluble Receptor. The Journal of Immunology 163: 4583-4589.

Knowles H.J. et al. (2012) Chondroclasts are mature osteoclasts which are capable of cartilage matrix resorption. Journal of the European Society of Pathology 461: 205–210.

Kobayashi K. et al. (2000) Tumor Necrosis Factor-α Stimulates Osteoclast Differentiation by a Mechanism Independent of the ODF/RANKL – RANK Interaction. J. Exp. Med 191: 275-285.

Kobayashi Y. et al. (2006) Prostaglandin E_2 enhances osteoclastic differentiation of precursor cells through protein kinase A- dependent phosphorylation of TAK1. The Journal of Biological Chemistry 280: 11395-11403.

Koch A.E. et al. (1994) Macrophage Inflammatory Protein-1α.J. Clin. Invest. 93: 921–928.

Koch A.E. (2005) Chemokines and their receptors in rheumatoid arthritis. Arthritis & Rheumatism 52: 710-721.

Kohno H. et al. (2014) CCL3 production by microglial cells modulates disease severity in murine models of retinal degeneration. J Immunol. 192: 3816–3827.

Kojima H. et al. (2013) IL-6-STAT3 signaling and premature senescence. JAK-STAT 2: e25763.

Kokkonen H. et al. (2010) Up-Regulation of Cytokines and Chemokines Predates the Onset of Rheumatoid Arthritis. Arthritis & Rheumatism 62: 383-3941.

Komano Y. et al. (2006) Identification of a human peripheral blod monocyte subset that differentiates into osteoclasts. Arthritis Research & Therapy 8: R152.

Kotake S. et al. (1996) Interleukin-6 and soluble interleukin-6 receptors in the synovial fluids from rheumatoid arthritis patients are responsible for osteoclast-like cell formaiton. Journal of Bone and Mineral Research 11: 88-95.

Kondo T. et al. (2011). Essentials roles of CCL3-CCR1 axis in the pathogenesis of antigen-induced arthritis. (Cytokine Poster Session 2 : Chemokines and their

Receptors). Cytokine 56: 80.

Kramer N. et al. (2013) *In vitro* cell migration and invasion assays. Mutation Research 752: 10-24.

Kudo O. et al. (2003) Interleukin-6 and interleukin-11 support human osteoclast formation by a RANKL-independent mechanism. Bone 32: 1–7.

Kukita T. et al. (2004) RANKL-induced DC-STAMP Is Essential for Osteoclastogenesis. J. Exp. Med200: 941-946.

Kuno K. & Matsushima K. (1994) The IL-1 receptor signalling pathway. Journal of Leukocyte Biology 56: 542-547.

Kusano K. et al. (1998) Regulation of Matrix Metalloproteinases (MMP-2, -3, -9, and -13) by Interleukin-1 and Interleukin-6 in Mouse Calvaria: Association of MMP Induction with Bone Resorption. Endocrinology 139: 1338–1345.

Kyrtsonis M.C. et al. (1996) Soluble interleukin-6 receptor (sIL-6R), a new prognostic factor in multiple myeloma. British Journal of Haematology 93: 398-400.

Lacey D.L. et al. (1998) Osteoprotegerin Ligand is a cytokine that regulates osteoclast differentiation and activation. Cell 93: 165-176.

Lader C.S. & Flanagan A.M. (1998) Prostaglandin E_2, interleukin 1α and tumor necrosis factor-α increase human osteoclast formation and bone resorption *in vitro*. Endocrinology 139: 3157-3164.

Lamas J.R. et al. (2013) Alternative splicing and poteolytic rupture contribute to the generation of soluble IL-6 receptors (sIL-6R) in rheumatoid arthritis. Cytokine 61: 720-723.

Lambiase A. et al. (1997) Immundeficiency and other clinical immunology. J Clin Immunol 100: 408-414.

Lauta V.M. (2003) A review of the cytokine network in multiple myeloma. Cancer 97: 2440-2452.

Lebre M.C. et al. (2011) Why CCR2 and CCR5 blockade failed and why CCR1 blockade might still be effective in the treatment of rheumatoid arthritis. PLOS one 6: e21772.

Lee S. et al. (2003) Interleukin-7 Is a Direct Inhibitor of in Vitro Osteoclastogenesis. Endocrinology 144: 3524–3531.

Lee S.H. et al. (2006) v-ATPase V 0 subunit d2 – deficient mice exhibit impaired osteoclast fusion and increased bone formation. Nature Medicine 12: 1403–1409.

Lee S.K. & Lorenzo J. (2006) Cytokines regulating osteoclast formation and function. CurrentOpinion in Rheumatology 18: 411–418.

Leeman M.F., McKay J.A. & Murray G.I., (2002) Matrix metalloproteinase 13 activity is associated with poor prognosis in colorectal cancer.J Clin Pathol 55: 758–762.

Lehenkari P. et al. (1998) carbonic anhydrase II plays a major role in osteoclast differentiation and bone resorption by effecting the steady state intracellular pH and Ca^{2+}. Experimental Cell Research 242: 128-137.

Lent van P.L.E.M. et al. (1995) Major Role for Interleukin 1 but Not for Tumor Necrosis Factor in Early Cartilage Damage in Immune Complex Arthritis in Mice. The Journal of Rheumatology 22: 2250-2258.

Lentzsch S. et al. (2003) Macrophage inflammatory protein 1-alpha (MIP-1α) triggers migration and signaling cascades mediating survival and proliferation in multiple myeloma (MM) cells.Blood 101: 3568–3573.

Leszczyński M. (2010) Image Preprocessing for Illumination Invariant Face Verification. Journal of Telecommunications and Information Technology 4: 19–25.

Lewis N.D. et al. (2014) CCR1 Plays a Critical Role in Modulating Pain through Hematopoietic and Non-Hematopoietic Cells. PLOS One 9: e105883.

Li Y-P. & Chen W. (1999) characterization of mouse cathepsin K gene, the gene promoter, and the gene expression. Jounral of Bone and Mineral Research 14: 487-499.

Lin T-H. et al. (2013) CCL2 increases αvβ3 integrin expression and subsequently promotes prostate cancer migration. Biochimica et Biophysica Acta 1830: 4917–4927.

Lind M. et al. (1995) IL-4 and IL-13, but not IL-10, are chemotactic factors for human osteoblasts. Cytokine 7: 78–82.

Liu C-C. & Howard G.A. (1991) Bone-cell changes in estrogen-induced bone-mass increase in mice: dissociation of osteoclasts from bone surfaces. The Anatomical Record 229: 240-250.

Loeser J.D. & Melzack R. (1999) Pain: an overview. Lancet 353: 1607-09.

Lorenzo J.A., Sousa S.L. & Leahy C.L. (1990) Inhibitory factor (LIF) inhibits basal bone resorption in fetal rat long bone cultures. Cytokine 2: 266–271.

Lubberts E. et al. (2004) Treatment With a Neutralizing Anti-Murine Interleukin-17 Antibody After the Onset of Collagen-Induced Arthritis Reduces Joint Inflammation, Cartilage Destruction, and Bone Erosion. Arthritis & Rheumatism 50: 650–659.

Luchin, A. et al., 2000. The Microphthalmia Transcription Factor Regulates Expression of the Tartrate-Resistant Acid Phosphatase Gene During Terminal Differentiation of Osteoclasts. *Journal of Bone and Mineral Research*, 15(3),

pp.451–460.

Lutter A-H. et al. (2010) A novel resorption assay for osteoclast functionality based on an osteoblast-derived native extracellular matrix. Journal of Cellular Biochemistry 109: 1025-1032.

Madhok R. et al. (1993) Serum interleukin 6 levels in rheumatoid arthritis: correlations with clinical and laboratory indices of disease activity. Annals of Rheumatic Diseases 52: 232-234.

Maina A.M. & Kraus H. (2012) successful treatment of osteitis fibrosa cystica from primary hyperparathyroidism. Case reports in Orthopedics 2012: 145760.

Mantovani A., Kaplanski G. & Farnarier C. (2003) IL-6 : a regulator of the transition from neutrophil to monocyte recruitment during inflammation. TRENDS in Immunology 24: 25–29.

Marenzana M. et al. (2013) Effect of sclerostin-neutralising antibody on periarticular and systemic bone in a murine model of rheumatoid arthritis : a microCT study. Arthritis Research & Therapy 15: R125.

Marinou I. et al. (2007) Association of interleukin-6 and interleukin-10 genotypes with radiographic damage in rheumatoid arthritis is dependent on autoantibody status. Arthritis & Rheumatism 56: 2549-2556.

Marksteiner J. et al. (2011) Five out of 16 plasma signalling proteins are enhanced in plasma of patients with mild cognitive impairment and Alzheimer's disease. Neurobiol. Aging 32: 539-540.

Maslinski W. et al. (2003) Unbalanced levels of bone resorption promoting factors in bone marrow from patients with rheumatoid arthritis in comparison to osteoarthritis. Arthritis Res Ther 5 (suppl 3): S23.

Massey H.M. & Flanagan A.M. (1999) Humna osteoclasts derive from CD14-positive monocytes. British Journal of Haematology 106: 167-170.

Matsuno H. et al. (2002) the role of TNF-α in the pathogenesis of inflammation and joint destruction in rheumatoid arthritis (RA): a study using human RA/SCID mouse chimera. Rheumatology 41: 329-337.

McClung M.R. et al. (2006) Denosumab in postmenopausal women with low bone mineral density. N Engl J Med 354: 821-831.

McInnes I.B. & Schett G. (2007) Cytokines in the pathogenesis of rheumatoid arthritis. Nature Reviews Immunology 7: 429–442.

McGonagle D. et al. (1999) The relationship between synovitis and bone changes in early untreated rheumatoid arthritis. Arthritis & Rheumatism 42: 1706-1711.

McQueen F.M. (2000) Magnetic resonance imaging in early inflammatory arthritis: what is its role? Rhuematology 39: 700-706.

Mediero A., Perez-aso M. & Cronstein B.N. (2014) Activation of EPAC1 / 2 is essential for osteoclast formation by modulating NF □ B nuclear translocation and actin cytoskeleton rearrangements. The FASEB Journal 28: 1–13.

Melo Soares D. et al. (2006) CCL3/macrophage inflammatory protein-1α induces fever and increases prostaglandin E_2 in cerebospinal fluid of rats: Effect of antipyretic drugs. Brain Research 1109: 83-92.

Merendino R.A. et al. (2004) Involvement of fractalkine and macrophage inflammatory protein-1 alpha in moderate- severe depression. Mediators of Inflammation 13: 205–208.

Michael H. et al. (2005) Estrogen and testosterone use different cellular pathways to inhibit osteoclastogenesis and bone resorption. Jounral of Bone and Mineral Research 20: 2224-2232.

Miguel de M., Kraychete D.C. & Nascimento R.J.M. (2014) Chronic pain: cytokines, lymphocytes and chemokines. Inflammation & Allergy - Drug Targets 13: 339-349.

Mihara M. et al. (2012) IL-6/IL-6 receptor system and its role in physiological and pathological conditions. Clinical Science 122: 143-159.

Minano F.J. et al. (1990) Macrophage inflammatory protein-1: unique action on the hypothalamus to evoke fever. Brain Research Bulletin 24: 849-852.

Mittal A.K. et al. (2014) Chronic Lymphocytic Leukemia Cells in a Lymph Node Microenvironment Depict Molecular Signature Associated with an Aggressive Disease. Molecular Medicine 20: 290–301.

Miyamoto K. et al. (2009) MCP-1 expressed by osteoclasts stimulates osteoclastogenesis in an autocrine/paracrine manner. Biochemical and Biophysical Communications 383: 373-377.

Miyamoto T. (2011) Regulators of Osteoclast Differentiation and Cell-Cell Fusion. Keio J Med 60: 101–105.

Mizutani K. et al. (2009) The Chemokine CCL2 Increases Prostate Tumor Growth and Bone Metastasis through Macrophage Recruitment. Neoplasia 11: 1235–1242.

Motyckova G. et al. (2001) Linking osteopetrosis and pycnodysostosis: Regulation of cathepsin K expression by the microphthalmia transcription factor family. PNAS 98: 5798-5803.

Mueller A. & Strange P.G. (2004) CCL3 acting via the chemokine receptor CCR5, leads to independent activation of Janus kinase 2 (JAK 2) and G_i proteins. FEBS Letters 570: 126-132.

Müller-Newen G. et al. (1998) Soluble IL-6 Receptor Potentiates the Antagonistic Activity of Soluble gp130 on IL-6 Responses. The Journal of Immunology 161: 6347-6355.

Muller L.O., Humphries P. & Rosendahl K., 2015. The joints in juvenile idiopathic arthritis. Insights Imaging: 275–284.

Murphy P.G. et al.(1999) Endogenous interleukin-6 contributes to hypersensitivity to cutaneous stimuli and changes in neuropeptides associated with chronic nerve constriction in mice. European Journal of Neuroscience 11: 2243–2253.

Nagae M. et al. (2006) Osteoclasts play a part in pain due to the inflammation adjacent to bone. Bone 39: 1107–1115.

Nakashima K. et al. (2002) The Novel Zinc Finger-Containing Transcription Factor Osterix Is Required for Osteoblast Differentiation and Bone Formation. Cell 108: 17–29.

Nakatani N. et al. (2006) Genome-wide expression analysis detects eight genes with robust alterations specific to bipolar I disorder : relevance to neuronal network perturbation. Human Molecular Genetics15: 1949–1962.

Nandakumar K.S., Svensson L. & Holmdahl R.(2003) Collagen Type II-Specific Monoclonal Antibody- Induced Arthritis in Mice. American Journal of Pathology 163: 1827–1837.

Naranjo A. et al. (2008) Cardiovascular disease in patients with rheumatoid arthritis : results from the QUEST-RA study. Arthritis Research & Therapy 10: R30.

Narni-mancinelliE. et al. (2007) Memory CD8 ⍰ T cells mediate antibacterial immunity via CCL3 activation of TNF / ROI^{+} phagocytes. JEM204: 2075-2087.

Neer R.M. et al. (2001) Effect of parathyroid hormone (1-34) on fractures and bone mineral density in postmenopausal woman with osteoporosis. N Engl J Med 344: 1434- 1441.

Nemeth E. et al. (2004) IL-6 mediates hypoferremia of inflammation by inducing the synthesis of the iron regulatory hornome hepcidin. Journal of Clinical Investigration 113: 1271-1276.

Nemunaitis J.(1993) Macrophage function activating cytokines : potential clinical application. Clinical Reviews in Oncology/Hematology 14: 153–171.

Nevius E. et al. (2015) Oxysterols and EB12 promote osteoclast precursor migration to bone surfaces and regulate bone mass homeostasis. J Exp. Med. 212: 1931-1946.

Nicholson G.C. et al. (2000) Induction of osteoclasts from CD14-positive human peripheral blood mononuclear cells by receptor activator of nuclear factor κβ ligand (RANKL). Clinical Science 99: 133-140.

Nijweide P. et al. (1982) Bone formation and calcification by osteoblast-like cells. The Journal of Cell Biology 93: 318-323.

Nogueira-barbosa M.H. et al. (2010) Magnetic resonance imaging in the evaluation

of periosteal reactions *. Radiol Bras.43: 266–271.

Nowell M.A. et al. (2003) Soluble IL-6 Receptor Governs IL-6 Activity in Experimental Arthritis: Blockade of Arthritis Severity by Soluble Glycoprotein 130. The Journal of Immunology 171: 3202-3209.

Nowell M.A. et al. (2009) Therapeutic targetting of IL-6 trans-signaling counteracts STAT3 control of experimental inflammatory arthritis.The Journal of Immunology 182: 613-622.

Oba Y. et al. (2015) MIP-1α utilizes both CCR1 and CCR5 to induce osteoclast formaiton and increase adhesion of myeloma cells to marrow stromal cells. Experimental Hematology 33: 272-278.

Obreja O. et al. (2002) Interleukin-6 in combination with its soluble IL-6 receptor sensitises rat skin nociceptors to heat , in vivo. Pain 96: 57–62.

Obreja O. et al.(2005) Fast modulation of heat-activated ionic current by proinflammatory interleukin 6 in rat sensory neurons. Brain 128: 1634–1641.

O'Brien C.A. et al. (1999) STAT3 activation in stromal/osteoblastic cells is required for induction of the receptor activator of NF-κβ ligand and stimulation of osteoclastogenesis by gp130-utilizing cytokines or interleukin-1 but not 1,25-Dihydroxyvitamin D_3 or parathyroid hormone. Journal of Biological Chemistry 274: 19301-19308.

Oddie G.W. et al. (2000) Structure, function and regulaiton of Tartrate-resistant acid phosphatase. Bone 27: 575-584.

Oh J.W., Revel M.& Chebath(1996) A soluble interleukin 6 receptor isolated from conditioned medium of human breast cancer cells is encoded by a differentially spliced mRNA. Cytokine 8: 401–409.

Oikawa T. et al. (2012) Tks5-dependent formation of circumferential podosomes/ invadopodia mediates cell-cell fusion. J. Cell Biol. 197: 553-568.

Oreffo R.O.C. et al. (1999) expression of estrogen receptor-alpha in cells of the osteoclast-lineage. Histochem Cell Biol 111: 125-133.

Oursler M.J. (2003) Direct and indirect effects of estrogen on osteoclasts. J Musculoskel Neuron Interact 3: 363–366.

Palma B.D. et al. (2016) Osteolytic lesions, cytogenetic features and bone marrow levels of cytokines and chemokines in multiple myeloma patients: Role of chemokine (C-C motif) ligand 20. Leukemia 30: 409-416.

Palmqvist P. et al. (2002) IL-6, Leukemia Inhibitory Factor, and Oncostatin M Stimulate Bone Resorption and Regulate the Expression of Receptor Activator of NF- κB Ligand, Osteoprotegerin, and Receptor Activator of NF- κB in Mouse Calvariae. The Journal of Immunology 169: 3353-3362.

Palmqvist P. et al. (2006). Inhibition of Hormone and Cytokine-stimulated

Osteoclastogenesis and Bone Resorption by Interleukin-4 and Interleukin-13 Is Associated with Increased Osteoprotegerin and Decreased RANKL and RANK in a STAT6-dependent Pathway*. The Journal of Biological Chemistry 281: 2414–2429.

Pardali E. & Waltenberger J. (2012) Monocyte function and trafficking in cardiovascular disease. Thrombosis and Haemostasis 108: 804–811.

Park S-J. et al. (2004) IL-6 regulates in vivo dendritic cell differentiation through STAT3 activation. Journal of Immunology 173: 3844-3854.

Partington G.A. et al. (2004) Mitf – PU . 1 interactions with the tartrate-resistant acid phosphatase gene promoter during osteoclast differentiation. Bone 34: 237–245.

Patel D.D. et al. (2001) CXCR3 and CCR5 ligands in rheumatoid arthritis synovium. Clinical Immunology 98: 39-45.

Pathak J.L. et al. (2015) CXCL8 and CCL20 Enhance Osteoclastogenesis via Modulation of Cytokine Production by Human Primary Osteoblasts. PLOS One 10: e0131041.

Peake N.J. et al. (2006) Interleukin-6 signalling in juvenile idiopathic arthritis is limited by proteolytically cleaved soluble inter-leukin-6 receptor. Rheumatology 45: 1485-1489.

Pearse R.N. et al. (2001) Multiple myeloma disrupts the TRANCE/osteoprotegerin cytokine axis to trigger bone destruction and promote tumour progression. PNAS 98: 11581-11586.

Perrin F.E. et al. (2005) Involvement of monocyte chemoattractant prtein-1, macrophage inflammatory protein-1α and interleukin-1β in Wallerian degeneration. Brain 128: 854-866.

Peruzzi B. et al. (2012) c-Src and IL-6 inhibit osteoblast differentiation and integrate IGFBP5 signalling. Nature Communications 3: 630.

Peters M. et al. (1996) the function of the soluble interleukin 6 (IL-6) receptor in vivo: sensitization of human soluble IL-6 receptor transgenic mice towards lL-6 and prolongation of the plasma half-life of IL-6. J. Exp. Med. 183: 1399-1406.

Pettit A.R. et al. (2001) TRANCE/RANKL knock-out mice are protected from bone erosion in a serum transfer model of arthritis. American Journal of Pathology 159: 1689-1699.

Pharoah D.S. et al. (2006) Expression of the inflammatory chemokines CCL5, CCL3 and CXCL10 in juvenile idiopathic arthritis, and demonstration of CCL5 production by an atypical subset of CD8+ T cells. Arthritis Research & Therapy 8: R50.

Phillips R.M. et al. (2003) Variations in eosinophil chemokine responses: An

investigation of CCR1 and CCR3 function, expression in atopy, and identification of a functional CCR1 promoter. Journal of Immunology 170: 6190-6201.

Pierroz D.D. et al. (2010) Are Osteoclasts Needed for the Bone Anabolic Response to Parathyroid Hormone? The Journal of Biological Chemistry 285: 28164–28173.

Piper K., Boyde A. & Jones S.J. (1992) The relationship between the number of nuclei of an osteoclast and its resorptive capability in vitro. Anatomy and Embryology 186: 291-299.

Podgorski I. et al. (2009) Bone Marrow-Derived Cathepsin K Cleaves SPARC in Bone Metastasis. The American Journal of Pathology 175: 1255–1269.

Polil V. et al. (1994) Interleukin-6 deficient mice are protected from bone loss caused by estrogen depletion. The EMBO Journal 13: 1189-1196.

Poole K.E.S. &Reeve J. (2005) Parathyroid hormone — a bone anabolic and catabolic agent Kenneth ES Poole and Jonathan Reeve. Current Opinion in Rheumatology 5: 612–617.

Quick M.L. et al.(2012) CCL2 and CCL3 are essential mediators of pelvic pain in experimental autoimmune prostatitis. Am J Physiol - Regulatory, Integrative and Comparative Physiology 303: R580-R589.

Quinn J.M.W. et al. (1998) A combination of osteoclast differentiation factor and macrophage-colony stimulating factor is sufficient for both human and mouse osteoclast formation. Endocrinology 139: 4424-4427.

Quinones M. et al. (2006) CC chemokine receptor (CCR)-2 prevents arthritis development following infection by *Mycobacterium avium*. J Mol Med 84: 503-512.

Raisz L.G. (1999) Physiology and Pathophysiology of Bone Remodeling. Clinical Chemistry 45: 1353–1358.

Raisz L.G. (2005) Pathogenesis of osteoporosis : concepts, conflicts, and prospects. J. Clin. Invest 115: 3318-3325.

Ralston S.H., Langston A.L. & Reid I.R. (2008) Pathogenesis and management of Paget ' s disease of bone. The Lancet 372: 155–163.

Ramos C.D.L. et al. (2005) MIP-1α [CCL3] acting on the CCR1 receptor mediates neutrophil migration in immune inflammation via sequential release of TNFα and LTB_4. Journal of Leukocyte Biology78: 167–177.

Rana R.S., Wu J.S. & Eisenberg R.L.(2009) Periosteal Reaction. AJR 193: 259–272.

Ravi A.K. et al. (2014) Increased levels of soluble interleukin-6 receptor and CCL3 in COPD sputum. Respiratory Research 15: 103.

Raza K. et al. (2005) Early rheumatoid arthritis is characterized by a distinct and

transient synovial fluid cytokine profile of T cell and stromal cell origin. Arthritis Research & Therapy 7: R784- 795.

Reale M. et al. (2011) Dysregulation of chemo-cytokine production in schizophrenic patients versus healthy controls. BMC Neuroscience 12: 13.

Reddy S. V et al. (1995) Characterization of the 5 ' -Flanking Region of the Human Tartrate-Resistant Acid Phosphatase (TRAP) Gene. Bone 16: 587–593.

Reid I.R. et al. (1990) Leukemia Inhibitory Factor : A Novel Bone-Active Cytokine. Endocrinology 126: 1416–1420.

Ren M. et al. (2010) Polymerization of MIP-1 chemokine (CCL3 and CCL4) and clearance of MIP-1 by insulin-degrading enzyme. The EMBO Journal 29: 3952-3966.

Ren K. & Dubner R. (2010) Interactions between the immune and nervous systems in pain. Nat Med. 16: 1267-1276.

Repeke C.E. et al. (2010) Non-inflammatory destructive periodontal disease: a clinical, microbiological, immunological and genetic investigation. J Appl Oral Sci, 20: 113–121.

Repeke C.E. et al. (2010) Evidences of the cooperative role of the cytokines CCL3, CCL4 and CCL5 and its recepotrs CCR1+ and CCR5+ in RANKL+ cell migration throughout experimental periodontitis in mice. Bone 46: 112-1130.

Richie A.M. & Francis M.L. (2003) Diagnostic Approach to Polyarticular Joint Pain. Am Fam Physician 68: 1151–1160.

Richter F. et al. (2010) Tumour necrosis factor causes persistent sensitization of joint nociceptors to mechanical stimuli in rats. Arthritis & Rheumatism 62: 3806-3814.

Riggs B.L., Khosla S. & Melton L.J. (2002) Sex Steroids and the Construction and Conservation of the Adult Skeleton. Endocrine Reviews 23: 279–302.

Ripley B.J.M. et al. (2005) Raised levels of interleukin 6 in systemic lupus erythematosus correlate with anaemia. Annuals of Rheumatic Diseases 64: 849-853.

Robak T. et al. (1998) Serum levels of interleukin-6 type cytokines and soluble interleukin-6 receptor in patients with rheumatoid arthritis. Mediators of Inflammation 7: 347–353.

Rocha F.A.C., Andrade L.E.C. & Jancar S. (1996) Immune complex induced arthritis in rats: role of lipid mediators on cell infiltration. Mediators of Inflammation 5: 104–109.

Rodan G.A. (1998) Bone homeostasis. Proc. Natl. Acad. Sci. 95: 13361–13362.

Rogers J., Shepstone L. & Dieppe P. (1997) Bone formers : osteophyte and

enthesophyte formation are positively associated. Annals of Rheumatic Diseases 56: 85–90.

Romas E. et al. (1996) The role of gp130-mediated signals in osteoclast development: regulation of interleukin 11 production by osteoblasts and distribution of its receptor in bone marrow cultures. J. Exp. Med. 183: 2581-2591.

Rood J.A. et al. (1997) Genomic organization and chromosome localization of the human cathepsin K gene (CTSK). Genomics 41: 169-176.

Roodman G.D. et al. (1992) Interleukin 6: A potential autocrine/paracrine factor in Paget's disease of bone. J. Clin. Invest. 89: 46-52.

Roodman G.D. (1999) Cell biology of the osteoclast. Experimental Hematology 27: 1229-1241.

Rose-John, S.(2012) IL-6 Trans-Signaling via the Soluble IL-6 Receptor : Importance for the Pro-Inflammatory Activities of IL-6. International Journal of Biological Sciences 8: 1237-1247.

Ross F.P. (2006) M-CSF, c-Fms, and Signaling in Osteoclasts and their Precursors.Ann. N.Y. Acad. Sci 1068: 110–116.

Sabroe I. et al. (2000) A Small Molecule Antagonist of Chemokine Receptors CCR1 and CCR3. The Journal of Biological Chemistry 275: 25985–25992.

Sago K. et al. (1999) The integrin $\alpha_v\beta_5$ is expressed on avian osteoclast precursors and regulated by retinoic acid. Journal of Bone and Mineral Research 14: 32-38.

Sanecka A. et al. (2011) DC-STAMP knock-down deregulates cytokine production and T-cell stimulatory capacity of LPS- matured dendritic cells. BMC Immunology 12: 57.

Sarma U. & Flanagan A.M. (1996) Macrophage colony-stimulating factor induces substantial osteoclast generation and bone resorption in human bone marrow cultures. Blood 88: 2531-2540.

Scheller J. et al. (2011) The pro- and anti-in fl ammatory properties of the cytokine interleukin-6. Biochemica et Biophysica Acta 1813: 878–888.

Schett G. (2007) Cells of the synovium in rheumatoid arthritis Osteoclasts. Arthritis Research & Therapy 9: 203.

Schett G. (2007) Erosive arthritis. Arthritis Research & Therapy 9: S2.

Schett G. (2007) Joint remodelling in inflammatory disease. Ann Rheum Dis 66: (Suppl III).

Schett G. (2007) How does joint remodelling work? Cell Adhesion & Migration 1: 102-103.

Schett G. & Teitelbaum S.L.(2009) Osteoclasts and Arthritis. Journal of Bone and Mineral Research 24: 1142–1146.

Scheven B.A.A. et al. (1999) Macrophage-Inflammatory Protein-1α Regulates Preosteoclast Differentiation in Vitro. Biochemical and Biophysical Research Communications 778: 773–778.

Schimmer R.C. et al. (1998) Streptococcal Cell Wall-Induced Arthritis: Requirements for IL-4, IL-10, IFN- γ, and Monocyte Chemoattractant Protein-1. The Journal of Immunology 16-: 1466-1471.

Schluger N.W. & Rom W.N. (1997) Early responses to infection: chemokines as mediators of inflammation. Current Opinion in Immunology 9: 504-508.

Schneider A. et al. (2005) Bone turnover mediates preferential localization of prostate cancer in the skeleton. Endocrinology 146: 1727-1736.

Schuett H. et al. (2012) Transsignaling of Interleukin-6 Crucially Contributes to Atherosclerosis in Mice. Aterioscler Thromb Vasc Biol 32: 281-290.

Schumacher N. et al. (2015) Shedding of endogenous interleukin-6 receptor (IL-6R) is governed by a disintegrin and metalloproteinase (ADAM) proteases while a full length IL-6R isoform localizes to circulating microvesicles. The Journal of Biological Chemistry 290: 26059-26071.

Seeuws S. et al. (2010) A multiparameter approach to monitor disease activity in collagen-induced arthritis. Arthritis Research & Therapy 12:R160.

Sharma S.M. et al. (2007) MITF and PU.1 Recruit p38 MAPK and NFATc1 to Target Genes during Osteoclast Differentiation*. The Journal of Biological Chemistry 282: 15921–15929.

Shi M. et al. (2015) The protective effects of chronic intermittent hypobaric hypoxia pretreatment against collagen-induced arthritis in rats. Journal of Inflammation 12:23.

Shidara K. et al. (2008) Serum Levels of TRAP5b , a New Bone Resorption Marker Unaffected by Renal Dysfunction, as a Useful Marker of Cortical Bone Loss in Hemodialysis Patients. Calcif Tissue Int 82: 278–287.

Sigaux J. et al. (2017) Immunogenicity of tocilizumab in patients with rheumatoid arthritis. Joint Bone Spine 84: 39-45.

Simon N.M. et al. (2008) A Detailed Examination of Cytokine Abnormalities in Major Depressive Disorder. Euro Neuropsychopharmacol. 18: 230–233.

Simpson A. & Horton M.A. (1989) Expression of the vitronectin recepotr during embryonic development; an immunohistological study of the ontogeny of the osteoclast in the rabbit. Br. J. Exp. Path. 70: 257-265.

Sims N.A. & Romas E. (2015) Is RANKL inhibition both anti-resorptive and anabolic in rheumatoid arthritis ? Arthritis Research & Therapy 17:328.

Sivina M. et al. (2011) CCL3 (MIP-1α) plasma levels and the risk for disease progression in chronic lymphocytic leukemia. Blood 117: 1662–1670.

Sleiman I. et al. (2004) Osteitis fibrosa cystica, coeliac disease and Turner syndrome: A case report. Digestive and Liver Disease 36: 486–488.

Soliman A.F. et al. (2016) Potential role of calprotectin as a monitoring biomarker for clinical and sonographic activity and treatment outcome in recent-onset rheumatoid arthritis. Egyptian Rheumatology & Rehabilitation 43: 143-149.

Song H-P. et al. (2015) Phenotypic characterization of type II collagen-induced arthritis in Wistar rats. Experimental and Therapeutic Medicine 10: 1483–1488.

Soysa N. S. et al. (2009) Three-dimensional characterization of osteoclast bone-resorbing activity in the resorption lacunae. J Med Dent Sci. 56: 107-112.

Soysa N.S. et al. (2012) Osteoclast formation and differentiation: An overview. J Med Dent Sci. 59: 65-74.

Sreeja R. et al. (2009) A scanning electron microscopic study of the patterns of external root resorption under different conditions. J Appl Oral Sci. 17: 481-486.

Srirangan S. & Choy E.H. (2010) The role of Interleukin 6 in the pathophysiology of rheumatoid arthritis. Therapeutic Advances in Musculoskeletal Disease 2: 247–256.

Stark Z. & Savarirayan R. (2009) Osteopetrosis. Orphanet Journal of Rare Diseases 4:5.

Strassle B.W. et al. (2010) Inhibition of osteoclasts prevents cartilage loss and pain in a rat model of degenerative joint disease. Osteoarthritis and Cartilage 18: 1319–1328.

Sundaram K. et al. (2007) RANK ligand signaling modulates the matrix metalloproteinase-9 gene expression during osteoclast differentiation. Experimental Cell Research313: 168-178.

Susa et al. M. (2004) Human primary osteoclasts: in vitro generation and applications as pharmacological and clinical assay. Journal of Translational Medicine 2:6.

Suzuki M. et al. (2010) Cytokine IL-6 and IL-1 synergistically enhanced the production of MMPs from synovial cells by up-regulating IL-6 production and IL-1 receptor I expression. Cytokine 51: 178–183.

Szekanecz Z. et al. (2010) Chemokines and chemokine receptors in arthritis. Front Biosci 2: 153-167.

Tak P.P. et al. (1997) Analysis of the synovial cell infiltrate in relation to local disease activity. Arthritis & Rheumatism 40: 217–225.

Takahashi N. et al. (1988) Osteoclast-like cell formation and its regulation by osteotropic hormones in mouse bone marrow cultures. Endocrinology 122: 1373-1382.

Takahashi K. et al. (2015) CCL3 and CCL4 are biomarkers for B cell receptor pathway activation and prognostic serum markers in diffuse large B cell lymphoma.British Journal of Haematology 171: 726–735.

Takano T. et al. (2014) Mesenchymal stem cells markedly suppress inflammatory bone destruction in rats with adjuvant-induced arthritis. Laboratory Investigation 94: 286–296.

Takayanagi H. et al. (2000) T-cell-mediated regulation of osteoclastogenesis by signalling cross-talk between RANKL and IFN-γ. Letter to Nature408: 600-605.

Takayanagi H. et al. (2002) Induction and activation of the transcription factor NFATc1 (NFAT2) integrate RANKL signaling in terminal differentiation of osteoclasts. Developmental Cell 3: 889-901.

Tamura T. et al. (1993) Soluble interleukin-6 receptor triggers osteoclast formation by interleukin 6. Proc. Natl. Acad. Sci.90: 11924–11928.

Tanaka K. et al. (2013) Anti-interleukin-6 receptor antibody prevents systemic bone mass loss via reducing the number of osteoclast precursors in bone marrow in a collagen-induced arthritis model. Clinical and Experimental Immunology 175: 172–180.

Taouli B. et al. (2002) Imaging of the hand and wrist in RA. Amm Rheum Dis 61: 687-869.

Teitelbaum S.L., Tondrovi M.M. & Ross F.P. (1997) Osteoclasts, macrophages, and the molecular mechanisms of bone resorption. J Leukoc Biol. 61: 381-388.

Teixeira A.L. et al. (2008) Increased serum lefels of CCL11/eotaxin in schizophrenia. Progress in Neuro-Psychopharmacology & Biological Psychiatry 32: 710-714.

Tenhumberg S. et al. (2008) Structure-guided optimization of the interleukin-6 trans-signaling antagonist sgp130. Journal of Biological Chemistry 282: 27200-27207.

Teramachi J. et al. (2014) Increased IL - 6 Expression in Osteoclasts Is Necessary But Not Suf fi cient for the Development of Paget ' s Disease of Bone. Journal of Bone and Mineral Research 29: 1456–1465.

Toh K. et al.(2004) Possible involvement of MIP-1 a in the recruitment of osteoclast progenitors to the distal tibia in rats with adjuvant-induced arthritis. Laboratory Investigation 84: 1092–1102.

Toma C.D. et al. (2007) Fusion of the wrist in rheumatoid arthritis. The Journal of Bone and Joint Surgery 89: 1620–1626.

Tomankova T. et al. (2014) Comparison of periprosthetic tissues in knee and hip

joints : differential expression of CCL3 and DC-STAMP in total knee and hip arthroplasty and similar cytokine pro fi les in primary knee and hip osteoarthritis. Osteoarthritis and Cartilage 22: 1851–1860.

Toraldo G. et al. (2003) IL-7 induces bone loss in vivo by induction of receptor activator of nuclear factor κβ ligand and tumor necrosis factor α from T cells. PNAS 100: 125–130.

Tregoning J.S. et al. (2010) The Chemokine MIP1 a / CCL3 Determines Pathology in Primary RSV Infection by Regulating the Balance of T Cell Populations in the Murine Lung. PLOS One 5: e9381.

Trentham D.E., Townes A.S. & Kang A.H. (1978) Autoimmunity to type II collagen: an experimental model of arthritis*. The Journal of Experimental Medicine 146: 857- 868.

Trifilo M.J. et al. (2003) CC Chemokine Ligand 3 (CCL3) Regulates $CD8^+$-T-Cell Effector Function and Migration following Viral Infection. Journal of Virology 77: 4004–4014.

Tsangari H. et al. (2004) Increased expression of IL-6 and RANK mRNA in human trabecular bone from fragility fracture of the femoral neck. Bone 35: 334-342.

Tsirakis G. et al. (2014) Increased serum levels of MIP-1alpha correlate with bone disease and angiogenic cytokines in patients with multiple myeloma. Med Oncol 31: 778.

Tzur et al. (2011) Optimizing Optical Flow Cytometry for Cell Volume-Based Sorting and Analysis. PLOS One 6: e16053.

Udagawa N. et al. (1996) Interleukin-6 and Soluble Interleukin-6 Receptors in the Synovial Fluids from Rheumatoid Arthritis Patients Are Responsible for Osteoclast-like Cell Formation. Journal of Bone and Mineral Research 11:1.

Udagawa N. et al. (2000) Osteoprotegerin Produced by Osteoblasts Is an Important Regulator in Osteoclast Development and Function*. Endocrinology 141: 3478–3484.

Uderhardt S. et al. (2010) Blockade of Dickkopf (DKK)-1 induces fusion of sacroiliac joints. Ann Rheum Dis 69: 592–597.

Urashima M. et al. (1996) Interleukin-6 promotes multiple myeloma cell growth via phosphoryltion of retinoblastoma protein. Blood 88: 2219-2227.

Vallet S. et al. (2007) MLN3897 , a novel CCR1 inhibitor , impairs osteoclastogenesis and inhibits the interaction of multiple myeloma cells and osteoclasts. Blood, 110: 3744–3752.

Vallet S. et al. (2011) A Novel Role for CCL3 (MIP-1α) in Myeloma-induced Bone Disease via Osteocalcin Downregulation and Inhibition of Osteoblast Function. Leukemia 25: 1174–1181.

Vangsness C.T. et al. (2011) Human knee synovial fluid cytokines correlated with grade of knee osteoarthritis. Bulletin of the NYU Hospital for Joint Diseases 69: 122-127.

Ved N. & Haller J.O. (2002) Periosteal reaction with normal-appearing underlying bone : a child abuse mimicker. Emergency Radiology 9: 278–282.

Vergunst C.E. et al. (2008) Modulation of CCR2 in Rheumatoid Arthritis. Arthritis & Rheumatism 58: 1931–1939.

Voskuyl A.E. (2006) The heart and cardiovascular manifestations in rheumatoid arthritis. Rheumatology 45: iv4-iv7.

Wada T. et al. (2006) RANKL – RANK signaling in osteoclastogenesis and bone disease. TRENDS in Molecular Medicine 12: 17-25.

Warshawsky H. et al. (1980) Direct in vivo demonstration by radioautography of specific binding sites for calcitonin in skeletal and renal tissues of the rat. Journal of Cell Biology 85: 682-694.

Watad A. et al. (2017) Anxiety disorder among rheumatoid arthritis patients: Insights from real-life data. Journal of Affective Disorders 213: 30-34.

Weissenbach M. et al. (2004) Interleukin-6 is a direct mediator of T cell migration. Eur. J. Immunol. 34: 2895-2906.

Weitzmann M.N. et al. (2000) Interleukin-7 stimulates osteoclast formation by up-regulating the T-cell production of soluble osteoclastogenic cytokines. Blood 96: 1873-1878.

Whitehead K.A., Langer R. & Anderson D.G.(2009) Knocking down barriers: advances in siRNA delivery. Nature Reviews8:129-138.

Wilson S.R. et al. (2009) Cathepsin K Activity-dependent Regulation of Osteoclast Actin Ring Formation and Bone Resorption*. The Journal of Biological Chemistry 284: 2584–2592.

Wintges K. et al. (2013) Imparied bone formation and increased osteoclastogenesis in mice lacking chemokine (C-C motif) ligand 5. Journal of Bone and Mineral Research 28: 2070-2080.

Witwicka H. et al. (2015) Studies of OC-STAMP in Osteoclast Fusion : A New Knockout Mouse Model , Rescue of Cell Fusion , and Transmembrane Topology. PLOS One 10: e0128275.

Wolf M. et al. (2003) Cathepsin D Specifically Cleaves the Chemokines Macrophage Inflammatory Protein-1α, Macrophage Inflammatory Protein-1β, and SLC That Are Expressed in Human Breast Cancer. American Journal of Pathology, 162: 1183–1190.

Wolpe S.D. et al. (1988) Macrophages secrete a novel heparin-binding protein with inflammatory and neutrophil chemokinetic properties. J. Exp. Med. 167: 570-

581.

Wong P.K.K. et al. (2006) Interleukin-6 Modulates Production of T Lymphocyte – Derived Cytokines in Antigen-Induced Arthritis and Drives Inflammation-Induced Osteoclastogenesis. Arthritis & Rheumatism 54: 158–168.

Wu Y. et al. (2005) Synovial Fibroblasts Promote Osteoclast Formation by RANKL in a Novel Model of Spontaneous Erosive Arthritis. Arthritis & Rheumatism 52: 3257–3268.

Wu Y. et al. (2008) CCL3-CCR5 Axis Regulates Intratumoral Accumulation of Leukocytes and Fibroblasts and Promotes Angiogenesis in Murine Lung Metastasis Process. The Journal of Immunology 181: 6384-6393.

Xing L., Xiu Y. & Boyce B.F. (2012) Osteoclast fusion and regulation by RANKL-dependent and independent factors. World J. Orthop. 18: 212–222.

Xue M. et al. (2007) A critical role for CCL2 and CCL3 chemokines in the regulation of polymorphonuclear neutrophils recruitment during corneal infection in mice. Immunology and Cell Biology 85: 525–531.

Yagi M. et al. (2005) DC-STAMP is essential for cell – cell fusion in osteoclasts and foreign body giant cells. JEM202: 345–351.

Yanaba K. et al. (2004) role of C-C chemokine receptors 1 and 5 and CCL3/macrophage inflammatory protein-1α in the cutaneous Arthus reaction: possible attenuation of their inhibitory effect by compensatory chemokine production. Eur. J. Immunol. 34: 3553-3561.

Yang S. et al. (1996) Functions of the M-CSF receptor on osteoclasts. Bone 18: 355-360.

Yang X. et al. (2006) Essential contribution of a chemokine, CCL3, and its receptor, CCR1, to hepatocellular carcinoma progression. Int. J. Cancer 118: 1869–1876.

Yang S. et al. (2013) Quantification of bone changes in a collagen- induced arthritis mouse model by reconstructed three dimensional micro-CT. Biological Procedures Online 15:8.

Yano S. et al. (2005) Functional Expression of β-Chemokine Receptors in Osteoblasts: Role of Regulated upon Activation, Normal T Cell Expressed and Secreted (RANTES) in Osteoblasts and Regulation of Its Secretion by Osteoblasts and Osteoclasts. Endocrinology 146: 2324–2335.

Yasuda H. (2013) RANKL , a necessary chance for clinical application to osteoporosis and cancer-related bone diseases. World J. Orthop. 18: 207–217.

Yoneda T. et al. (2011) Involvement of acidic microenvironment in the pathophysiology of cancer-associated bone pain. Bone 48: 100-105.

Yoshitake F. et al. (2008) Interleukin-6 Directly Inhibits Osteoclast Differentiation by Suppressing Receptor Activator of NF-κB Signaling Pathways. The Journal of

Biological Chemistry 283: 11535–11540.

Yoshizaki K. et al. (1998) Therapy of rheumatoid arthritis by blocking IL-6 signal transduction with a humanized anti-IL-6 receptor antibody. Springer Seminars in Immunopatholgy 20: 247–259.

Yu X. et al. (2004) CCR1 Chemokines Promote the Chemotactic Recruitment, RANKL Development, and Motility of Osteoclasts and Are Induced by Inflammatory Cytokines in Osteoblasts. Journal of Bone and Mineral Research 19: 2065–2077.

Zhang N. et al. (2005) A proinflammatory chemokine, CCL3, sensitizes the heat- and capsaicin-gated ion channel TRPV1. PNAS 102: 4536-4541.

Zhang X., Huang J. & McNaughton P.A.(2005) NGF rapidly increases membrane expression of TRPV1 heat-gated ion channels. The EMBO Journal 24: 4211–4223.

Zhang W. et al. (2009) NAD(P)H oxidase-dependent regulation of CCL2 production during retinal inflammation. Invest. Opthalmol. Vis. Sci. 50: 3033-3040.

Zheng M.H. et al. (1994) Carbonic anhydrase II gene transcript in cultured osteoclasts from neonatal rats: effect of calcitonin. Cell Tissue Res. 276: 7-13.

Zucchetto A. et al. (2009) Cell Adhesion Molecule-1 Are Interchained by Sequential Events Sustaining Chronic Lymphocytic Leukemia Cell Survival. Cancer Res. 69: 4001–4009.

Appendices

Appendix 1 – MATLAB code for automated counting algorithm

```
%show original image
figure(1); imagesc(I);
set(gca,'XTick',0); set(gca,'XTickLabel',{' '}); xlabel(' '); % --- clear axes labels
set(gca,'YTick',0); set(gca,'YTickLabel',{' '}); ylabel(' ');
```

```
%set parameters
P.conn = 4;
P.noise_thresh = 50;

%produce the threshed, filled and denoised binary image
I_temp.level = graythresh(I); % -- determine default threshold
I_temp.BW_threshed = im2bw(I,I_temp.level); % -- make binary image using thresh
I_temp.BW_comp = imcomplement(I_temp.BW_threshed); % -- complement binary image
I_temp.BW_filled = imfill(I_temp.BW_comp,'holes'); % -- fill in any holes
I_temp.BW_denoised = bwareaopen(I_temp.BW_filled,P.noise_thresh); % remove all objects < noise_thresh
```

```
%count number of objects in filled and noisy image
I_temp.cc_filled = bwconncomp(I_temp.BW_filled, P.conn); % identify objects in noisy image
I_temp.cc_denoised = bwconncomp(I_temp.BW_denoised, P.conn); % identify objects in final image

%show the noisy and denoised binary images
figure(2); imagesc(I_temp.BW_filled); colormap gray; axis image;
set(gca,'XTick',0); set(gca,'XTickLabel',{' '}); xlabel(' '); % --- clear axes labels
set(gca,'YTick',0); set(gca,'YTickLabel',{' '}); ylabel(' ');
xlabel(strcat(int2str(I_temp.cc_filled.NumObjects),' objects')); % -- add no. of objects to x-axis

figure(3); imagesc(I_temp.BW_denoised); colormap gray; axis image;
set(gca,'XTick',0); set(gca,'XTickLabel',{' '}); xlabel(' '); % --- clear axes labels
set(gca,'YTick',0); set(gca,'YTickLabel',{' '}); ylabel(' ');
xlabel(strcat(int2str(I_temp.cc_denoised.NumObjects),' objects')); % -- add no. of objects to x-axis
```

```
%normalise image to produce constant background illumination
I_user.I.gray = rgb2gray(handles.I.original); %from RGB into gray
I_user.DCT_norm = DCT_normalization(I_user.I.gray); % normalization code
I_user.DCT_norm = I_user.DCT_norm/255; % norm to values between [0 1]

cd(path.image)

%produce the threshed, filed and denoised image again
I_user.level = graythresh(I_user.DCT_norm);
I_user.BW_threshed = im2bw(I_user.DCT_norm,I_user.level);
I_user.BW_comp = imcomplement(I_user.BW_threshed); % -- complement binary image
I_user.BW_filled = imfill(I_user.BW_comp,'holes'); % -- fill in any holes
I_user.BW_denoised = bwareaopen(I_user.BW_filled,P.noise_thresh); % remove all objects < noise_thresh

%count number of objects in filled and noisy image
I_user.cc_filled = bwconncomp(I_user.BW_filled, P.conn);
I_user.cc_denoised = bwconncomp(I_user.BW_denoised, P.conn);

%show the normalised image
figure(4); imagesc(I_user.BW_denoised); colormap gray; axis image;
set(gca,'XTick',0); set(gca,'XTickLabel',{' '}); xlabel(' '); % --- clear axes labels
set(gca,'YTick',0); set(gca,'YTickLabel',{' '}); ylabel(' ');
xlabel(strcat(int2str(I_user.cc_denoised.NumObjects),' objects'));
```

```
%Outline binary objects counted
outline= bwperim(handles.I.BW_denoised);
handles.I.original_outlined = handles.I.original;
handles.I.original_outlined(outline) = 0;

%show segmented image
figure(5); imagesc(handles.I.original_outlined); axis image;
set(gca,'XTick',0); set(gca,'XTickLabel',{' '}); xlabel(' '); % --- clear axes labels
set(gca,'YTick',0); set(gca,'YTickLabel',{' '}); ylabel(' ');
xlabel(strcat(int2str(I_user.cc_denoised.NumObjects),' objects'));


%define x and y dimensions
x_dim = size(handles.I.original,1);
y_dim = size(handles.I.original,2);

%set up histogram bins
temp_bins_1 = [1:100:2000]; temp_bins_2 = [2001 1000000]; % -- for lauren
bins.pixels = [temp_bins_1 temp_bins_2]; % -- combine bins

%loop through objects/cells and assign them to a hist bin
bins.counts = zeros(1,length(bins.pixels));
bins.bwMat = false(x_dim,y_dim,length(bins.pixels)); % -- set up false logical image matrix for bins


count_H2 = 0;

%keyboard

for i = 1:1:handles.I.cc_denoised.NumObjects % -- loop through denoised objects, in order objects found

    curr_obj.logical = false(size(handles.I.BW_denoised)); % -- set up false logical image
    curr_obj.logical(handles.I.cc_denoised.PixelIdxList{i}) = true; % -- set current object (starts with biggest one) to true
    curr_obj.area = size((find(curr_obj.logical)),1); % -- count number of true pixels

    for b = 1:1:(length(bins.pixels)-1) % -- loop through hist bins to see which one object falls into

        thresh = bins.pixels(b);
        thresh_next = bins.pixels(b+1)-1;

        if ((curr_obj.area > thresh) && (curr_obj.area <= (thresh_next)))

            bins.bwMat(:,:,b) = bins.bwMat(:,:,b) | curr_obj.logical; % add bits of current object to relevant bin
            bins.counts(b) = bins.counts(b) +1;


            % --- LJ & AKH - 28/01/2013 --- took this bit of code out
            % because breaking code as no data in hist2 for some images
%             % save out to variable information about hist2
%             if (thresh == 101) && (thresh_next == 200)
%
%                 % create new variable to save hist data to
%                 count_H2 = count_H2 +1;
%                 HIST2_areas(count_H2) = curr_obj.area;
%
%             end % if

        end % if

    end
```

```
end

%handles.I.HIST2_areas = HIST2_areas; % ---- taken out, see comment 28/01/2014

total_counted = sum(bins.counts); % -- check counts the right number of objects

%show the histogram with bins
figure(6); bar(bins.counts);
axis([0 22 0 max(bins.counts)+20]);
h = findobj(gca,'Type','patch'); set(h,'FaceColor','b','EdgeColor','w');


% -- insert object counts on the histogram bars
for l = 1:1:length(bins.counts)

    text(l-0.25,bins.counts(l)+5,int2str([bins.counts(l)]))

end
```

Appendix 2- Quantification of Pit Depths

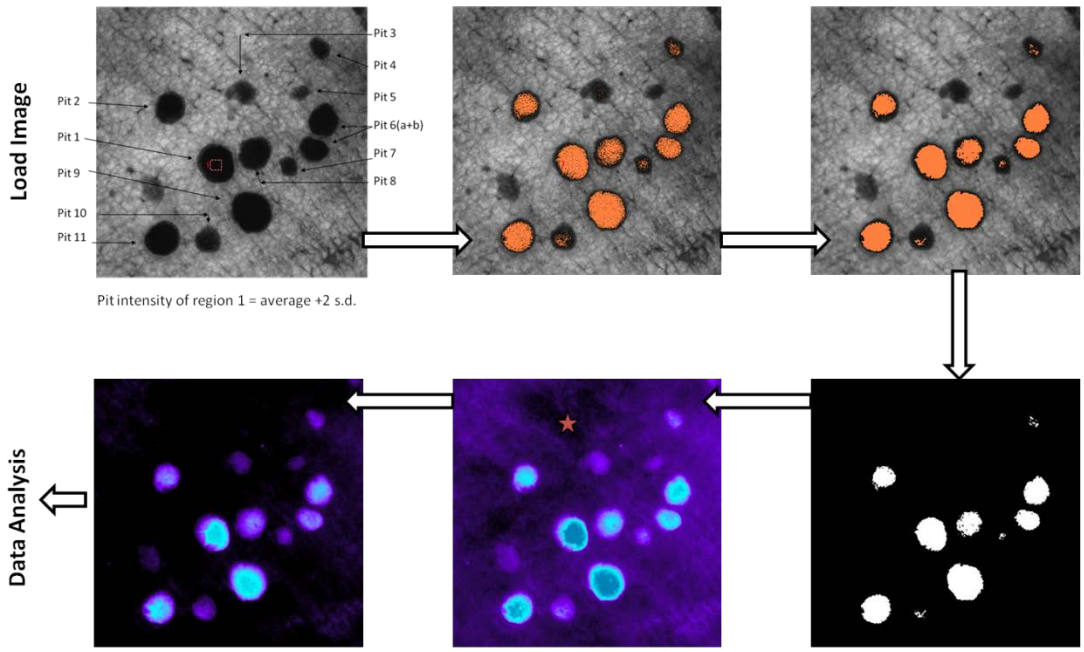

Appendix 2 –Flow diagram for the calculation of depth and volume of pits from the analysis of 3-D confocal stacks. Data collected at x60 was loaded into metamorph and the average intensity of a pit was defined. Through the application of an inclusive threshold and a median filter, both background noise and data slices below the base of the pit were removed. A binary image was then produced which could be summed to allow the removal of background signal and facilitate the creation of an intensity profile for each pit.